The American Journal of Human Genetics, Volume *108*

Supplemental information

Targeted long-read sequencing identifies missing disease-causing variation

Danny E. Miller, Arvis Sulovari, Tianyun Wang, Hailey Loucks, Kendra Hoekzema, Katherine M. Munson, Alexandra P. Lewis, Edith P. Almanza Fuerte, Catherine R. Paschal, Tom Walsh, Jenny Thies, James T. Bennett, Ian Glass, Katrina M. Dipple, Karynne Patterson, Emily S. Bonkowski, Zoe Nelson, Audrey Squire, Megan Sikes, Erika Beckman, Robin L. Bennett, Dawn Earl, Winston Lee, Rando Allikmets, Seth J. Perlman, Penny Chow, Anne V. Hing, Tara L. Wenger, Margaret P. Adam, Angela Sun, Christina Lam, Irene Chang, Xue Zou, Stephanie L. Austin, Erin Huggins, Alexias Safi, Apoorva K. Iyengar, Timothy E. Reddy, William H. Majoros, Andrew S. Allen, Gregory E. Crawford, Priya S. Kishnani, University of Washington Center for Mendelian Genomics, Mary-Claire King, Tim Cherry, Jessica X. Chong, Michael J. Bamshad, Deborah A. Nickerson, Heather C. Mefford, Dan Doherty, and Evan E. Eichler

Supplemental Data

Supplemental Text

Clinical summary and prior testing for simple structural variant cases

All nine cases beginning with "BK" are from the Study of Autism Genetics Exploration (SAGE) collection, five cases of which have been previously described[5] and four (BK397-101, BK430-103, BK482-101, BK487-101) are samples collected after the publication.

Individual S016 has a known duplication in *CTNND2* confirmed by clinical mate-pair sequencing to be tandem.[1]

Individual S023 presented with developmental delay, epilepsy, and hypothyroidism. A SNP array identified a mosaic region of 18p11.32 and 18q21.31q23 with copy number between 1 and 2. Evaluation of chromosomes revealed that this individual was mosaic for a ring chromosome 18 in ~40% of cells.

Individual S046 presented with developmental delay and was found to have an unbalanced translocation between chromosomes 4 and 15. A single-nucleotide polymorphism (SNP) array identified a copy state of 1 at 4q35.1q35.2 and a copy state of 3 at 15q26.1q26.3.

Individual S060 was diagnosed with campomelic dysplasia, vertebral anomalies, neurogenic bowel and bladder, and bilateral moderate conductive hearing loss. Karyotype revealed 46,XY,t(12;17)(q13.3;q25). Because of high suspicion for campomelic dysplasia associated with a *SOX9* variant sequencing of *SOX9* was undertaken which was negative. SNP microarray was used in an attempt to localize the translocation breakpoints if they were associated with a deletion or duplication but was unrevealing.

Individual S063 was from a family with severe bilateral breast and ovarian cancer in which clinical evaluation failed to identify a pathogenic variant in either *BRCA1* or *BRCA2*. Long-read sequencing on a PacBio platform after CRISPR-Cas9 excision of *BRCA1* and *BRCA2* revealed a SINE-VNTR-Alu retrotransposon insertion that created a pseudoexon in *BRCA1*.

Clinical summary and prior testing for cases that underwent phasing

Individual S071 was referred to genetics for global developmental delay. Trio exome sequencing revealed two variants of uncertain clinical significance, one a *de novo* variant, in *METTL5* that could not be phased.

Individual S086 carried a diagnosis of epilepsy. Panel testing on an exome backbone revealed an inherited pathogenic variant in *KIAA1109* and a *de novo* mosaic variant. These variants could not be phased by the clinical laboratory.

Clinical summary and prior testing for repeat expansion cases

Individual S011 was an individual with clinically confirmed expansions in *ATXN3* (74 and 28 repeats) and *ATXN8OS* (80 and 25 repeats). Individual 04-01 (proband), 04-02 (mother), 04-03 (father), 06-01 (proband), 06-02 (mother), and 06-03 (father) were previously described.[3]

Clinical summary and prior testing for complex structural variant cases

Individual S014 presented prenatally with agenesis of the corpus callosum and ventriculomegaly. At birth the child was noted to have mild dysmorphic features and pelviectasis without hydroureter. A SNP array identified a complex pathogenic heterozygous deletion within 6q25.2 to 6q25.3, which included *ARID1B* and perhaps explained most of his clinical findings.

Individual S020 presented with hypotonia, developmental delay, epilepsy, and dysmorphic features. A SNP array revealed deletions of 4q13.2q13.3, 4q13.3, and 14q11.2. Karyotyping identified rearrangements among chromosomes 2, 14, 10, and 4 that involved the deleted regions and also 2p23, 2p25, 10q21.2, 10q21.1, and 10q22.3.

Individual S021 presented with developmental delay and was found by microarray and karyotype to be mosaic for complex changes to chromosome 8 that included loss of 8p23.2–pter (copy number 1), mosaic loss of a segment within 8p23.2–8p23.1 (copy number 1–2), and mosaic gain of 8q22.1–qter (copy number 2–3). Karyotype identified one cell line with a derivative chromosome 8 that consists of a terminal duplication of 8q, from 8q22.1 to qter, and a terminal deletion of 8p, from 8p23.2 to pter. The duplicated region of 8q is present on distal 8p, such that 8q22.1 to qter is present at both ends of the derivative chromosome 8. The other cell line has a terminal deletion of 8p, from 8p23.1 to pter.

Individual S022 presented with hemihypertrophy of unclear etiology. A standard Beckwith-Wiedemann workup including *CDKN1C* sequencing and deletion/duplication analysis was unremarkable. A SNP array identified a focal amplification of 4q with the copy state reported as more than 4 with an adjacent 27.5 Mbp region of homozygosity on 4q. A SNP array also identified a duplication of 15q11.2. Metaphase and interphase FISH confirmed that the focal amplification of 4q was more than 4.

Individual S035 presented with developmental delay and was found on array to have duplications of both 8q24.3 and 16p13.11.

Individual S036 underwent genetic testing for expressive language delay, microcephaly, and mild dysmorphic features. A SNP array revealed four noncontiguous deletions of chromosome 10 at 10p12.2p12.1, 10p11.21, and 10q21.1 (two deletions in this interval). Karyotype revealed a translocation between chromosomes 6 and 18 at 6q22.2 and 18p11.2 as well as a pericentric inversion of chromosome 10 at 10p11.2q11.2.

Individual S082 was referred for genetic testing because of gross motor delay and multiple congenital anomalies. SNP array revealed two pathogenic CNVs, a 10q25.2 deletion involving *RBM20*, and a complex chromosome 17 duplication and deletion involving *RAI1* and *PMP22*.

Individual S083 was prenatally diagnosed with multiple congenital anomalies, including imperforate anus and vertebral anomalies. SNP array after birth revealed a 4p16.3 deletion and 4p16.3p15.2 duplication. The deletion overlaps the Wolf-Hirschhorn syndrome critical region.

Clinical summary and prior testing for missing variant cases

Individual S002 presented with early-onset obesity, type 2 diabetes, cone-rod dystrophy, and sensorineural hearing loss. Clinical testing by SNP array was unremarkable and exome sequencing identified a single paternally inherited stop-gain variant in *ALMS1*, the gene associated with Alström syndrome, a recessive disorder that fit the phenotype well. Subsequent exon-level array revealed no deletions or duplications in the gene.

Individual S003 was an individual with renal failure, retinal degeneration, and essential tremor. A SNP array was unremarkable, trio exome revealed a single variant in *NPHP4*, and deletion/duplication analysis of NPHP4 was unremarkable. Clinical RNA testing was sent, which was interpreted as indeterminate.

Individual S004 presented with agenesis of the corpus callosum, microcephaly, poor growth, lactic acidosis, and global developmental delay. The SNP array was unremarkable, trio exome sequencing revealed a single pathogenic variant in *VARS2*, and deletion/duplication analysis of the gene was unremarkable.

Individual S008 was an individual with biochemically confirmed Lesch-Nyhan syndrome. Clinical testing included karyotype and sequencing of exons on an exome backbone, both of which were unremarkable.

Individual S009 presented with concern for Duchenne muscular dystrophy due to a family history of the disease. The proband's maternal uncle passed away at age 29 from the disease without a molecular diagnosis. Molecular testing in the proband included SNP array, targeted exon sequencing, and deletion/duplication analysis, all of which were unremarkable. Analysis of muscle biopsy by immunohistochemistry revealed staining indicative of a dystrophinopathy, but dystrophin 1 antibody staining (rod domain) was more than classically seen in Duchenne type dystrophy.

Individual S013 presented with oculocutaneous albinism and platelet dysfunction, suggesting Hermansky-Pudlak syndrome, but SNP array and exome sequencing only identified a single paternally inherited stop in *HPS1*, one of several genes associated with this recessive disorder.

Individual S018 presented with elevated phenylalanine consistent with phenylketonuria. Panel testing revealed a single pathogenic variant in *PAH*.

Individual S025 presented in their early twenties with disease characteristics in the macula of both eyes consistent with recessive Stargardt disease. No other systemic issues or family history was reported. Research sequencing revealed a single inherited pathogenic variant and research whole-genome short-read sequencing failed to identify a second hit. After identification of a 1,500 bp insertion in the first intron of *ABCA4* with LRS visual reanalysis of the short-read data confirmed an 11 bp target site duplication at the same position.

Individual S047 presented at 18 months old with failure to thrive, marked hepatomegaly, and fasting hypoglycemia. A liver biopsy was performed revealing increasing glycogen content, decreased glucose-1-phosphate to glucose ratio, and no measurable debranching enzyme. A diagnosis of Glycogen Storage Disease Type IIIa was suspected. Sequencing of the *AGL* gene revealed a single heterozygous frameshift variant in exon 10 resulting in a premature stop codon (c.1276delG, p.Ile437X) on one allele. A second variant was not identified.

Individual S056 presented with end-stage renal disease related to nephronophthisis, rhizomelic/metaphyseal skeletal dysplasia, retinal dystrophy, developmental delays, hyperparathyroidism, and hepatic fibrosis. A ciliopathy gene panel revealed a single heterozygous pathogenic variant in *WDR19* and deletion/duplication analysis of the gene was unremarkable.

Supplementary Figures

Figure S1. Binary segmentation figures.

To complement existing SV callers and independently guide the refinement of CNV breakpoints, we applied the binary segmentation method to the sequencing depth profiles of each CNV region. The coordinates of each region were further refined through visual validation. Due to the sensitivity of the binary segmentation method to duplicated genomic sequences, 6 of the 29 regions could not have their breakpoints refined by this method; these were refined using a combination of existing SV callers and visual refinement of sequencing depth profile. The script used to generate these images as well as the coverage for each target region is available on GitHub.

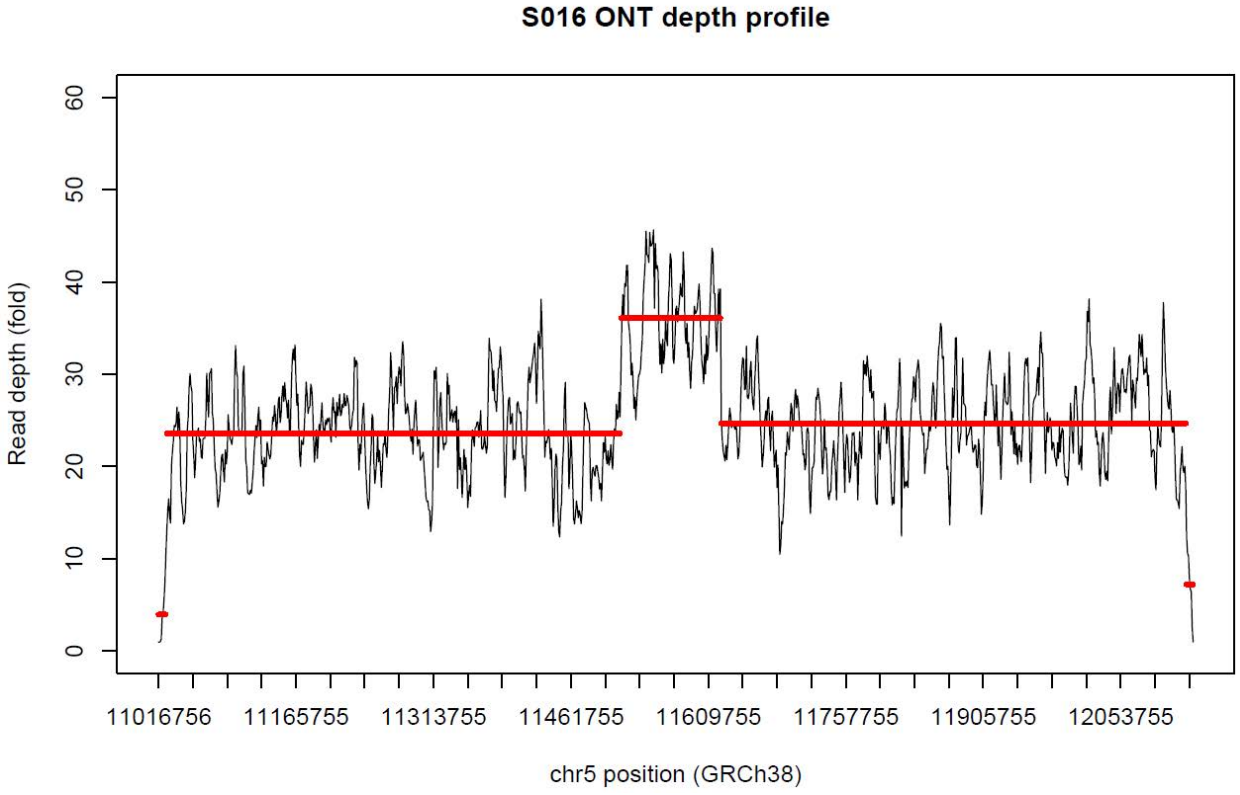

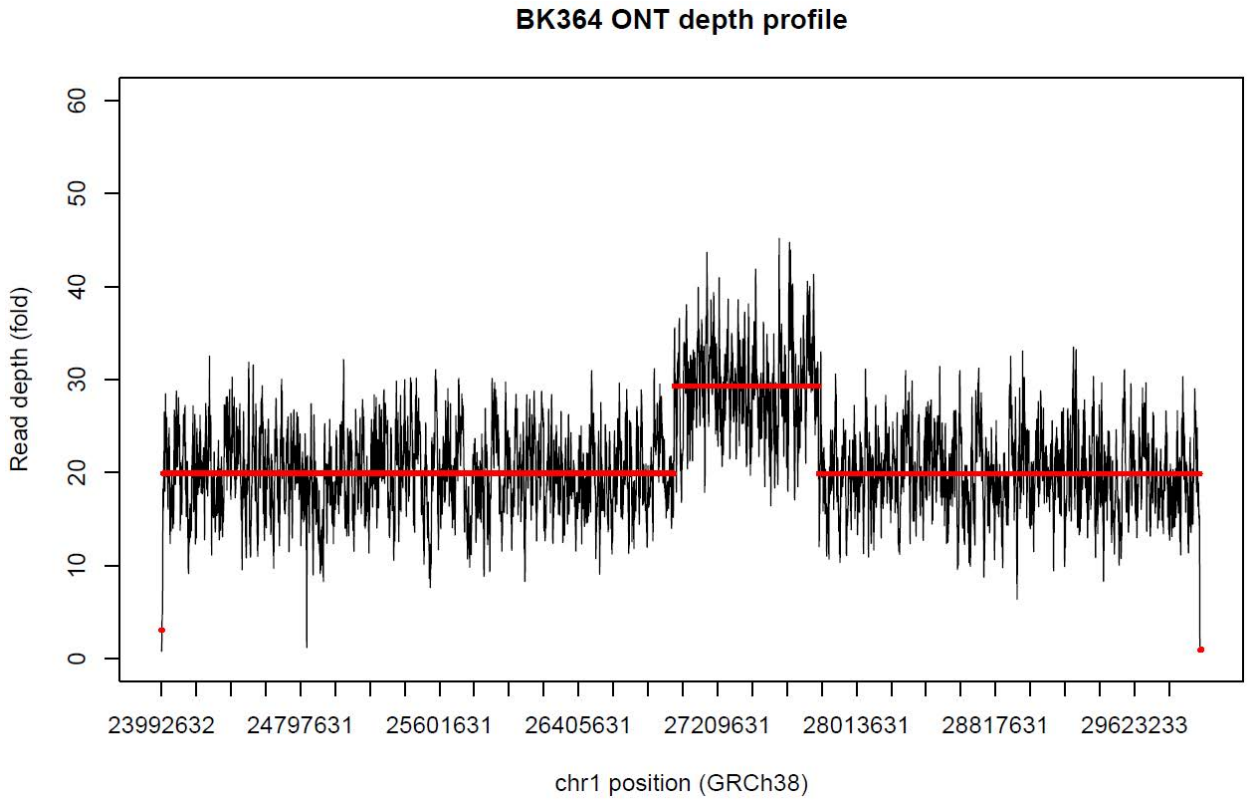
BK364 ONT depth profile
Read depth (fold)
0
10
20
30
40
50
60
23992632
24797631
25601631
26405631
27209631
28013631
28817631
29623233
chr1 position (GRCh38)

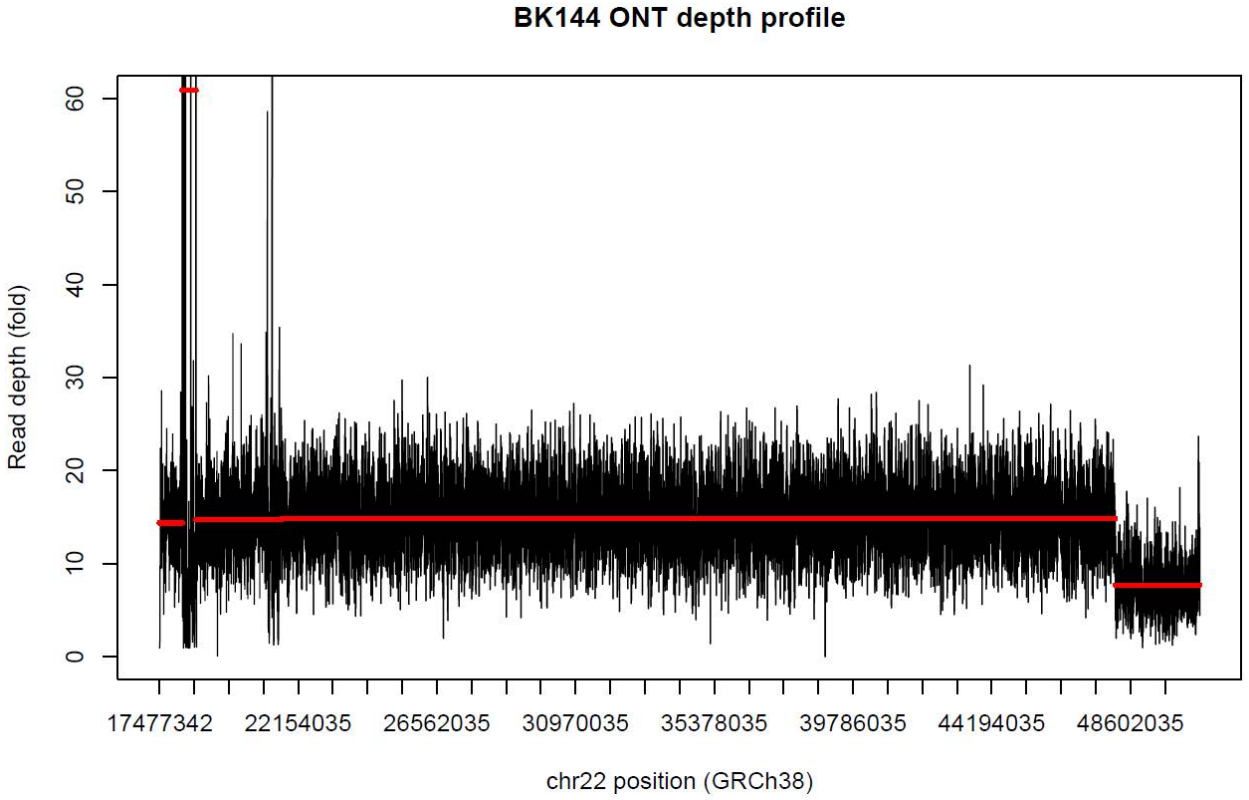
BK144 ONT depth profile
Read depth (fold)
0
10
20
30
40
50
60
17477342
22154035
26562035
30970035
35378035
39786035
44194035
48602035
chr22 position (GRCh38)

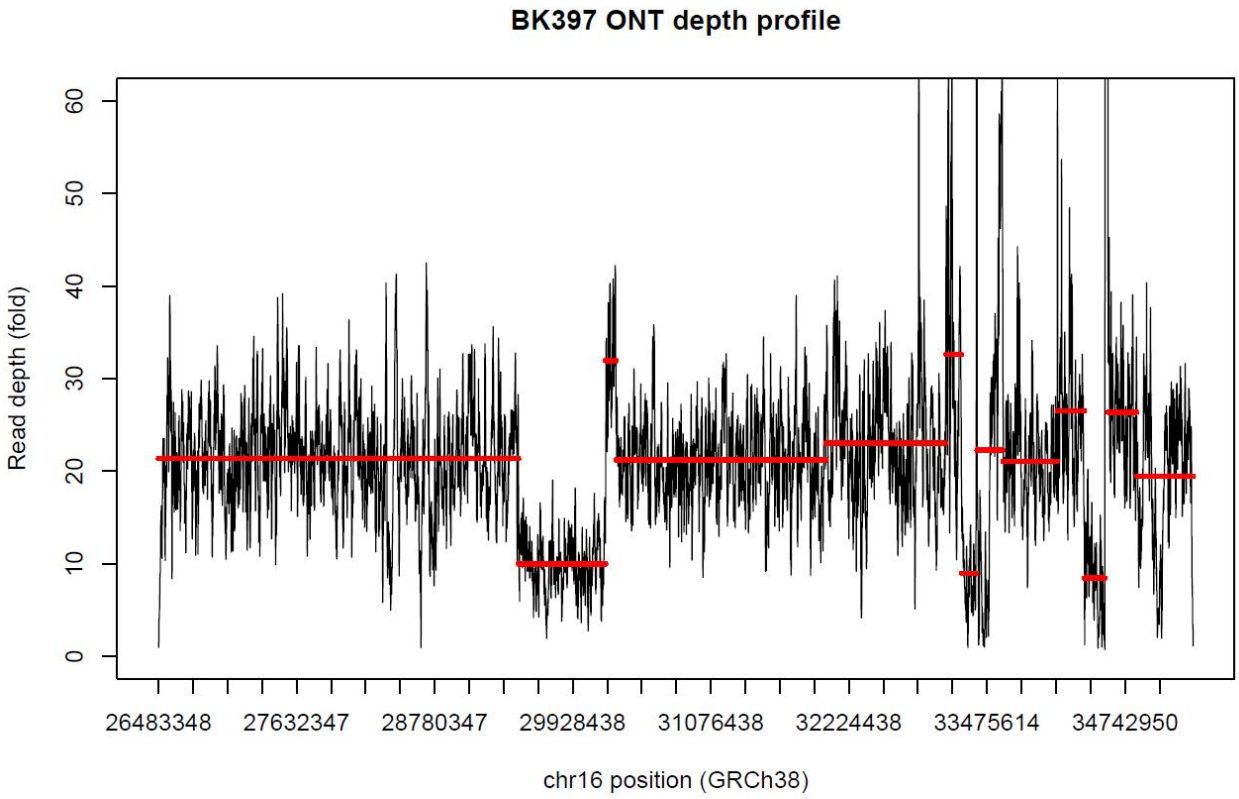
BK397 ONT depth profile
Read depth (fold)
0
10
20
30
40
50
60
26483348
27632347
28780347
29928438
31076438
32224438
33475614
34742950
chr16 position (GRCh38)

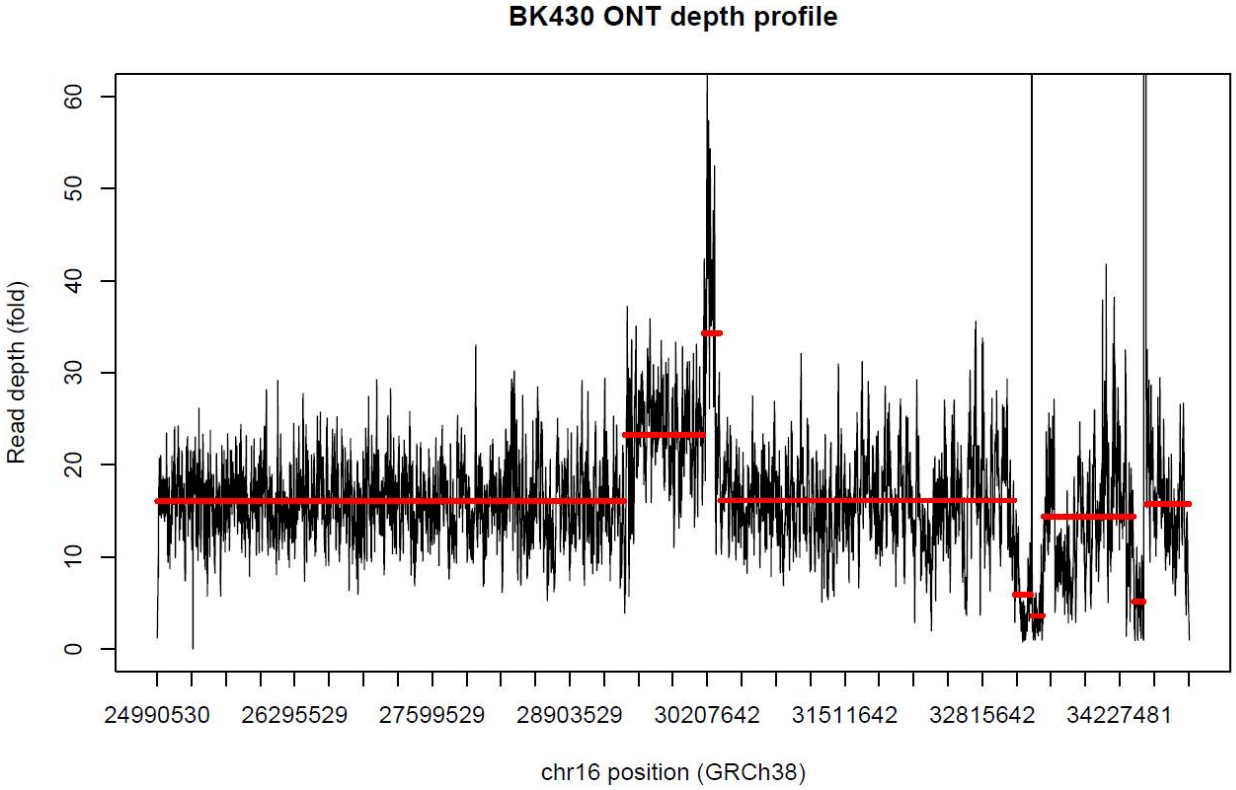
BK430 ONT depth profile
Read depth (fold)
0
10
20
30
40
50
60
24990530
26295529
27599529
28903529
30207642
31511642
32815642
34227481
chr16 position (GRCh38)

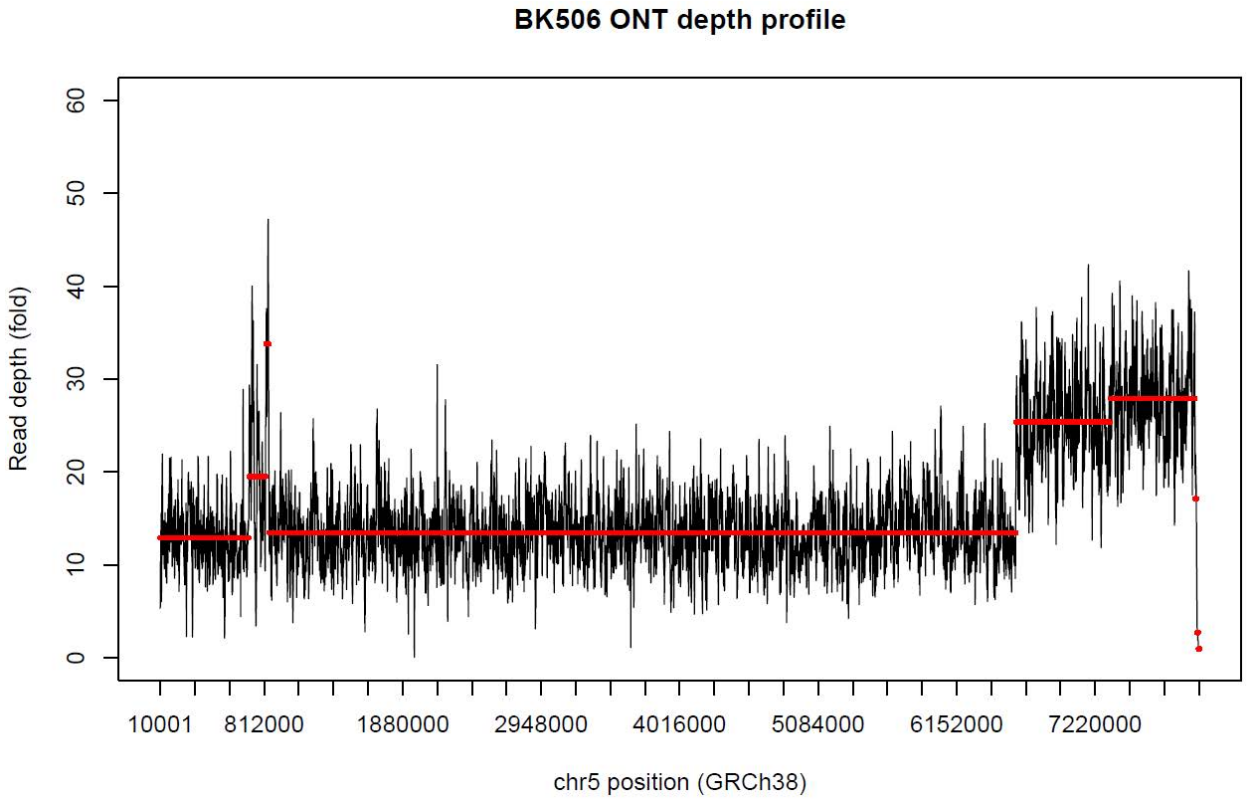
BK506 ONT depth profile
Read depth (fold)
0
10
20
30
40
50
60
10001
812000
1880000
2948000
4016000
5084000
6152000
7220000
chr5 position (GRCh38)

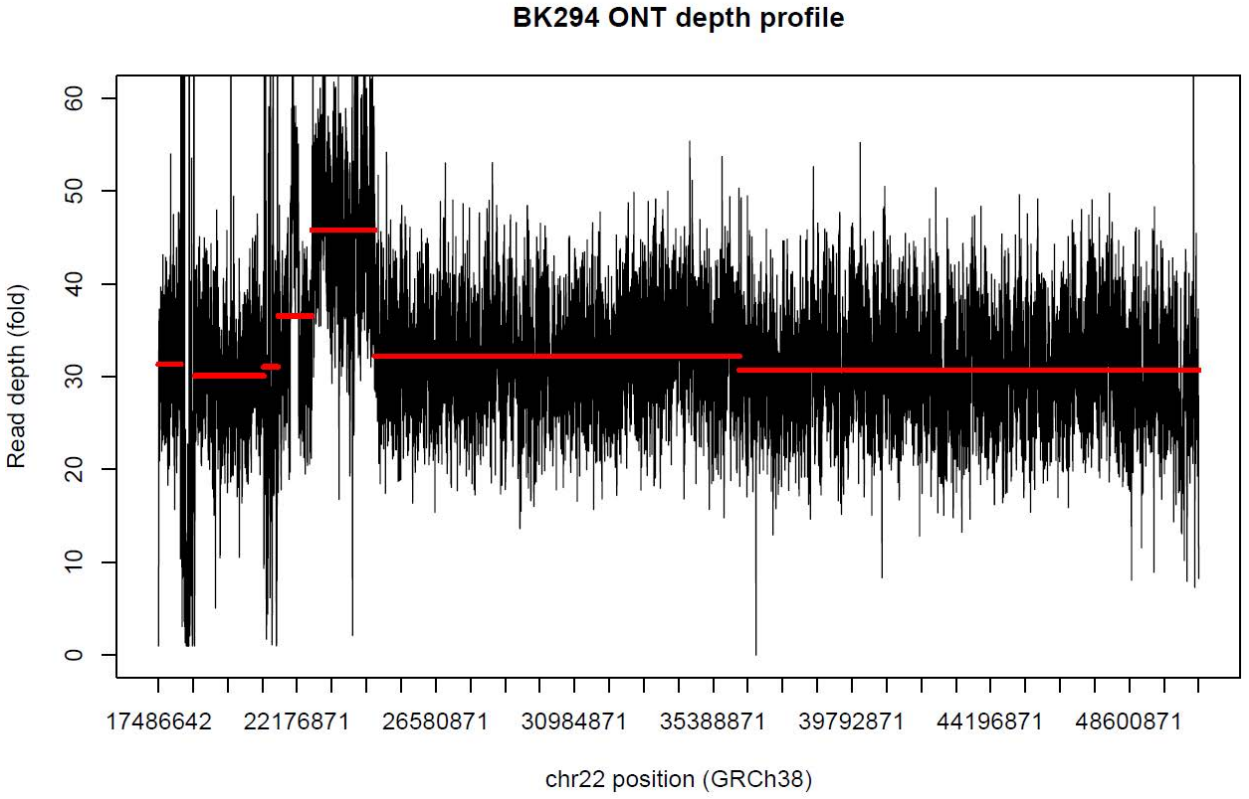
BK294 ONT depth profile
Read depth (fold)
0
10
20
30
40
50
60
17486642
22176871
26580871
30984871
35388871
39792871
44196871
48600871
chr22 position (GRCh38)

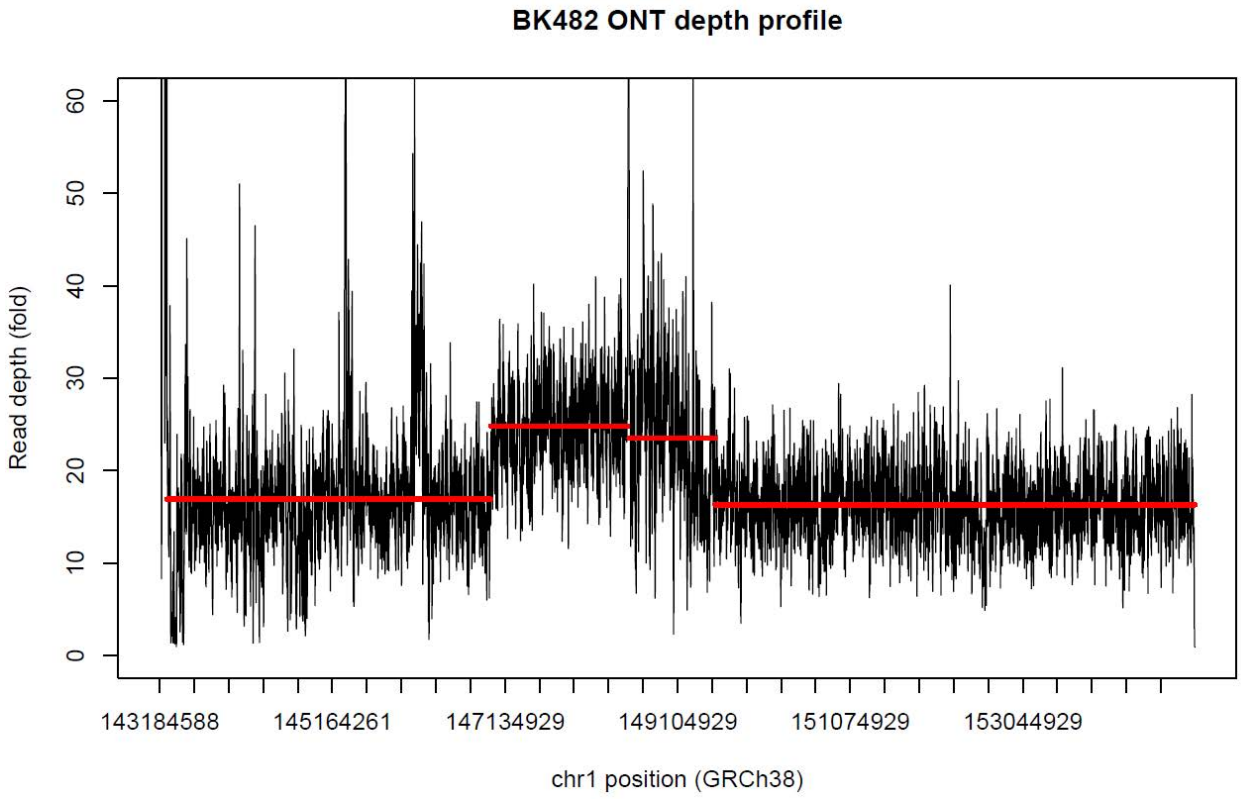
BK482 ONT depth profile
Read depth (fold)
0
10
20
30
40
50
60
143184588
145164261
147134929
149104929
151074929
153044929
chr1 position (GRCh38)

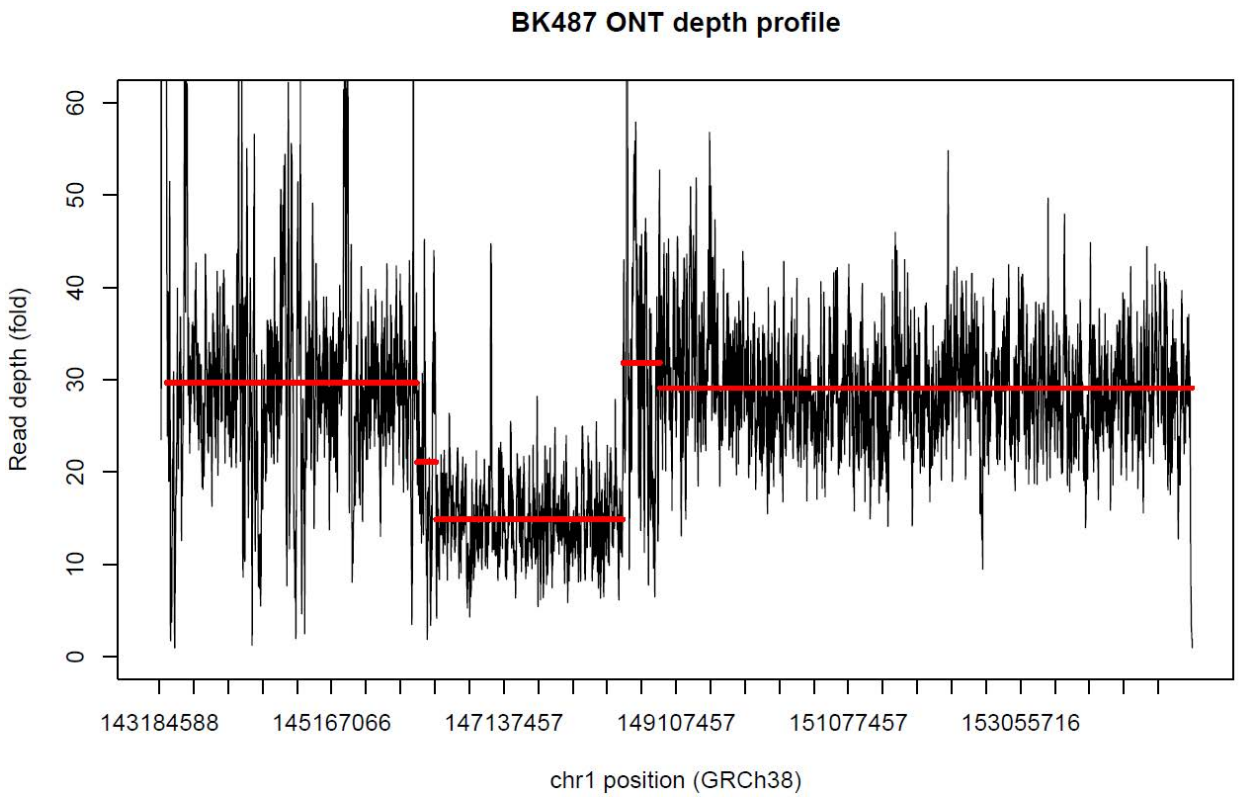
BK487 ONT depth profile
Read depth (fold)
0
10
20
30
40
50
60
143184588
145167066
147137457
149107457
151077457
153055716
chr1 position (GRCh38)

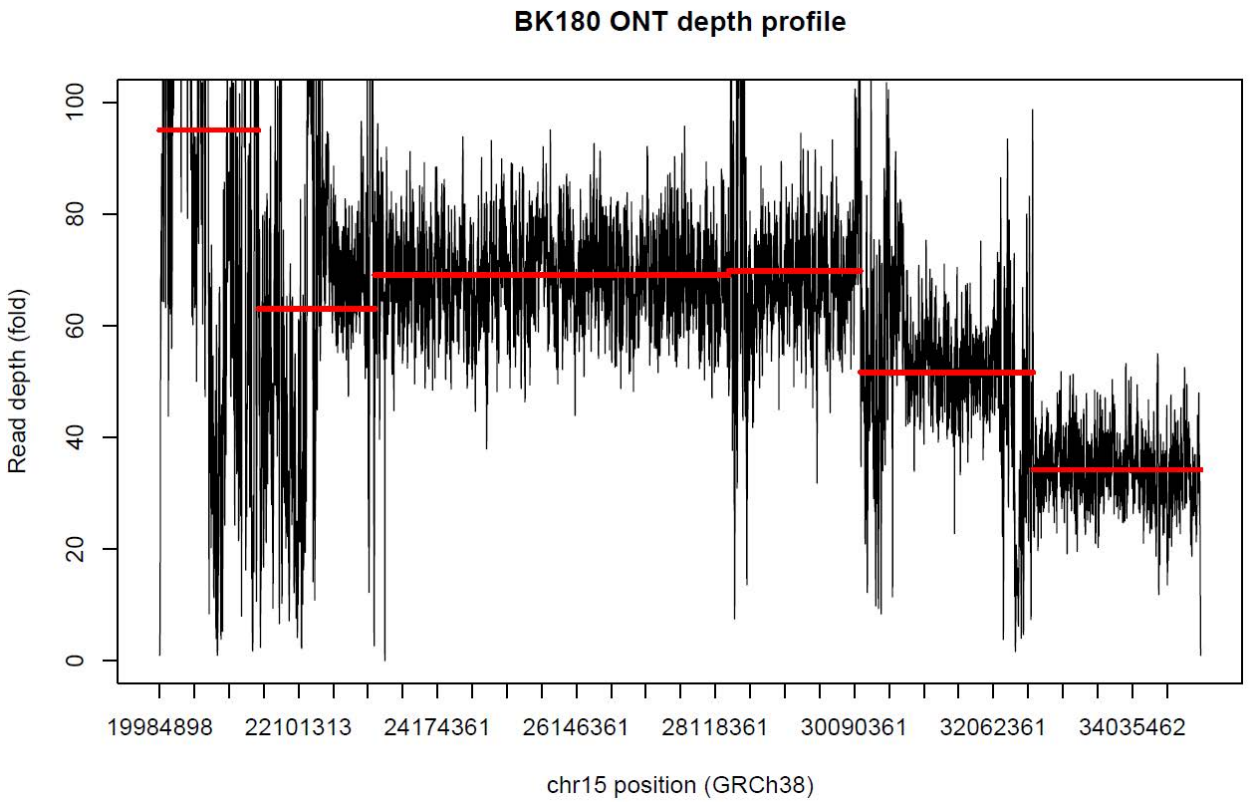
BK180 ONT depth profile
Read depth (fold)
0
20
40
60
80
100
19984898
22101313
24174361
26146361
28118361
30090361
32062361
34035462
chr15 position (GRCh38)

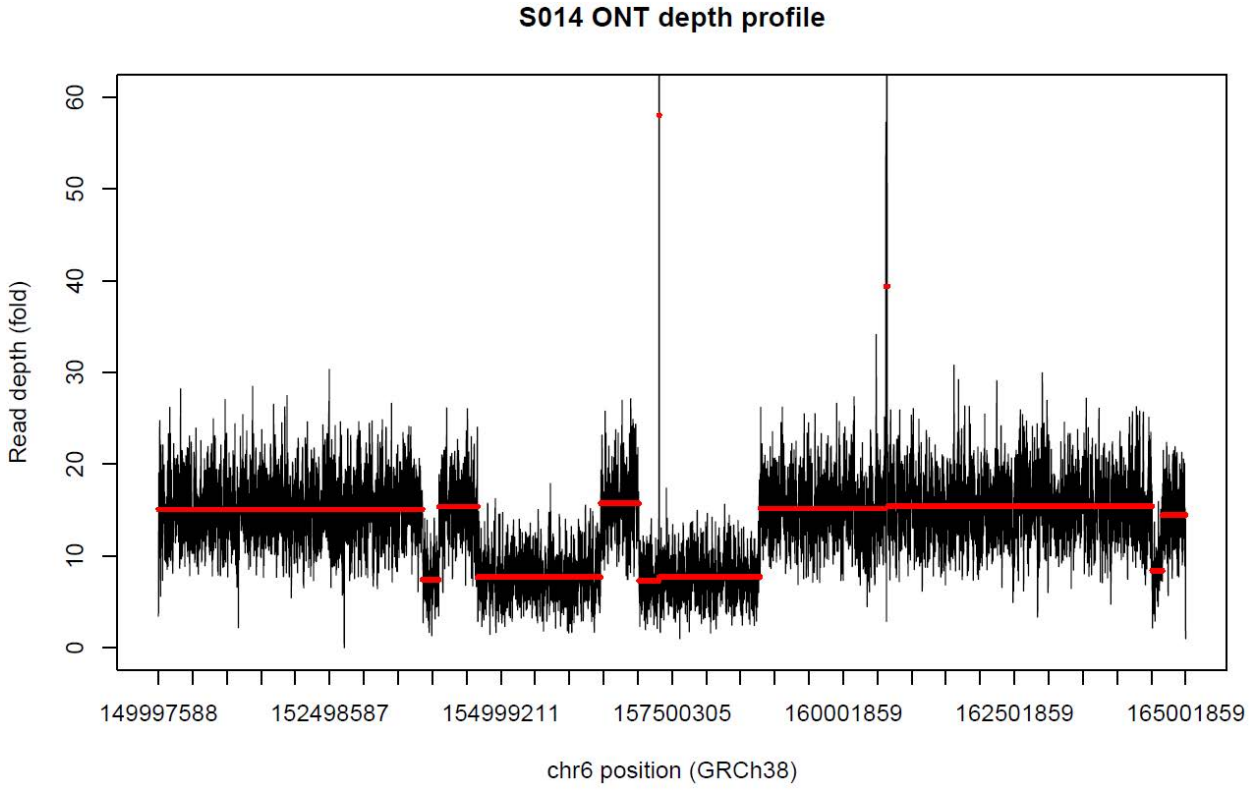
S014 ONT depth profile
Read depth (fold)
0
10
20
30
40
50
60
149997588
152498587
154999211
157500305
160001859
162501859
165001859
chr6 position (GRCh38)

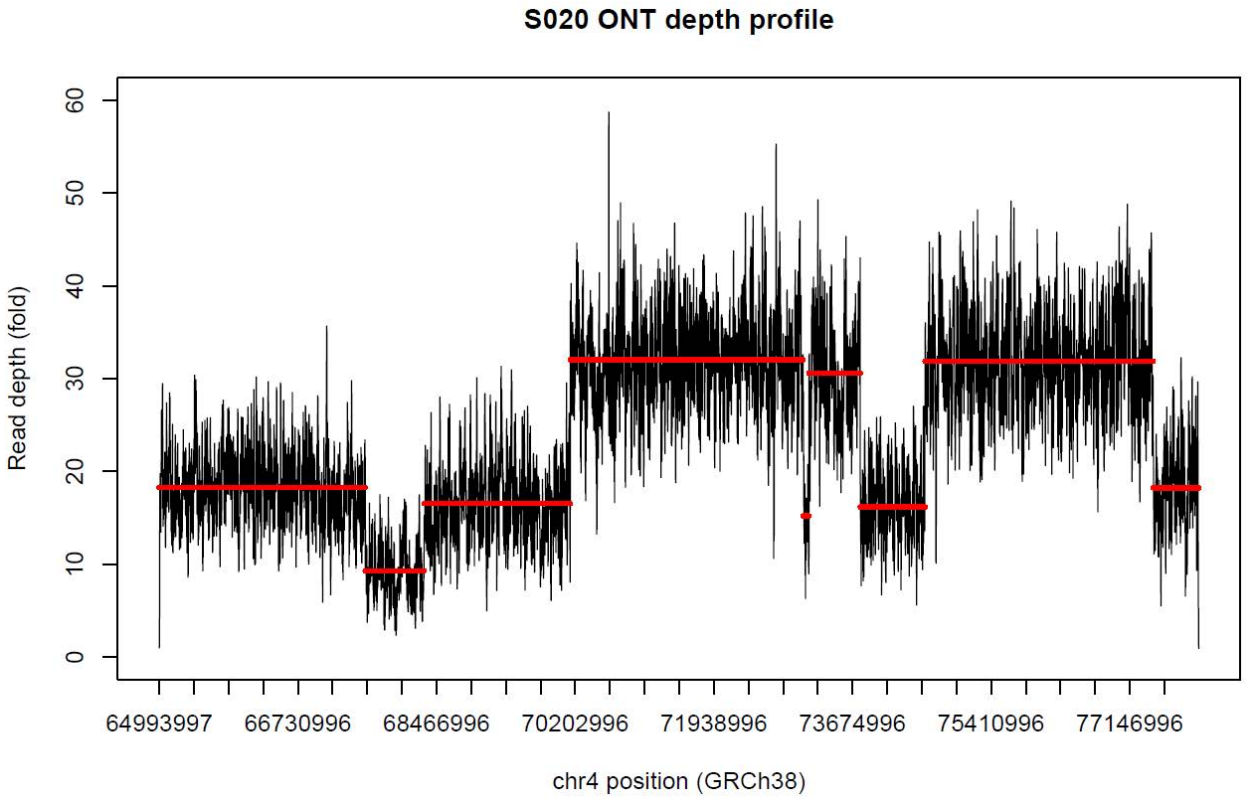
S020 ONT depth profile
Read depth (fold)
0
10
20
30
40
50
60
64993997
66730996
68466996
70202996
71938996
73674996
75410996
77146996
chr4 position (GRCh38)

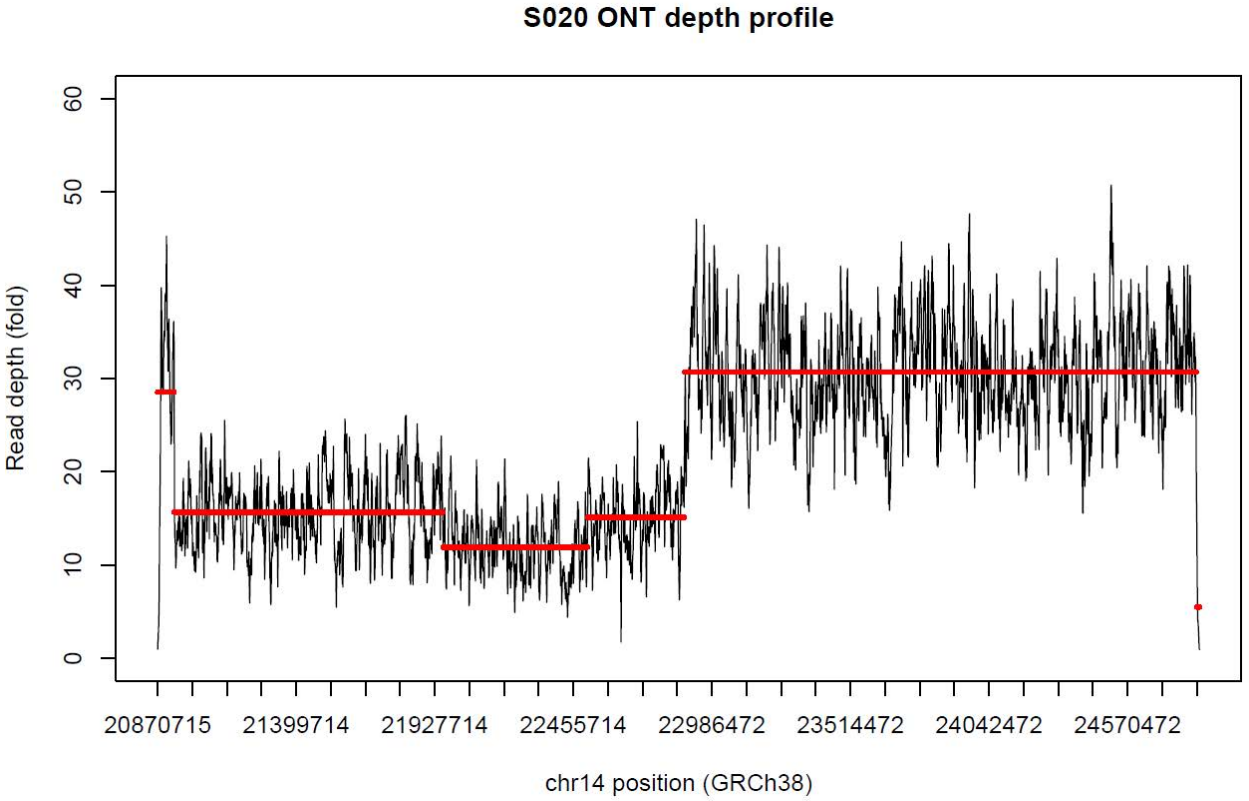
S020 ONT depth profile
Read depth (fold)
0
10
20
30
40
50
60
20870715
21399714
21927714
22455714
22986472
23514472
24042472
24570472
chr14 position (GRCh38)

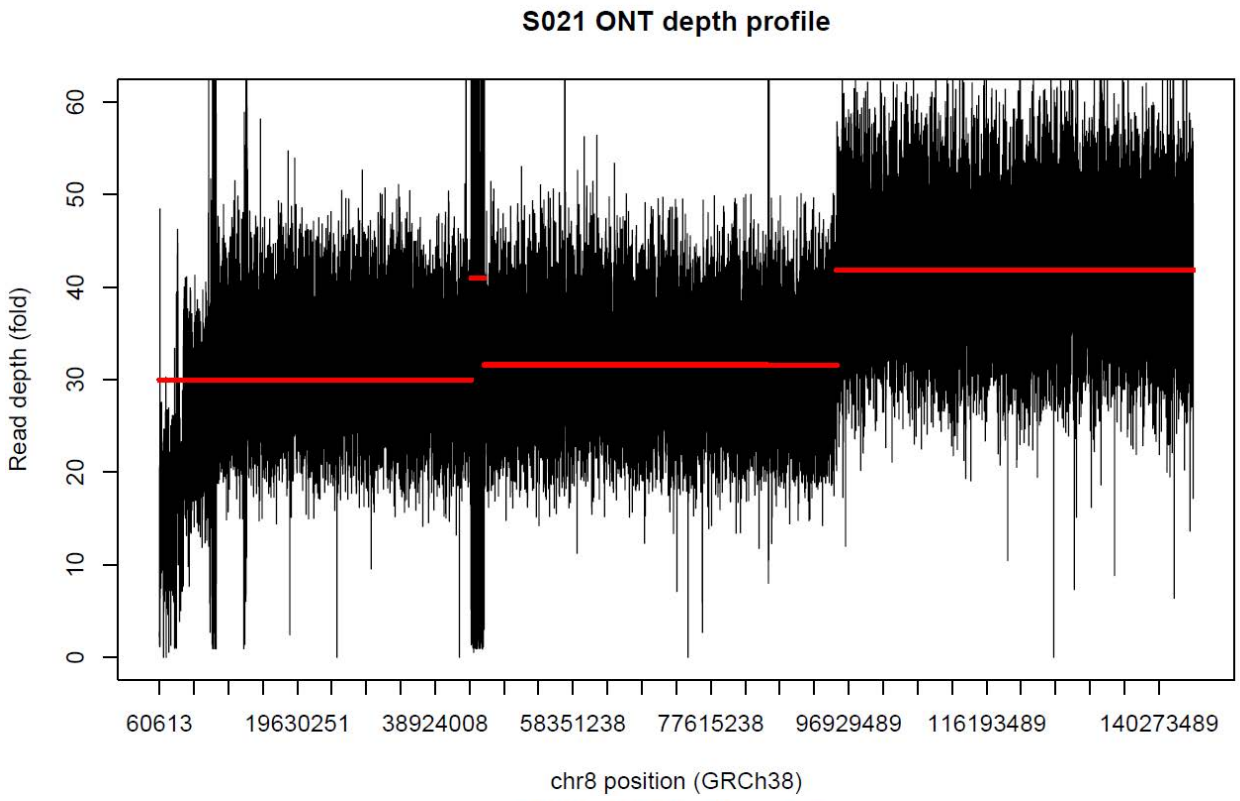
S021 ONT depth profile
Read depth (fold)
0
10
20
30
40
50
60
60613
19630251
38924008
58351238
77615238
96929489
116193489
140273489
chr8 position (GRCh38)

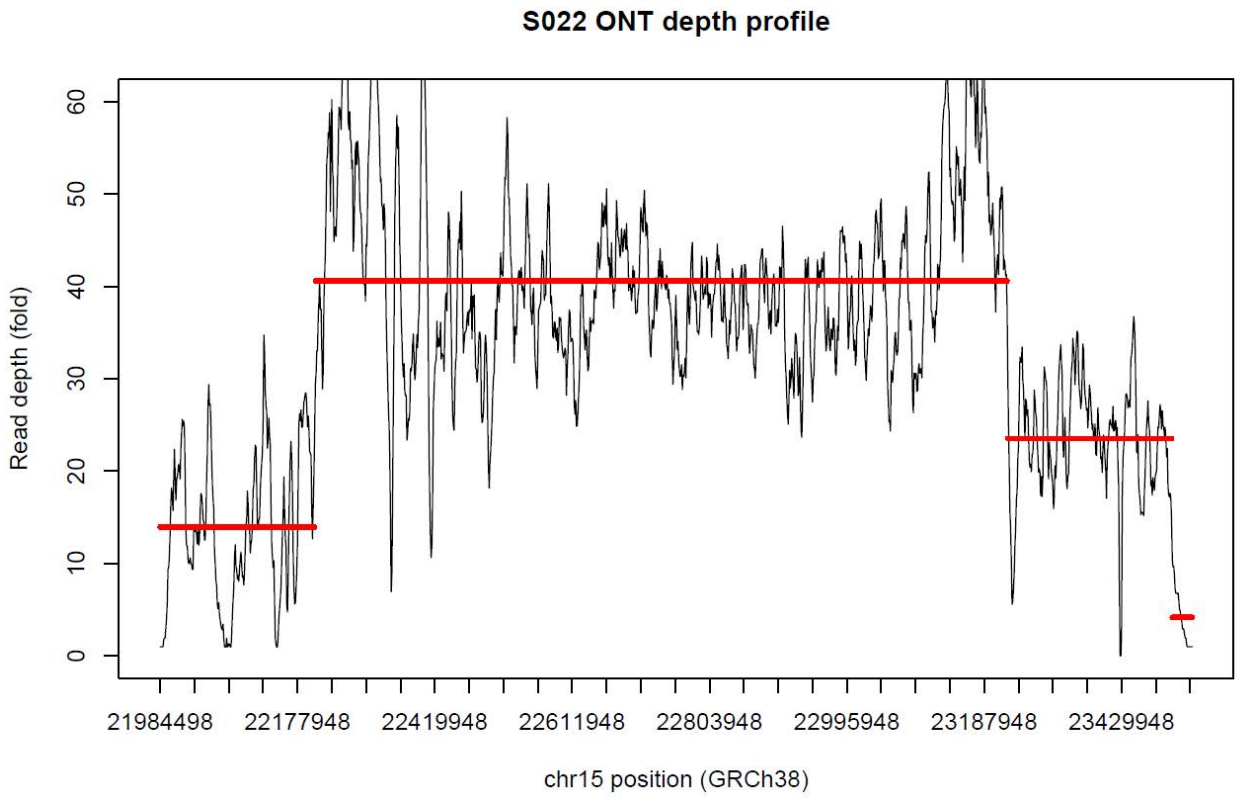
S022 ONT depth profile
Read depth (fold)
0
10
20
30
40
50
60
21984498
22177948
22419948
22611948
22803948
22995948
23187948
23429948
chr15 position (GRCh38)

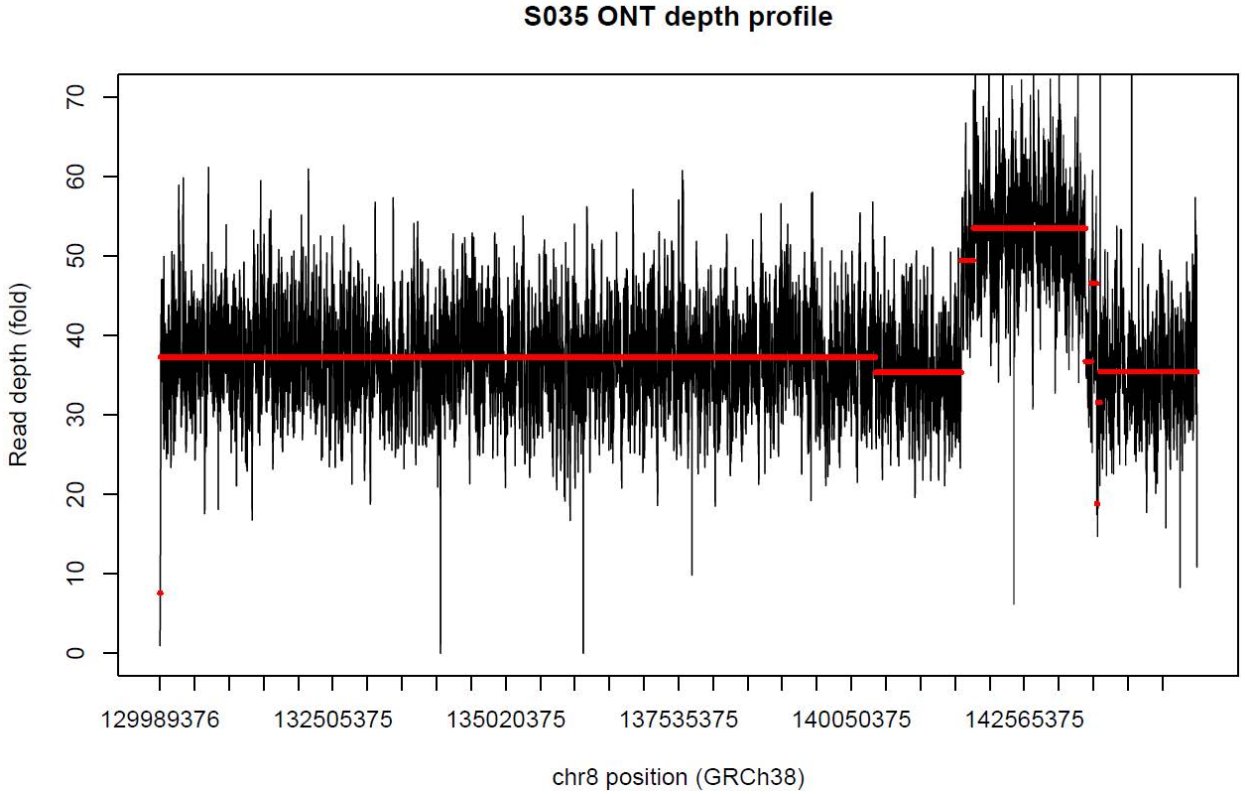
S035 ONT depth profile
Read depth (fold)
0
10
20
30
40
50
60
70
129989376
132505375
135020375
137535375
140050375
142565375
chr8 position (GRCh38)

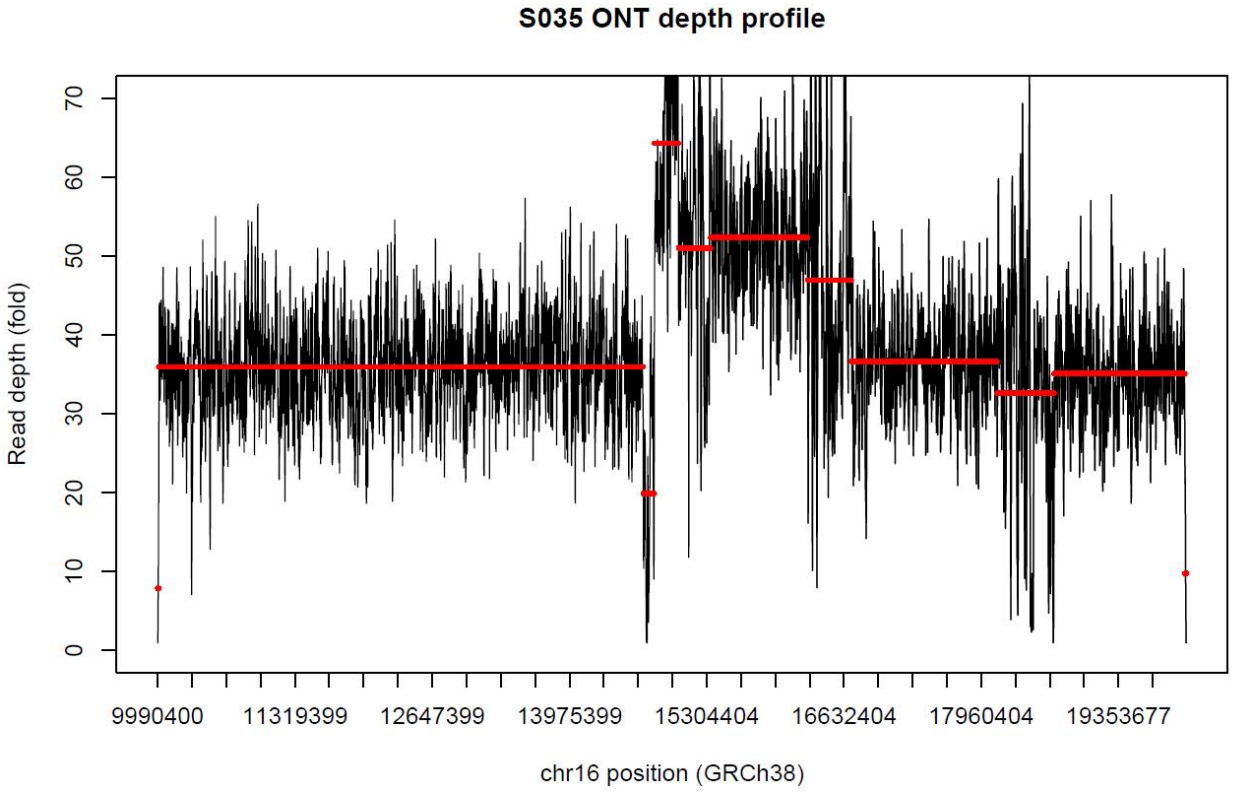
S035 ONT depth profile
Read depth (fold)
0
10
20
30
40
50
60
70
9990400
11319399
12647399
13975399
15304404
16632404
17960404
19353677
chr16 position (GRCh38)

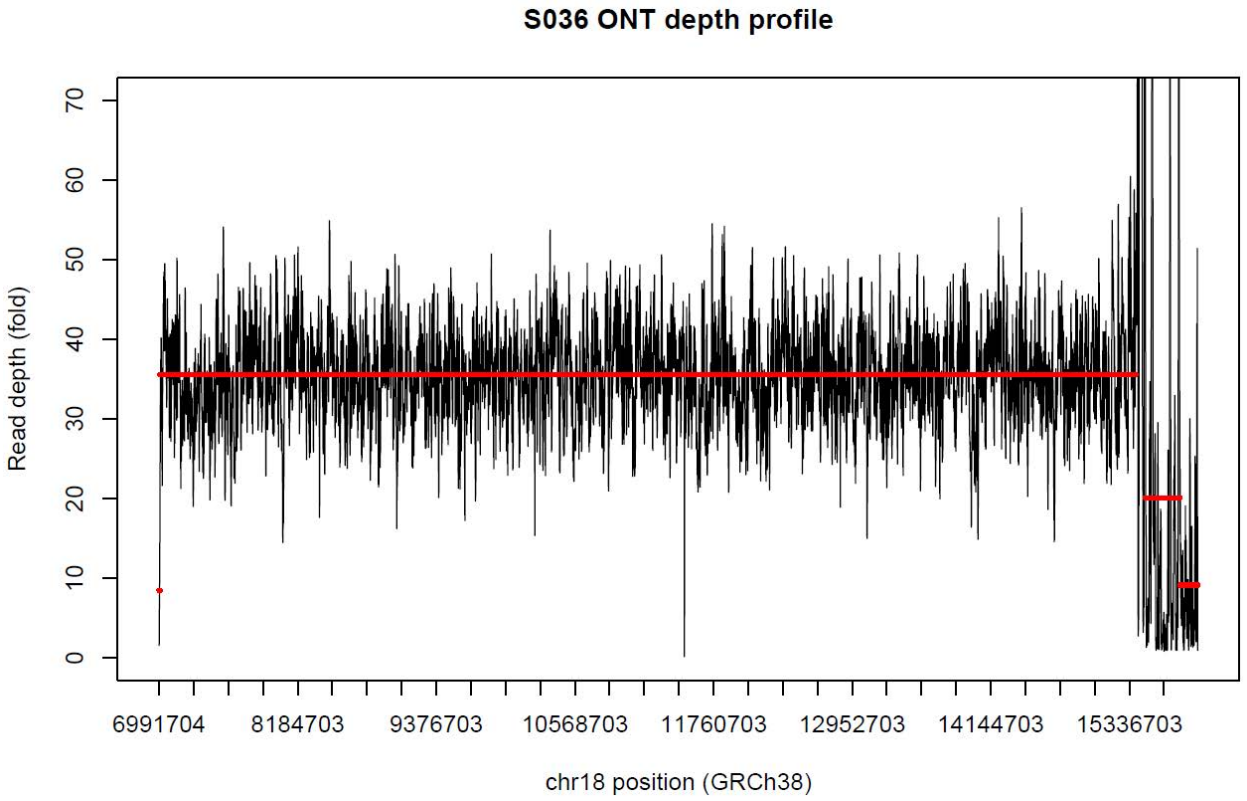
S036 ONT depth profile
Read depth (fold)
0
10
20
30
40
50
60
70
6991704
8184703
9376703
10568703
11760703
12952703
14144703
15336703
chr18 position (GRCh38)

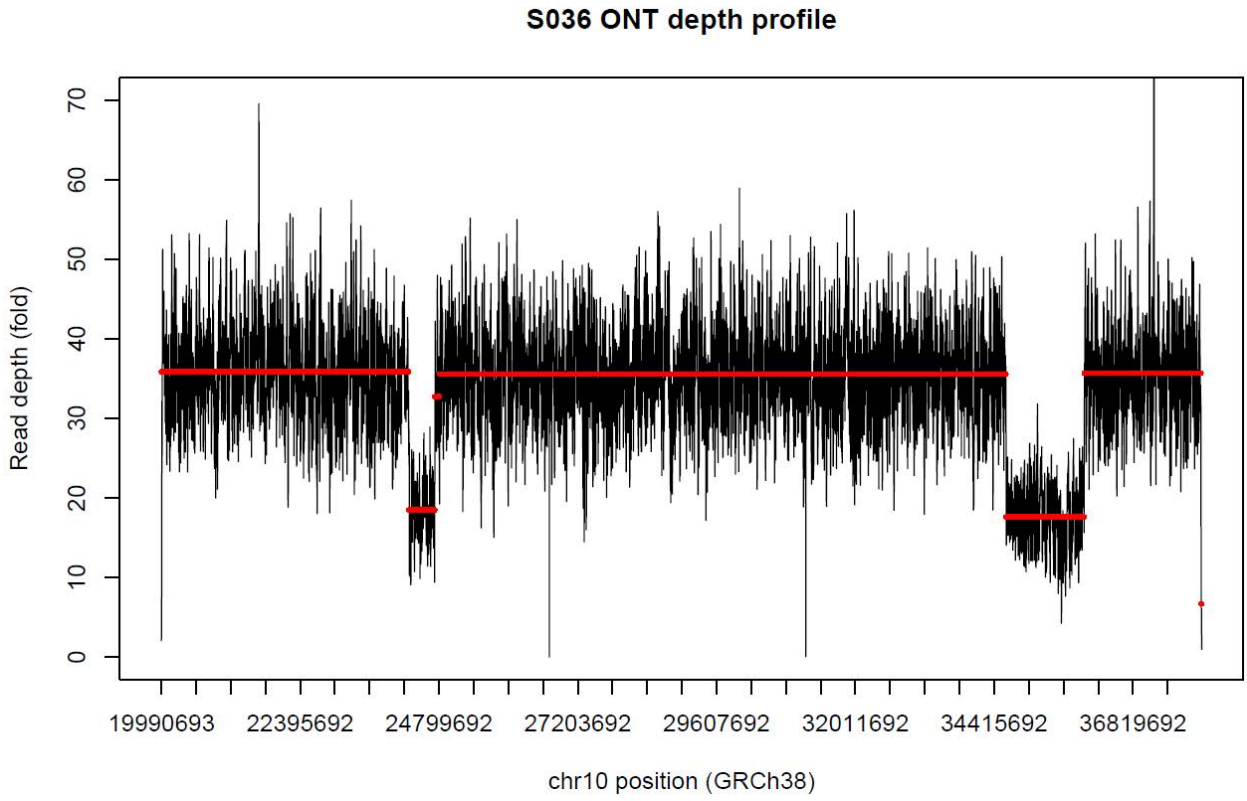
S036 ONT depth profile
Read depth (fold)
0
10
20
30
40
50
60
70
19990693
22395692
24799692
27203692
29607692
32011692
34415692
36819692
chr10 position (GRCh38)

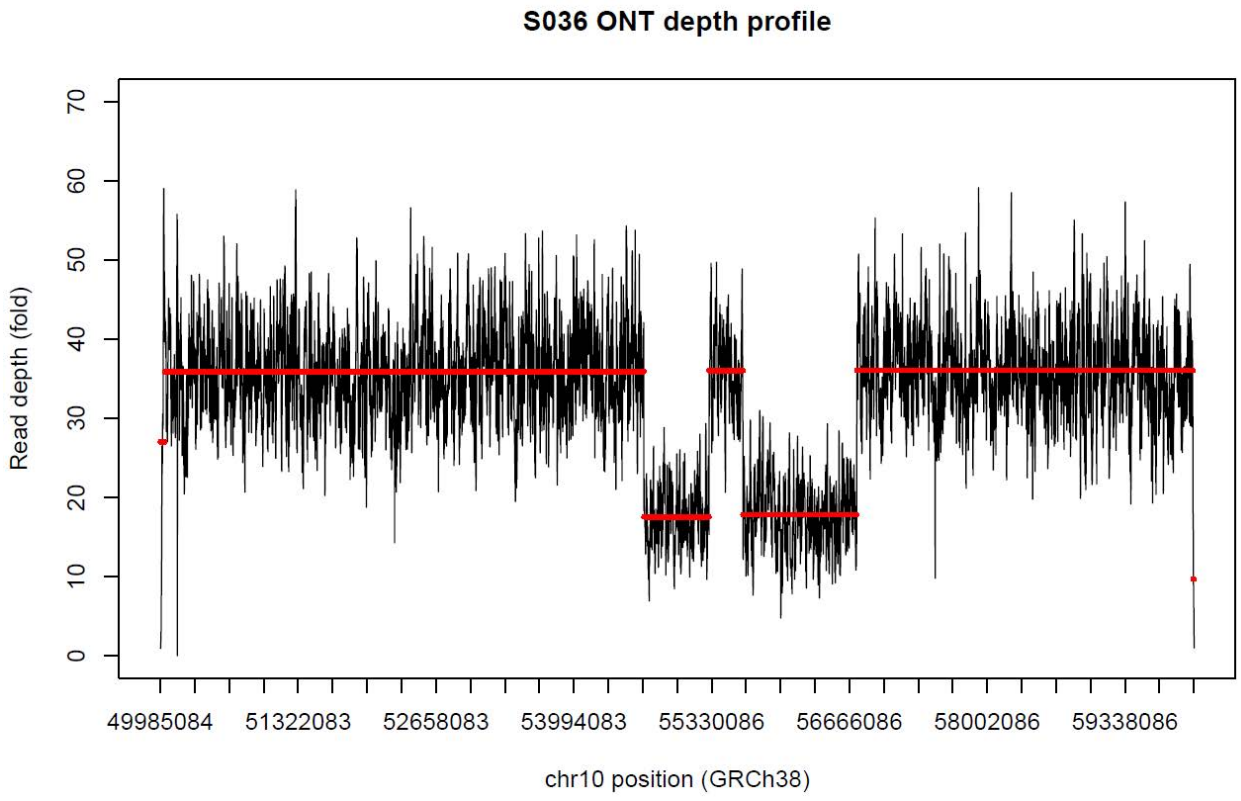
S036 ONT depth profile
Read depth (fold)
0
10
20
30
40
50
60
70
49985084
51322083
52658083
53994083
55330086
56666086
58002086
59338086
chr10 position (GRCh38)

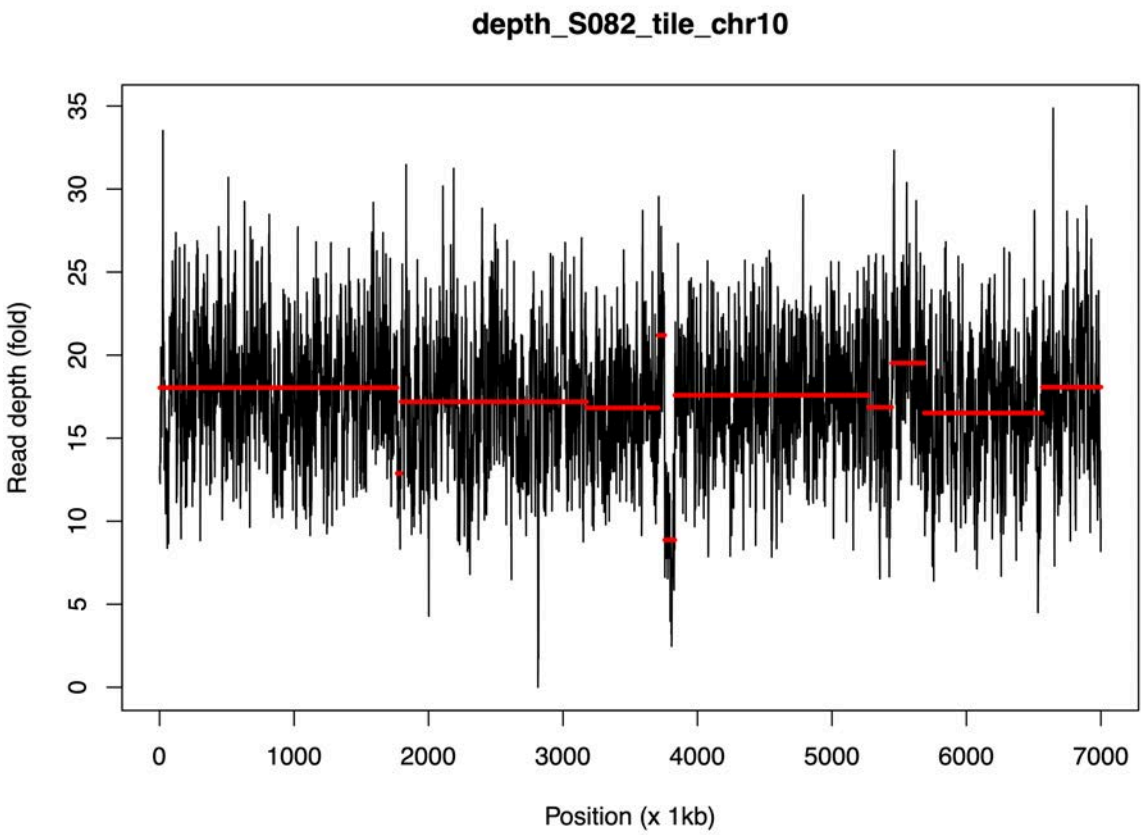
depth_S082_tile_chr10
Read depth (fold)
0
5
10
15
20
25
30
35
0
1000
2000
3000
4000
5000
6000
7000
Position (x 1kb)

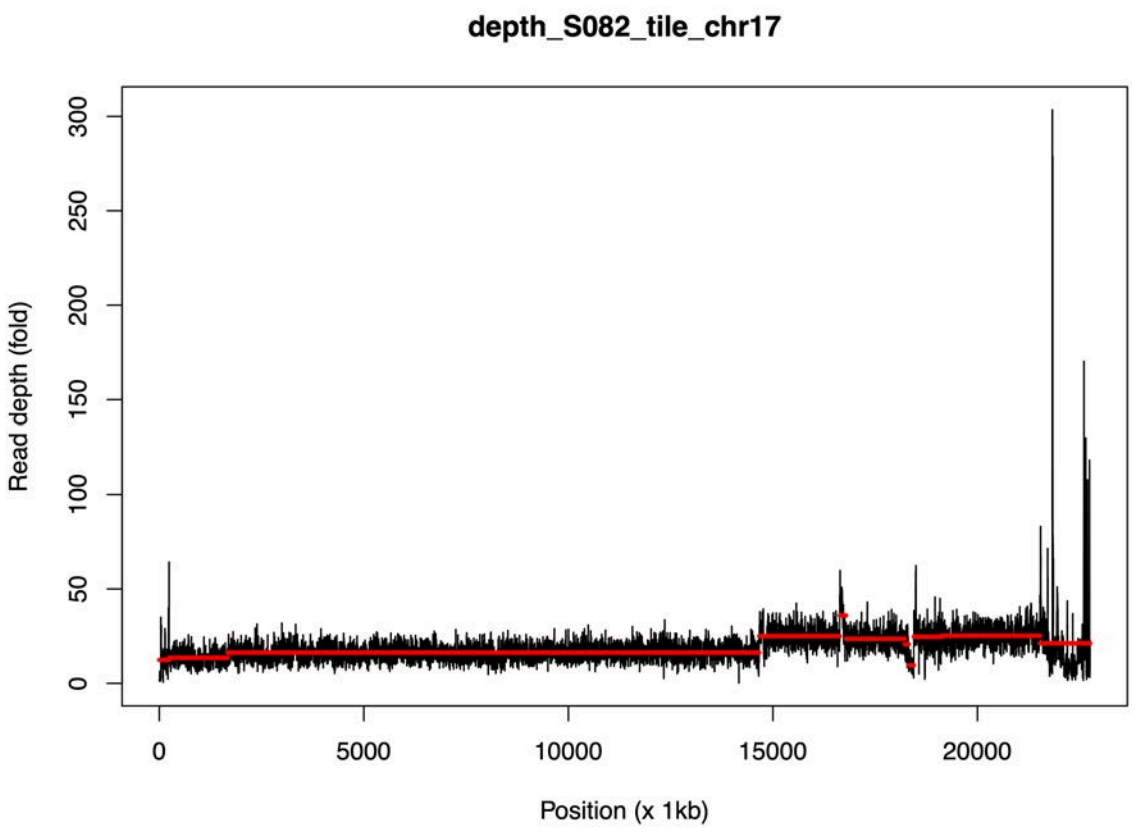
depth_S082_tile_chr17
Read depth (fold)
0
50
100
150
200
250
300
0
5000
10000
15000
20000
Position (x 1kb)

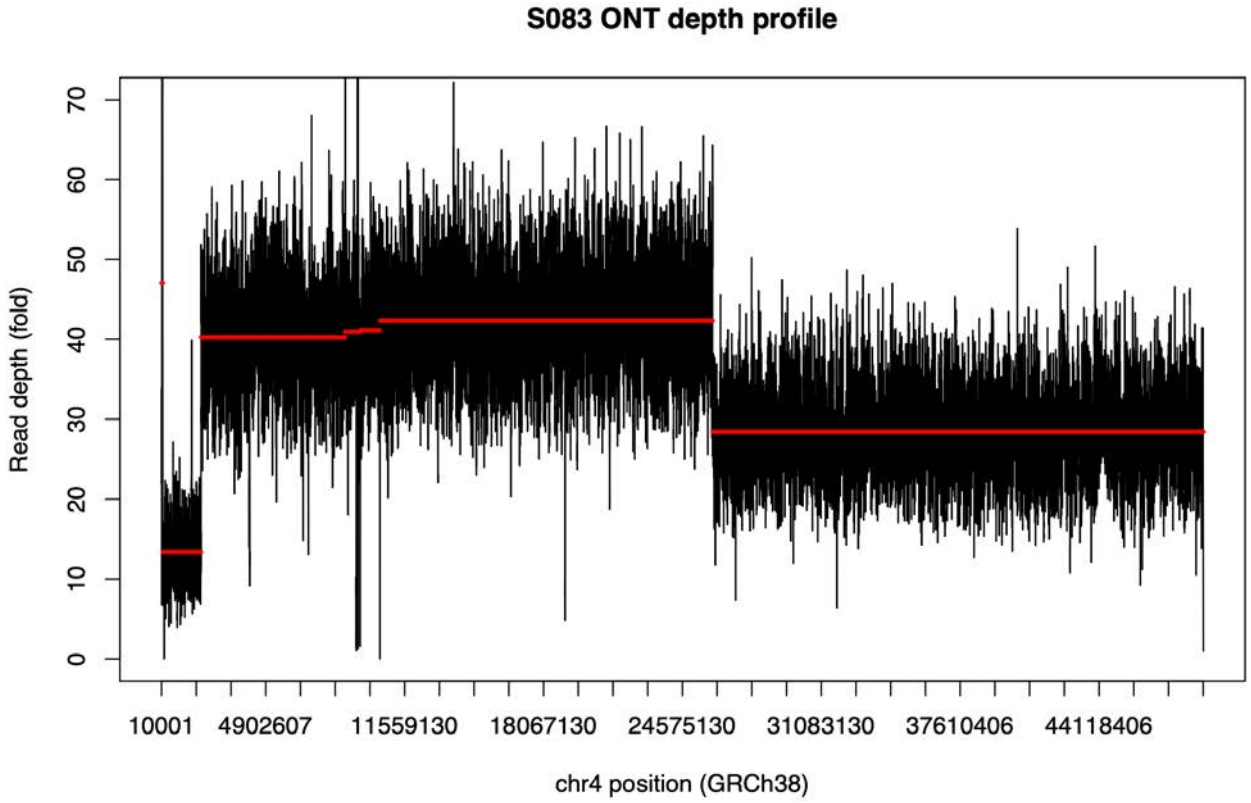
S083 ONT depth profile
Read depth (fold)
0
10
20
30
40
50
60
70
10001
4902607
11559130
18067130
24575130
31083130
37610406
44118406
chr4 position (GRCh38)

Figure S2. BK144-03, known 22q13.3 deletion.

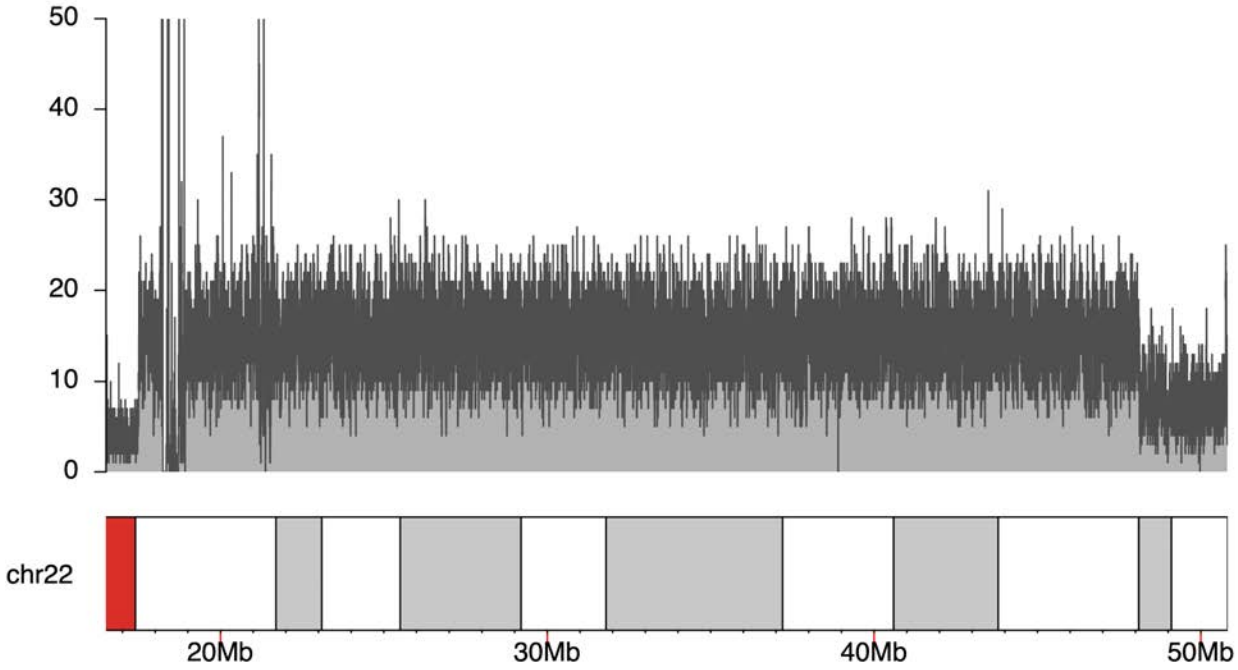

A. Coverage of the target region.

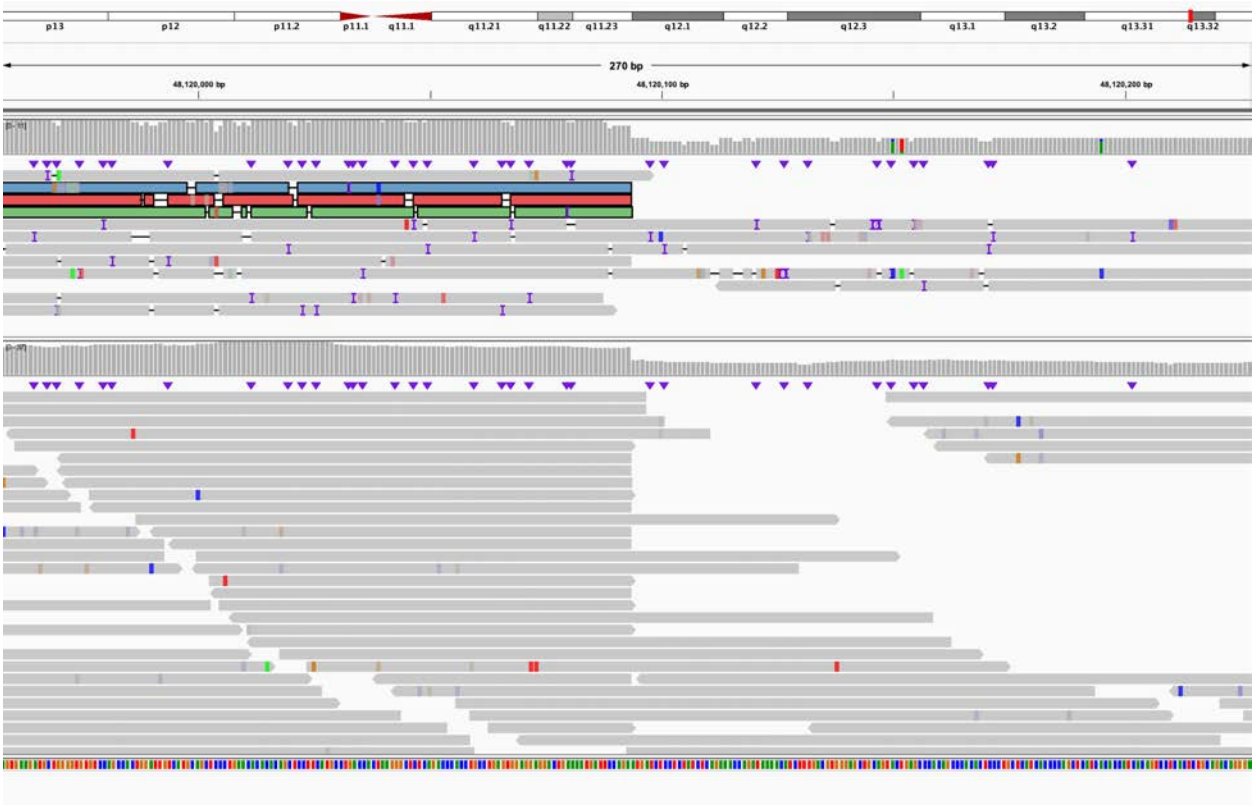

B. Centromere proximal end of deletion, long-read BAM file is top track, short-read BAM is bottom track. Long reads that span the deletion breakpoint are highlighted with color; IGV view is chr22:48,119,958-48,120,228.

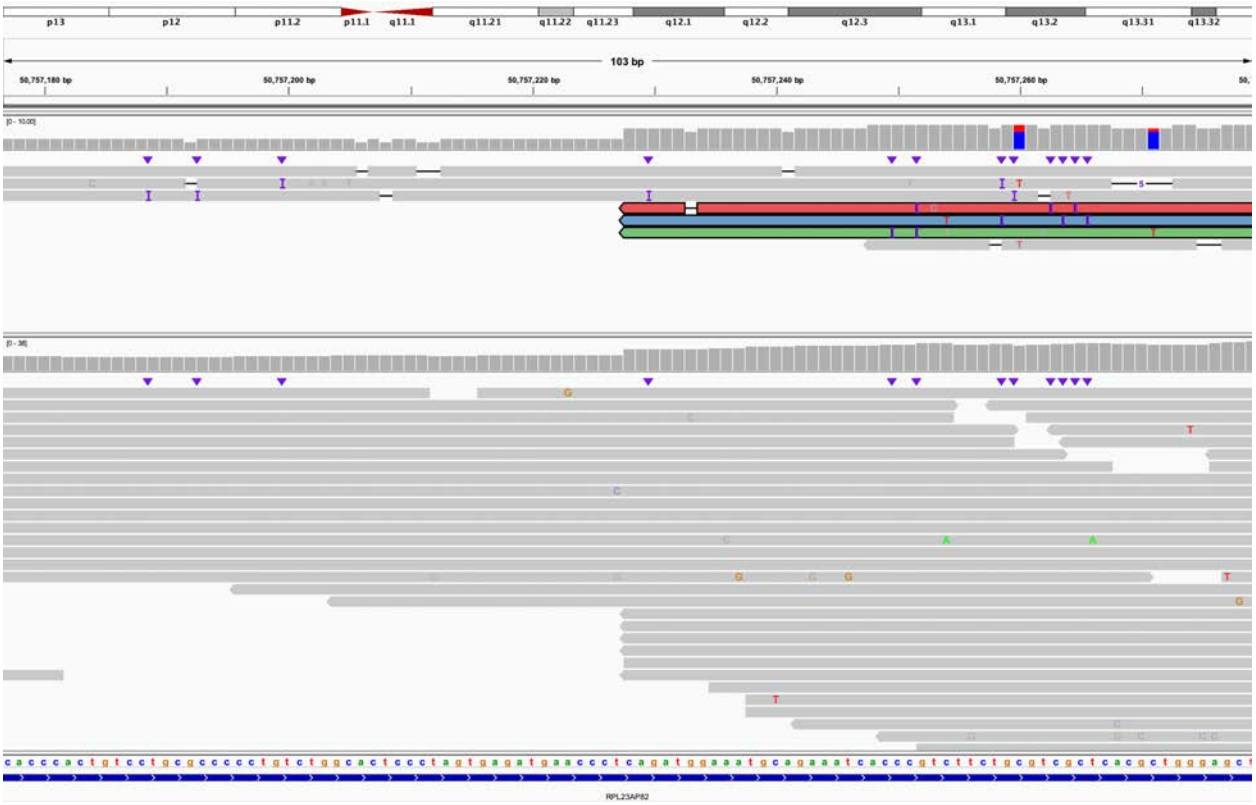

C. Telomere proximal end of deletion, long-read BAM file is the top track while short-read file is the bottom track. Long reads that span the deletion are colored as in (B); IGV view is chr22:50,757,177-50,757,279.

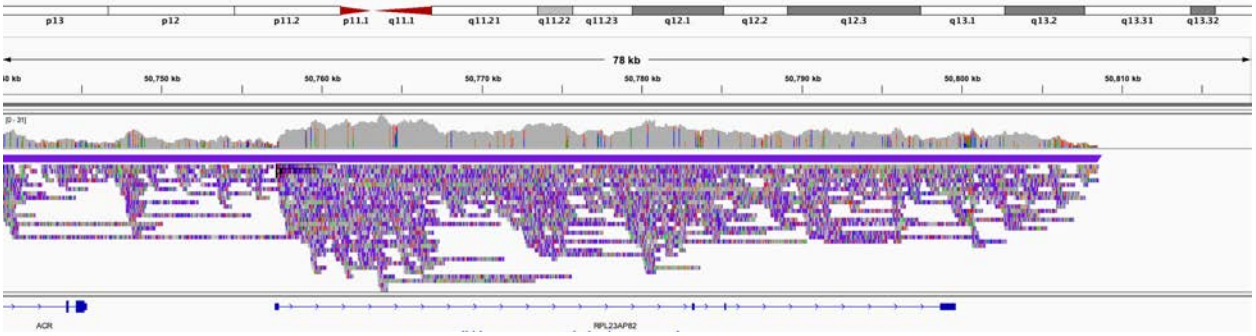

D. IGV view of only long reads at the end of chromosome 22; view is chr22:50,739,987-50,818,468.

Figure S3. BK180-03, known 15q11-q13 duplication.

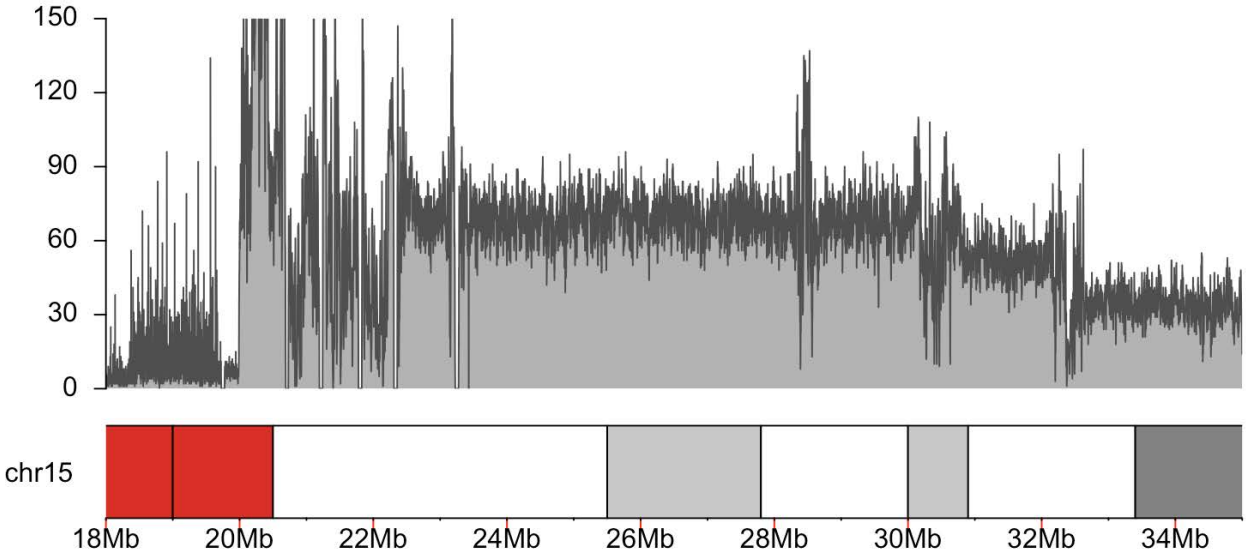

Coverage of target region in 15q. No definitive duplication breakpoint was found using targeted long reads.

Figure S4. BK294-03, known 22q11.2 duplication.

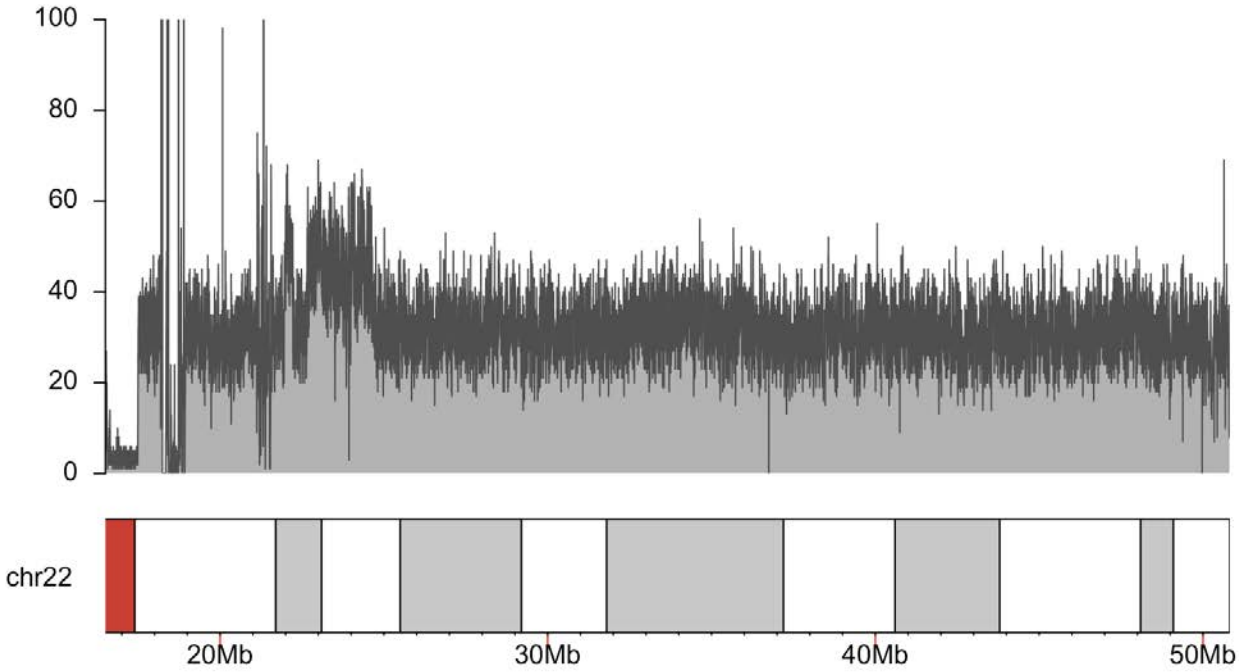

Coverage of chromosome 22 target region. No definitive duplication breakpoint was found using targeted long reads.

Figure S5. BK364-03, known 1p36.11 duplication.

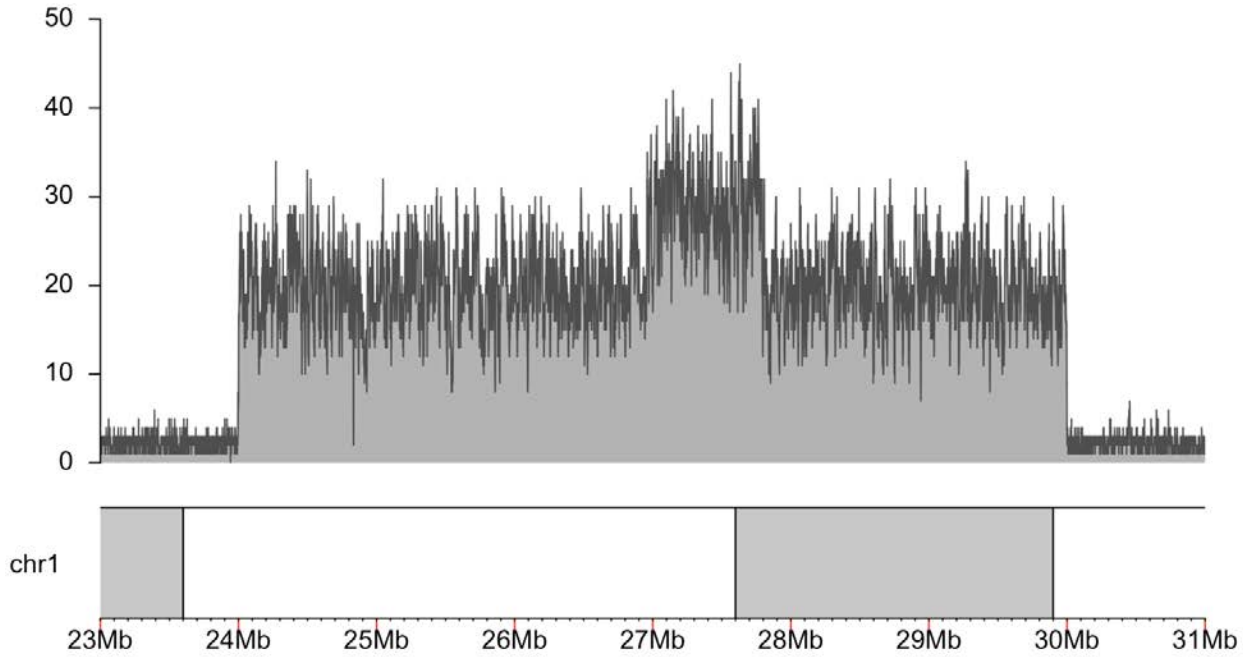

A. Coverage of target region demonstrating the presence of a duplication.

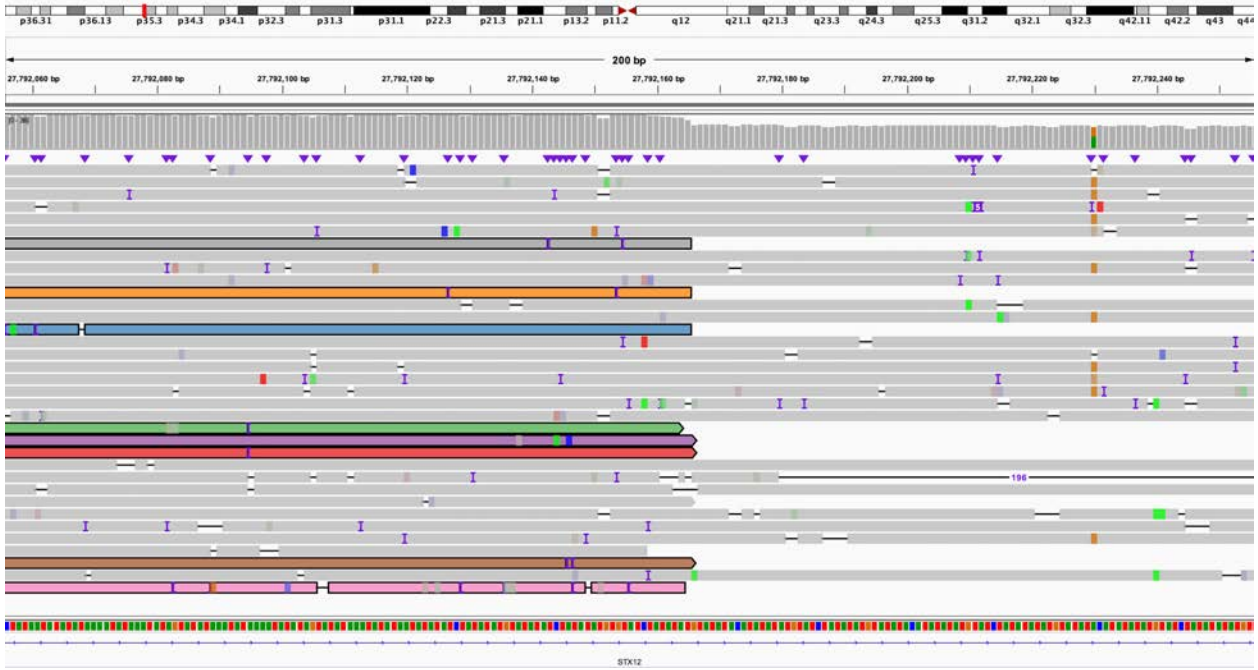

B. IGV view of 3' end, or centromere-proximal end of the duplication, reads that define the deletion breakpoint are represented by colors. IGV view is of chr1:27,792,056-27,792,256.

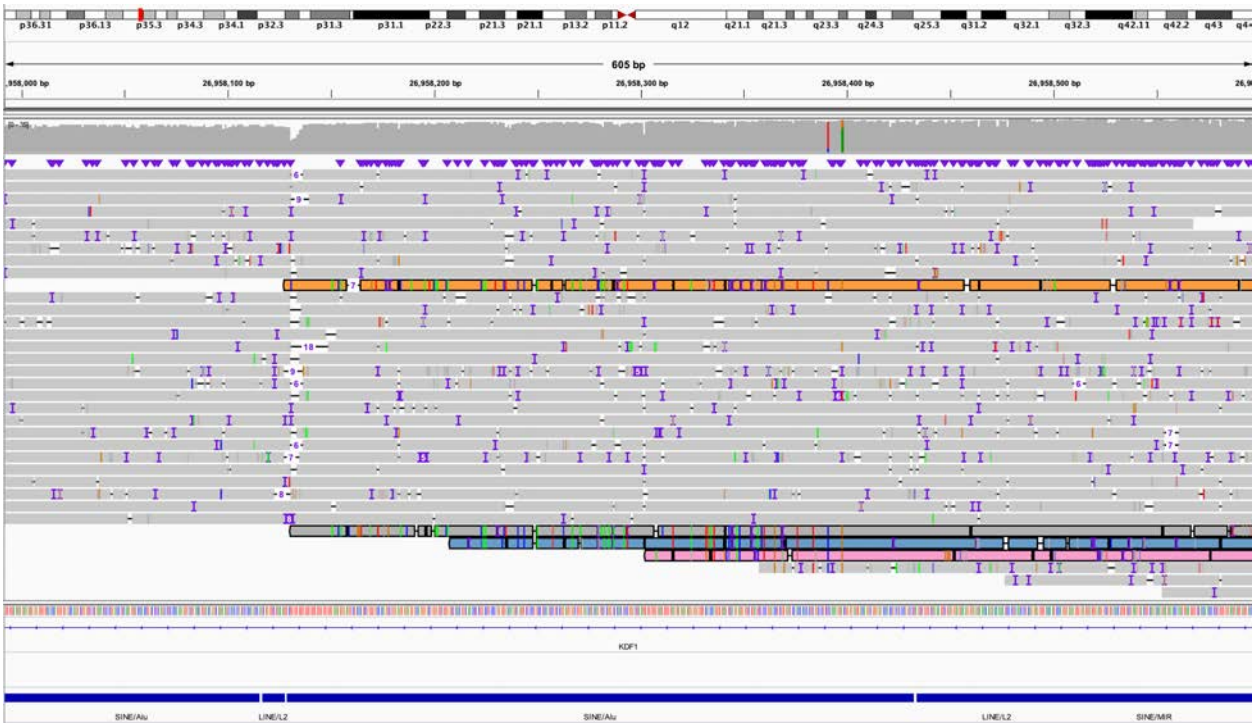

C. Reads from B are split and align to the 5' end, or telomere-proximal end of the duplication. The region contains several repetitive elements, as shown in the bottom track. IGV view is of chr1:26,956,878-26,959,178.

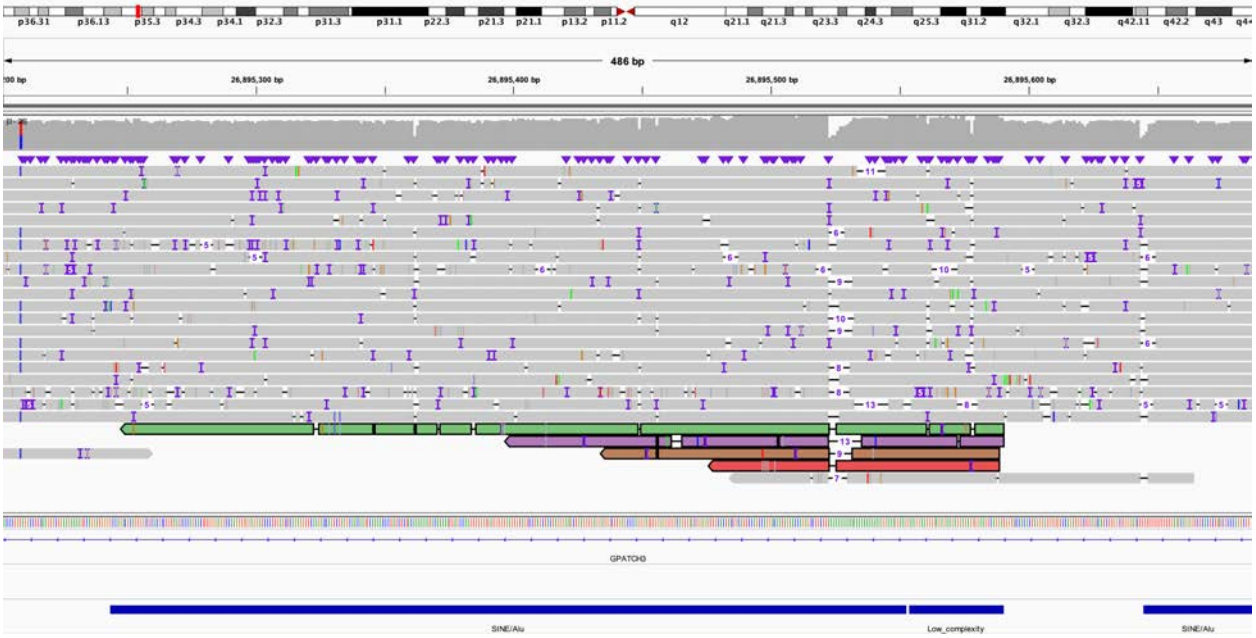

D. Fragments of four reads seen in B align incorrectly to a region outside of the duplicated region that includes a SINE/Alu and low-complexity region (bottom track); these fragments are notably shorter than those in C. IGV view is of chr1:26,895,202-26,895,689.

Figure S6. BK397-101, known 16p11.2 deletion.

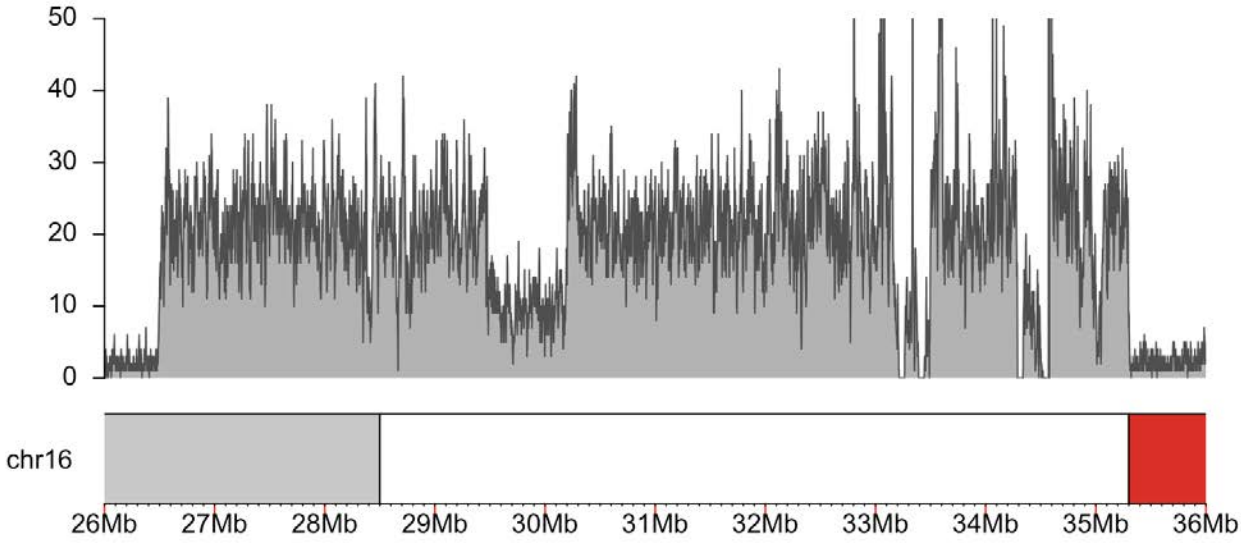

Coverage of chromosome 16 target region. No definitive deletion breakpoint was found using targeted long reads.

Figure S7. BK430-103, known 16p11.2 duplication.

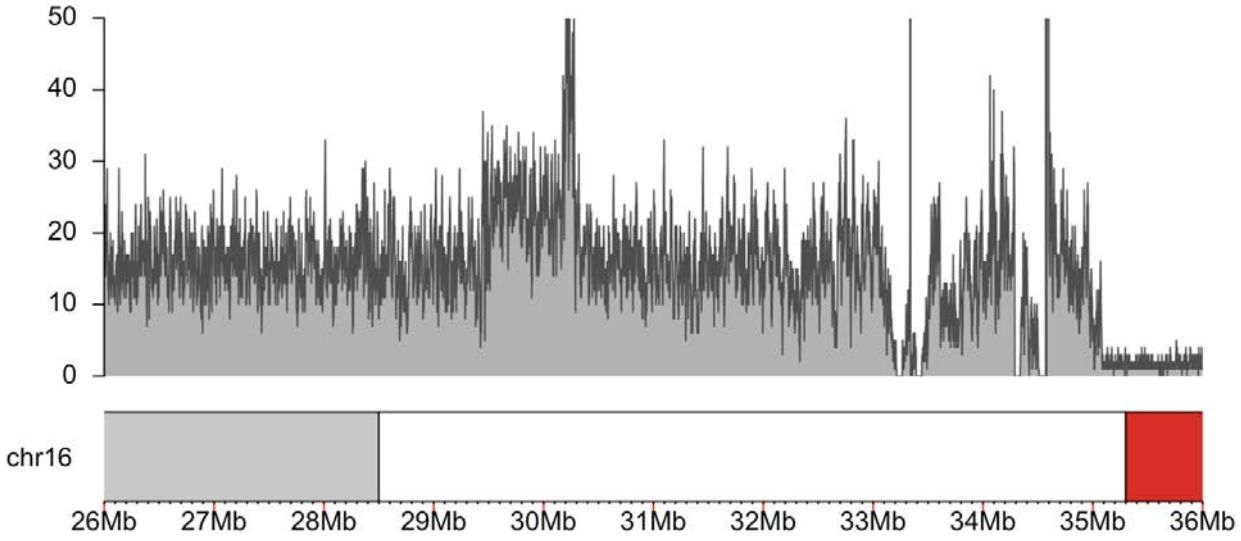

Coverage of chromosome 16 target region. No definitive duplication breakpoint was found using targeted long reads.

Figure S8. BK482-101, known 1q21.1 duplication.

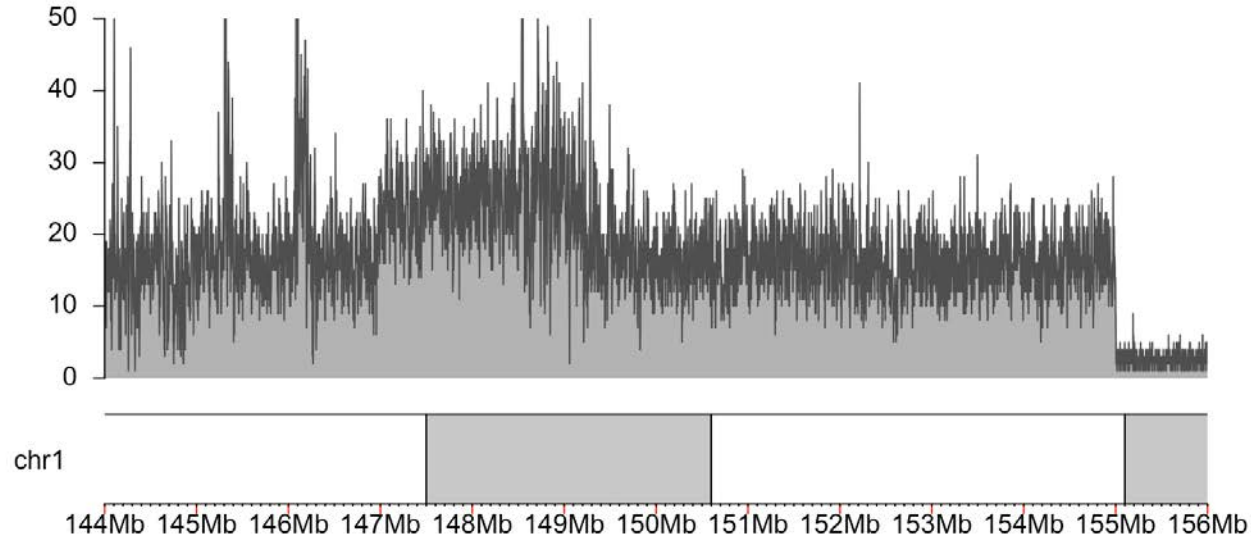

Coverage of chromosome 1 target region. No definitive duplication breakpoint was found using targeted long reads.

Figure S9. BK487-101, known 1q21 deletion.

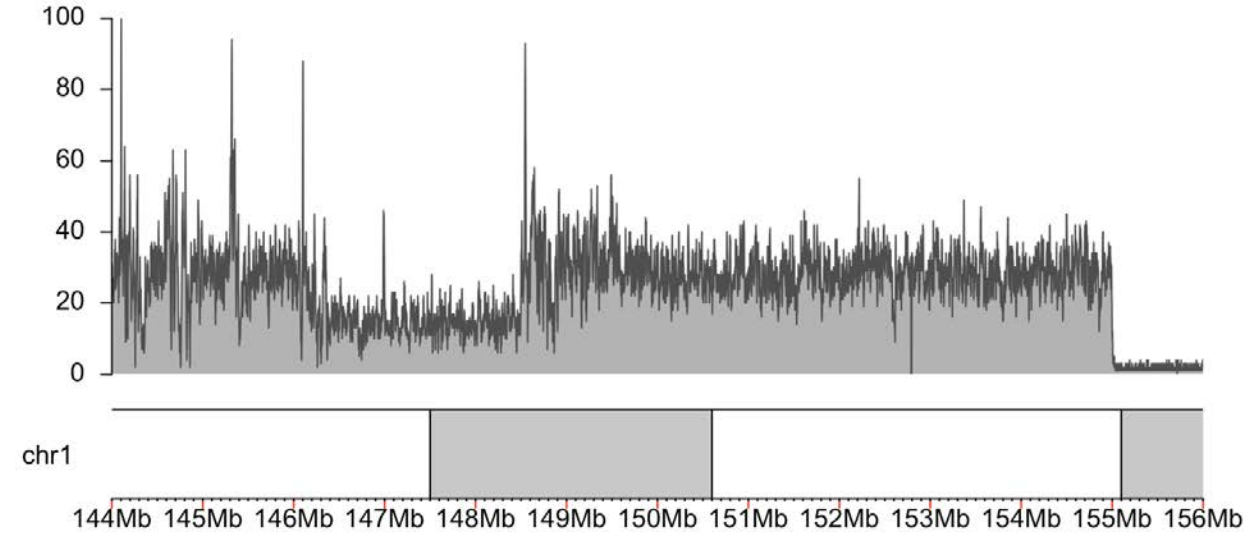

Coverage of chromosome 1 target region. No definitive deletion breakpoint was found using targeted long reads.

Figure S10. BK506-03, known 5p15.33 deletion.

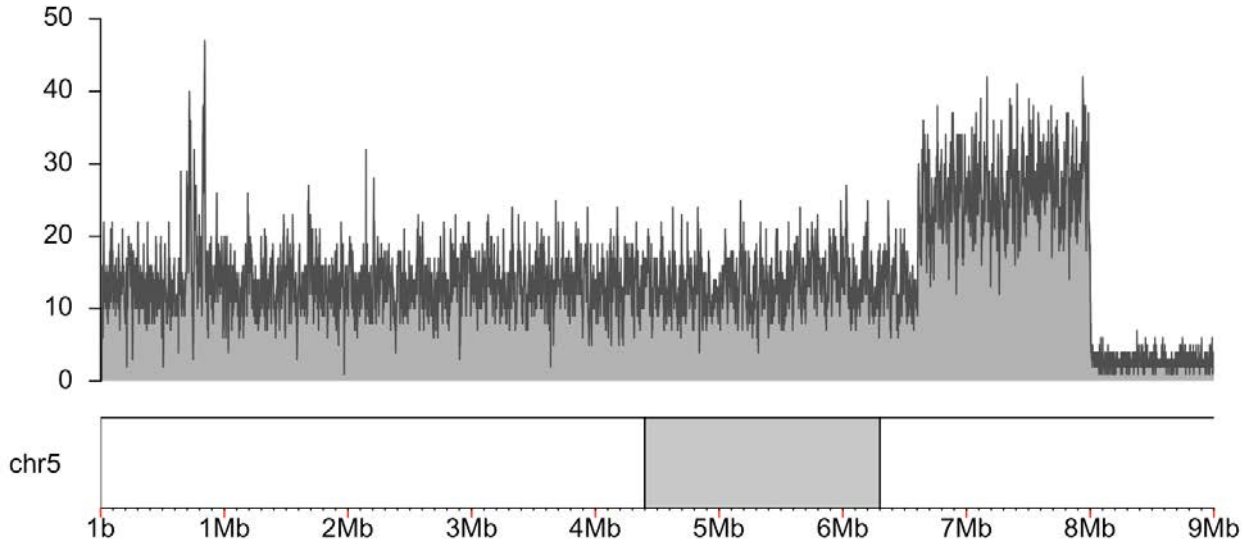

A. Coverage of chromosome 5 target region.

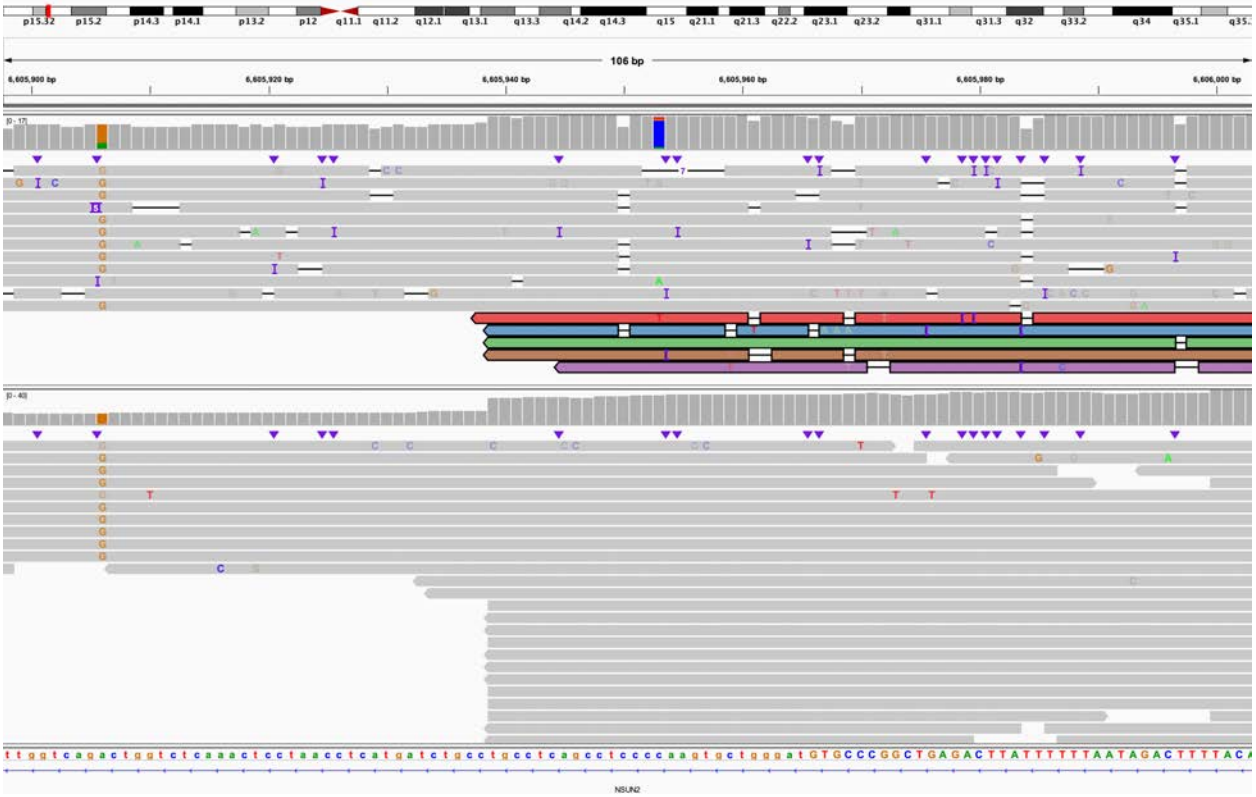

B. Breakpoint of the chromosome 5 deletion in IGV: long-read data is top track; short-read data is bottom track. Colors in top track correspond to colors of reads in C. View is of chr5:6,605,898-6,606,003.

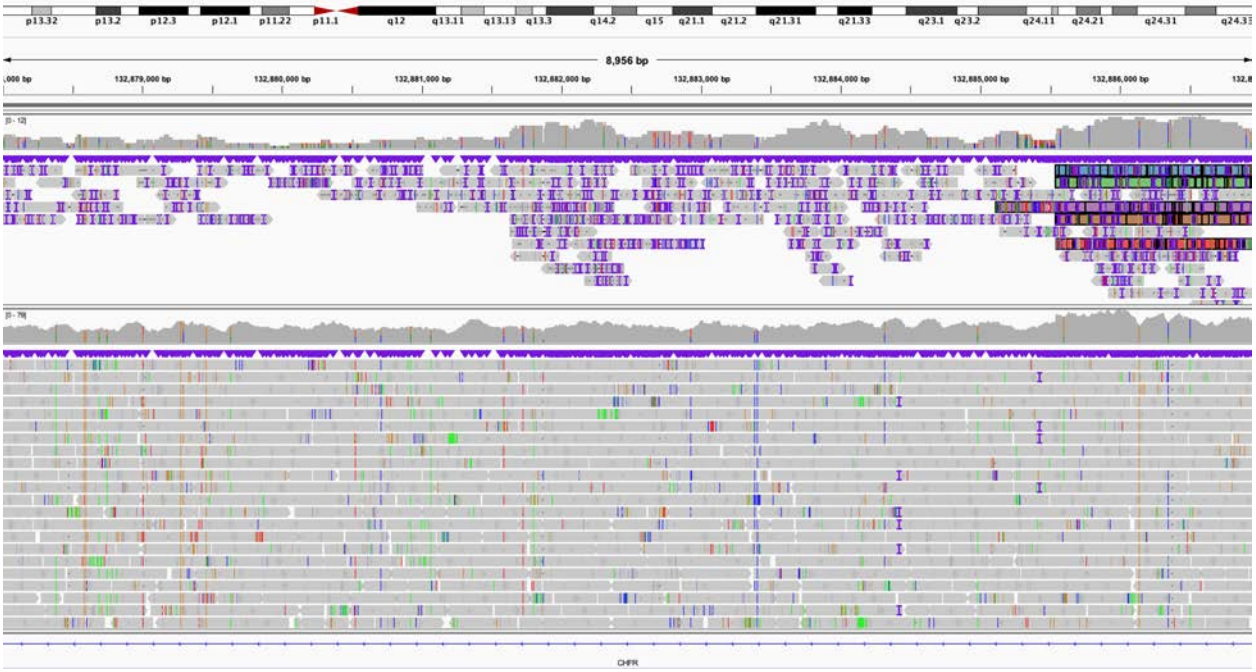

C. View of both long-read (top track) and short-read (bottom track) data from BK506-03 showing the centromere-proximal sequence is not deleted, but the telomere-proximal sequence is present in three copies. Long reads in the top track can be matched with those from B by their color. IGV view is chr12:132,877,990-132,886,995.

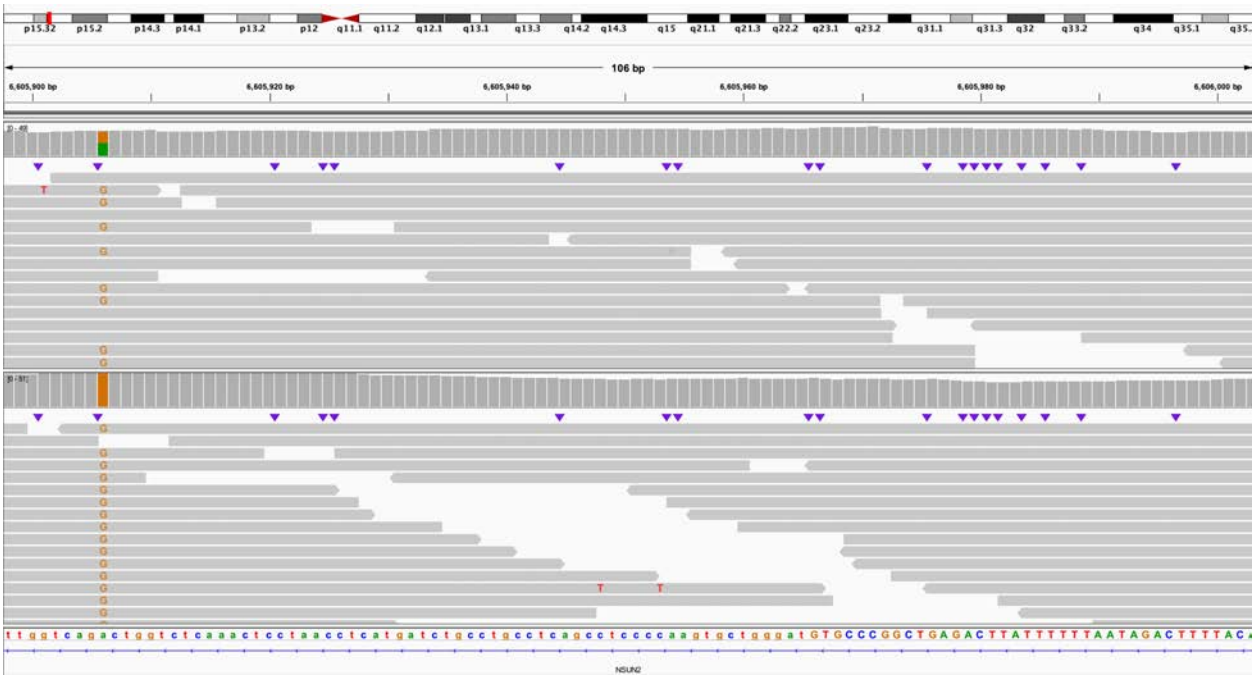

D. View of short-read sequencing data at the chromosome 5 breakpoint from the parents of BK506-03 (BK506-01 and BK506-02). IGV view is chr5:6,605,898-6,606,003.

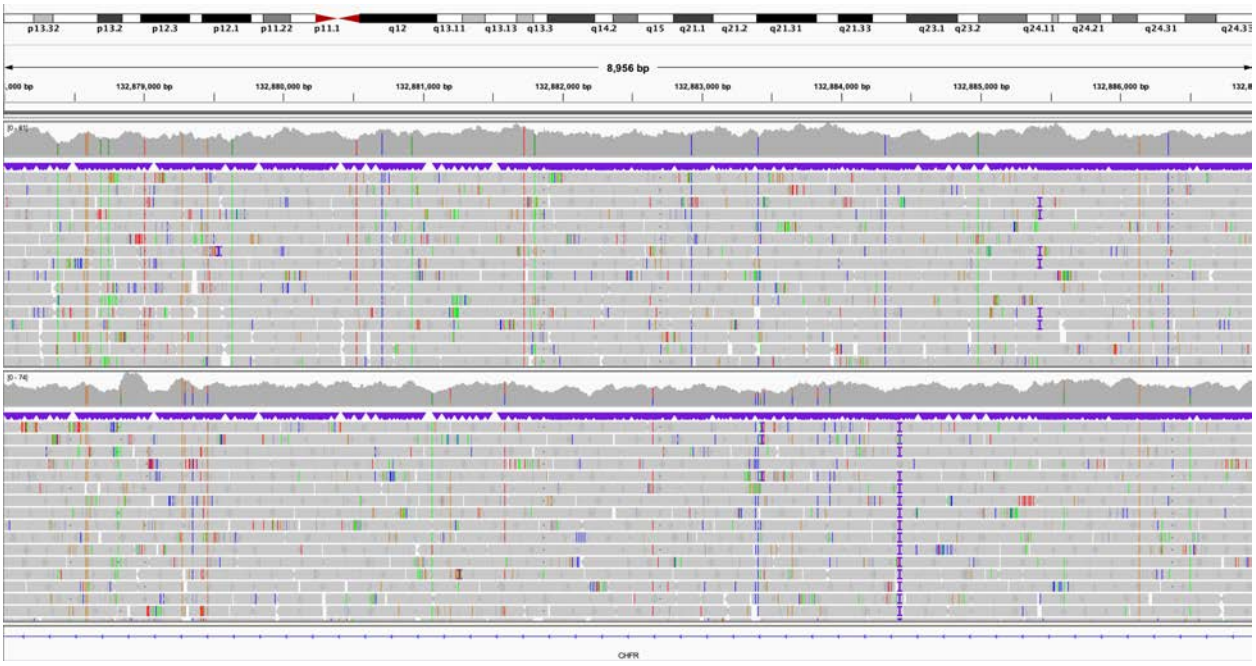

E. View of short-read sequencing data at the chromosome 12 breakpoint from the parents of BK506-03. IGV view is chr12:132,877,990-132,886,995.

Figure S11. S016, known tandem duplication within *CTNND2*.

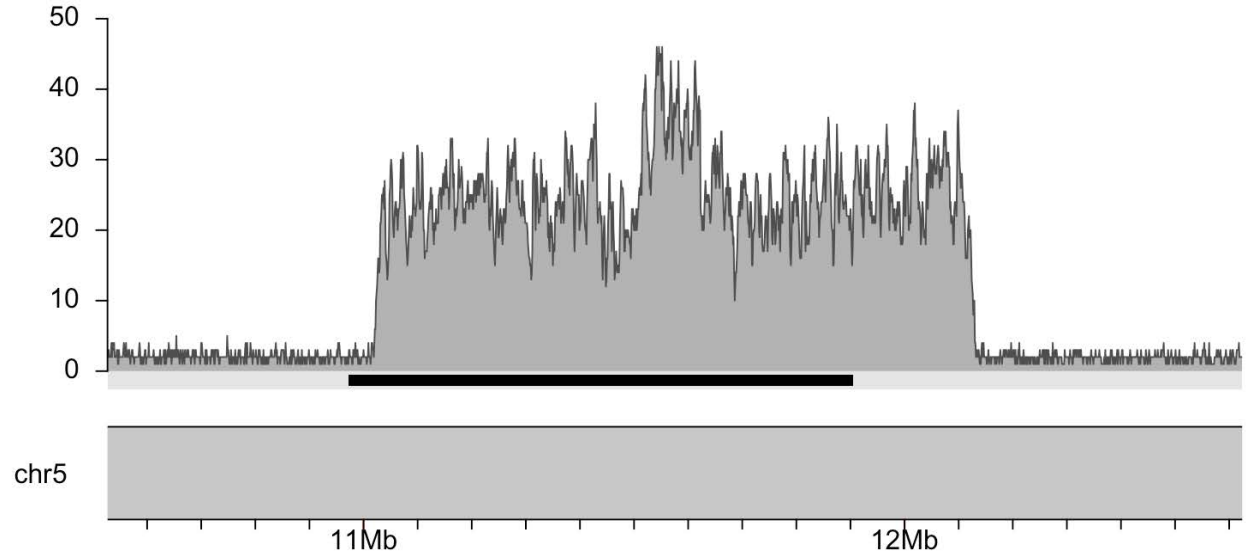

A. Coverage of duplication within *CTNND2*, gene body of *CTNND2* is represented by the black bar below the coverage graph.

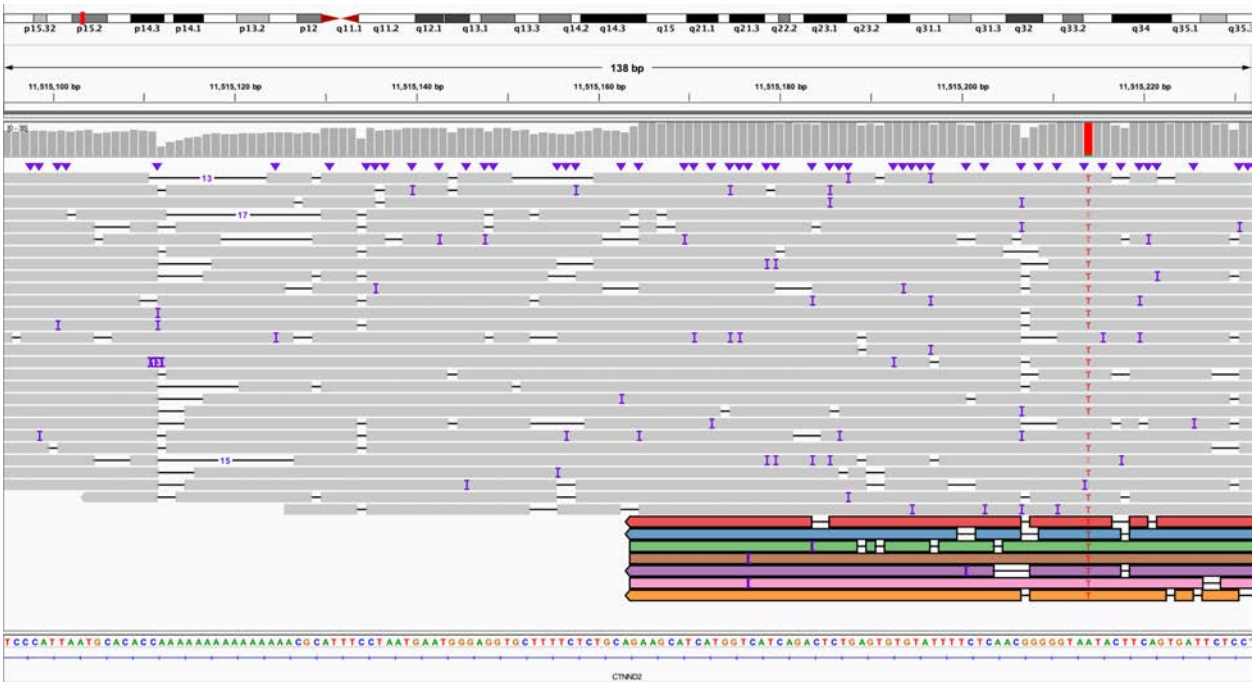

B. Reads in the telomere-proximal end of the duplication, colors correspond to reads in C. The orientation of reads in B and C confirm that it is a tandem duplication as previously shown.[1] IGV view of chr5:11,515,095-11,515,232.

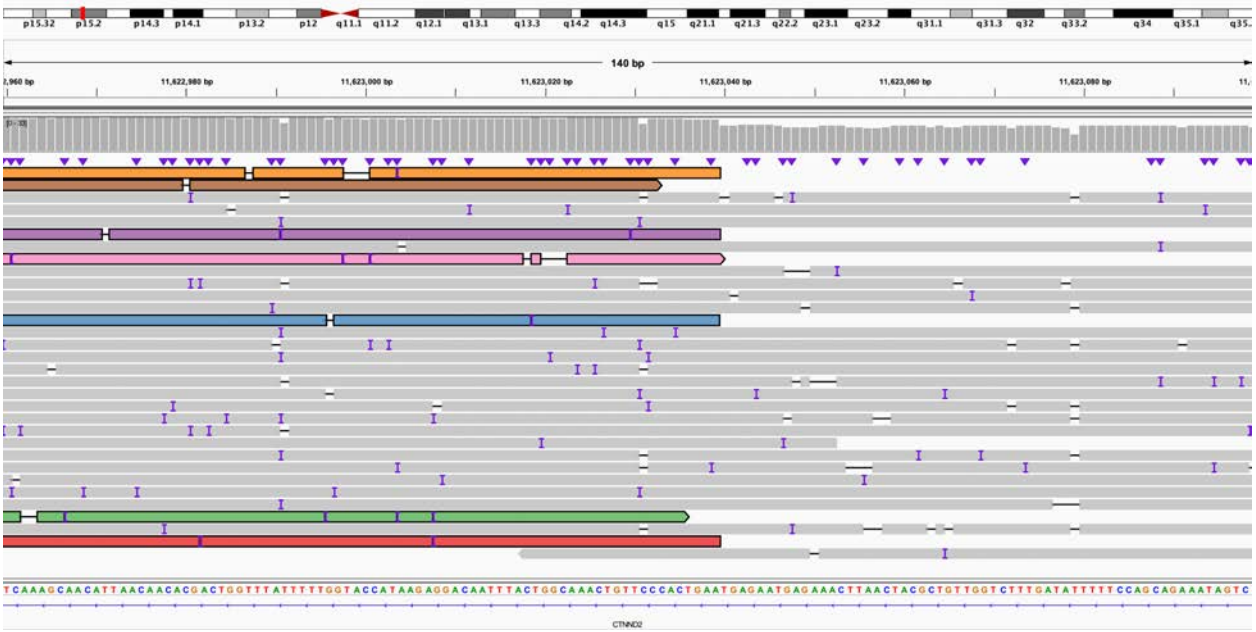

C. Reads from the centromere-proximal end of the duplication, colors correspond to reads in B. IGV view is of chr5:11,622,960-11,623,099.

Figure S12. S023, mosaic ring 18 present in 40% of cells.

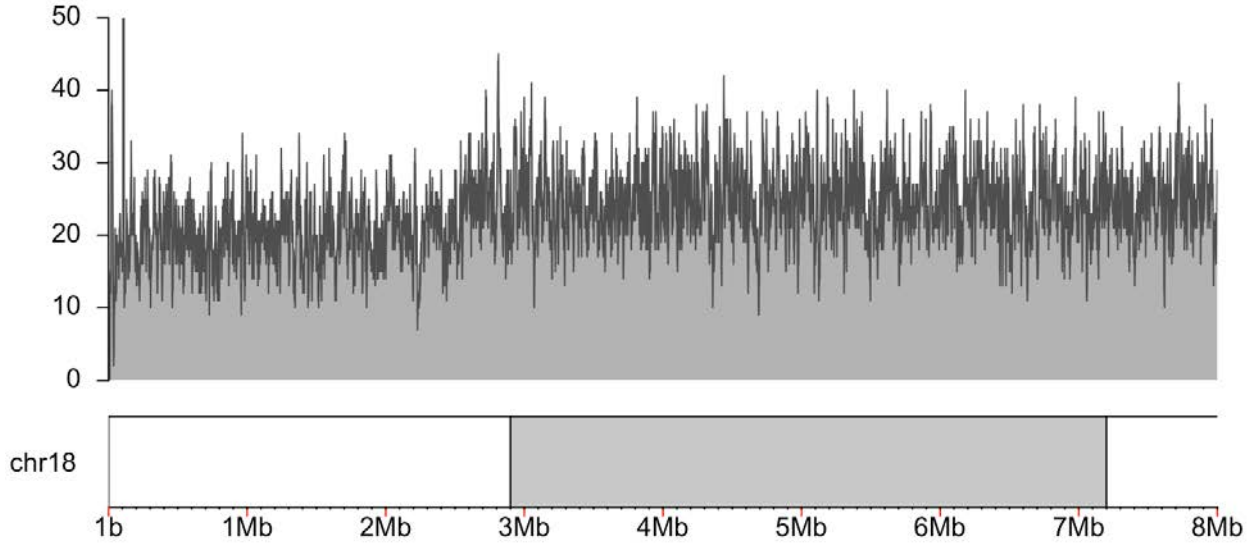

A. Coverage of chromosome 18p target region shows mosaic copy loss.

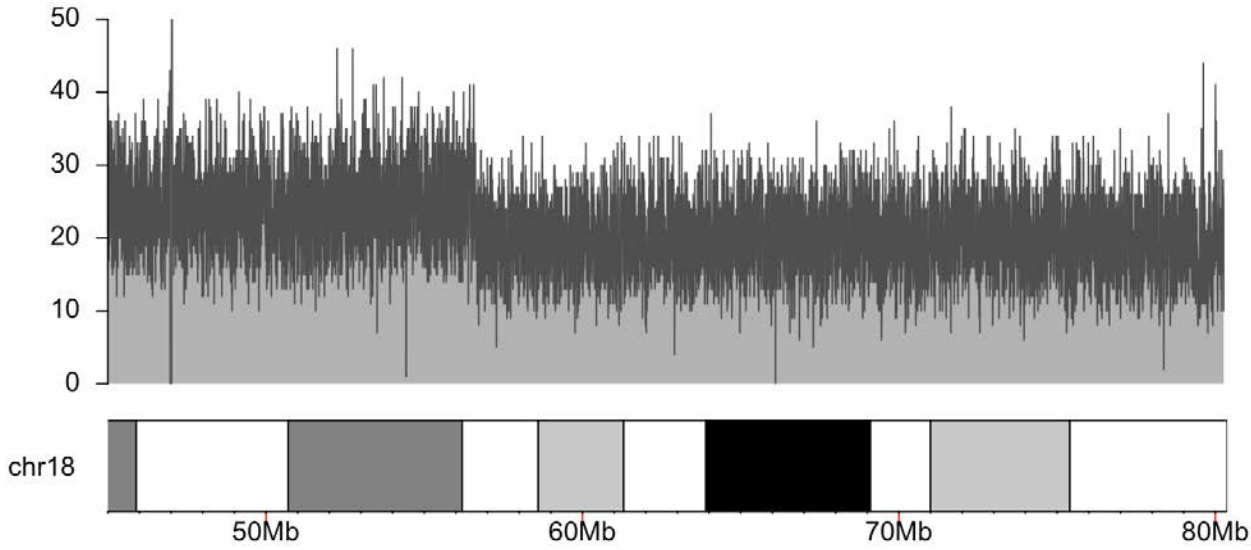

B. Coverage of chromosome 18q target region shows mosaic copy loss.

Figure S13. S046, known unbalanced translocation between chromosomes 4 and 15.

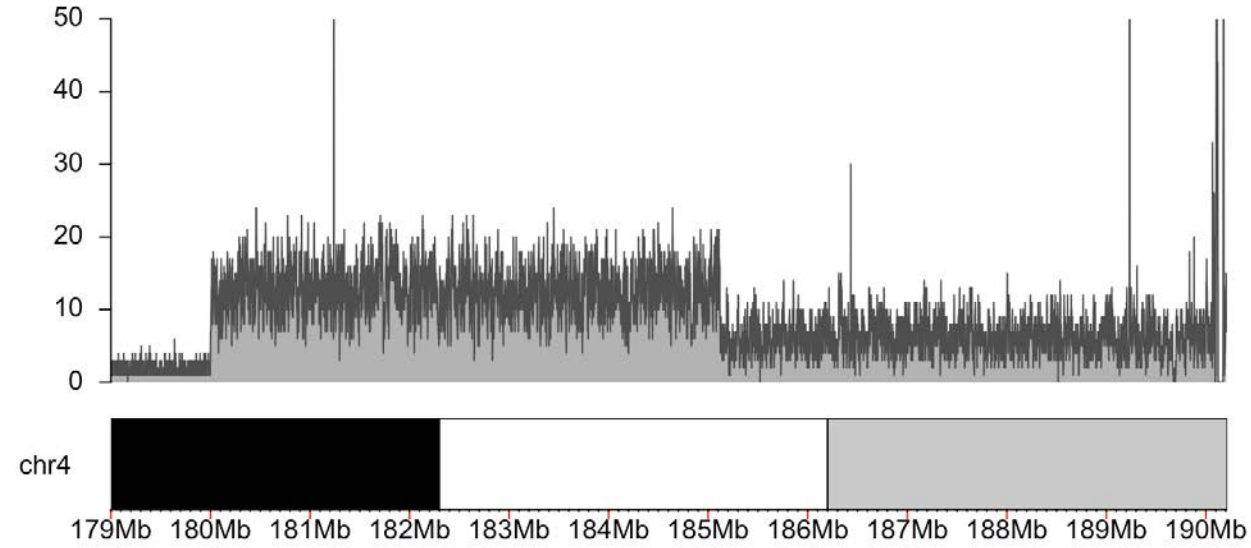

A. Coverage of chromosome 4 target region showing a distal deletion.

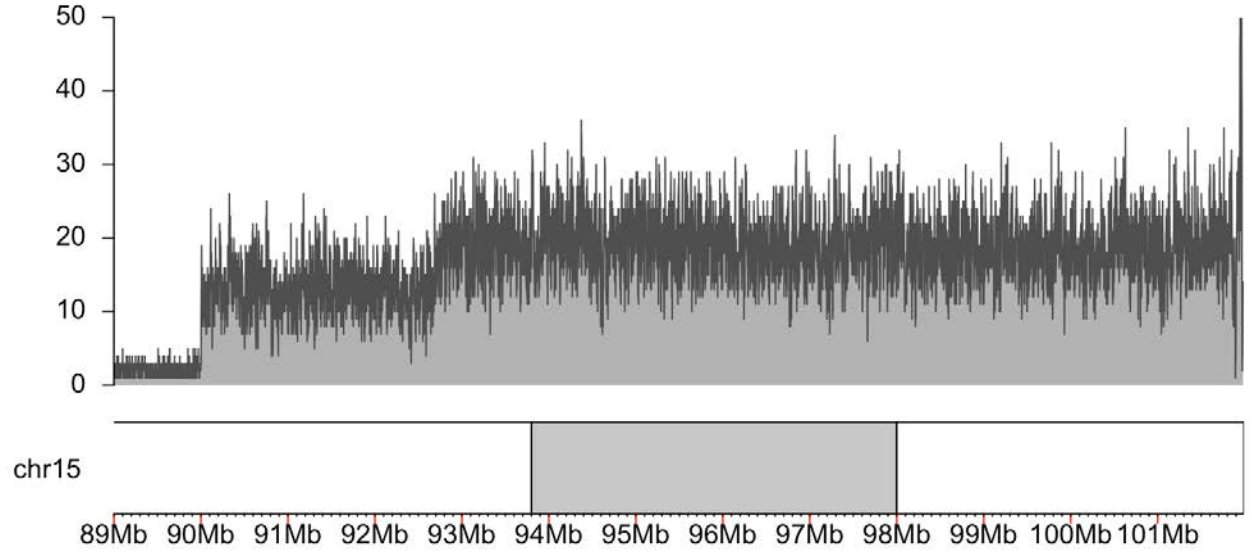

B. Coverage of chromosome 15 target region showing a distal gain.

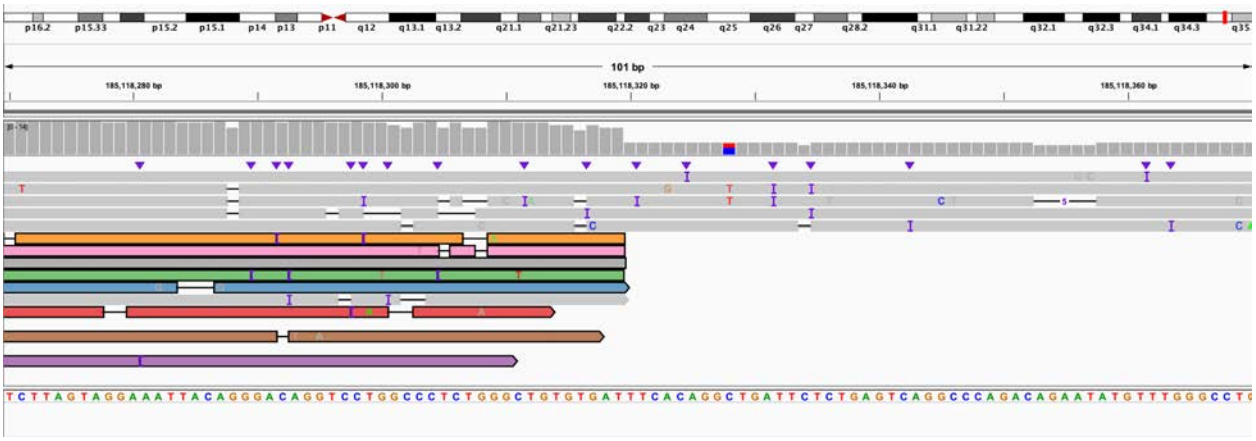

C. IGV view of reads spanning the translocation breakpoint. Reads are colored to correspond to reads in D. IGV view is of chr4:185,118,270-185,118,370.

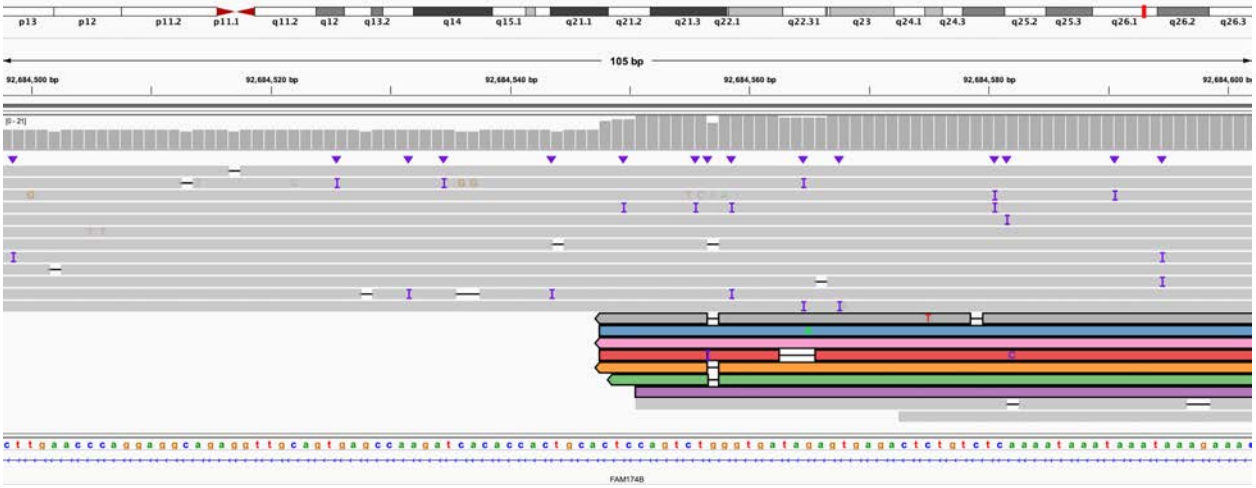

D. View of reads spanning the translocation breakpoint on chromosome 15. IGV view is of chr15:92,684,498-92,684,602.

Figure S14. S060, known translocation between chromosomes 12 and 17 thought to affect *SOX9*.

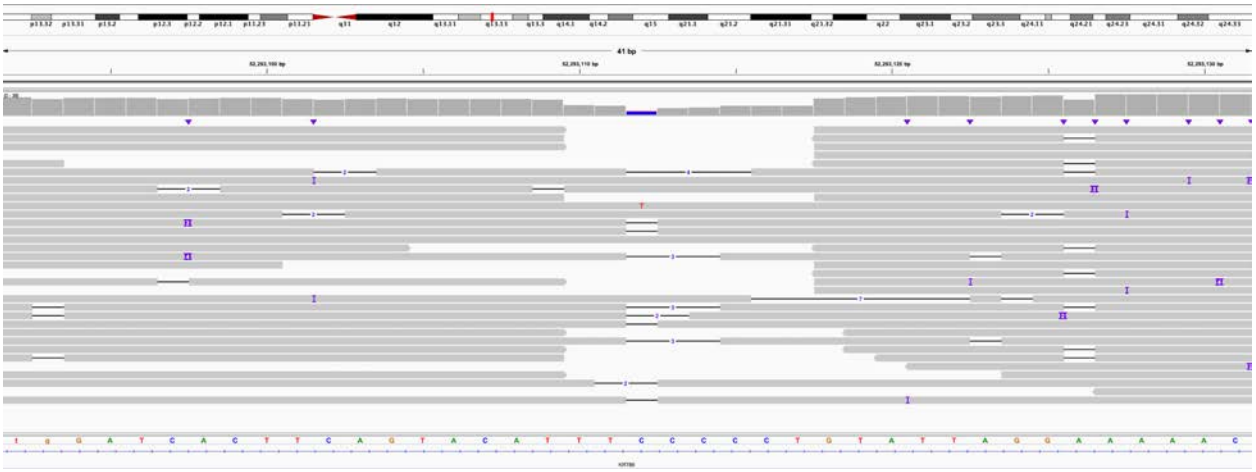

A. Screenshot of chromosome 12 showing translocation breakpoints. IGV view is of chr12:52,293,092-52,293,131.

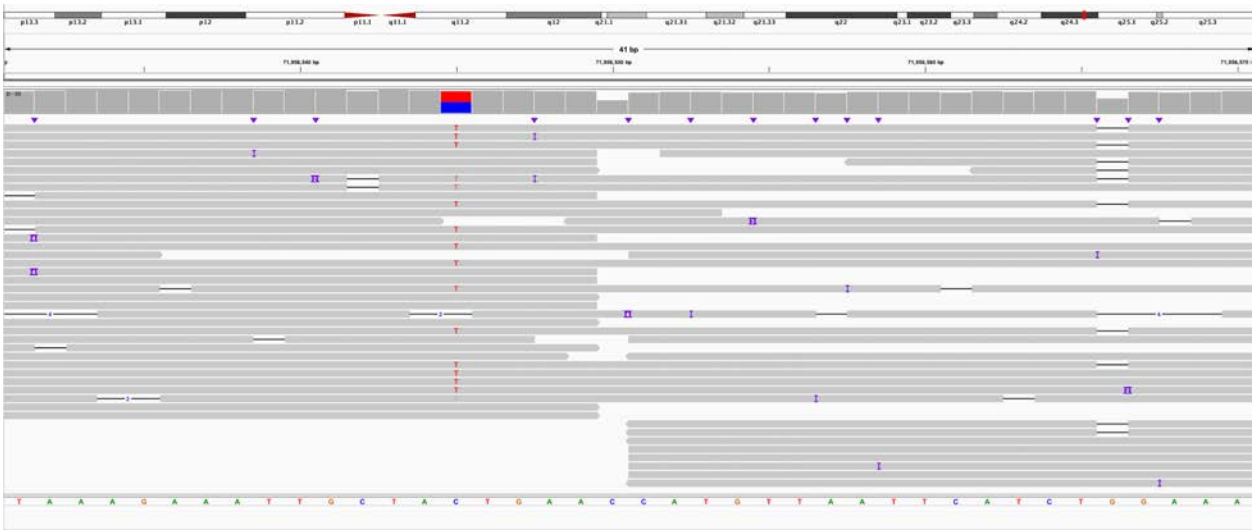

B. Screenshot of chromosome 17 showing translocation breakpoints. IGV view is of chr17:71,956,531-71,956,570.

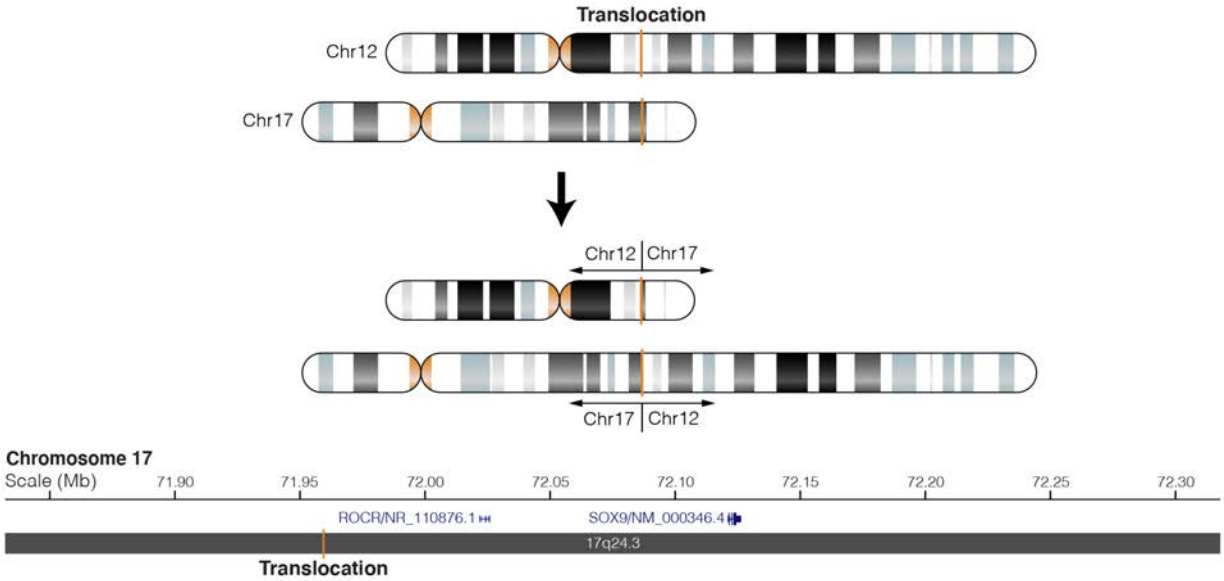

C. Cartoon of chromosome 12 and 17 translocations and breakpoints.

Figure S15. S063, known SVA insertion in *BRCA1*.

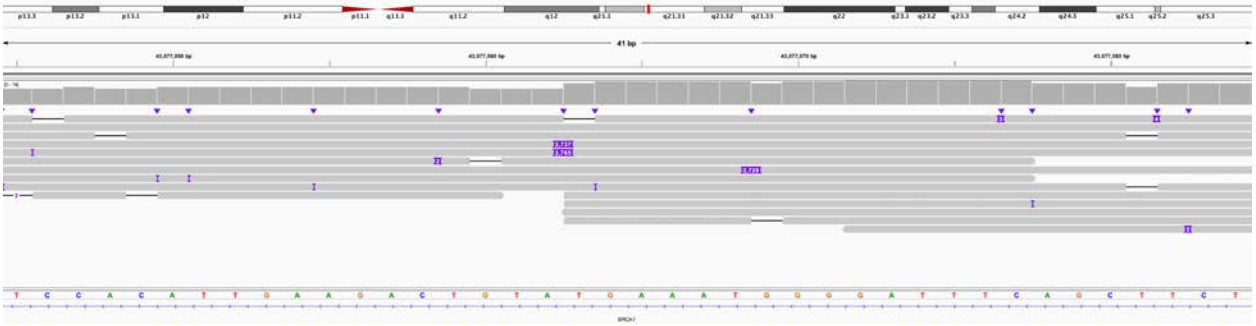

IGV view of known SVA insertion into *BRCA1*. IGV view is of chr17:43,077,045-43,077,084. This insertion was previously reported by Walsh and colleagues.[2]

Figure S16. S011 (*ATXN3* and *ATXN8OS*), evaluation of repeat length in an individual.

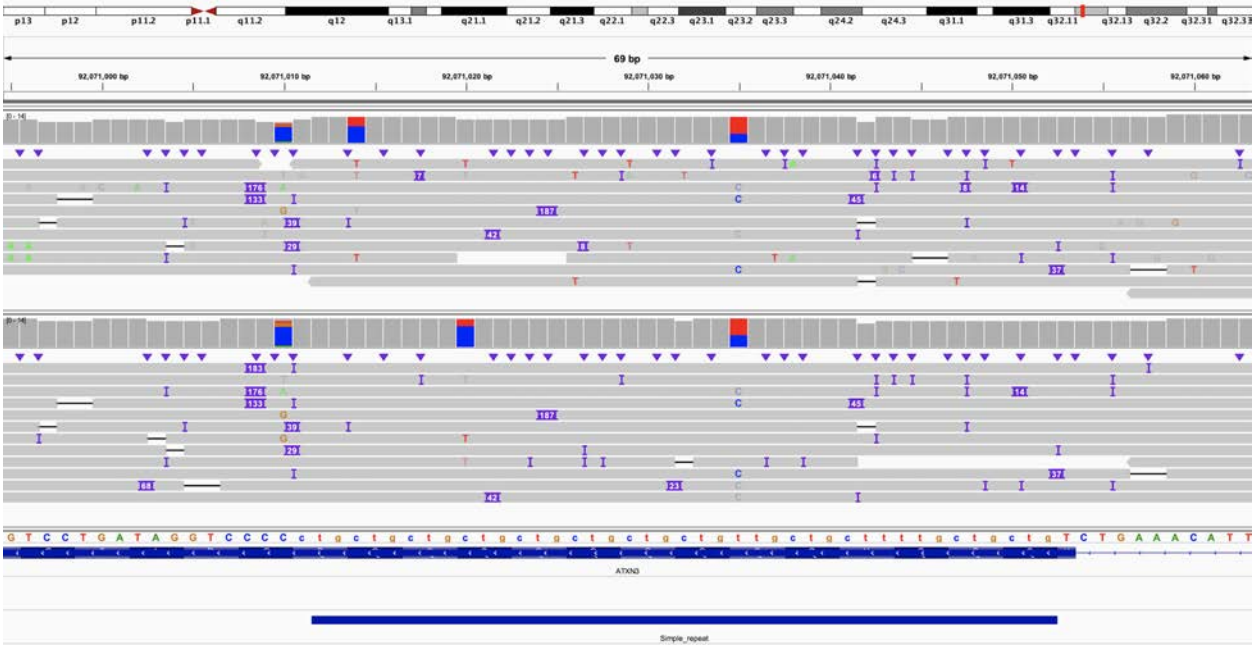

A. T-LRS of an individual known to carry a heterozygous repeat expansion in *ATXN3*. Three reads carry the expansion and span the region. IGV view of chr14:92,070,974-92,071,079. For both A and B reads aligned to the reference using minimap2 with default parameters is the top panel and reads aligned with modified parameters as outlined in the methods is the bottom panel.

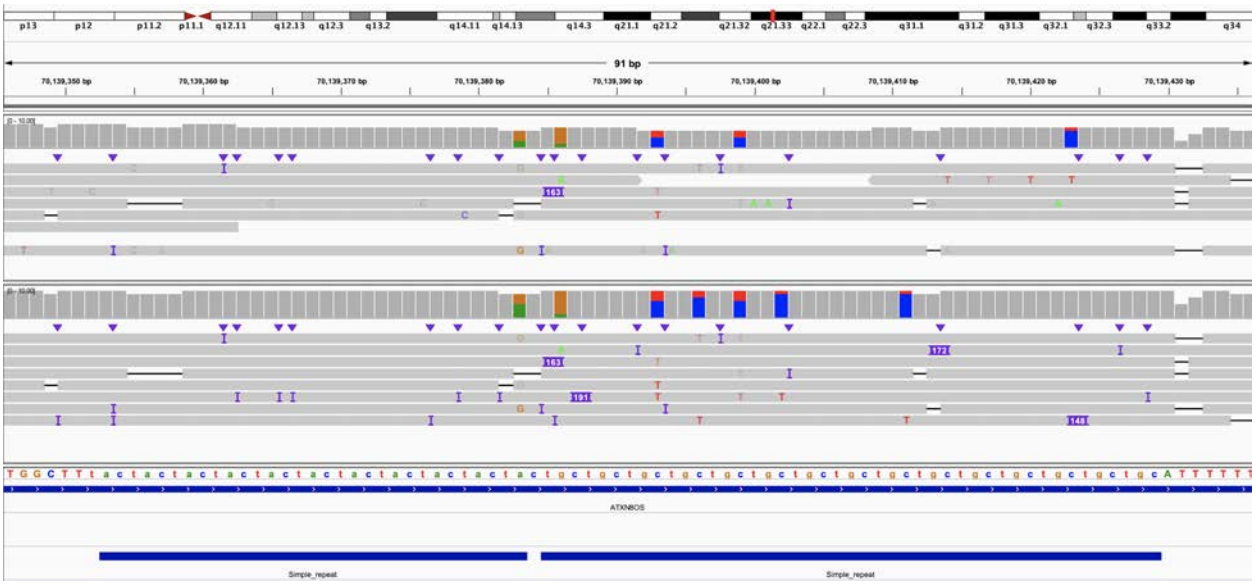

B. This individual was also known to carry a heterozygous expansion in *ATXNOS8*. In the minimap2 alignment with default parameters, a single read carries the full expansion and spans the region (top panel), but with modified parameters four reads can be found spanning the interval (bottom panel). IGV window is chr13:70,139,346-70,139,436.

Figure S17. S039 (*FMR1*), evaluation of repeat length and methylation status.

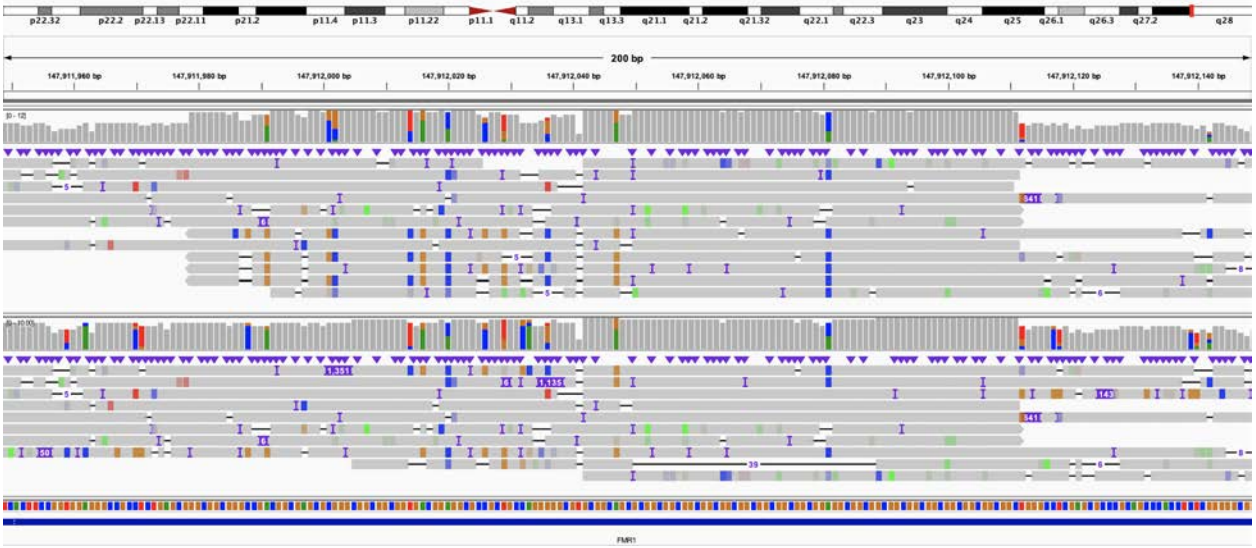

A. Screenshot of CGG repeat expansion in 5' UTR of *FMR1* from an individual known to carry an expansion. DNA was obtained from Coriell (Table S1). Top panel represents minimap2 run with default parameters; bottom panel is minimap2 run with parameters meant to reduce split reads. In the bottom panel, two reads with insert sizes of approximately 1,350 bp can be seen that are not present in the top panel. IGV view is chrX:147,911,949-147,912,149.

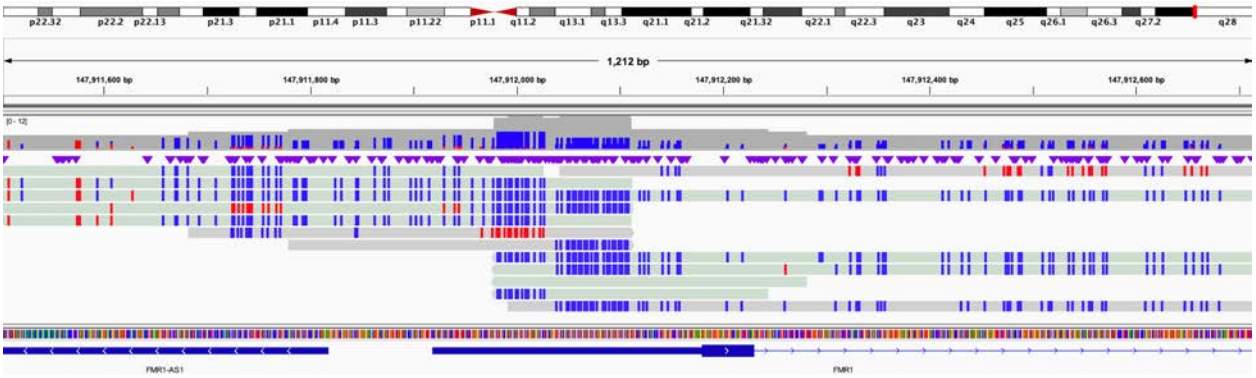

B. Methylation analysis of 5' UTR of *FMR1* reveals that the region around the CGG expansion is no longer methylated. The region shown is larger than in panel A. IGV view is chrX:147,911,502-147,912,719.

Figure S18. S040 (*FXN*), known repeat expansion.

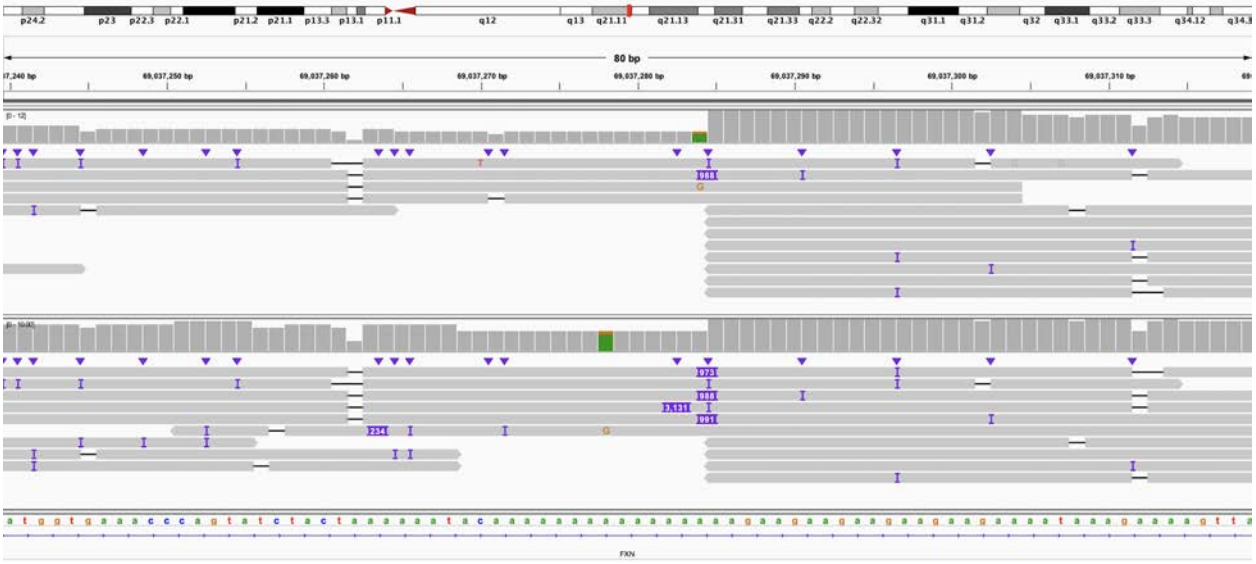

IGV view of a sample from an individual with a heterozygous expansion in *FXN*. Sample is from a cell line obtained from Coriell (Table S1). Top panel is reads aligned with minimap2 using default parameters; bottom panel is parameters that reduce the number of split reads. IGV view is from chr9:69,037,240-69,037,319.

Figure S19. S041 (*FXN*), known repeat expansion.

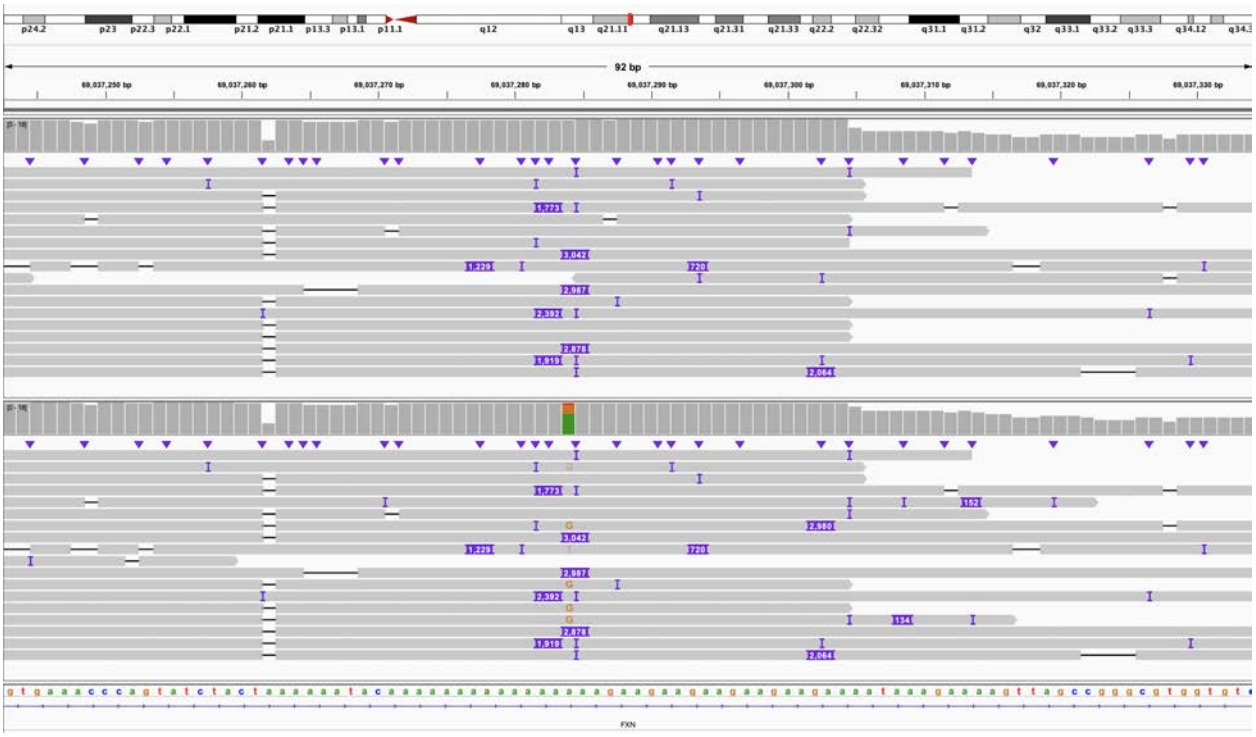

IGV view of a case known to be heterozygous for two different repeat expansions in *FXN*; DNA was obtained from Coriell (Table S1). Reads aligned with minimap2 and default parameters are in the top panel; reads aligned with minimap2 and parameters meant to decrease the number of reads broken by the aligner are in the bottom panel. IGV view is from chr9:69,037,243-69,037,334.

Figure S20. 04-01, 04-02, and 04-03 (*XYLT1*), evaluation of repeat length in family 04 from LaCroix *et al.* 2019.

3

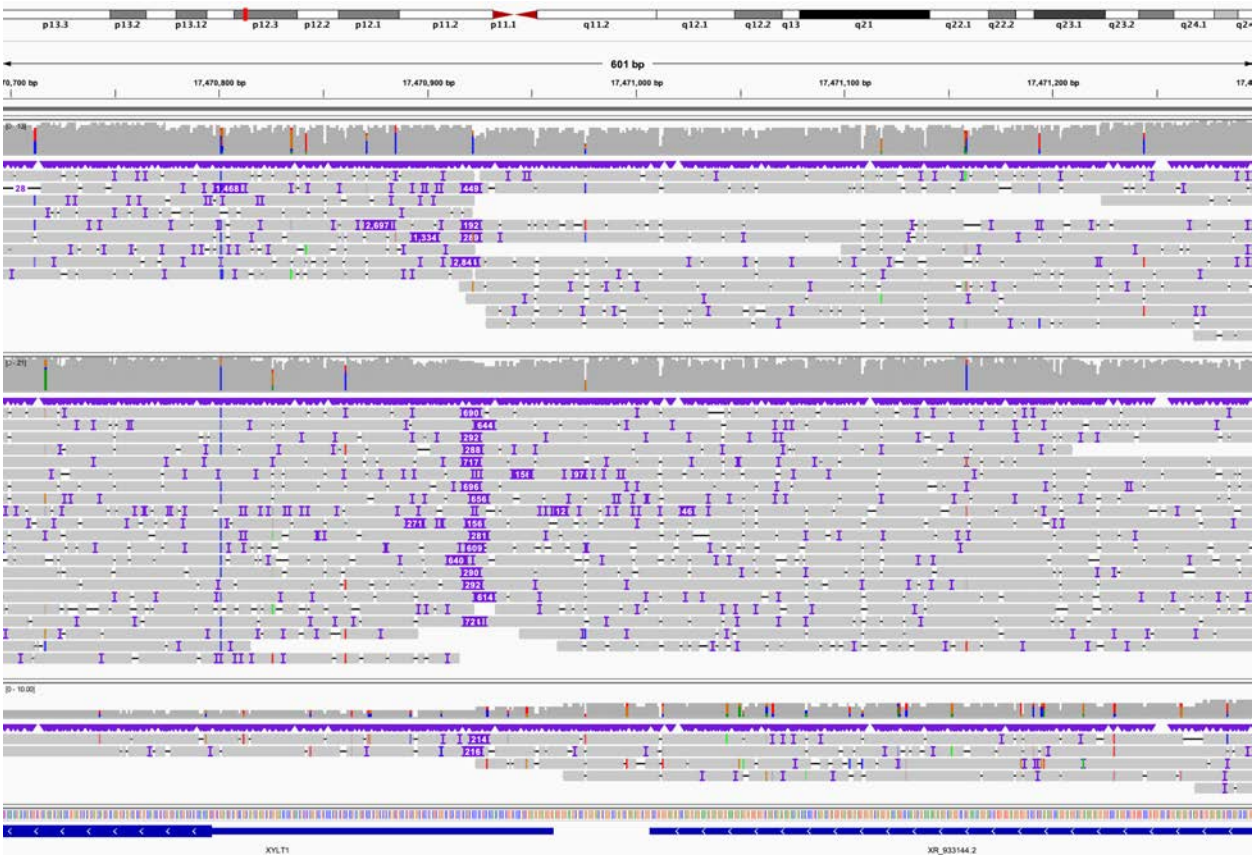

A. Screenshot of expansion in 5' UTR of *XYLT1* in family 04 from LaCroix *et al*., 2019.[32] The proband (top) inherited a permutation allele from his mother and a *de novo* deletion from his father; the mother (middle) has a wild-type allele and permutation allele, while the father has two wild-type alleles (bottom).

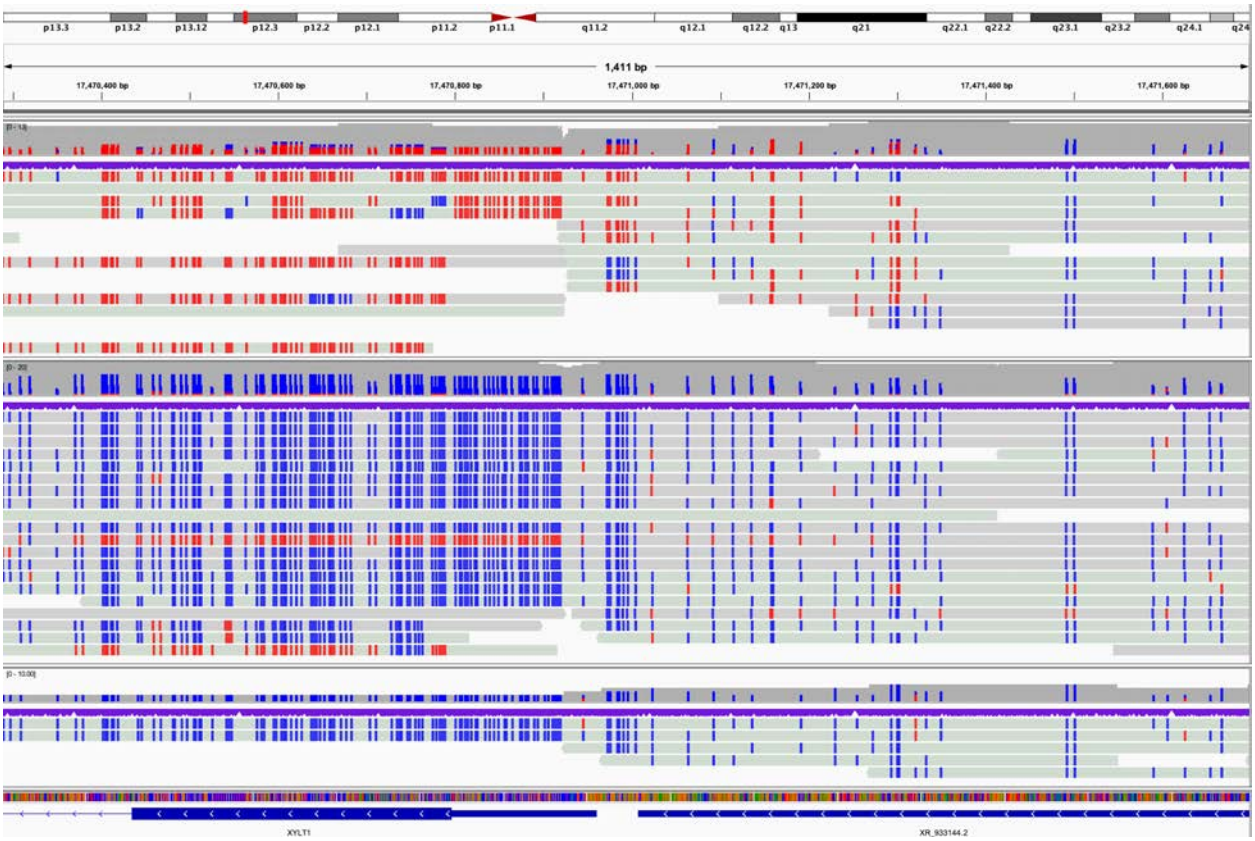

B. Methylation was called and assigned to each read and shows that all reads in the proband are methylated (red), while most in the mother are unmethylated (blue), and both in the father are unmethylated. IGV view from chr16:17,470,696-17,471,299. B. IGV view from chr16:17,470,288-17,471,705.

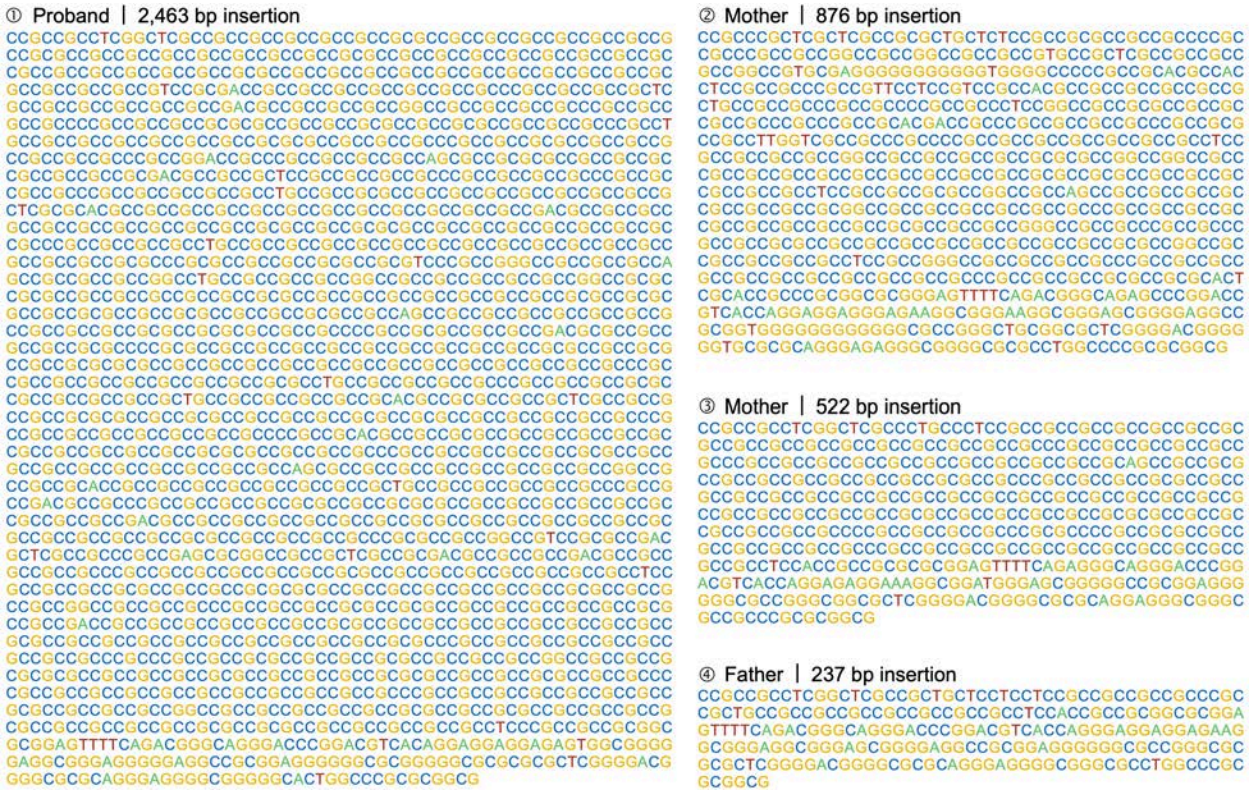

C. Sequence of the GCC repeat haplotypes as determined by PacBio CLR sequencing is consistent with the Southern blots and the lengths identified using ONT.

Figure S21. 06-01, 06-02, and 06-03 (*XYLT1*), evaluation of repeat length in family 06 from LaCroix *et al.* 2019.

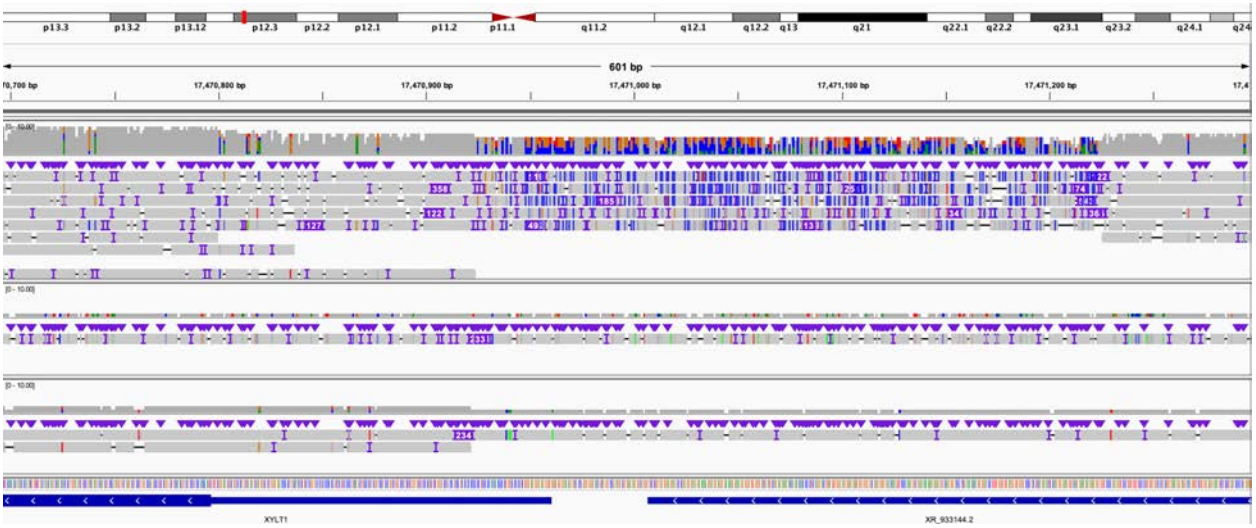

A. IGV view of proband (top), mother (middle), and father (bottom) from family 06 from LaCroix *et al*., 2019.[33] Only a single read was recovered spanning the GGC repeat in both the mother and father. IGV view is from chr16:17,470,696-17,471,299.

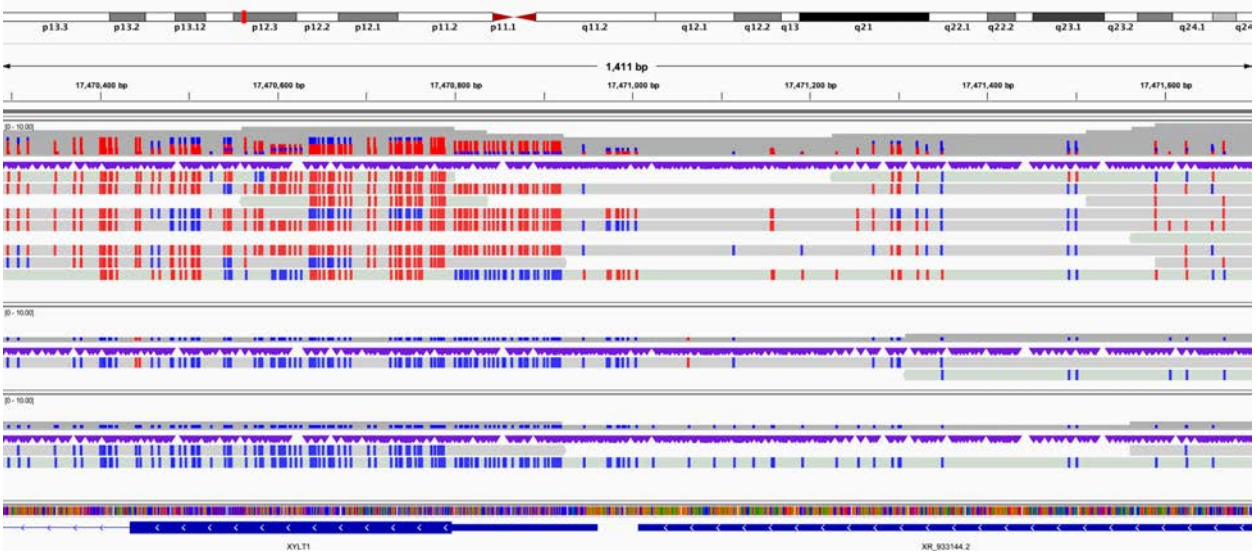

B. IGV view of reads converted to show methylation status; order is the same as in A but the view is slightly larger to show methylation of the first exon of *XYLT1* in the proband. IGV view from chr16:17,470,288-17,471,705.

Figure S22. S071, Phasing of inherited and *de novo* variants in METTL5.

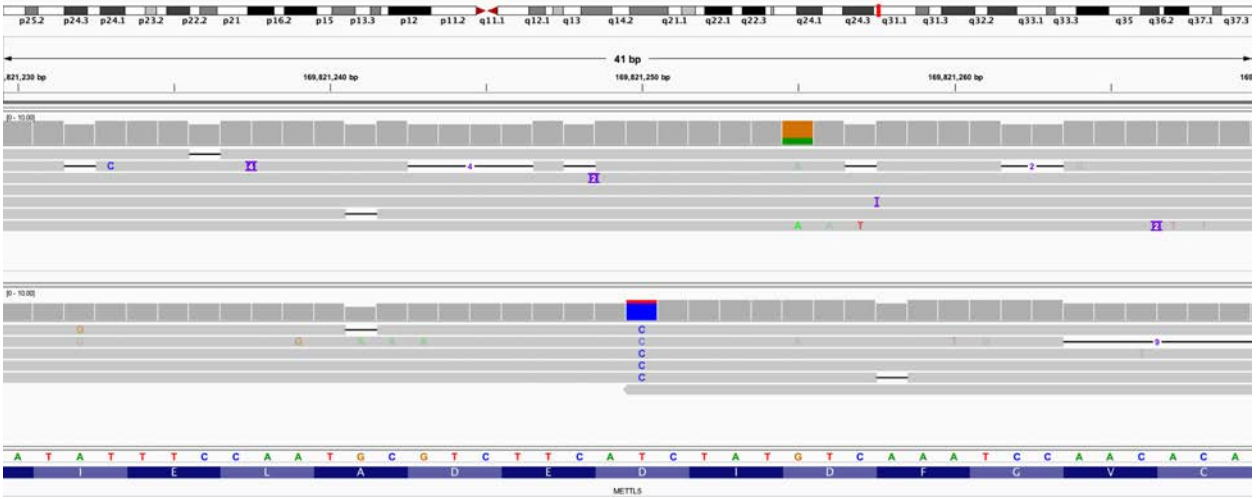

A. View of paternally inherited c.248 A>G (p.D83G), IGV view is chr2:169,821,230-169,821,269. Haplotype 1 is the top track, haplotype 2 is the bottom.

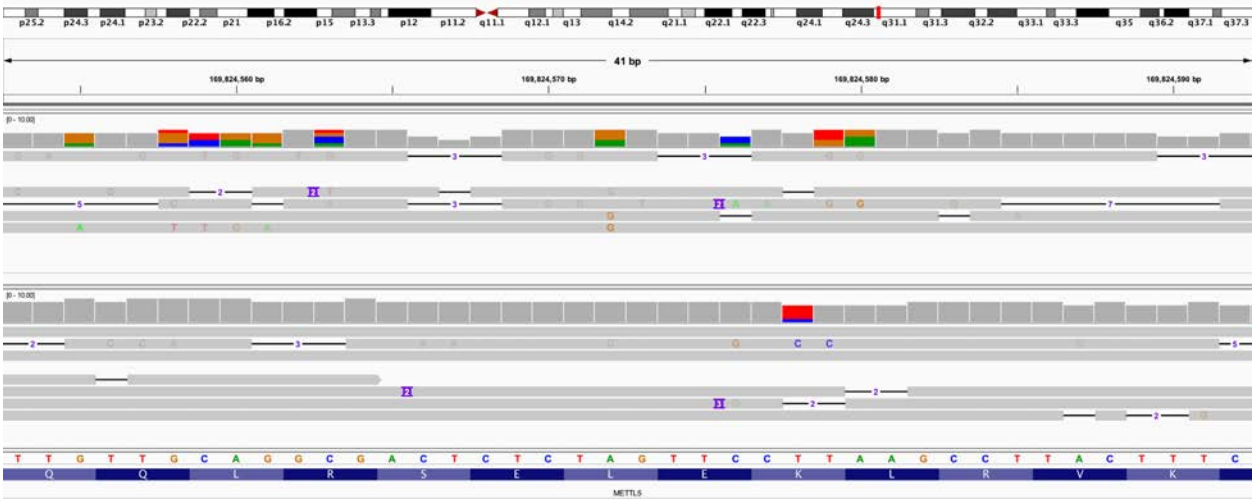

B. View of *de novo* c.26T>C(p.L9P), IGV view is chr2:169,824,553-169,824,592. Haplotype 1 is the top track, haplotype 2 is the bottom.

Figure S23. S086, Phasing of known inherited and *de novo* mosaic variant in KIAA1109.

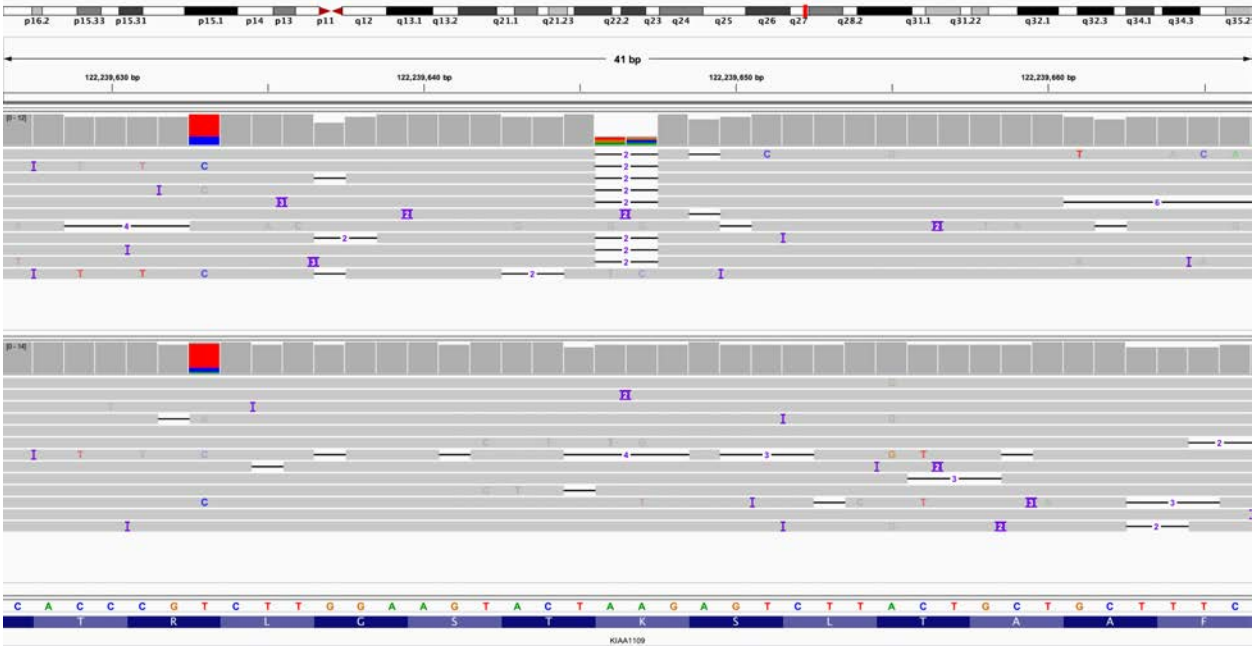

A. View of maternally inherited 2bp deletion, IGV view is of chr4:122,239,627-122,239,666. Haplotype 1 is top track, haplotype 2 is bottom.

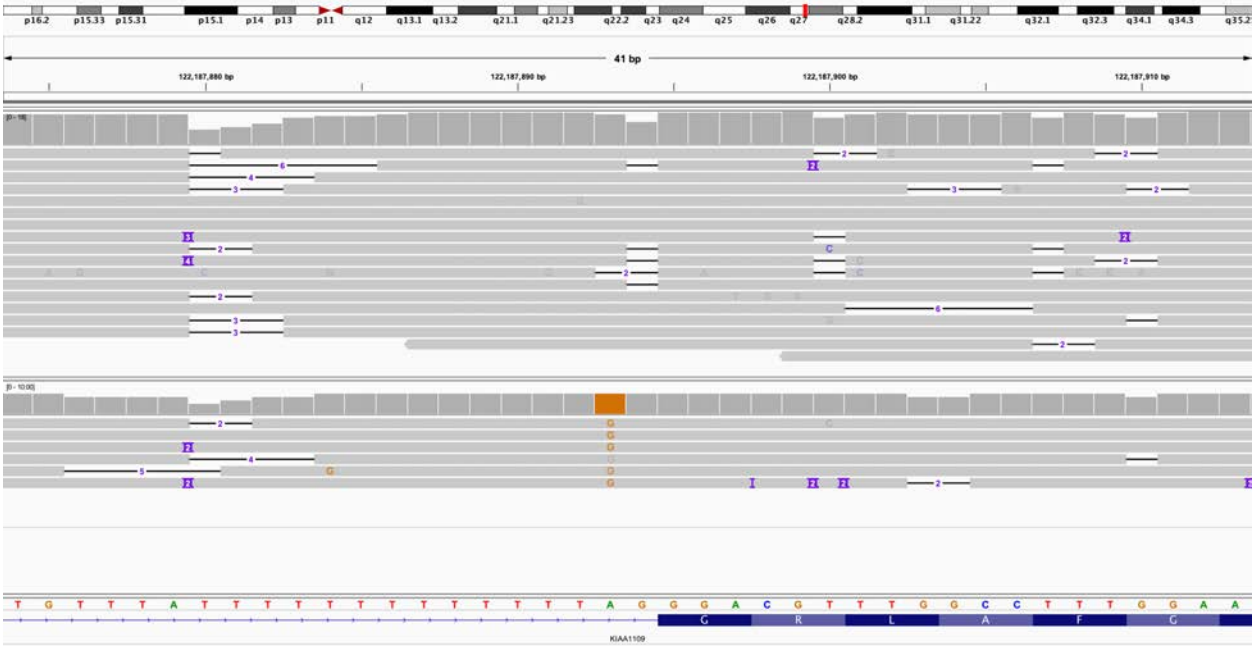

B. View of *de novo* A>G with reported allele fraction of 16%. IGV view is of chr4:122,187,874-122,187,913. Haplotype 1 is top track, haplotype 2 is bottom.

Figure S24. S014, three noncontiguous deletions of chromosome 6 identified by CMA.

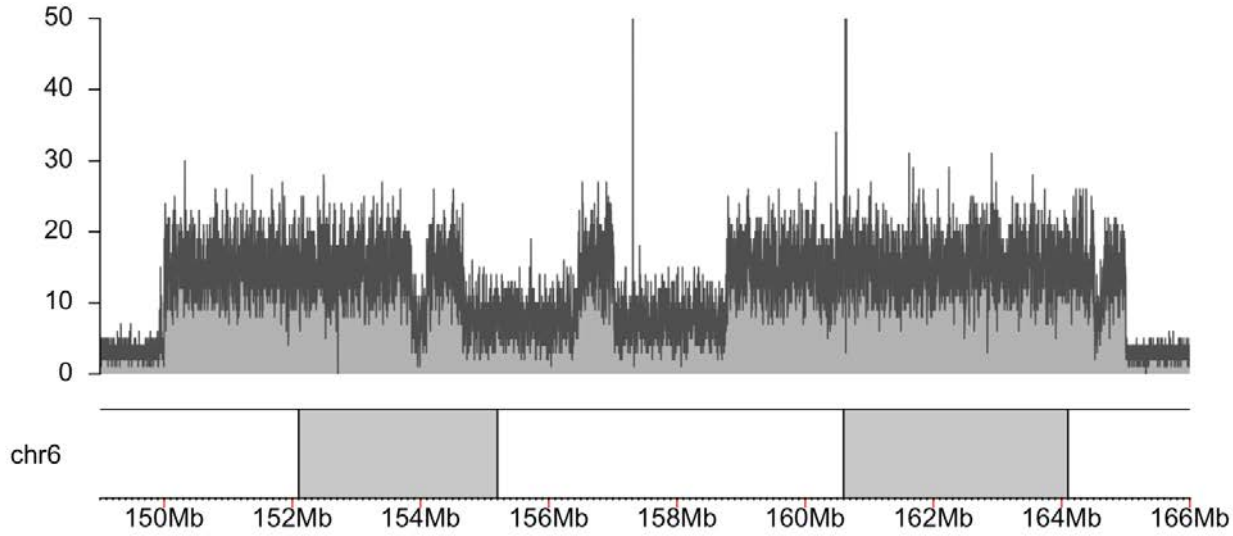

A. Coverage of chromosome 6 target region.

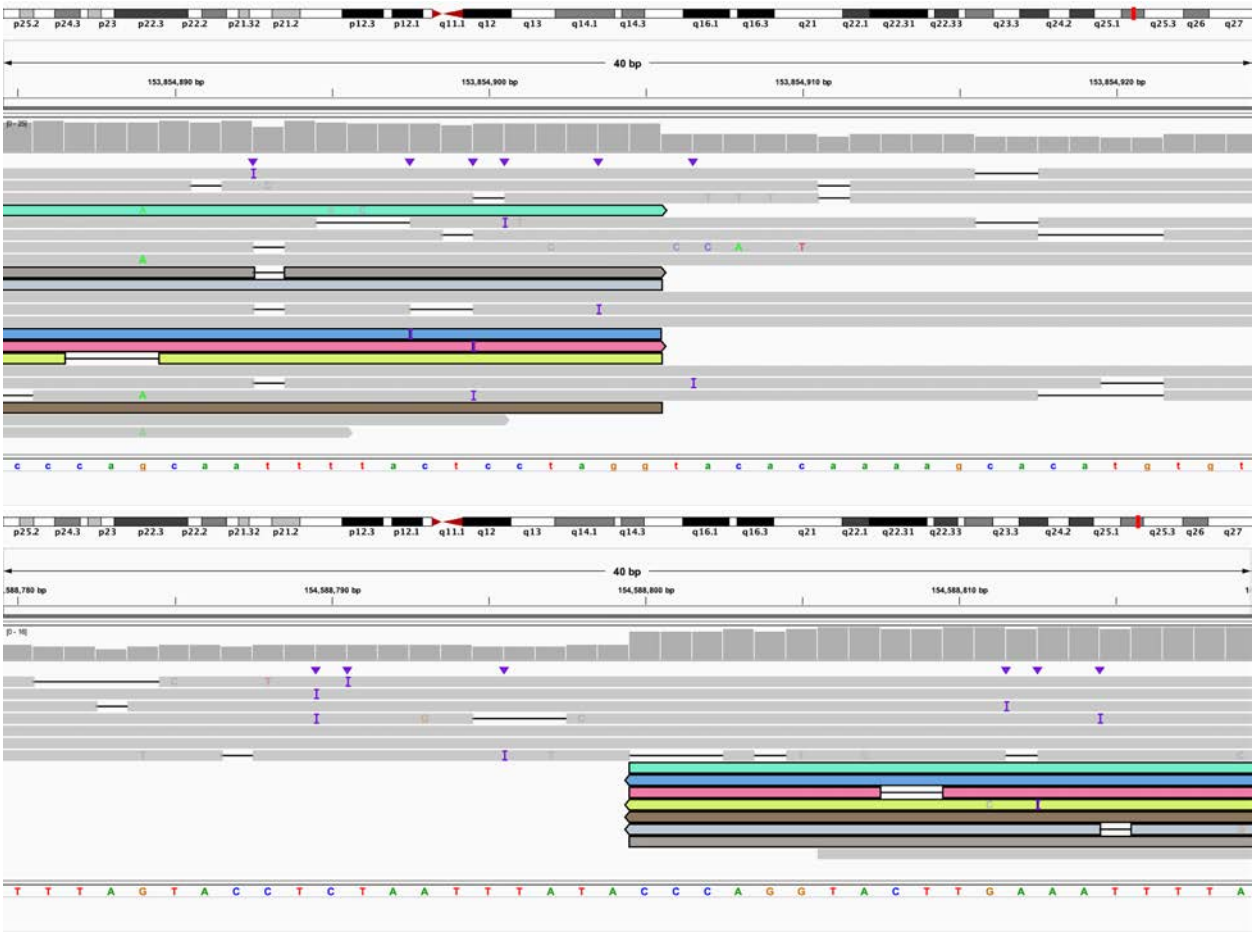

B: 3' end of fragment A (IGV: chr6:153,854,885-153,854,924) connects to 5' end of fragment E (IGV: chr6:154,588,780-154,588,819).

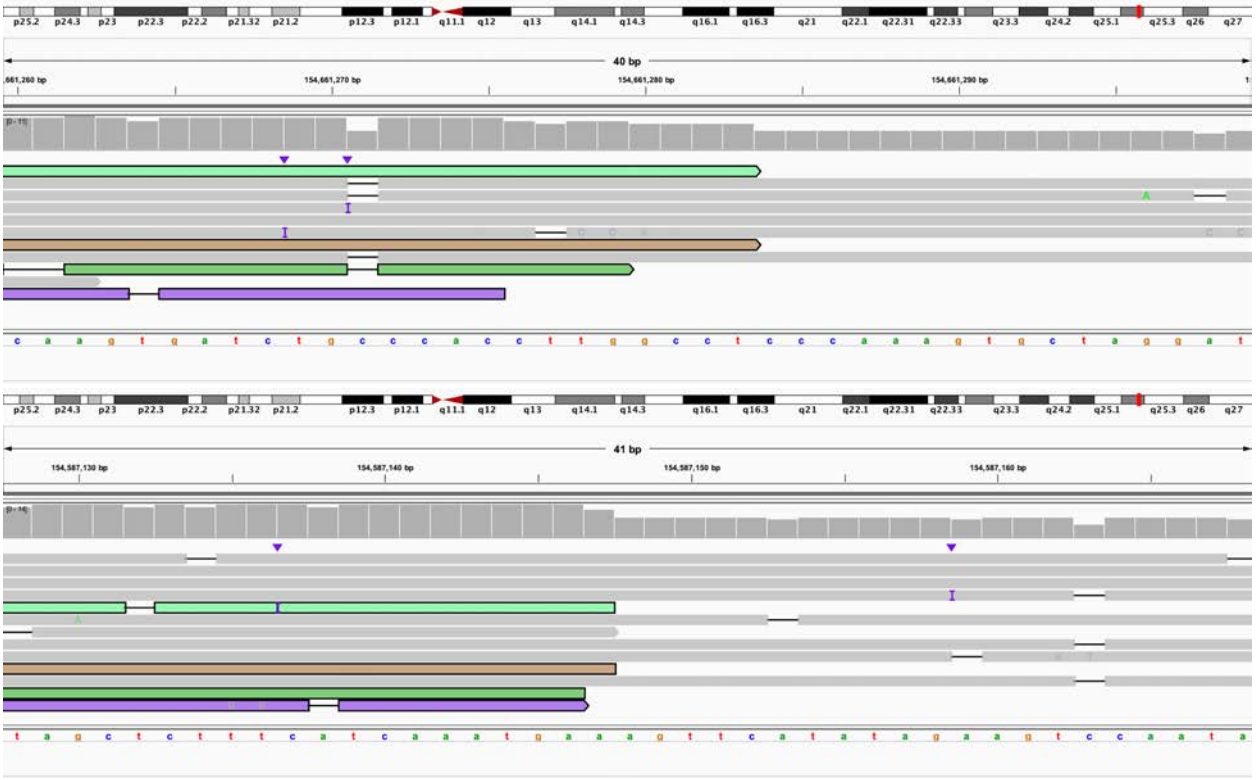

C: 3' end of fragment E (IGV: chr6:154,661,260-154,661,299) connects to 3’ end of fragment C (IGV: chr6:154,587,128-154,587,168).

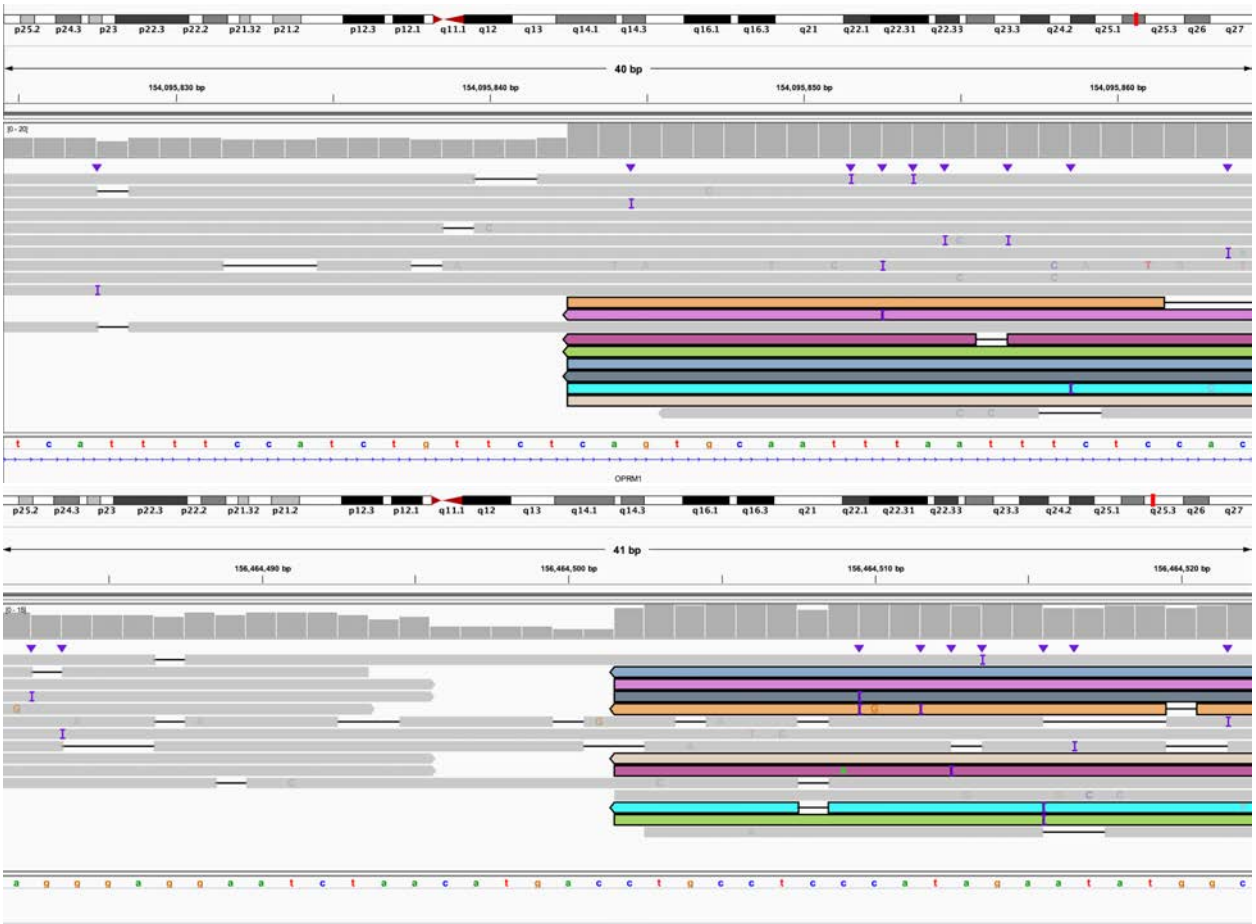

D: 5' end of fragment C bisects *OPRM1* (IGV: chr6:154,095,825-154,095,864) and connects to 5' end of fragment I (IGV: chr6:156,464,482-156,464,522).

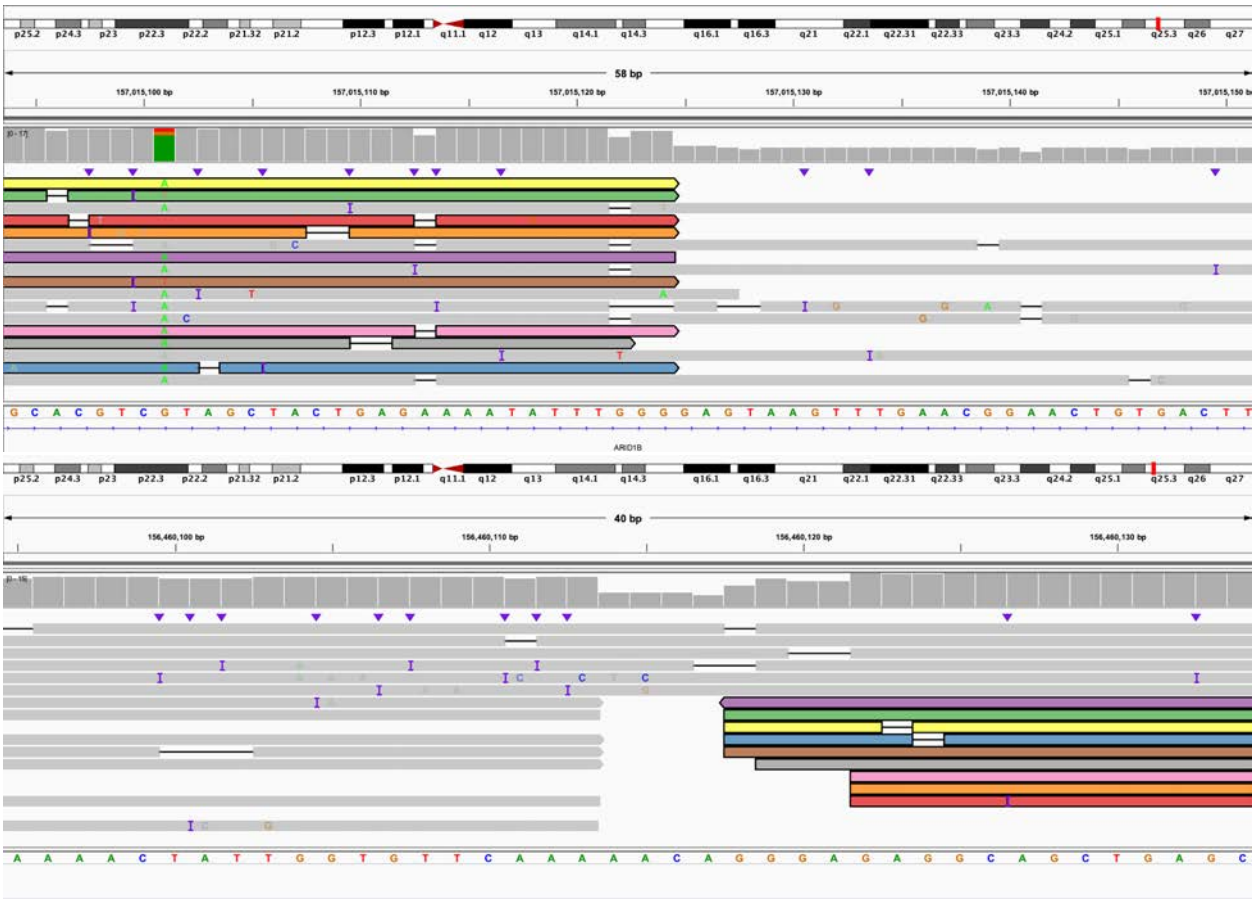

E: 3' end of fragment I bisects *ARID1B* (IGV: chr6:157,015,094-157,015,151) and connects to 5' end of fragment H (IGV: chr6:156,460,095-156,460,134).

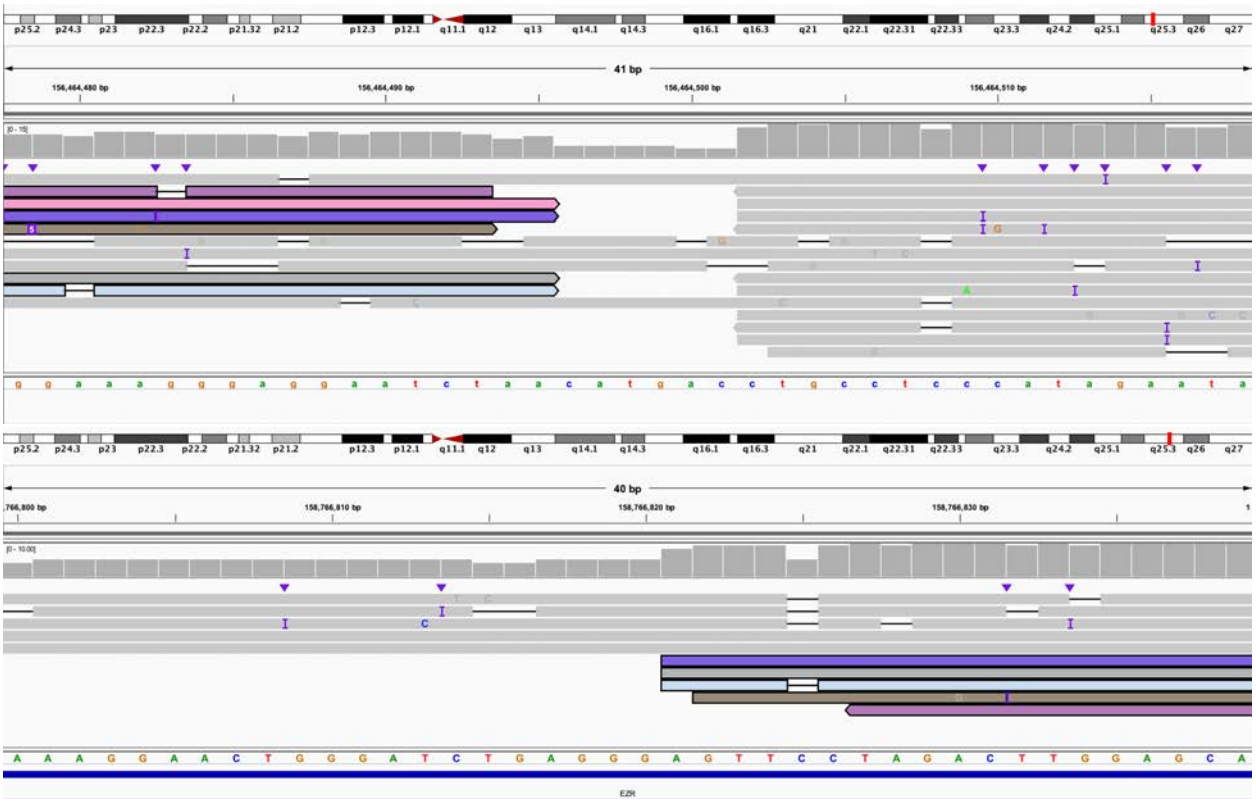

F: 3' end of fragment H (IGV: chr6:156,464,478-156,464,518) connects to 5' end of fragment K and bisects *EZR* (IGV: chr6:158,766,800-158,766,839).

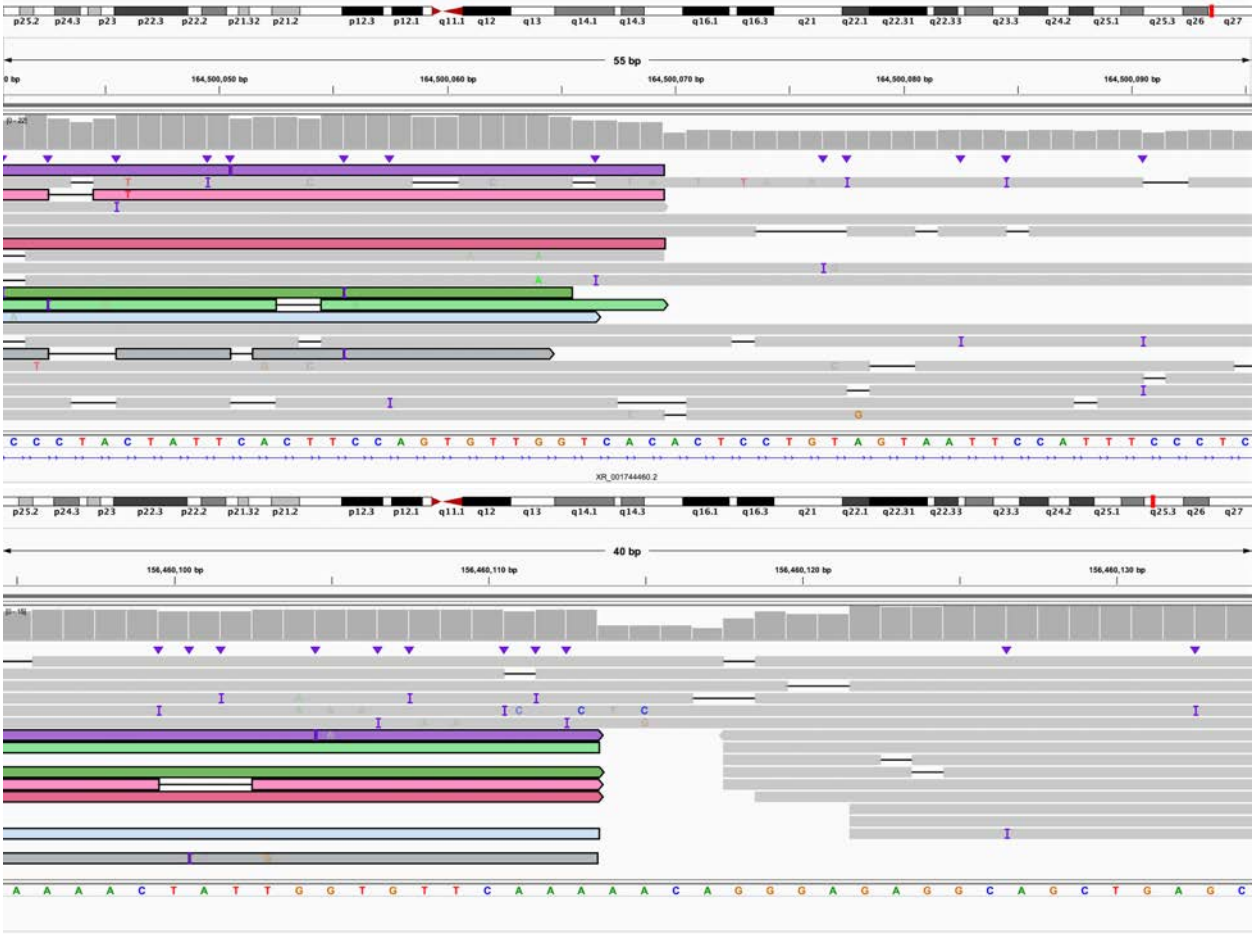

G: 3' end of fragment K bisects *XR_001744460.2* (IGV: chr6:164,500,041-164,500,095) and connects to 3' end of fragment G (IGV: chr6:156,460,095-156,460,134).

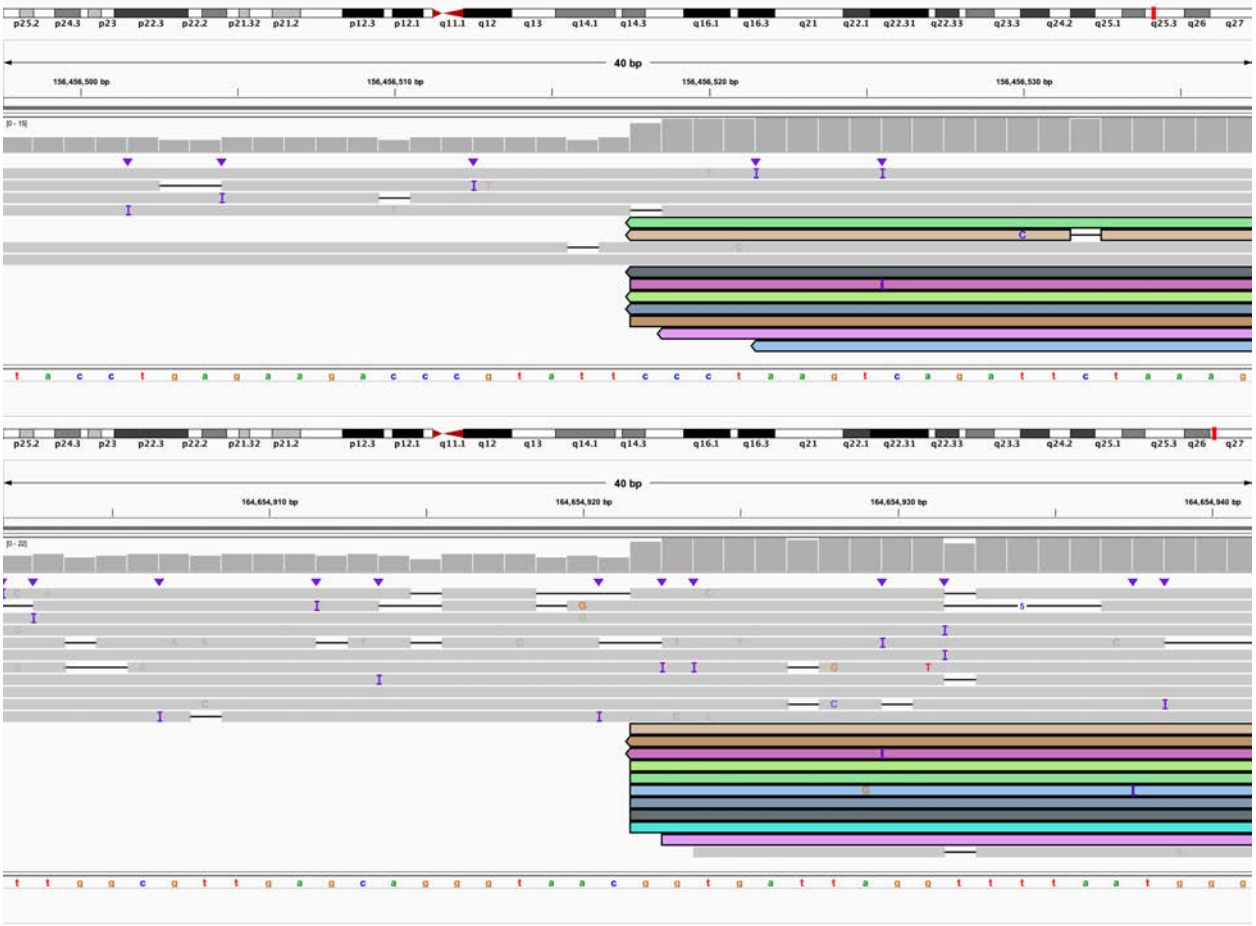

H: 5' end of fragment G (IGV: chr6:156,456,498-156,456,537) connects to 5' end of fragment M (IGV: chr6:164,654,902-164,654,941).

Figure S25. S020, individual with three deletions identified on array and multiple rearrangements on karyotype.

In panels J-AG Nanopore data is the top track and PacBio HiFi data is the bottom track.

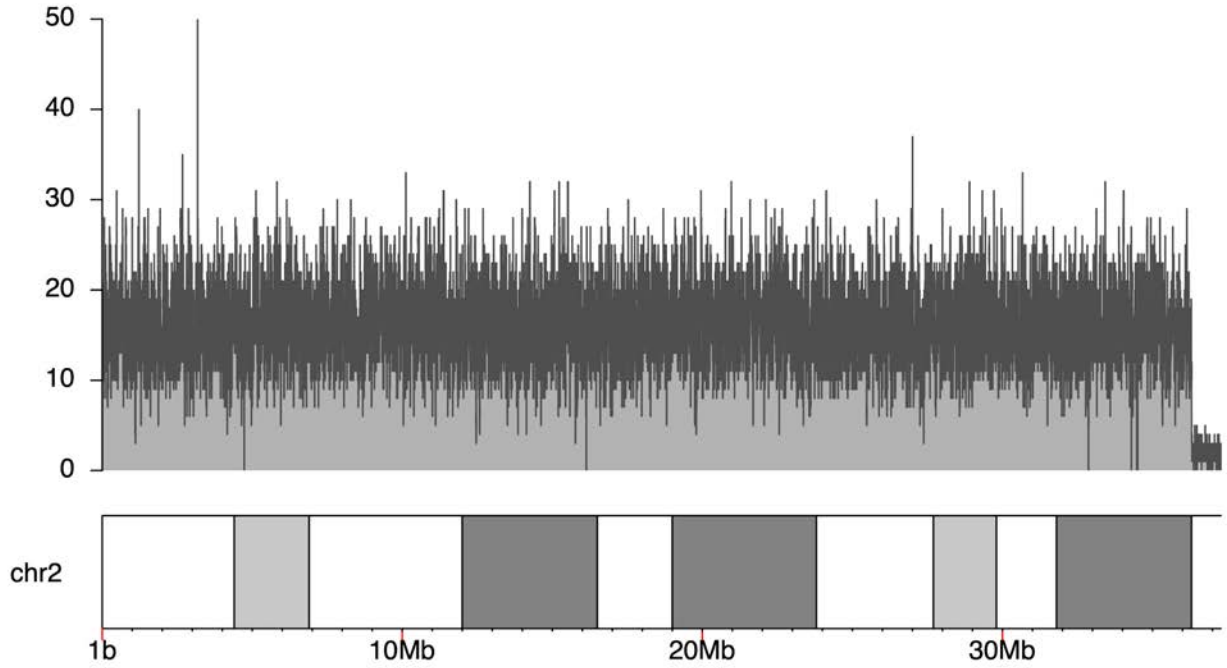

A: Coverage of chromosome 2 target region from readfish experiment 1.

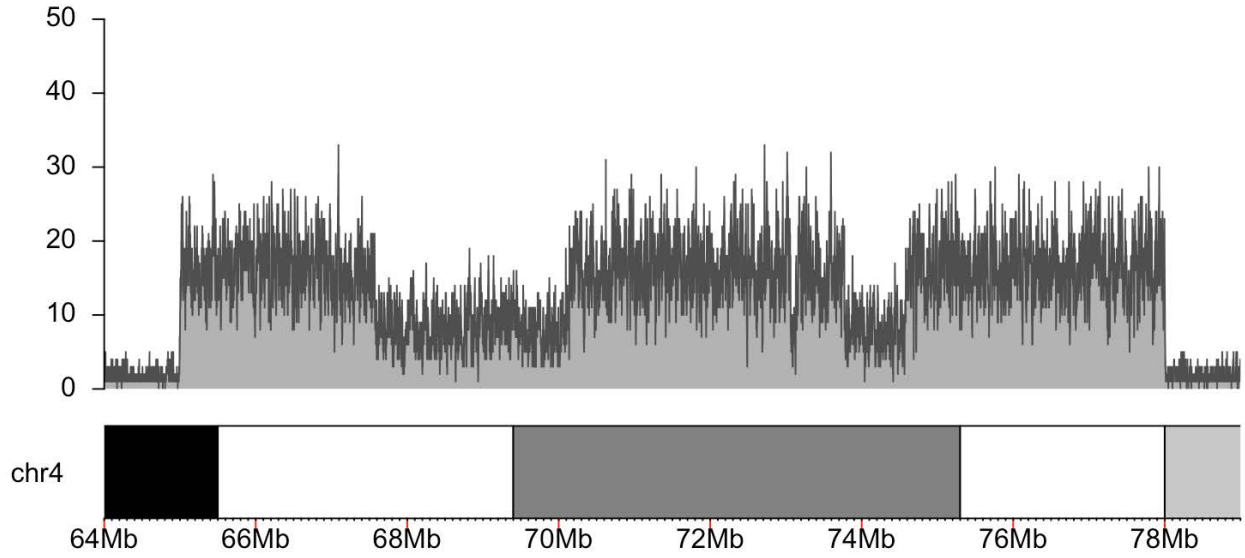

B: Coverage of chromosome 4 target region from readfish experiment 1.

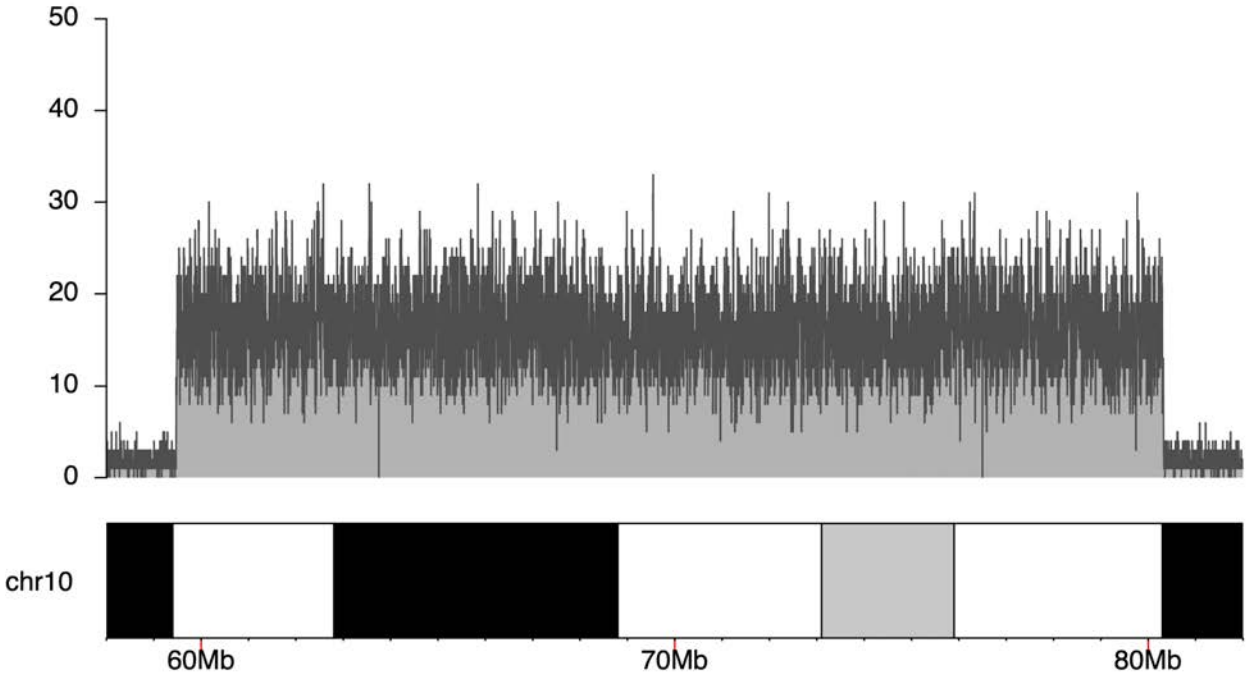

C: Coverage of chromosome 10 target region from readfish experiment 1.

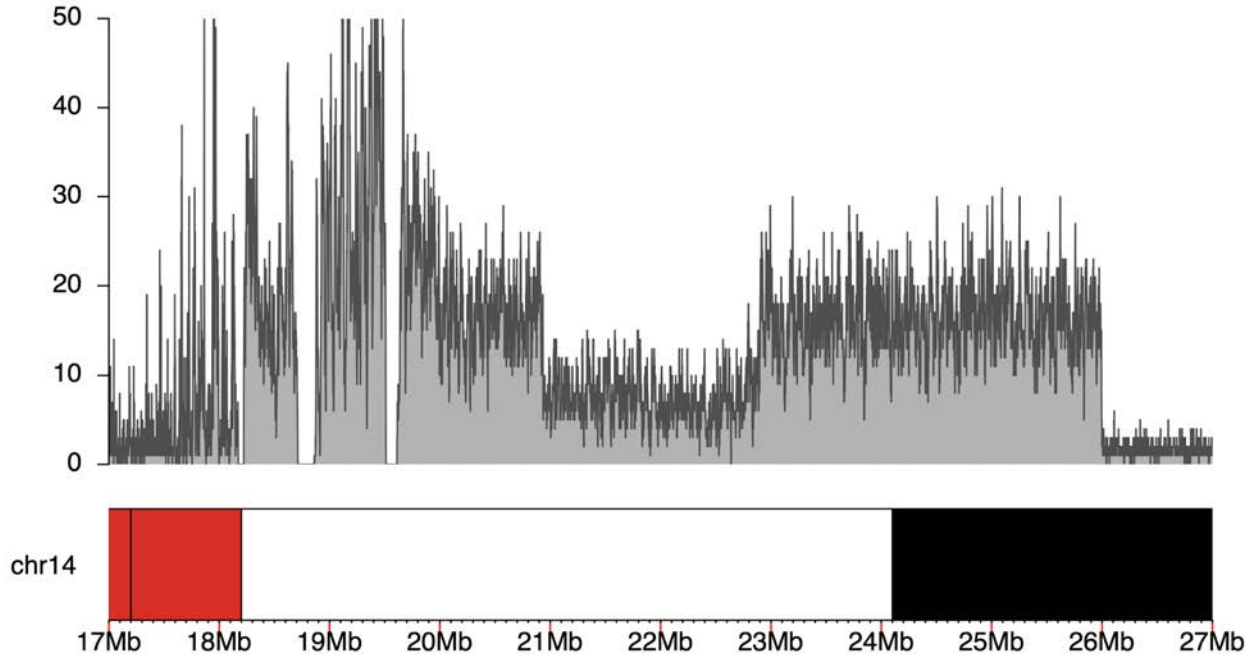

D: Coverage of chromosome 14 target region from readfish experiment 1.

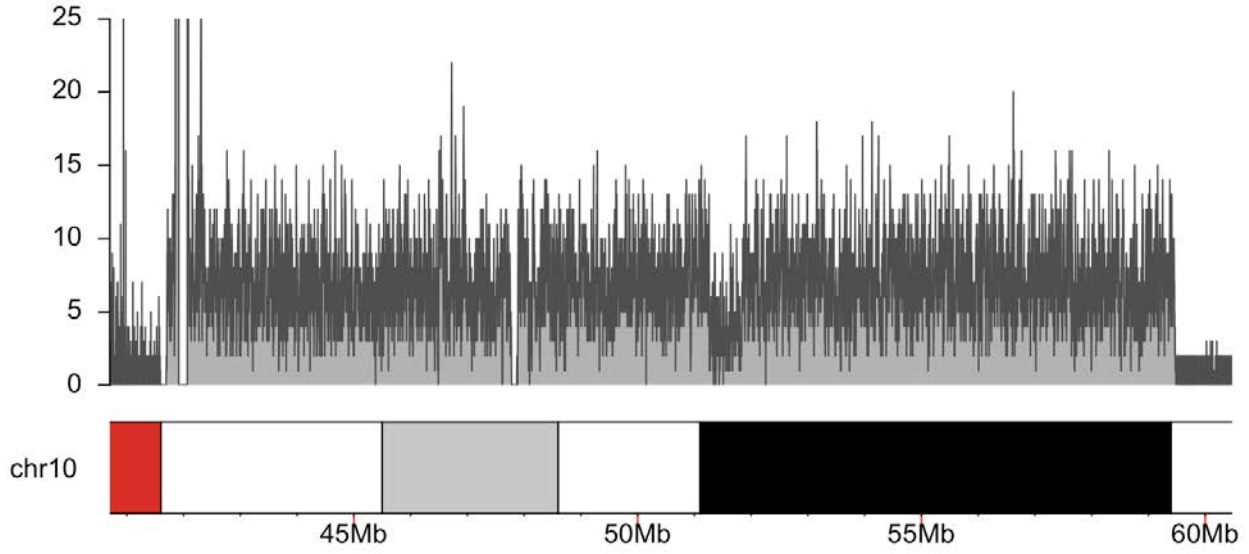

E: Coverage of chromosome 10 target region from readfish experiment 2.

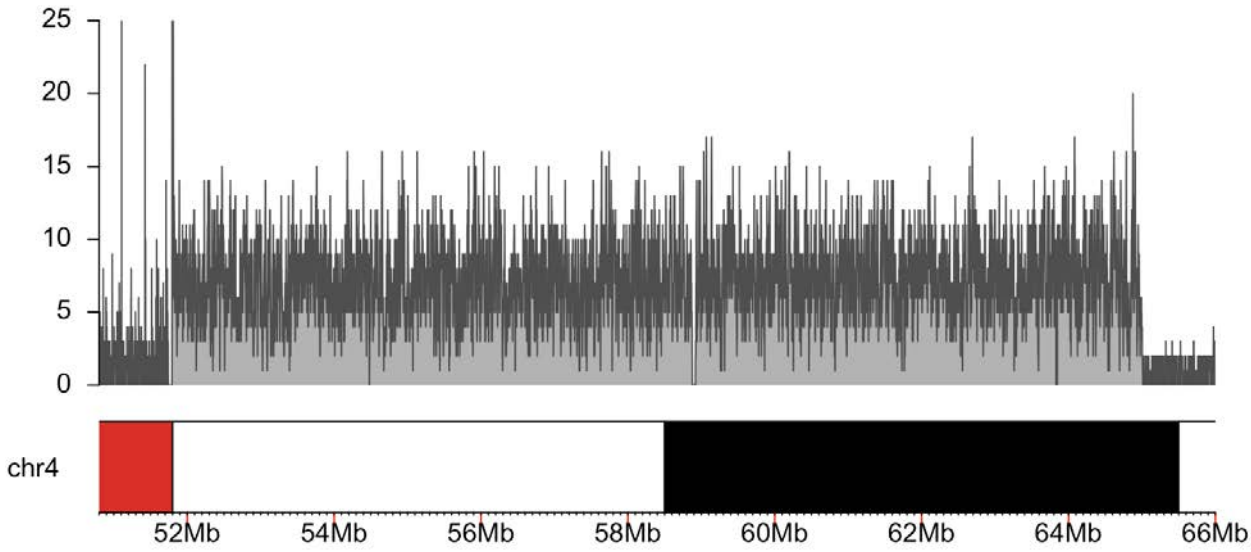

F: Coverage of first chromosome 4 target region from readfish experiment 2.

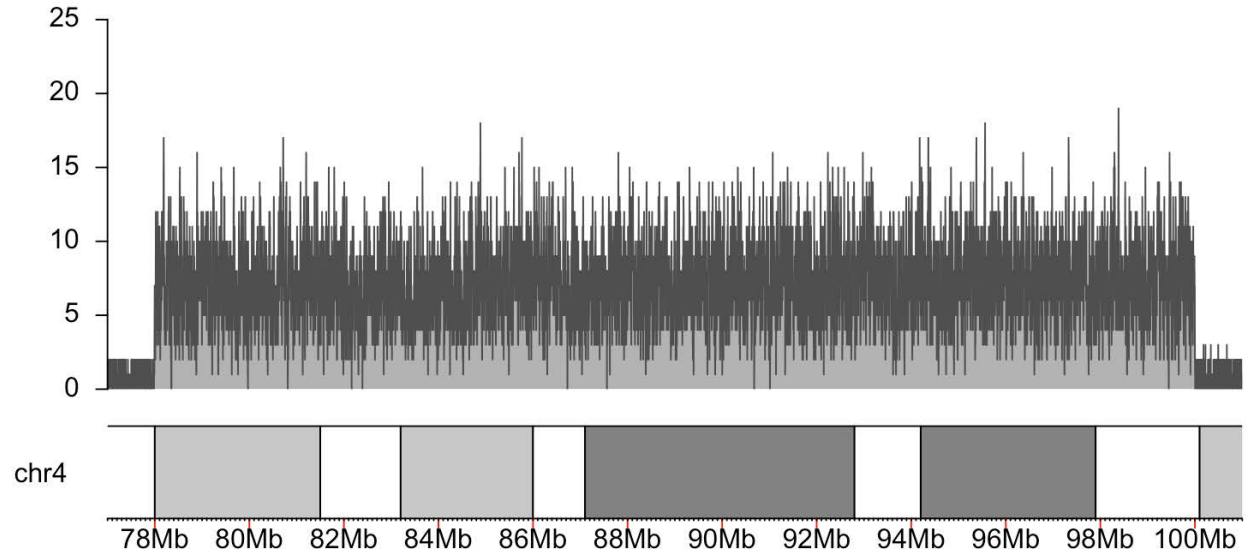

G: Coverage of second chromosome 4 target region from readfish experiment 2.

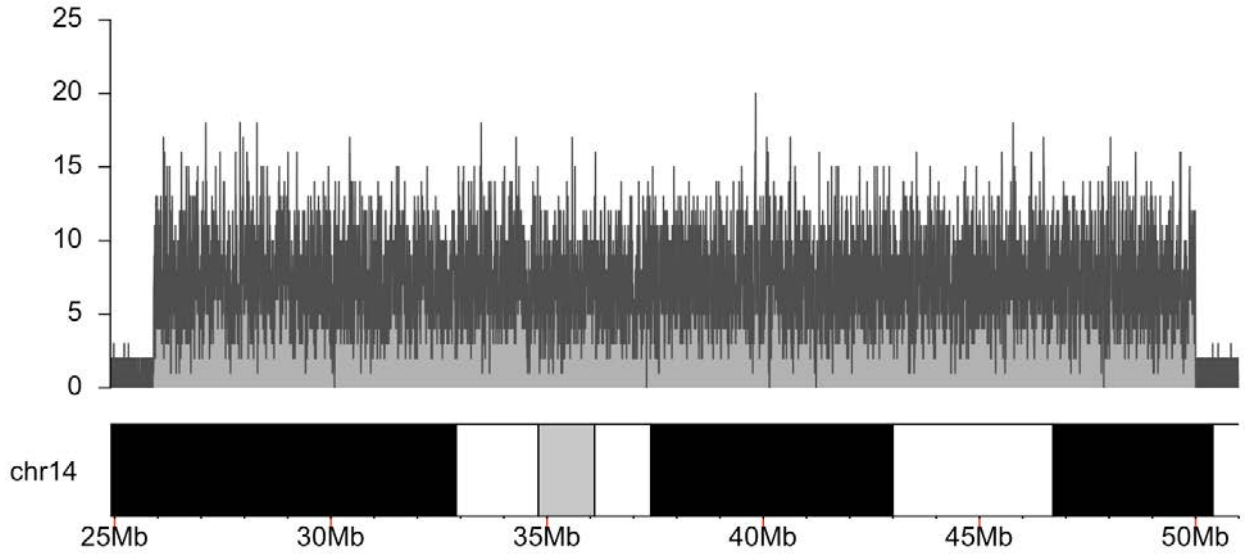

H: Coverage of chromosome 14 target region from readfish experiment 2.

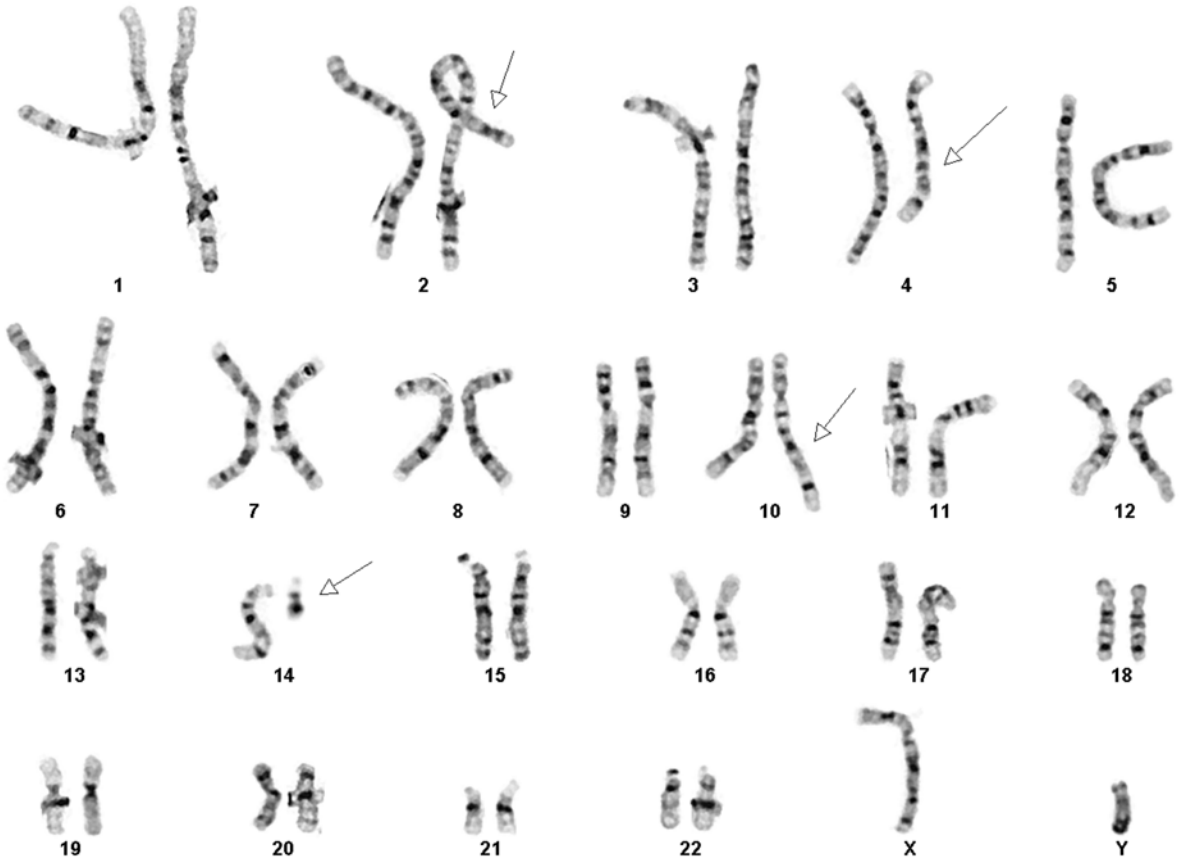

I: Karyotype of the case, arrows point to abnormal chromosomes.

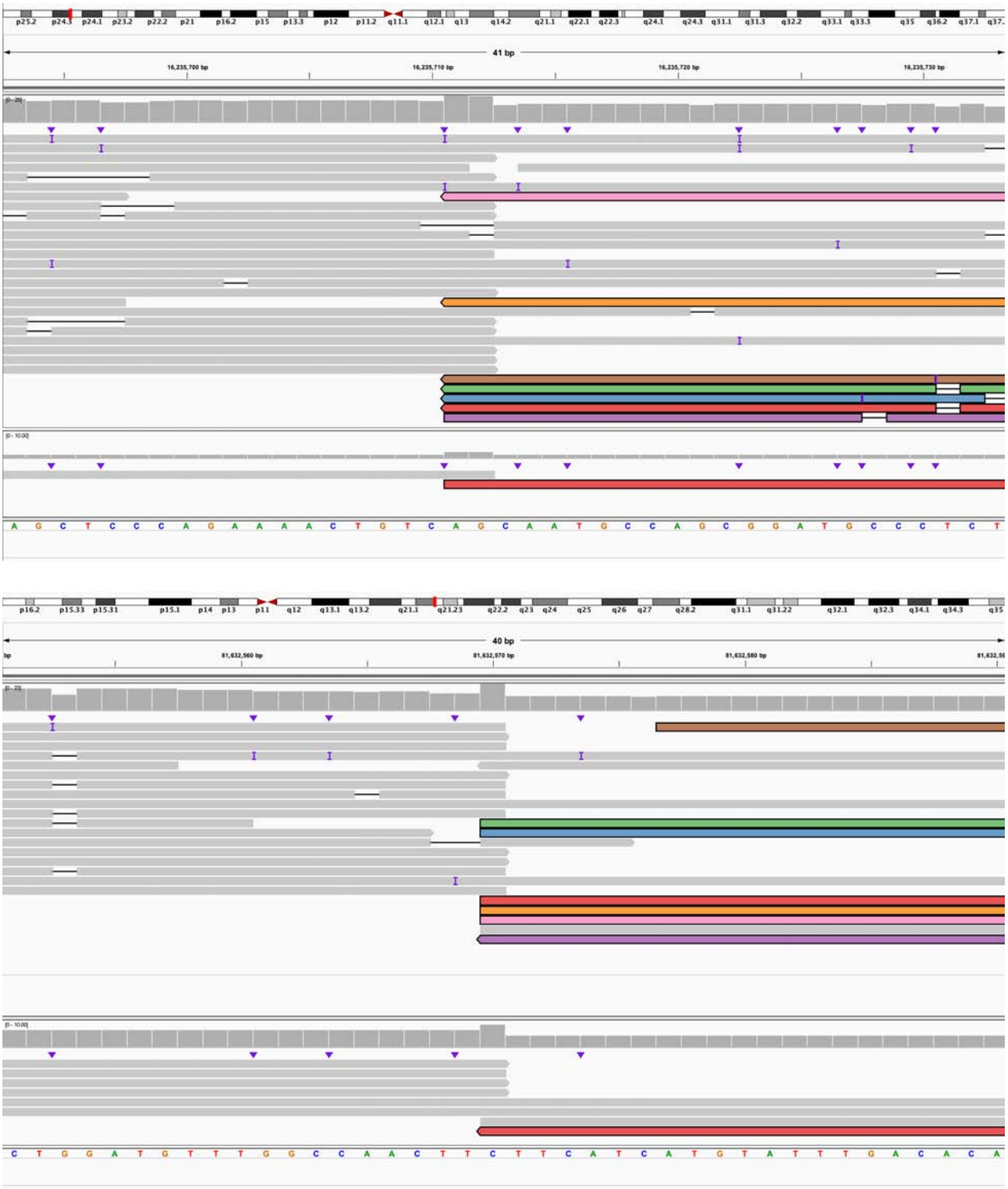

J. The 5' end of 2:C (IGV: chr2:16,235,693-16,235,733) is connected to the 5' end of 4:N (IGV: chr4:81,632,551-81,632,590). This is the entirety of derivative chromosome 2.

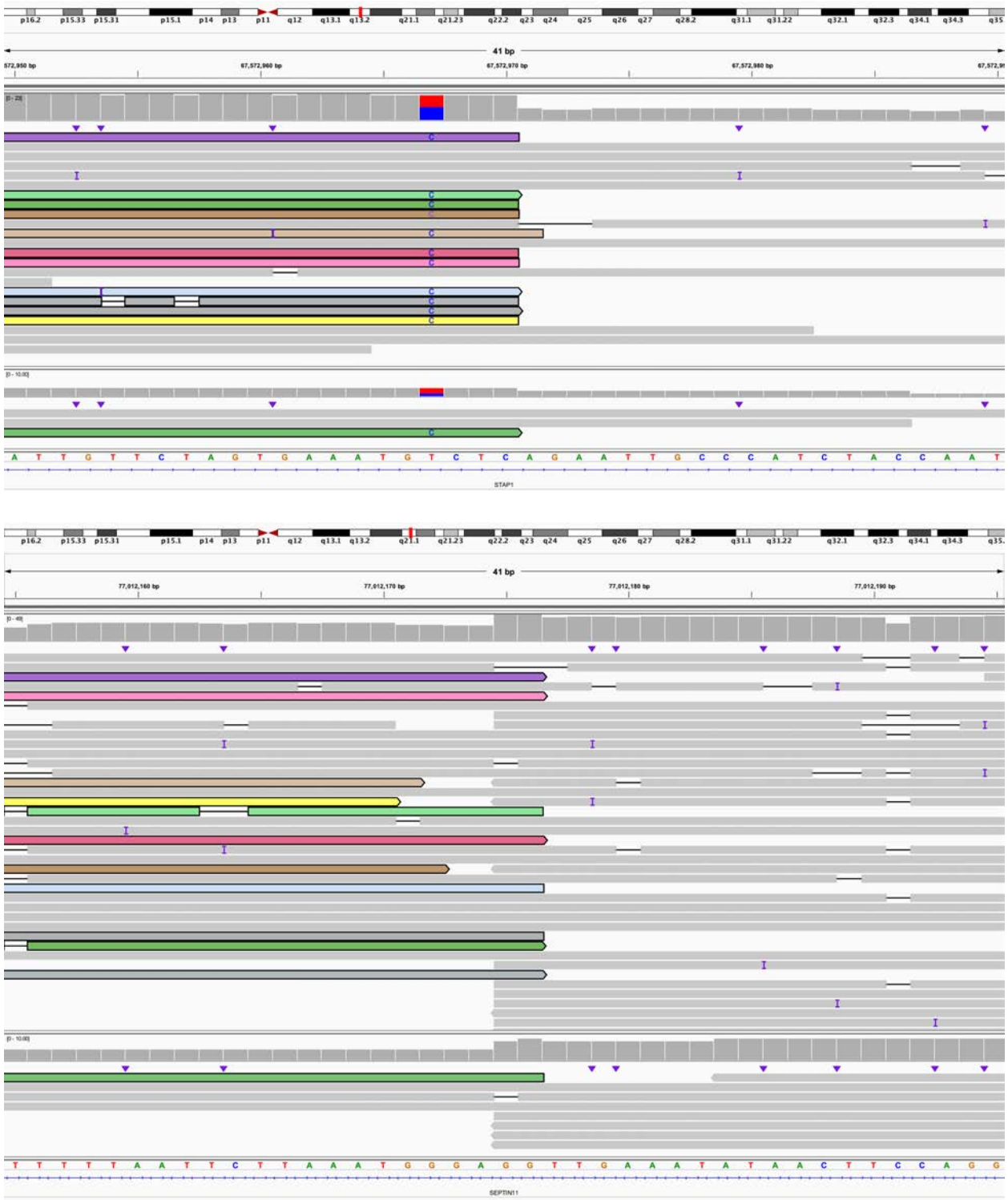

K. The 3' end of 4:A bisects *STAP1* (IGV: chr4:67,572,950-67,572,990) and is connected to the 3' end of 4:K and bisects *SEPTIN11* (IGV: chr4:77,012,155-77,012,195). This is the beginning of derivative chromosome 4.

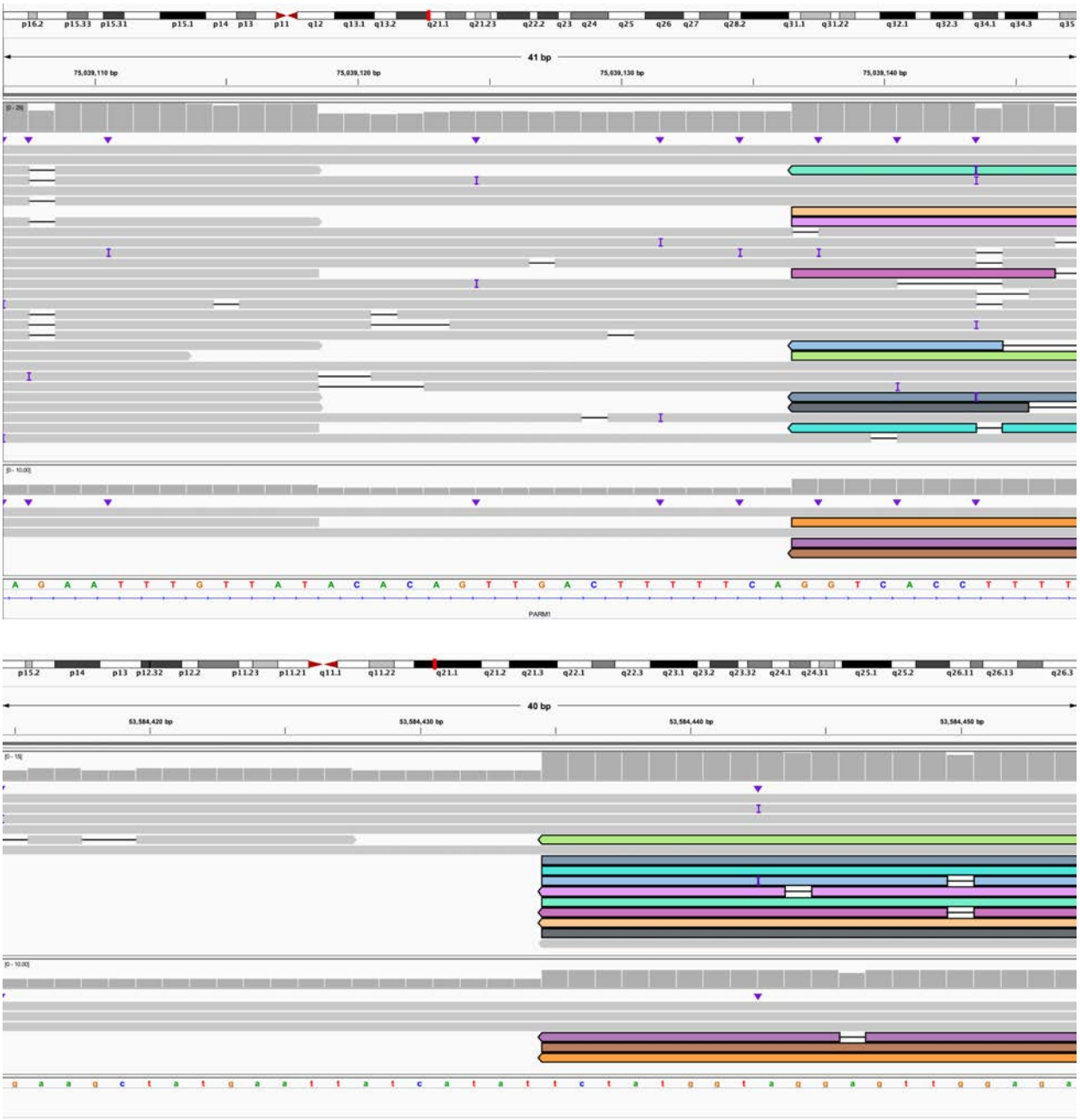

L. The 5' end of 4:K bisects *PARM1* (IGV: chr4:75,039,107-75,039,147) and is connected to the 5' end of 10:I (IGV: chr10:53,584,415-53,584,454). This is within derivative chromosome 4.

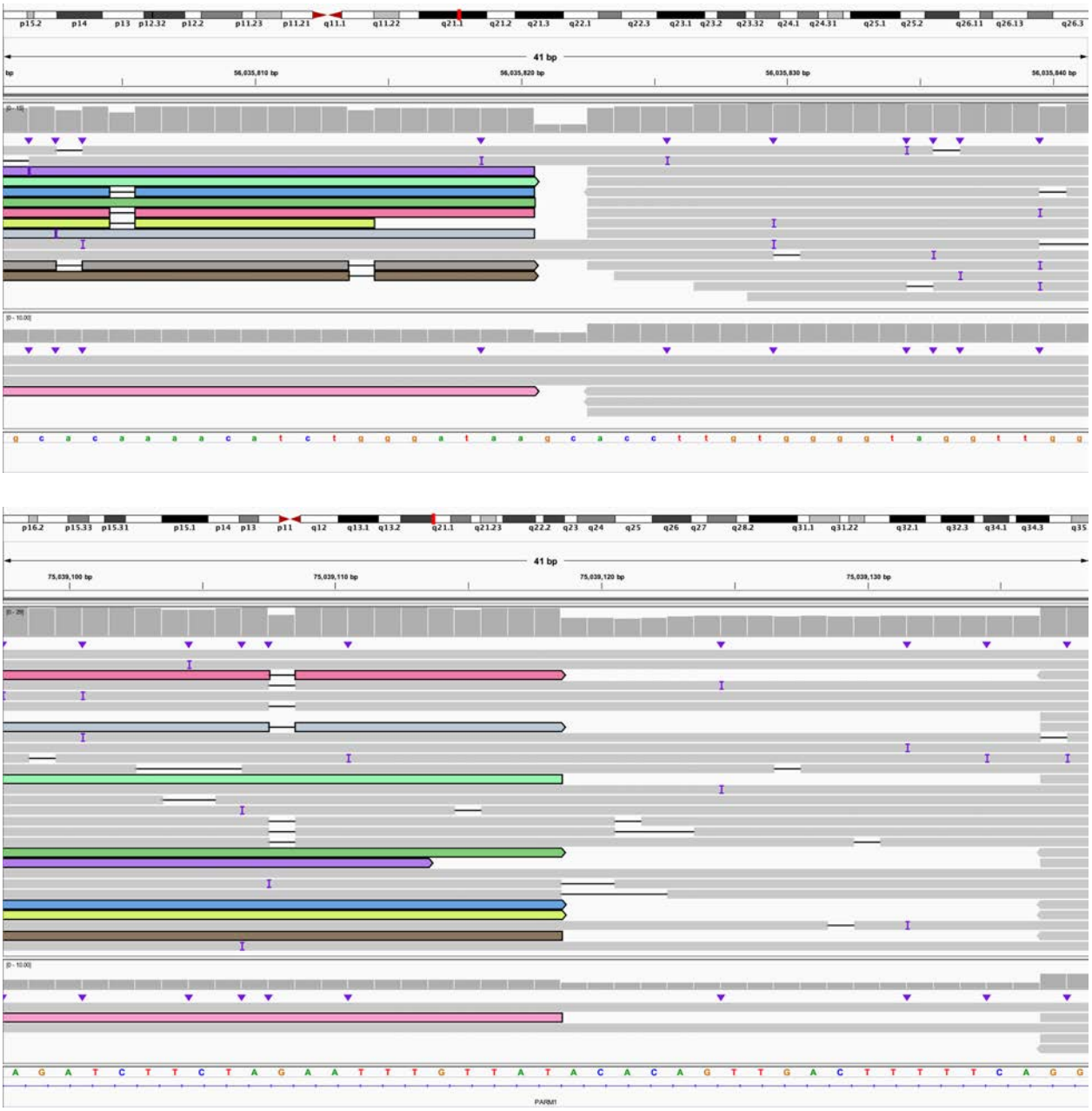

M. The 3' end of 10:I (IGV: chr10:56,035,801-56,035,841) is connected to the 3' end of 4:J and bisects *PARM1* (IGV: chr4:75,039,098-75,039,138). This is within derivative chromosome 4.

N. The 5' end of 4:J bisects *XR_938881.1* (IGV: chr4:74,831,229-74,831,268) and is connected to the 3' end of 4:M (IGV: chr4:81,632,550-81,632,590). This is within derivative chromosome 4.

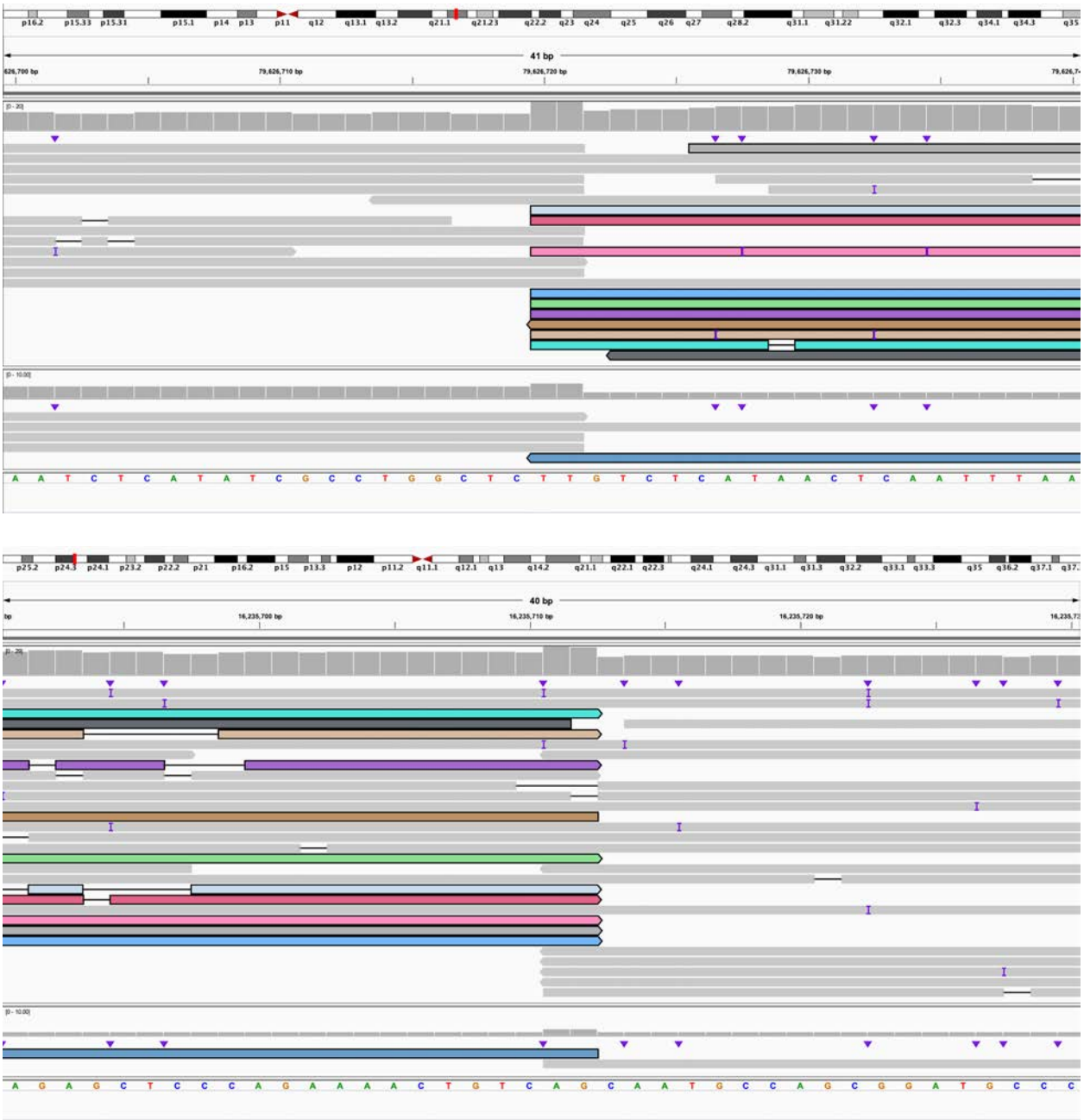

O. The 5' end of 4:M (IGV: chr4:79,626,700-79,626,740) is connected to the 3' end of 2:B (IGV: chr2:16,235,691-16,235,730). This is within derivative chromosome 4.

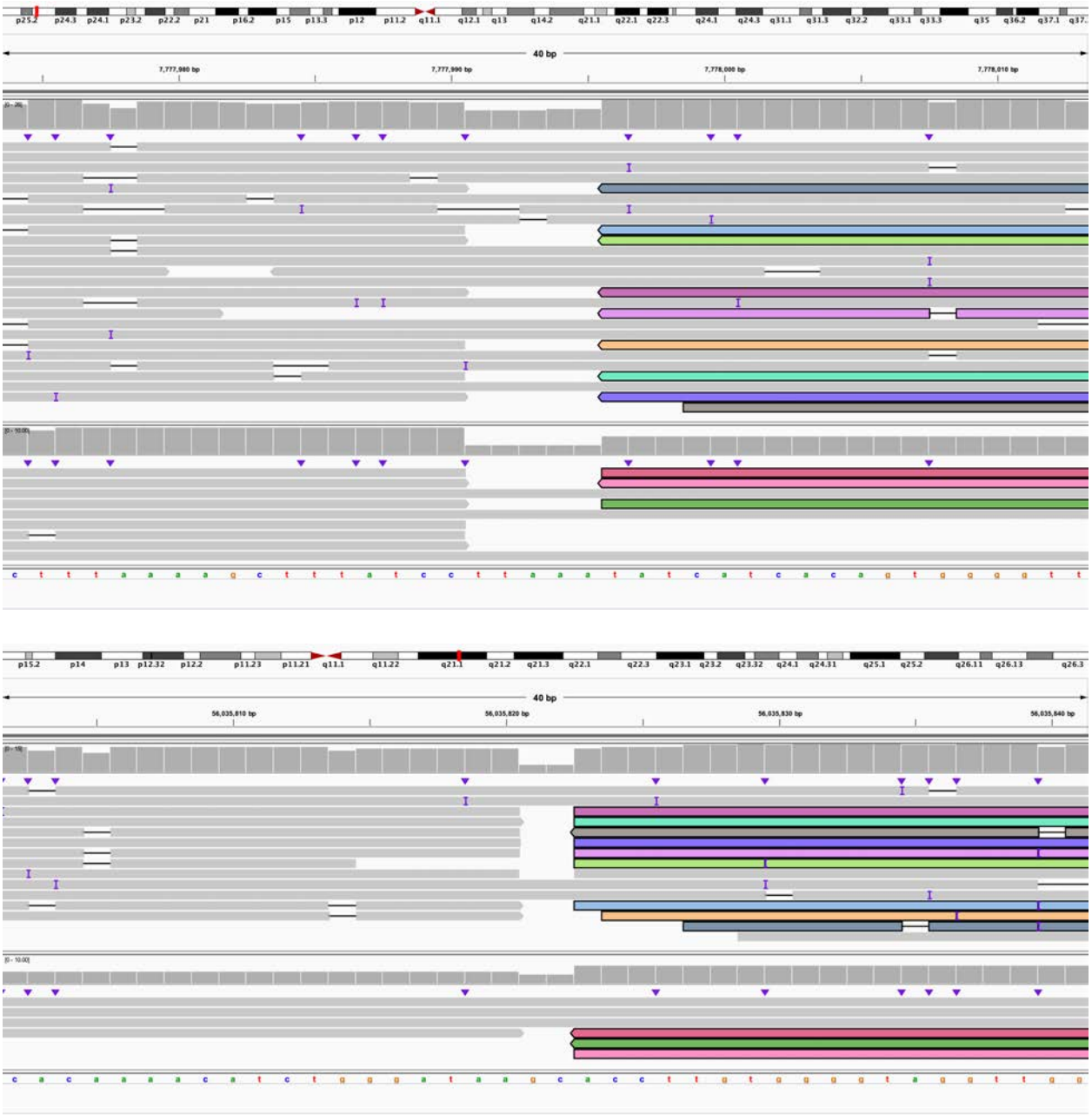

P. The 5' end of 2:B (IGV: chr2:7,777,974-7,778,013) is connected to the 5' end of 10:J (IGV: chr10:56,035,802-56,035,841). This is within derivative chromosome 4.

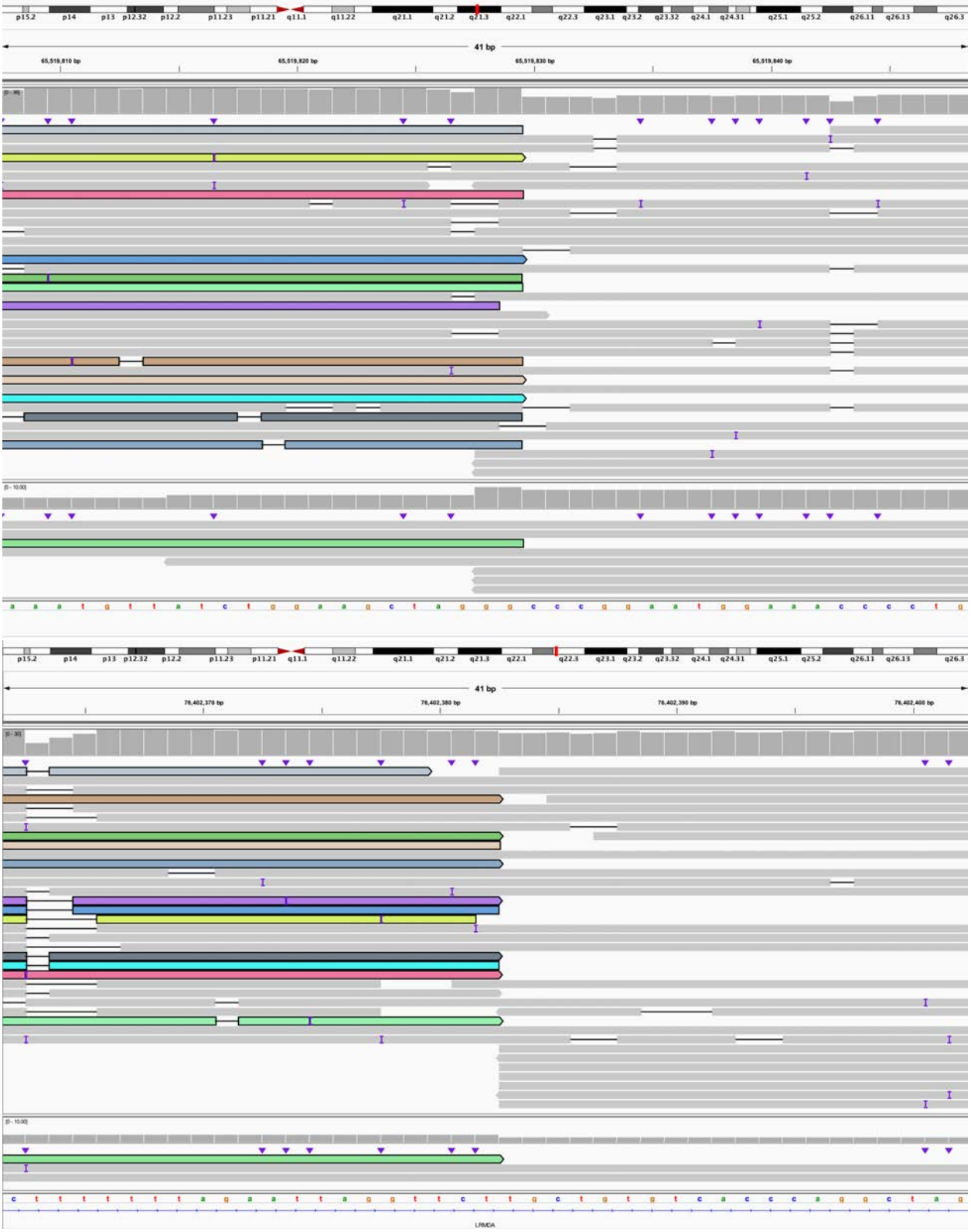

Q. The 3' end of 10:J (IGV: chr10:65,519,808-65,519,848) is connected to the 3' end of 10:M and bisects *LRMDA* (IGV: chr10:76,402,362-76,402,402). This is within derivative chromosome 4.

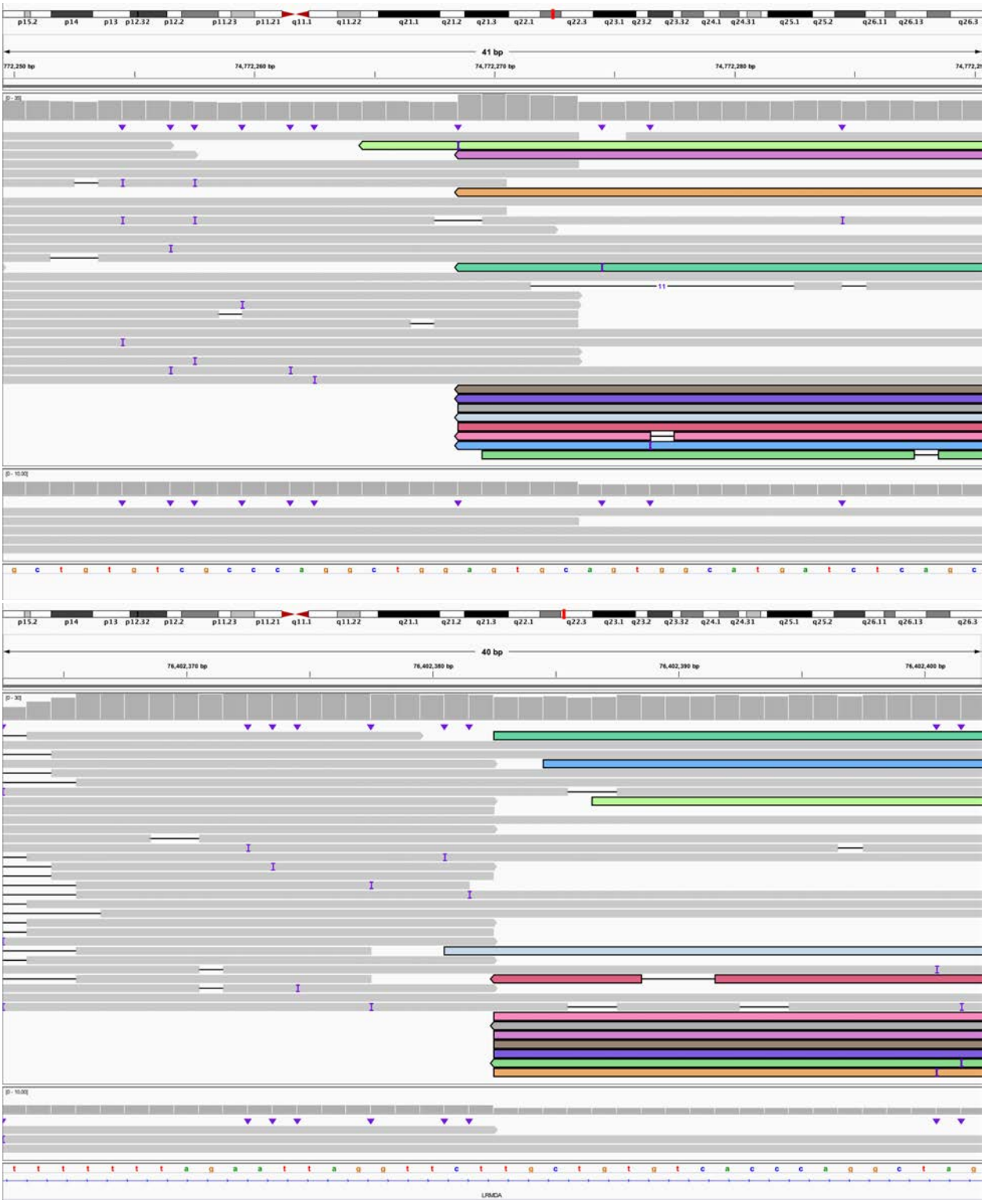

R. The 5' end of 10:M (IGV: chr10:74,772,250-74,772,290) is connected to the 5' end of 10:N and bisects *LRMDA* (IGV: chr10:76,402,363-76,402,402). This is the end of derivative chromosome 4.

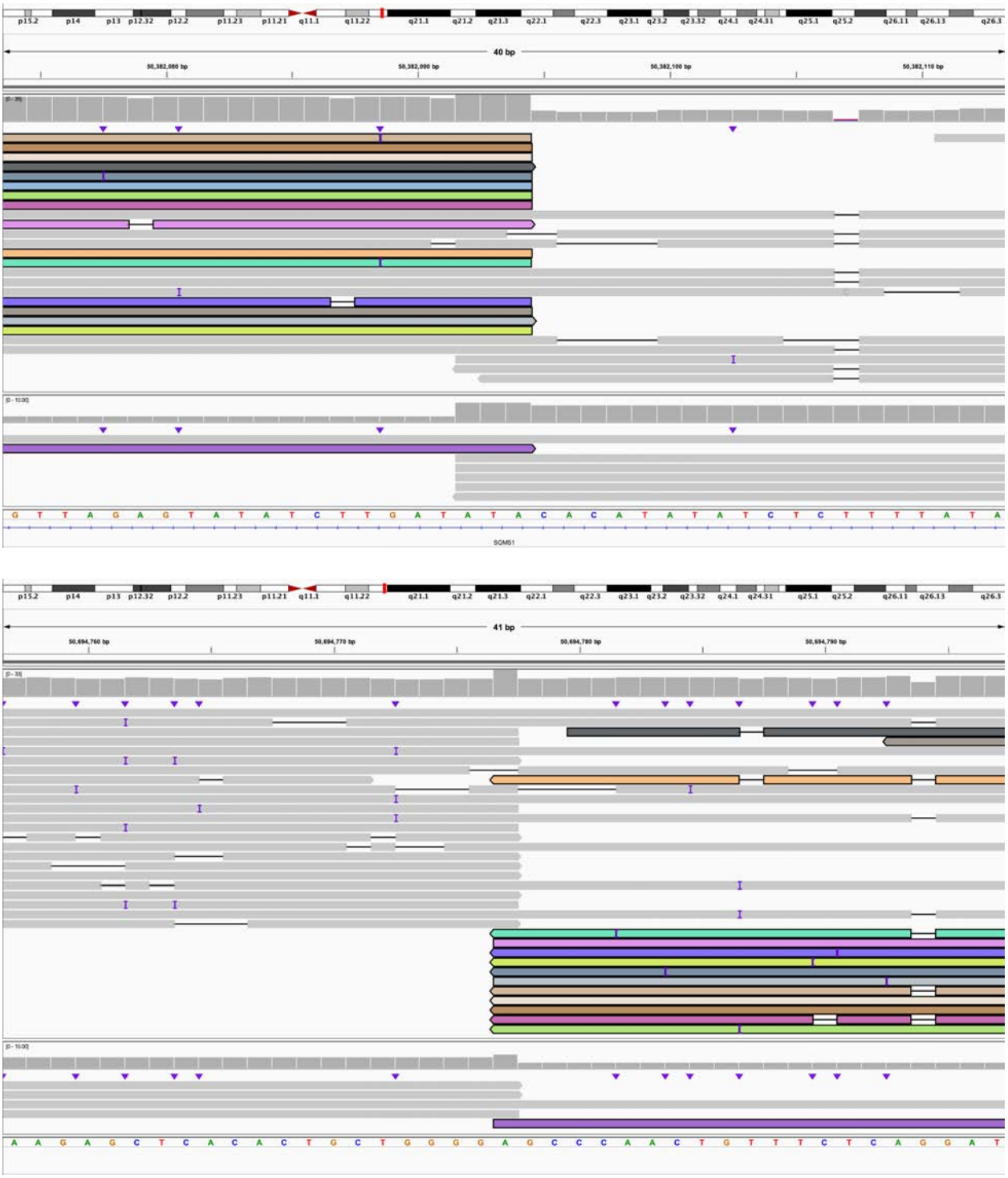

S. The 3' end of 10:A bisects *SGMS1* (IGV: chr10:50,382,074-50,382,113) and is connected to the 5' end of 10:D (IGV: chr10:50,694,757-50,694,797). This is the beginning of derivative chromosome 10.

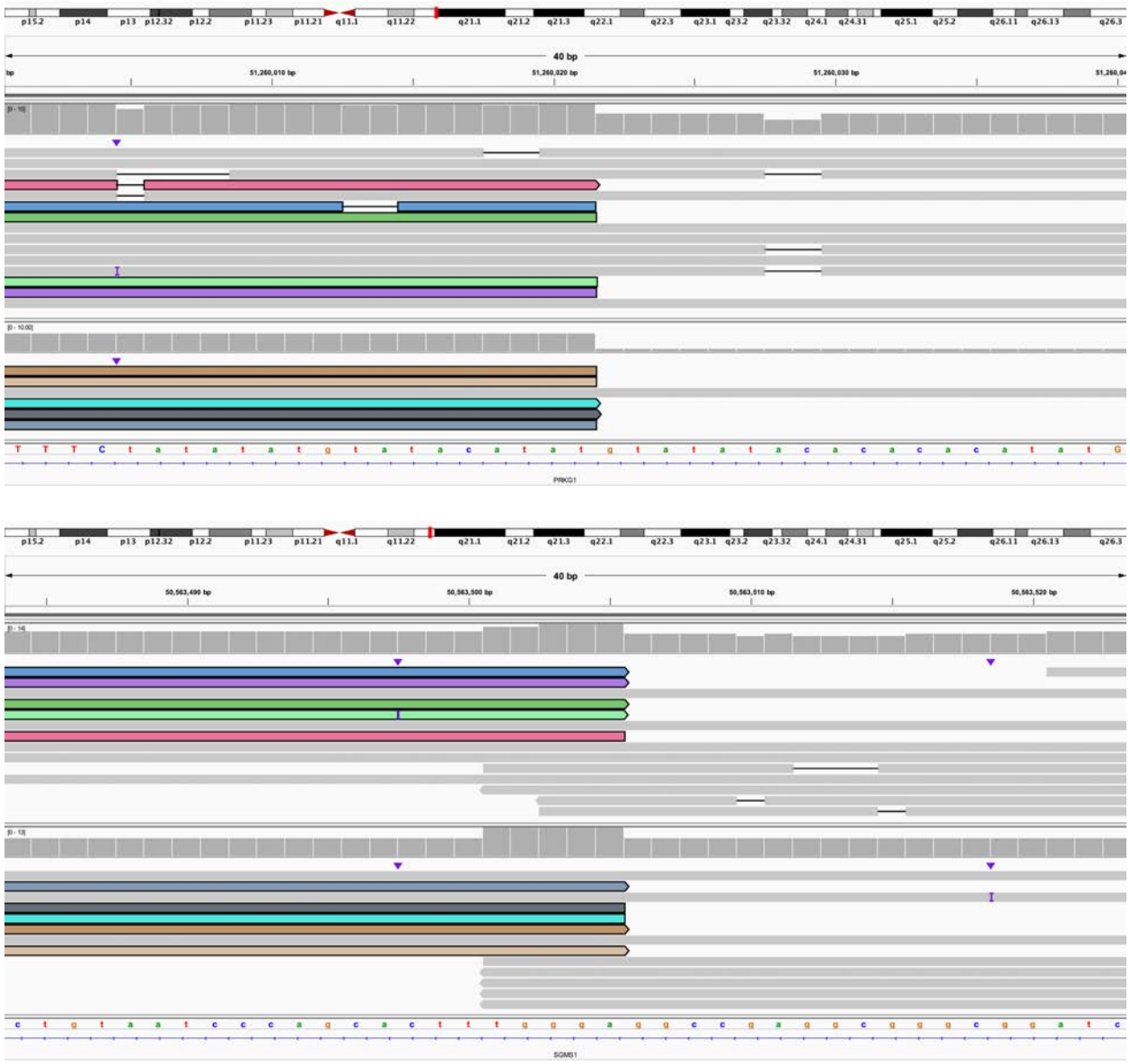

T. The 3' end of 10:D bisects *PRKG1* (IGV: chr10:51,260,001-51,260,040) and is connected to the 3' end of 10:B which bisects *SGMS1* (IGV: chr10:50,563,484-50,563,523). This is within derivative chromosome 10.

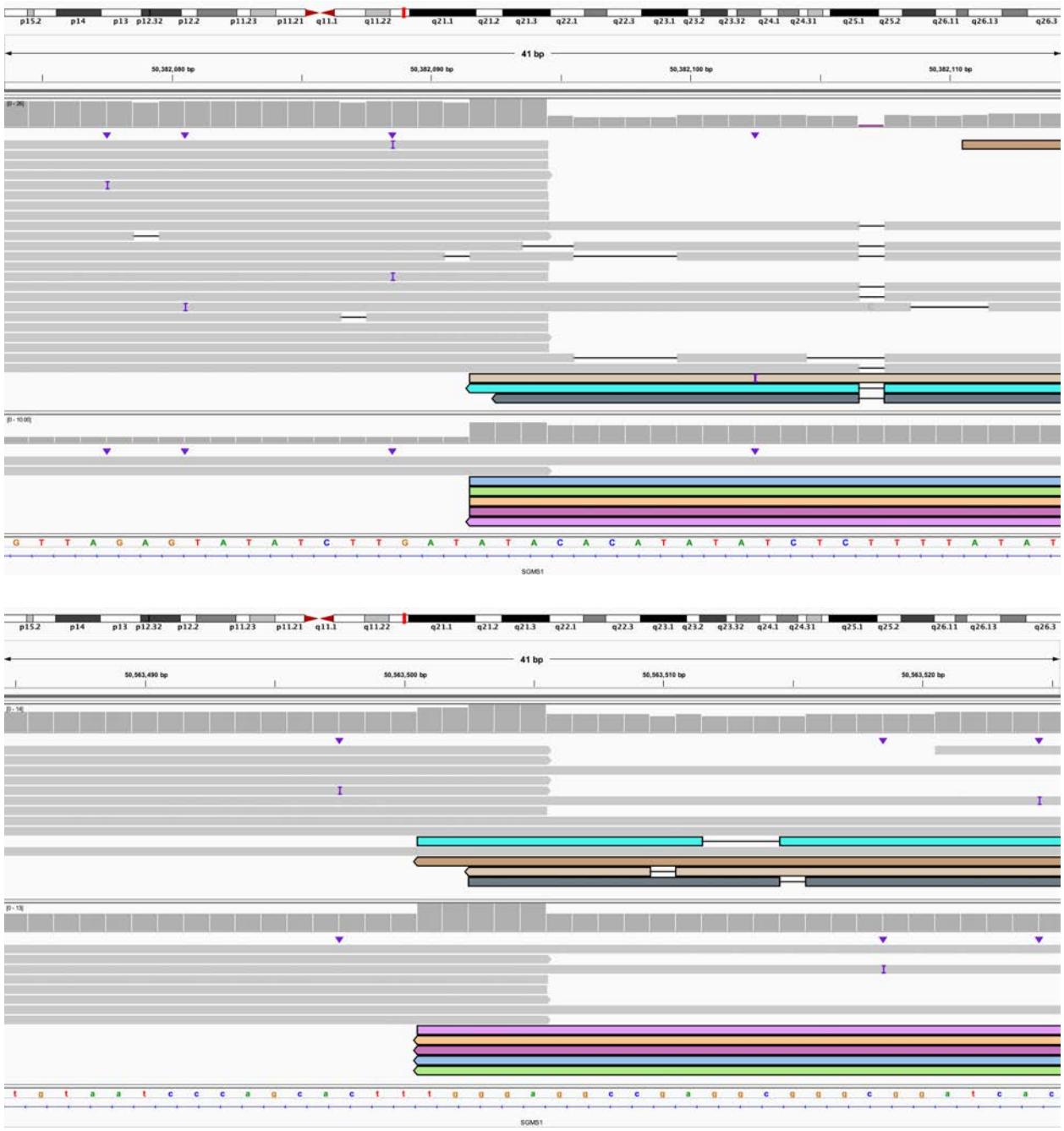

U. The 5' end of 10:B bisects *SGMS1* (IGV: chr10:50,382,074-50,382,114) and is connected to the 5' end of 10:C and bisects *SGMS1* (IGV: chr10:50,563,485-50,563,525). This is within derivative chromosome 10.

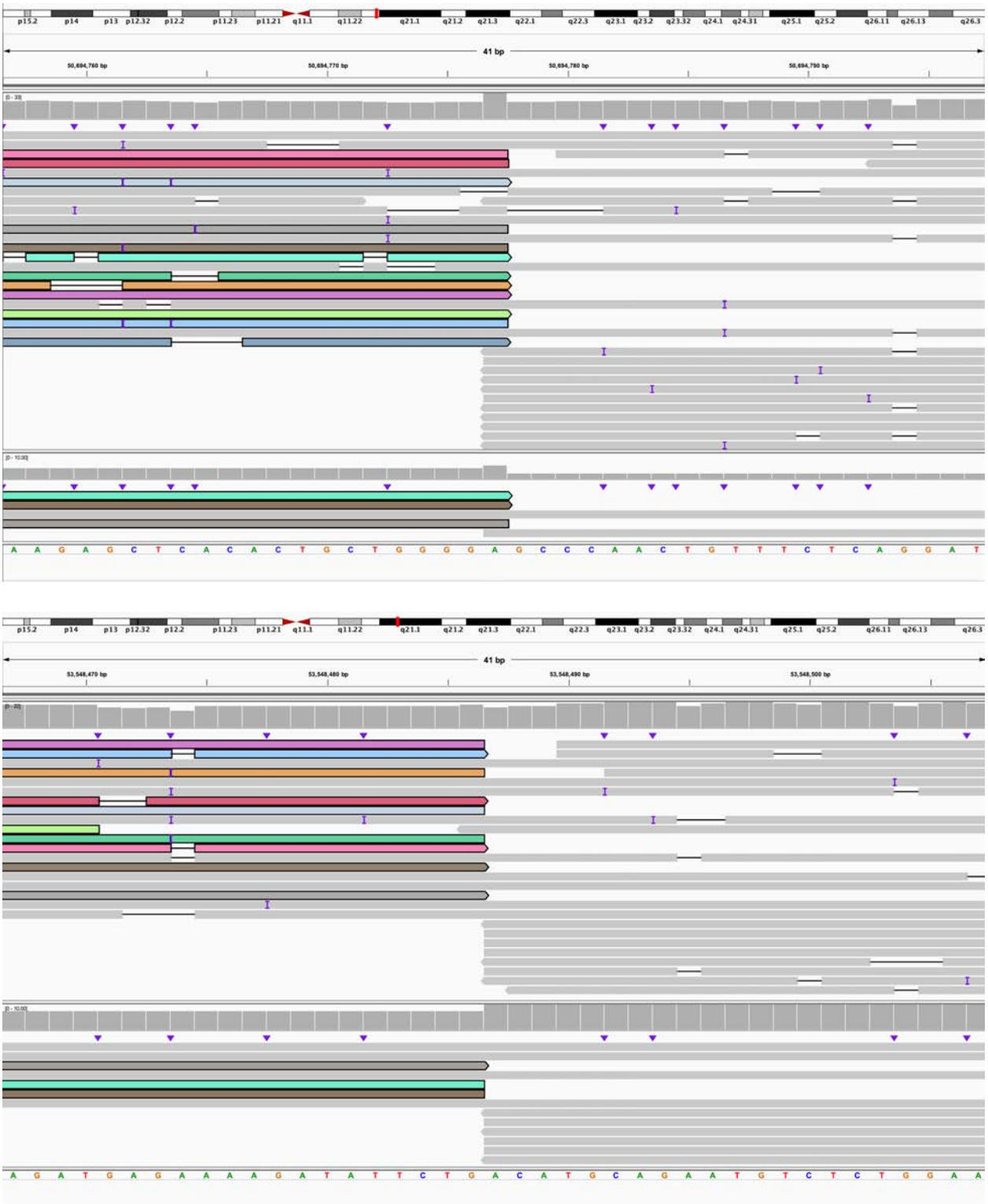

V. The 3' end of 10:C (IGV: chr10:50,694,757-50,694,797) is connected to the 3' end of 10:F (IGV: chr10:53,548,467-53,548,507). This is within derivative chromosome 10.

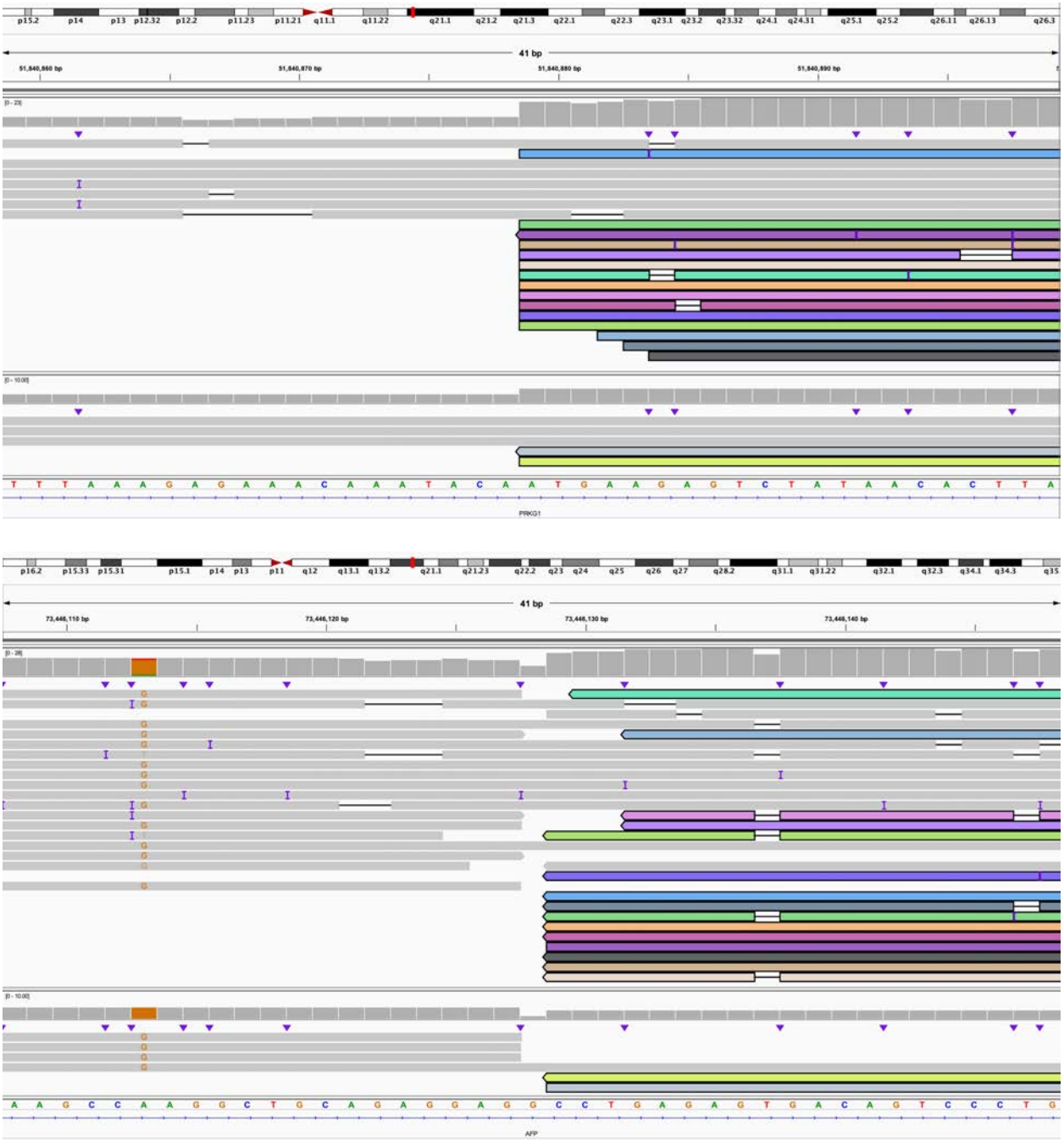

W. The 5' end of 10:F bisects *PRKG1* (IGV: chr10:51,840,859-51,840,899) and is connected to the 5' end of 4:F and bisects *AFP* (IGV: chr4:73,446,108-73,446,148). This is within derivative chromosome 10.

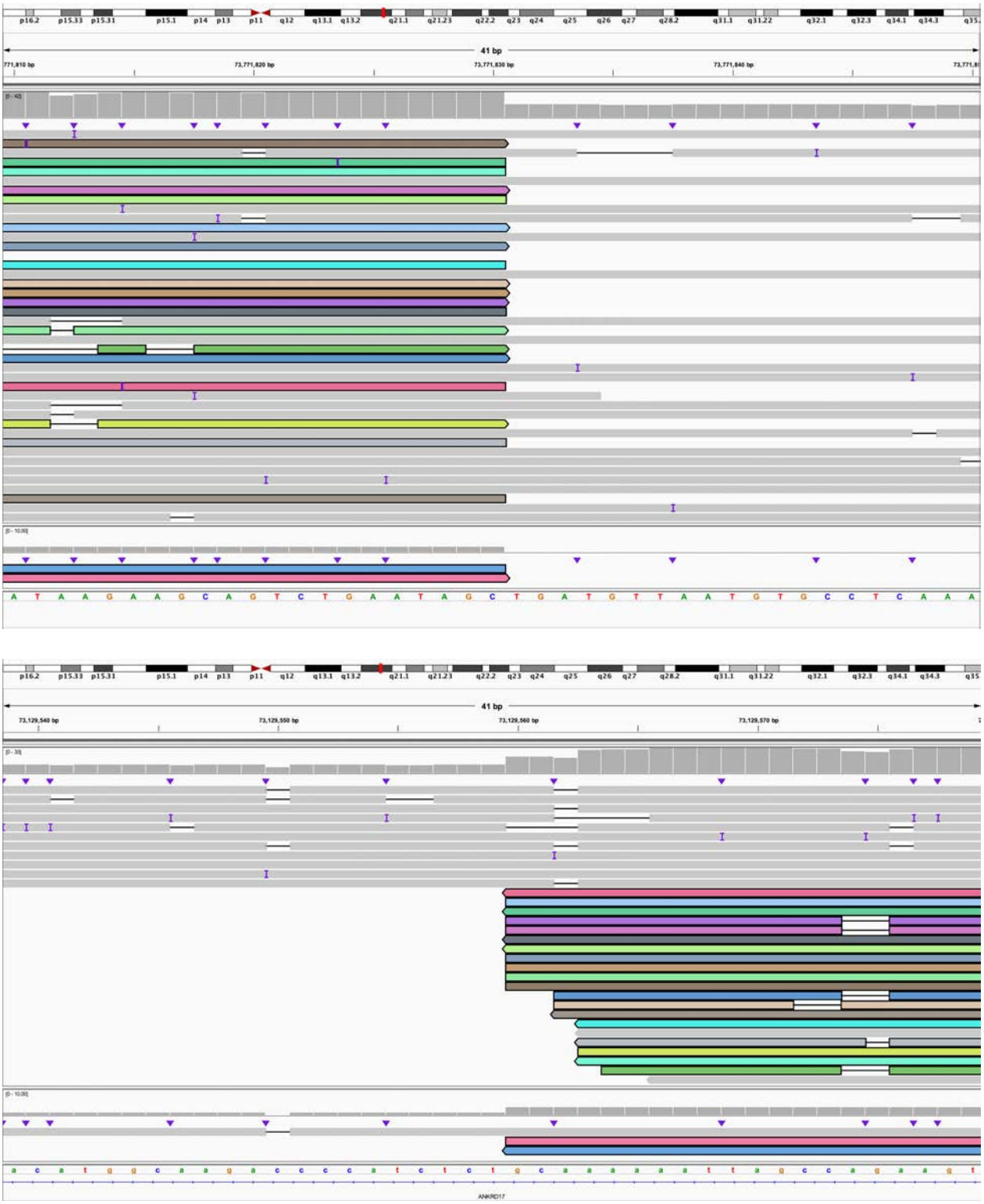

X. The 3' end of 4:F (IGV: chr4:73,771,810-73,771,850) is connected to the 5' end of 4:E which bisects *ANKRD17* (IGV: chr4:73,129,539-73,129,579). This is within derivative chromosome 10.

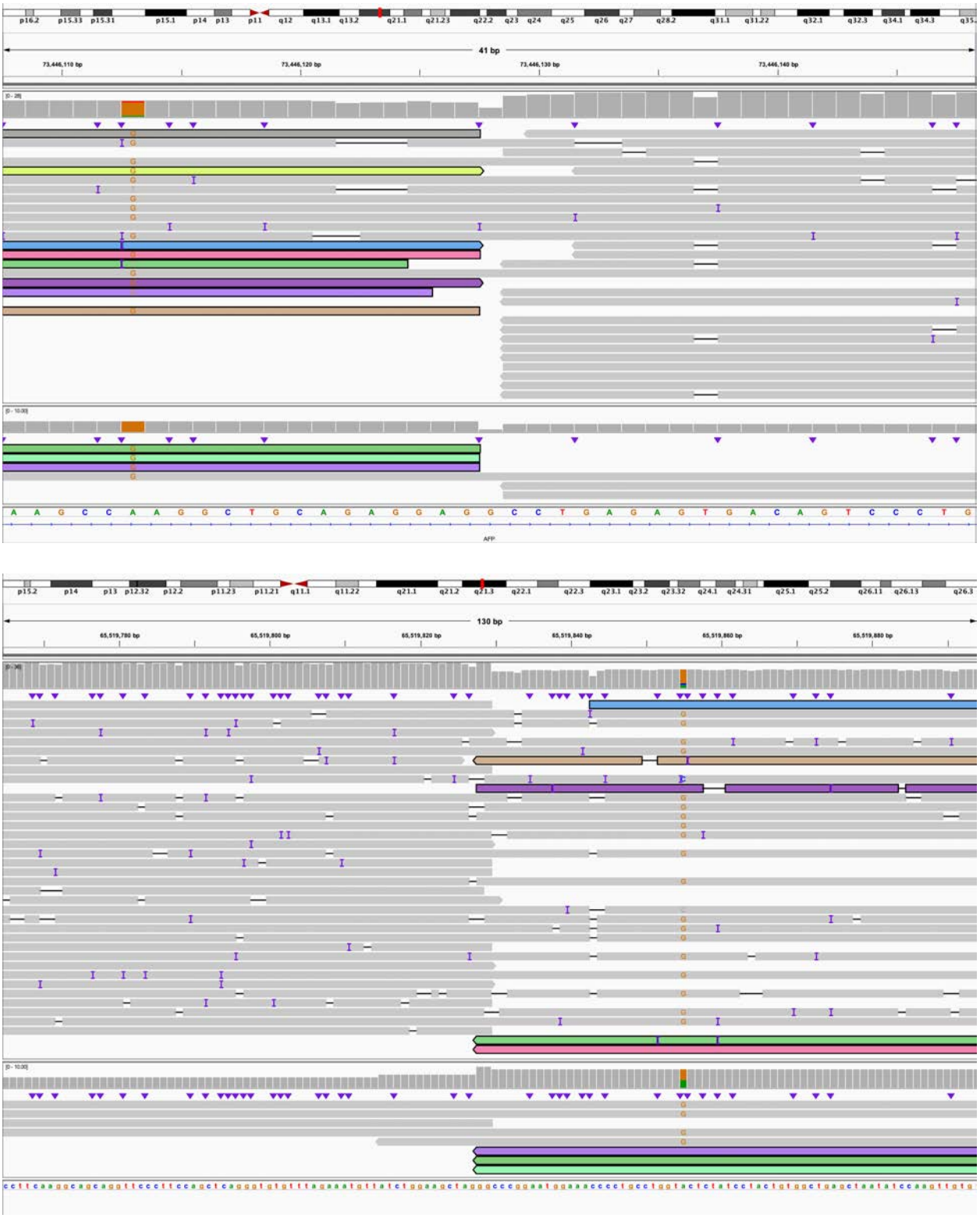

Y. The 3' end of 4:E bisects *AFP* (IGV: chr4:73,446,108-73,446,148) and is connected to the 5' end of 10:K (IGV: chr10:65,519,765-65,519,894). This is within derivative chromosome 10.

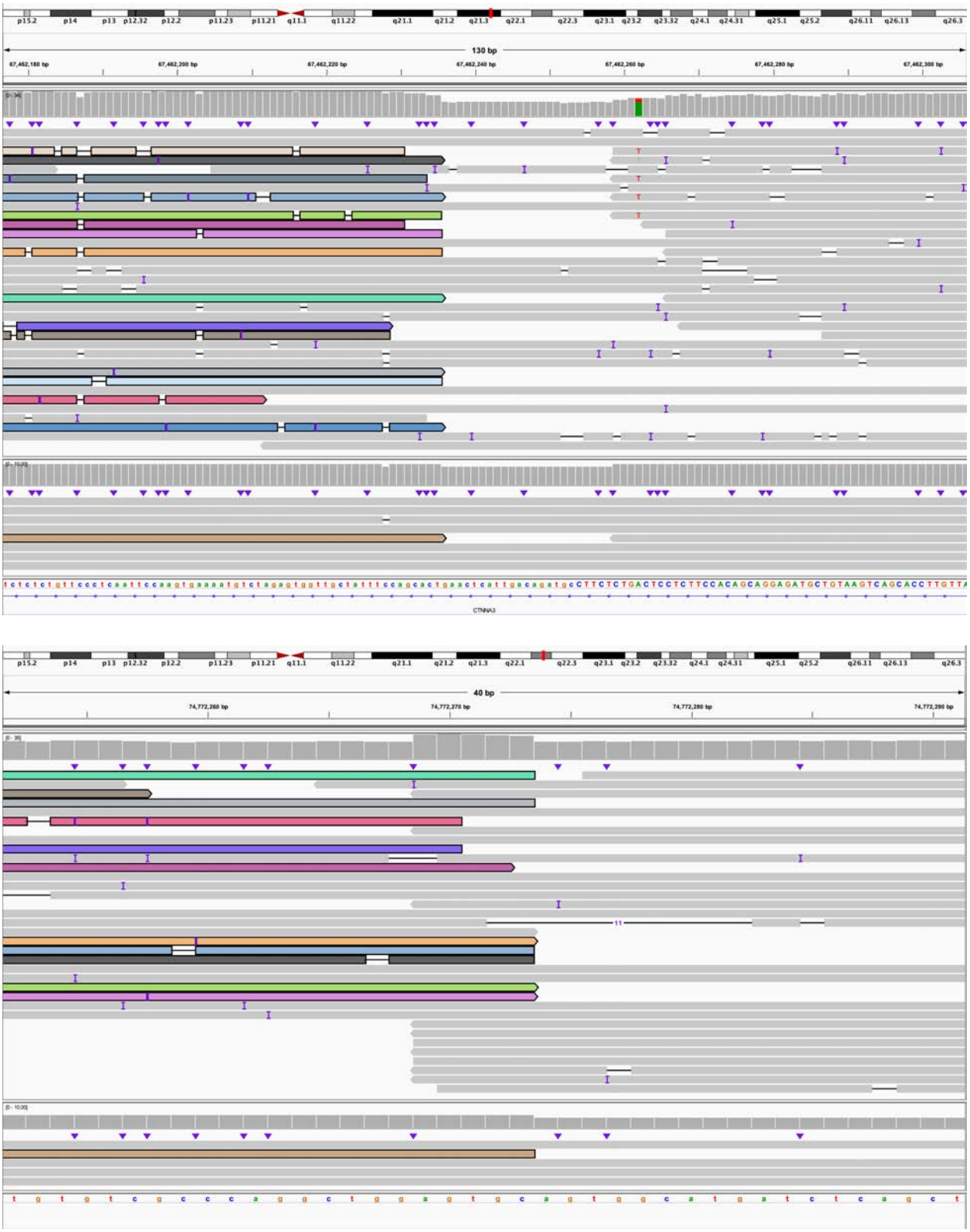

Z. The 3' end of 10:K bisects *CTNNA3* (IGV: chr10:67,462,177-67,462,306) and is connected to the 3' end of 10:L (IGV: chr10:74,772,252-74,772,291). This is within derivative chromosome 10.

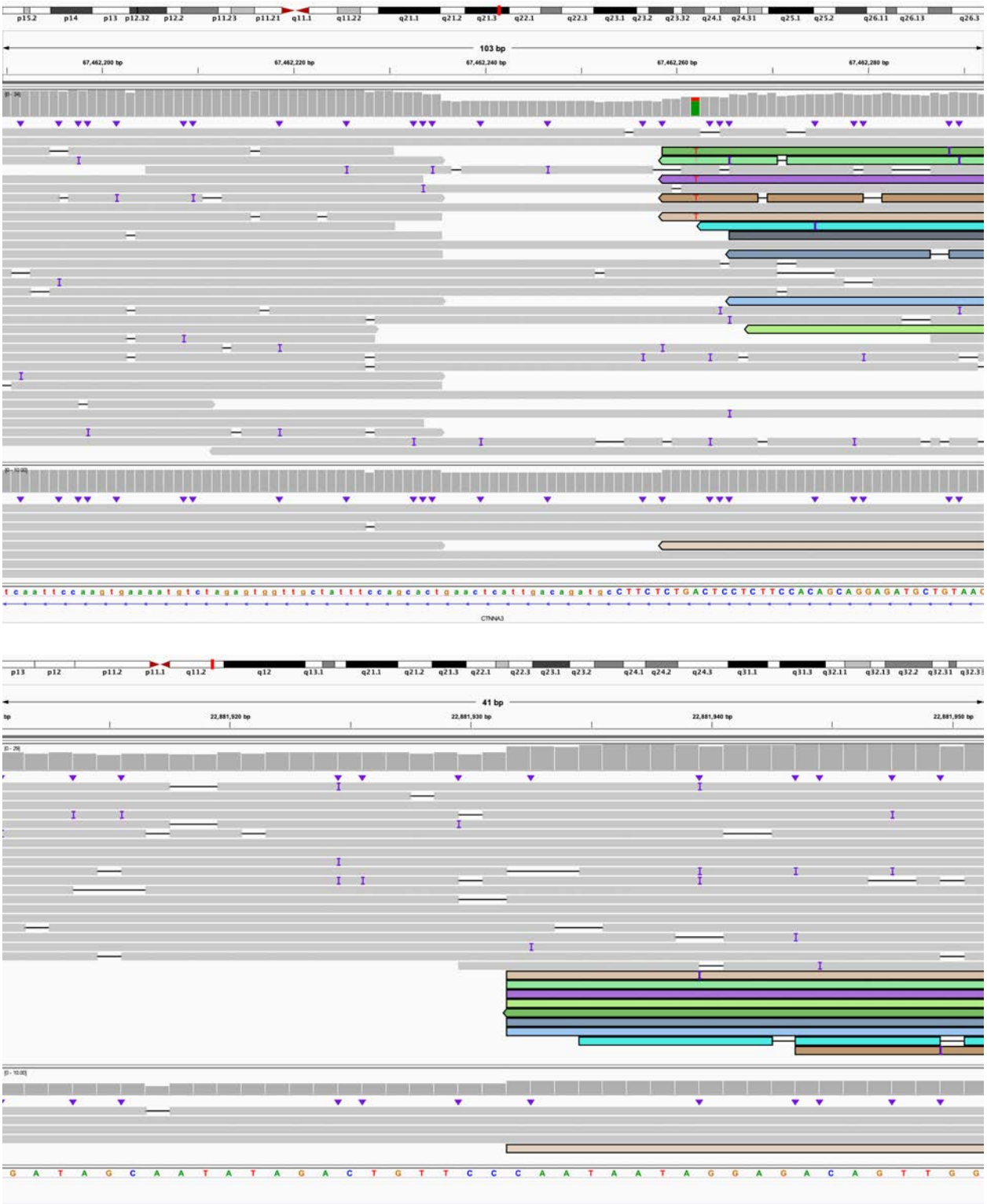

AA. The 5' end of 10:L bisects *CTNNA3* (IGV: chr10:67,462,190-67,462,292) and is connected to the 5' end of 14:C (IGV: chr14:22,881,911-22,881,951). This is the end of derivative chromosome 10.

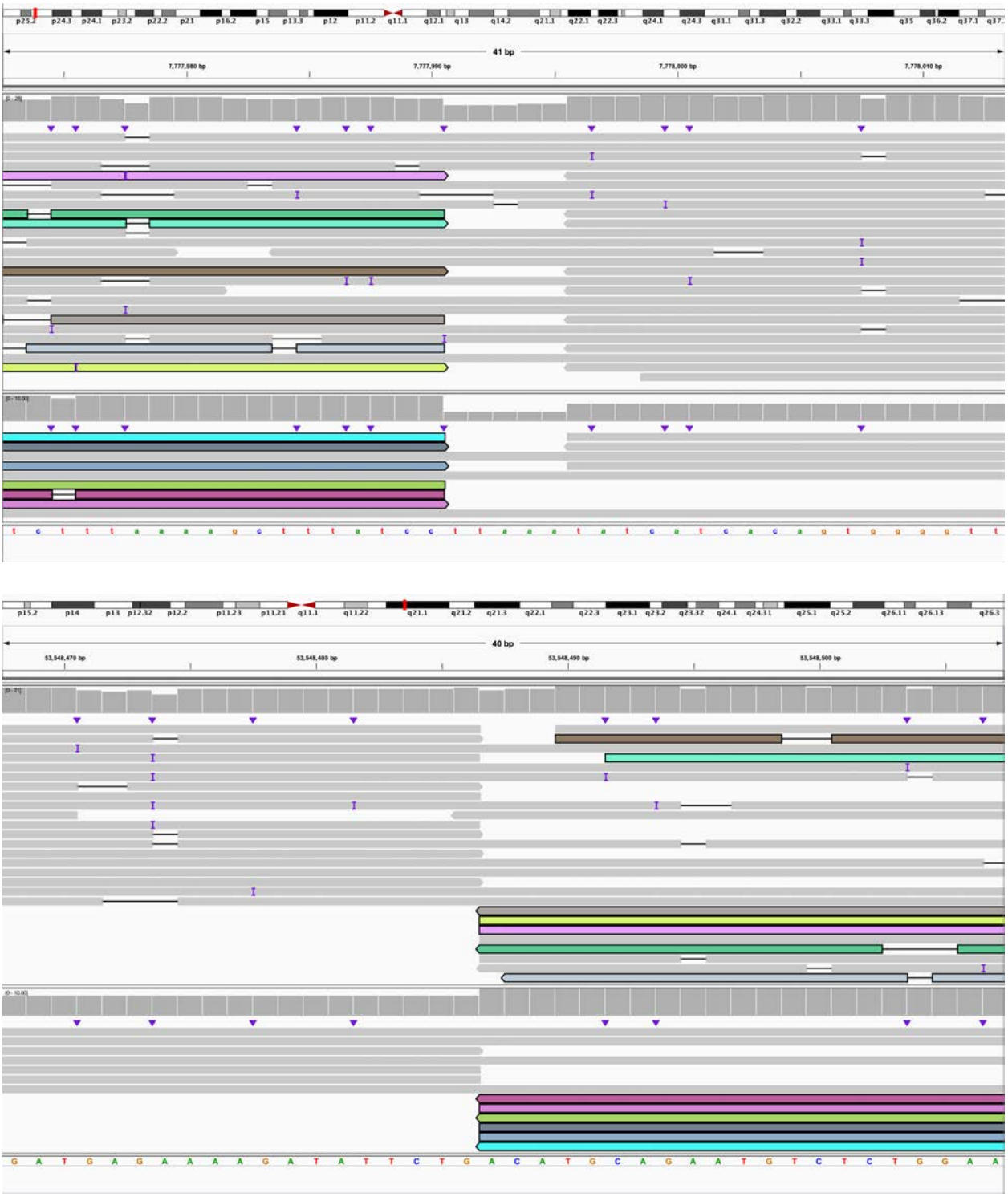

AB. The 3' end of 2:A (IGV chr2:7,777,973-7,778,013) is connected to the 5' end of 10:G (IGV chr10:53,548,468-53,548,507). This is the beginning of derivative chromosome 14.

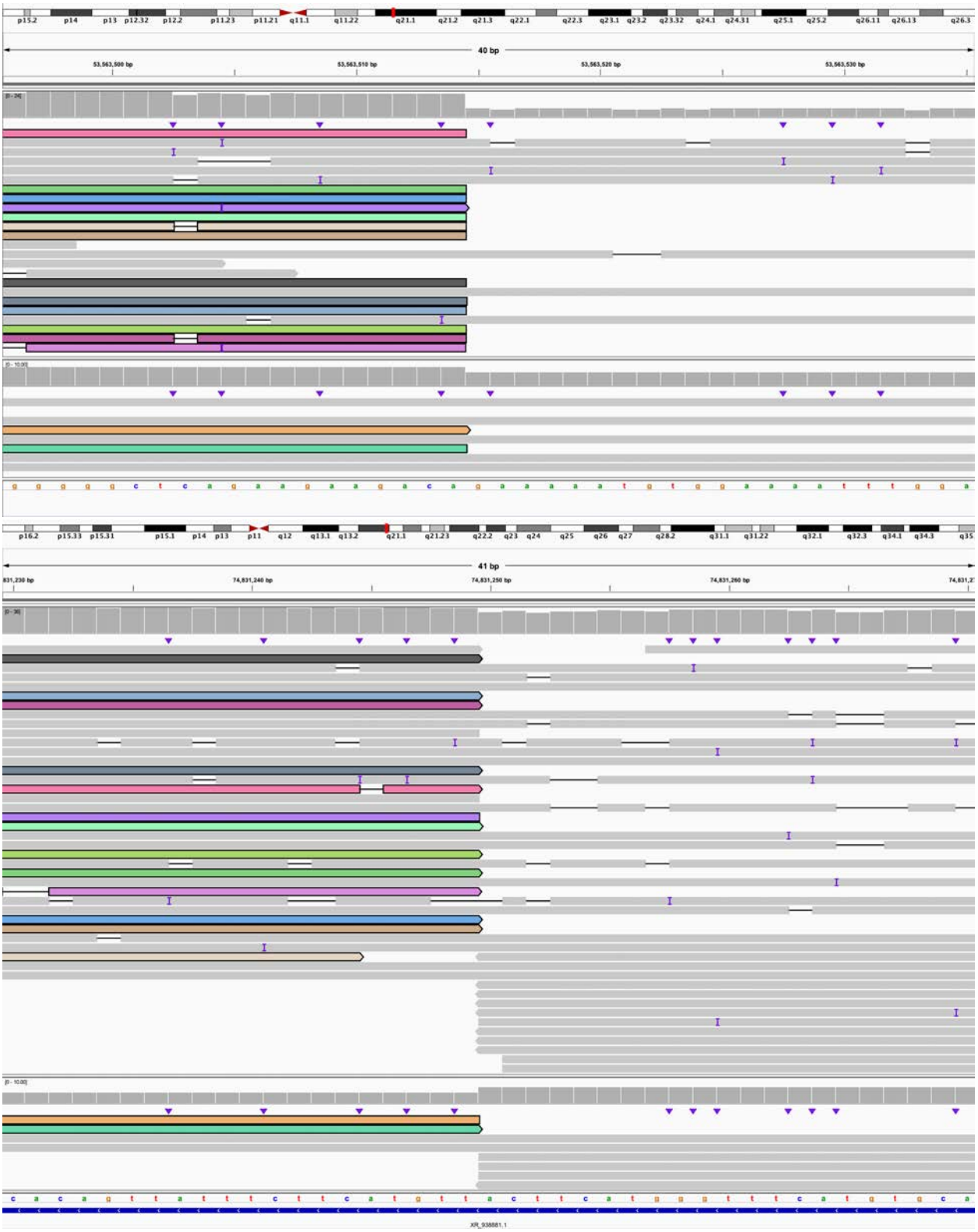

AC. The 3' end of 10:G (IGV: chr10:53,563,496-53,563,535) is connected to the 3' end of 4:I and bisects *XR_938881.1* (IGV: chr4:74,831,230-74,831,270). This is within derivative chromosome 14.

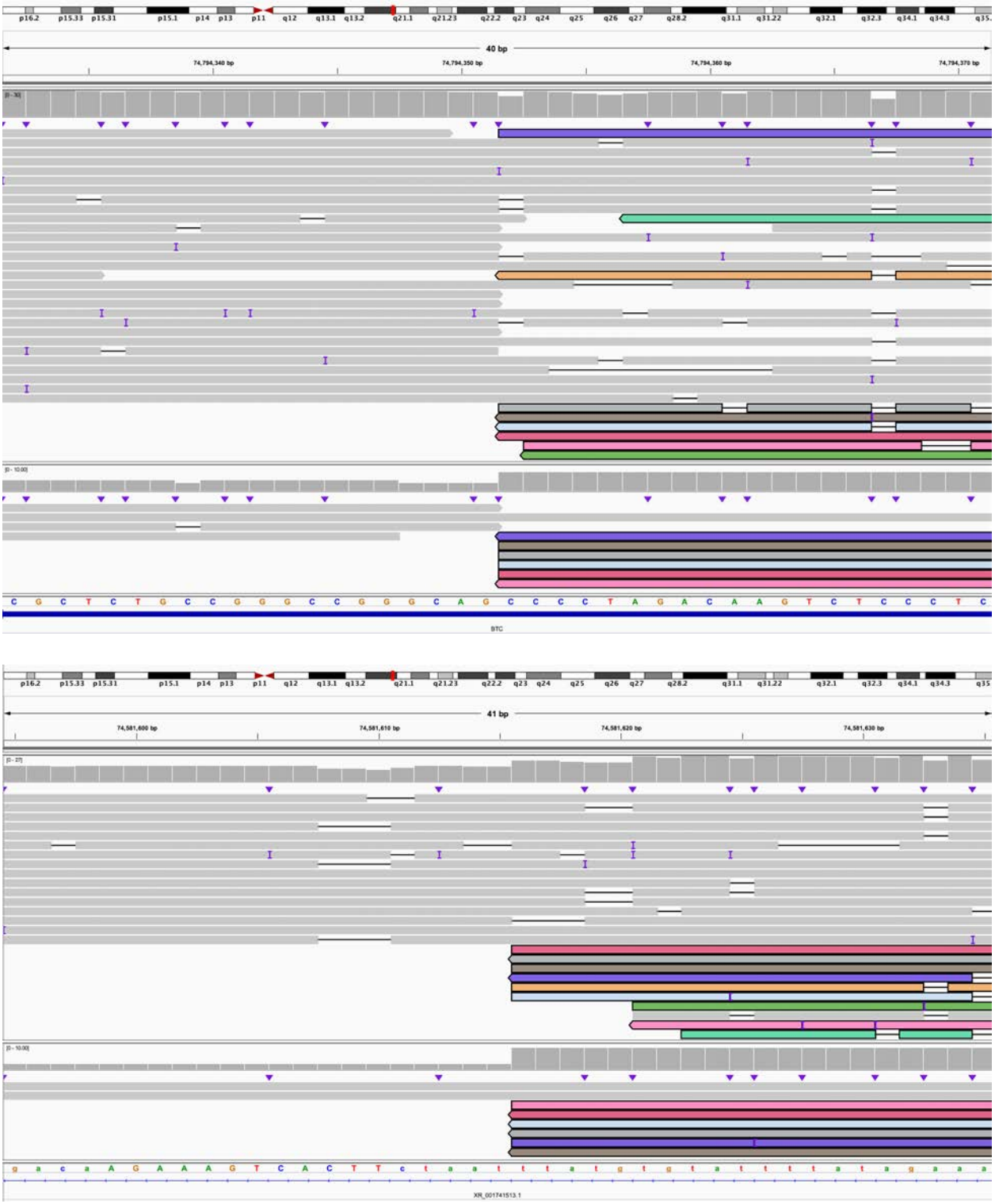

AD. The 5' end of 4:I bisects *BTC* (IGV: chr4:74,794,332-74,794,371) and is connected to the 5' end of 4:H and bisects *XR_001741513.1* (IGV: chr4:74,581,595-74,581,635). This is within derivative chromosome 14.

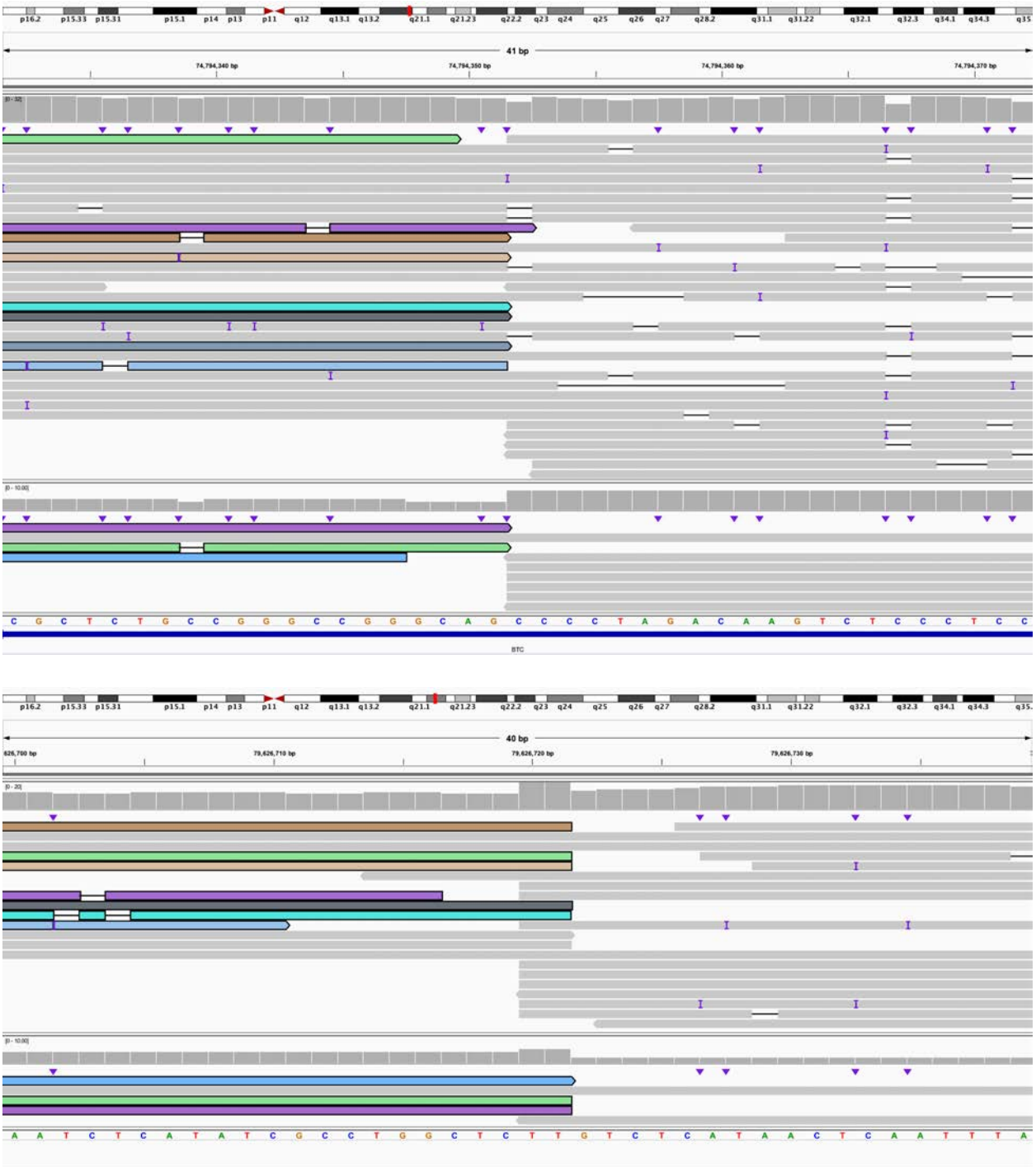

AE. The 3' end of 4:H bisects *BTC* (IGV: chr4:74,794,332-74,794,372) and is connected to the 3' end of 4:L (IGV: chr4:79,626,700-79,626,739). This is within derivative chromosome 14.

AF. The 5' end of 4:L bisects *SEPTIN1* (IGV: chr4:77,012,155-77,012,195) and connects to the 5' end of 4:C and bisects *CSN1S2BP* (IGV: chr4:70,140,480-70,140,520). This is within derivative chromosome 14.

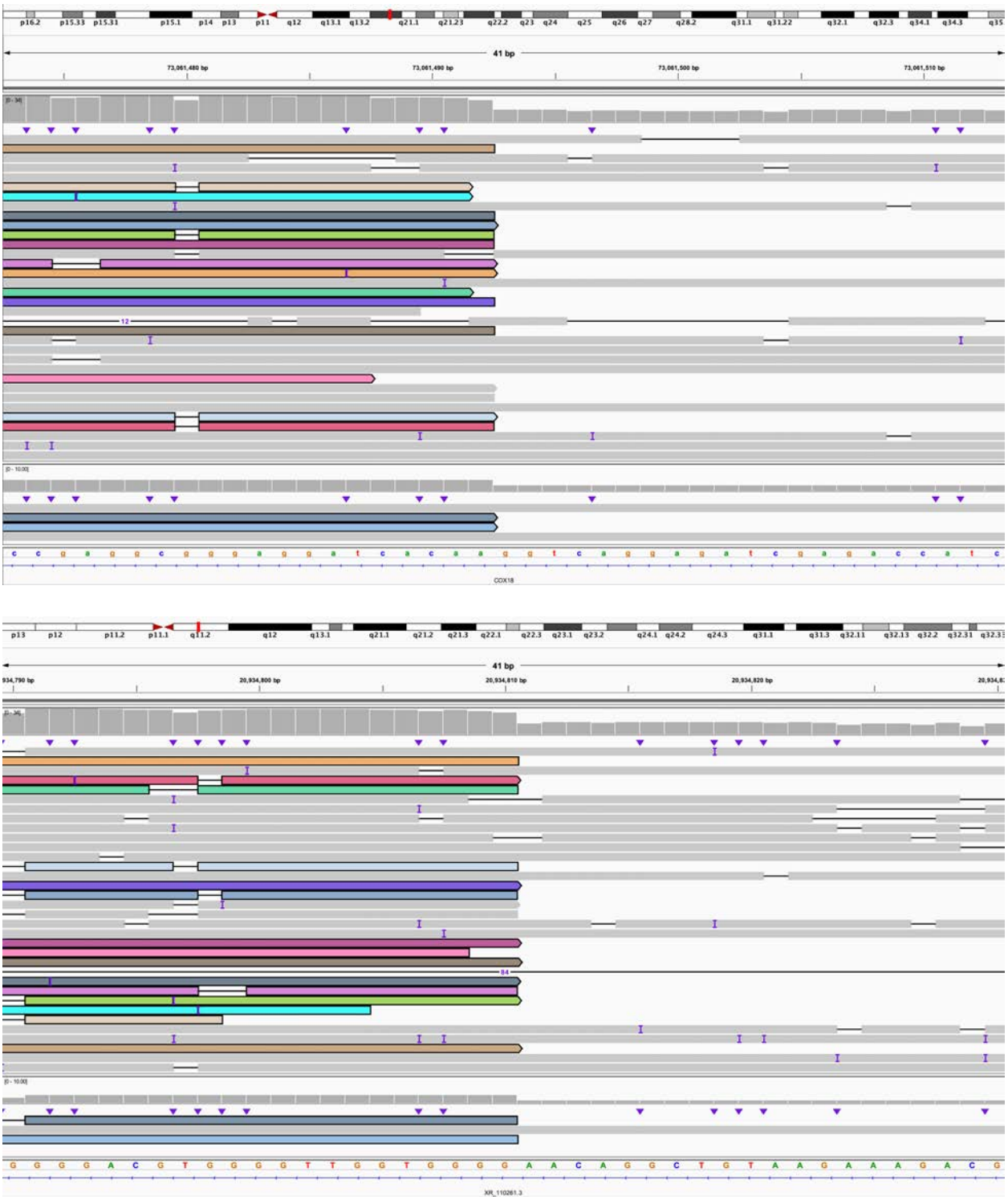

AG. The 3' end of 4:C bisects *COX18* (IGV: chr4:73,061,473-73,061,513) and is connected to the 3' end of 14:A and bisects *XR_110261.3* (IGV: chr14:20,934,790-20,934,830). This is the end of derivative chromosome 14.

Figure S26. S021, mosaic loss of 8p and mosaic gain of 8q.

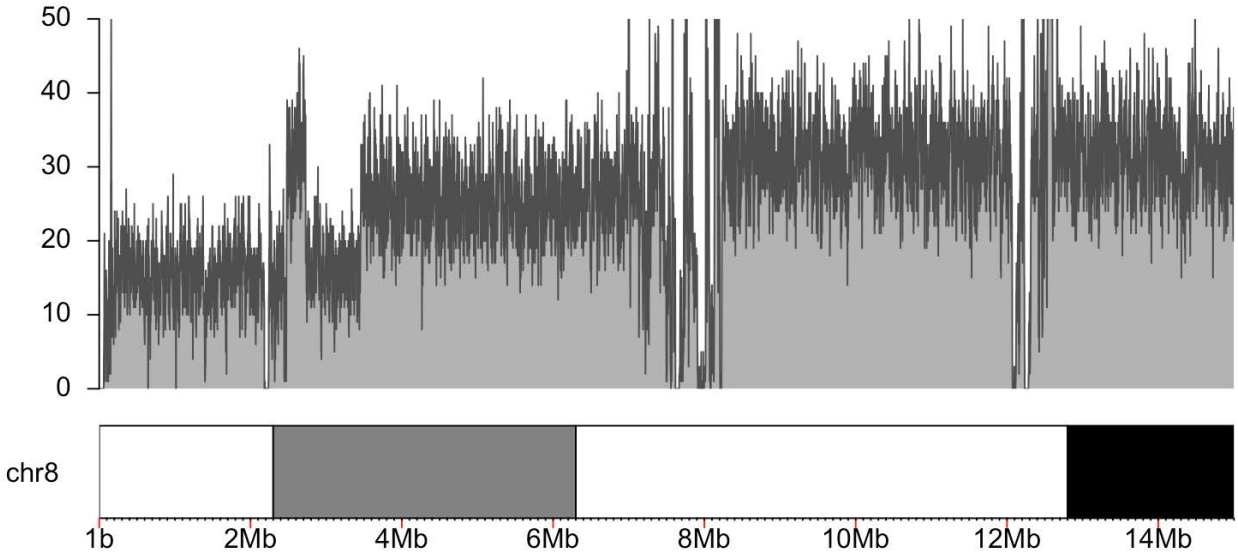

A. Coverage of chr8:1-15,000,000. This demonstrates the presence of a deletion of one chromosome from the telomere to 3,458,035. Also apparent is the mosaic region between 3,469,752 and 7,186,524, then the normal copy state after the defensin locus. The duplication around 2 Mbp is frequently observed in SNP array studies and is often not reported on the array as it is considered benign (see panels B–D for details).

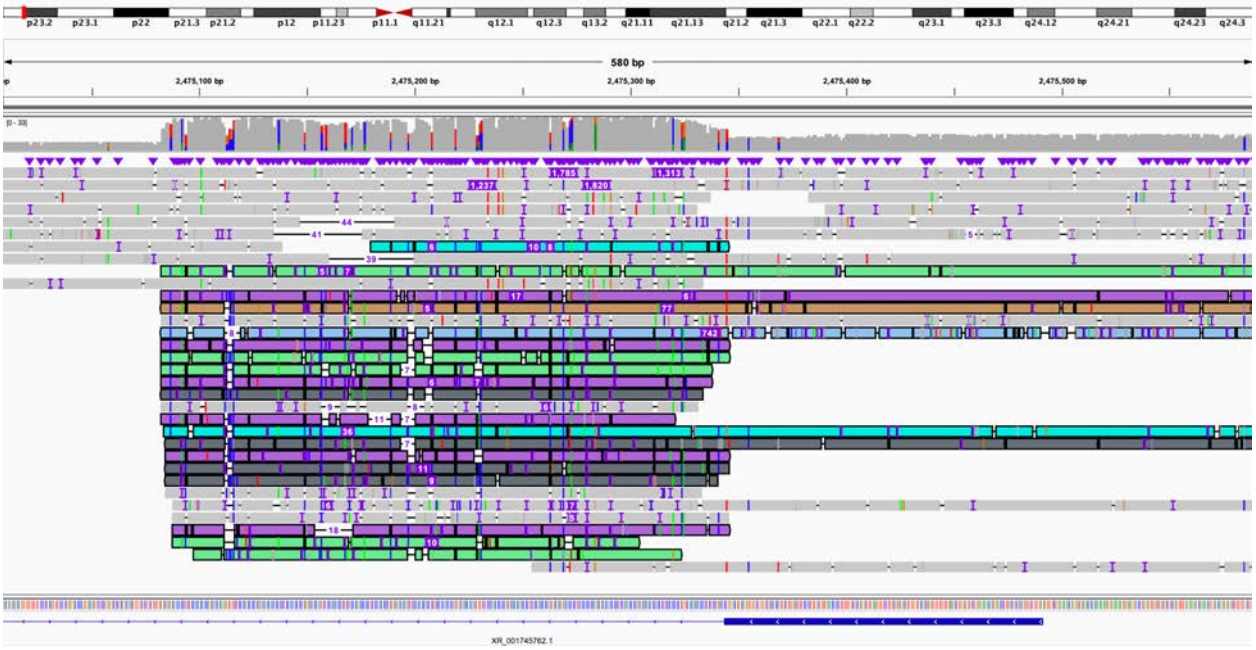

B. The 5' end of the duplication observed in the coverage plot in A begins at approximately chr8:2,475,083, within a VNTR. Read color shows that reads were split and re-aligned to the repetitive region. IGV view is of chr8:2,475,009-2,475,591.

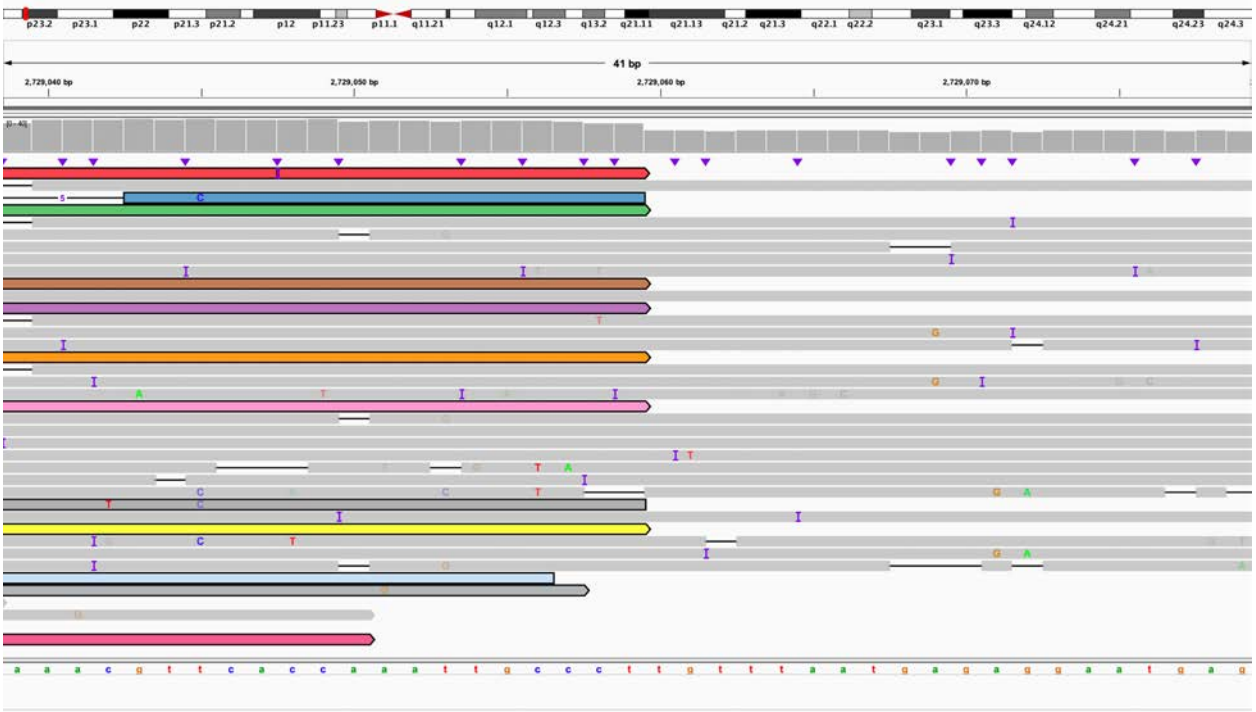

C. The 3' end of the duplication observed in A ends at chr8:2,729,059, meaning the duplication is approximately 254 kbp. IGV view is of chr8:2,729,039-2,729,079. Reads are linked to those shown in panel D and color is consistent between the two.

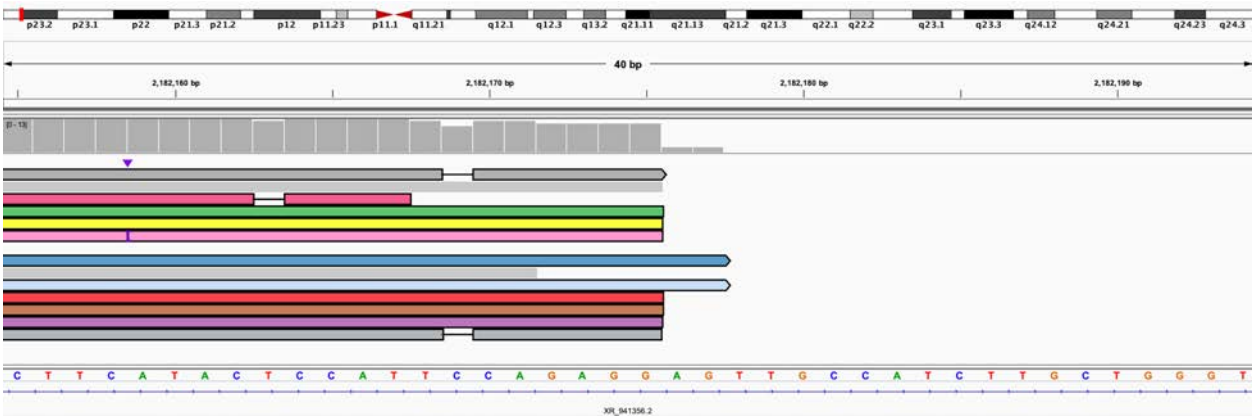

D. Reads from the 3' end of the duplication shown in C link to the beginning of a deletion on chr8 at chr8:2,182,175. The orientation of the reads suggests that the duplication is inverted. IGV view is of chr8:2,182,155-2,182,194.

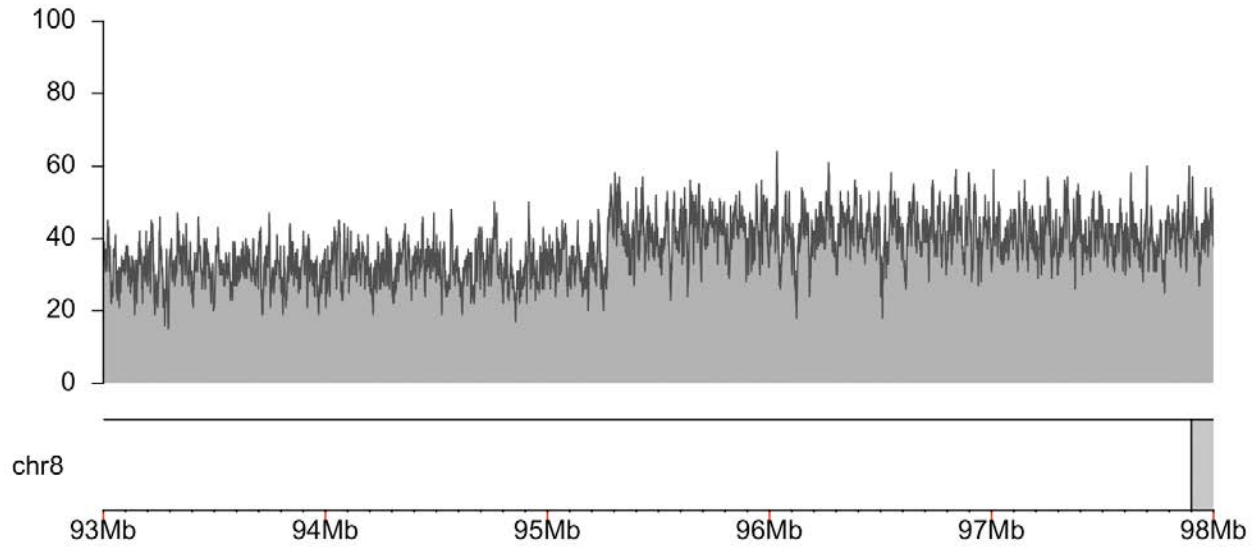

E: Coverage of chr8:93,000,000-98,000,000 demonstrating the increase of copy state from 2 to 3 observed on array at 95,270,423. No definitive breakpoint could be identified in the long-read data.

Figure S27. S022, focal amplification of 4q with adjacent region of homozygosity, duplication of 15q11.2.

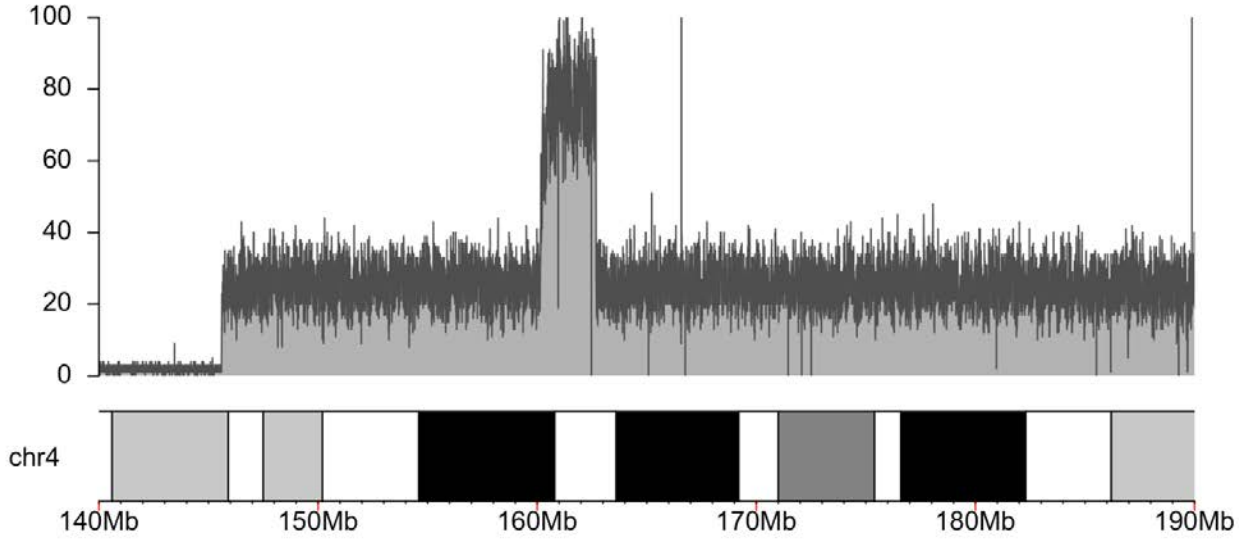

A. Coverage of the 4q target region shows the presence of an amplification.

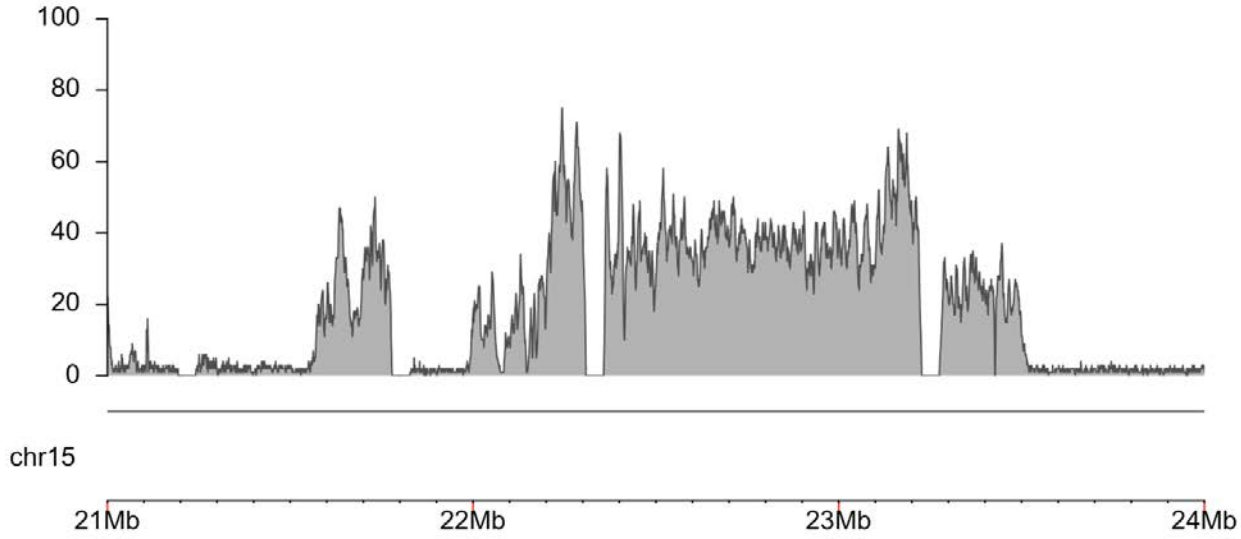

B. Coverage of 15q11.2 target region, regions with no coverage represent regions of the reference genome denoted as 'N'.

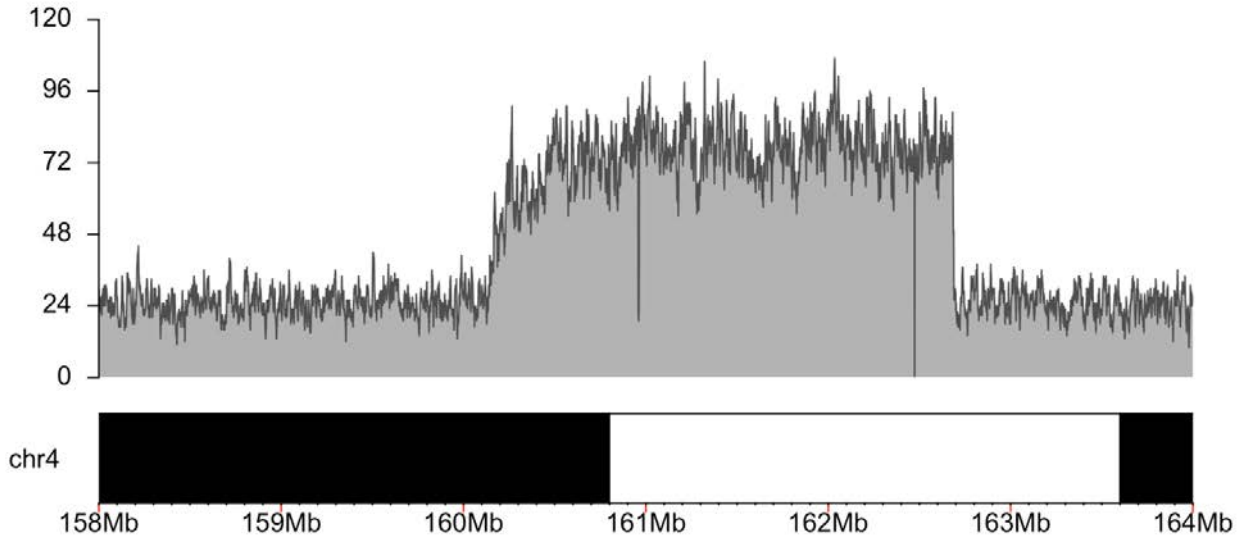

C. Coverage of the focal amplification of 4q.

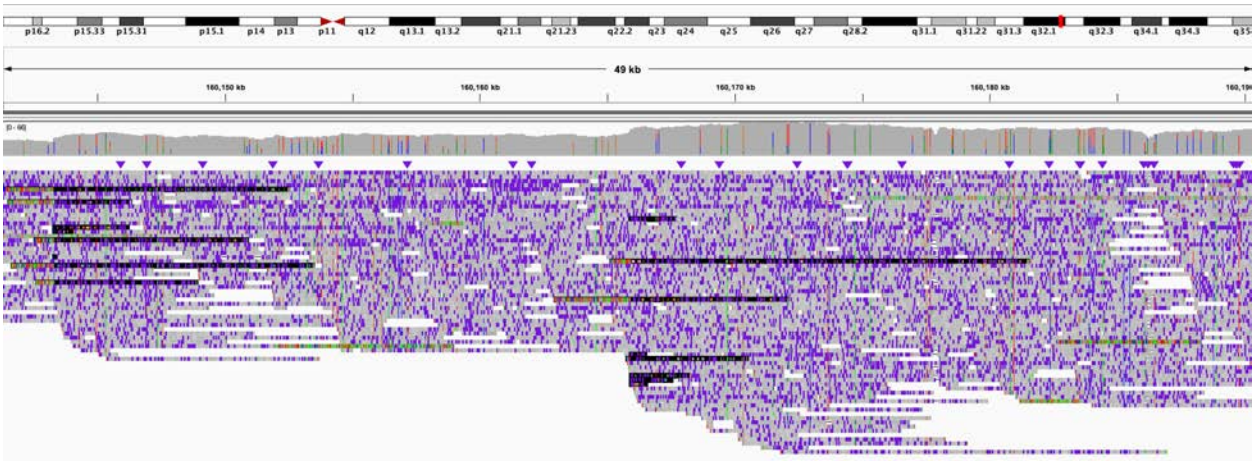

D. View of the beginning of the focal amplification of 4q, this is the centromere-proximal side and includes the second increase in coverage. Within this region, copy number estimate increases from 2x to 4x in a stepwise fashion (Table S9). Reads that span both breakpoints are highlighted. IGV view is of chr4:160,141,260-160,190,550.

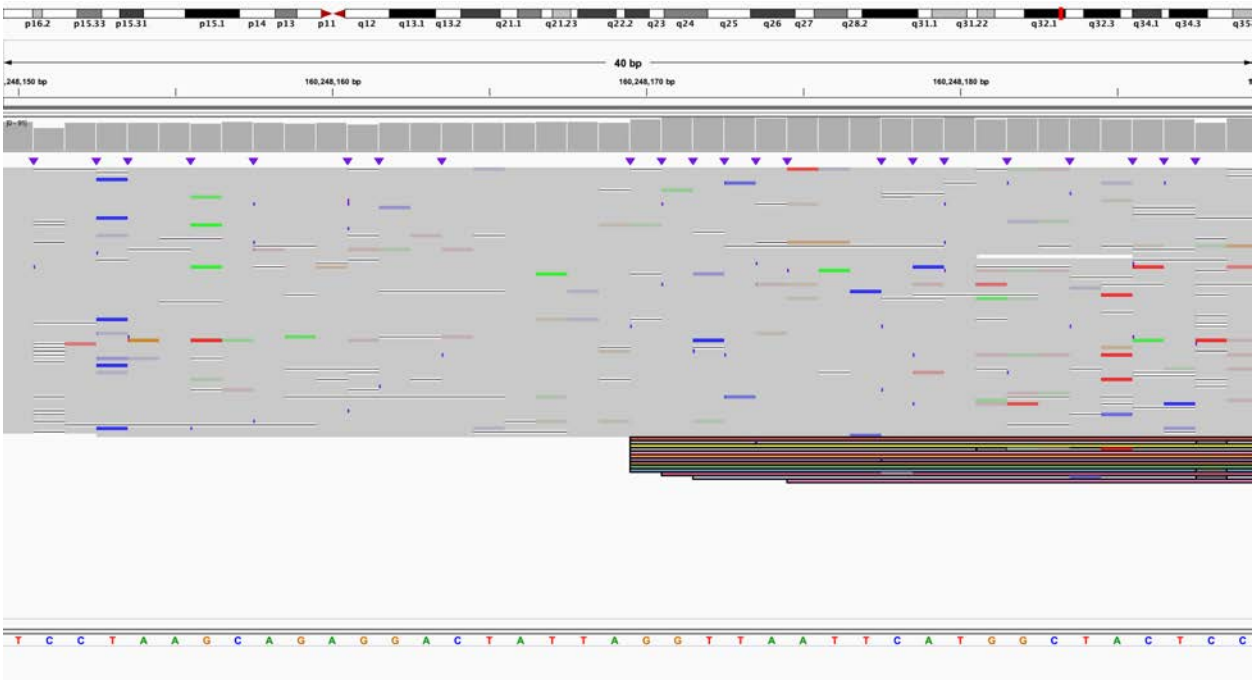

E. View of the third centromere-proximal breakpoint and amplification. Copy number estimate in this region increases from 4x to 5x (Table S9). IGV view is of chr4:160,248,150-160,248,189.

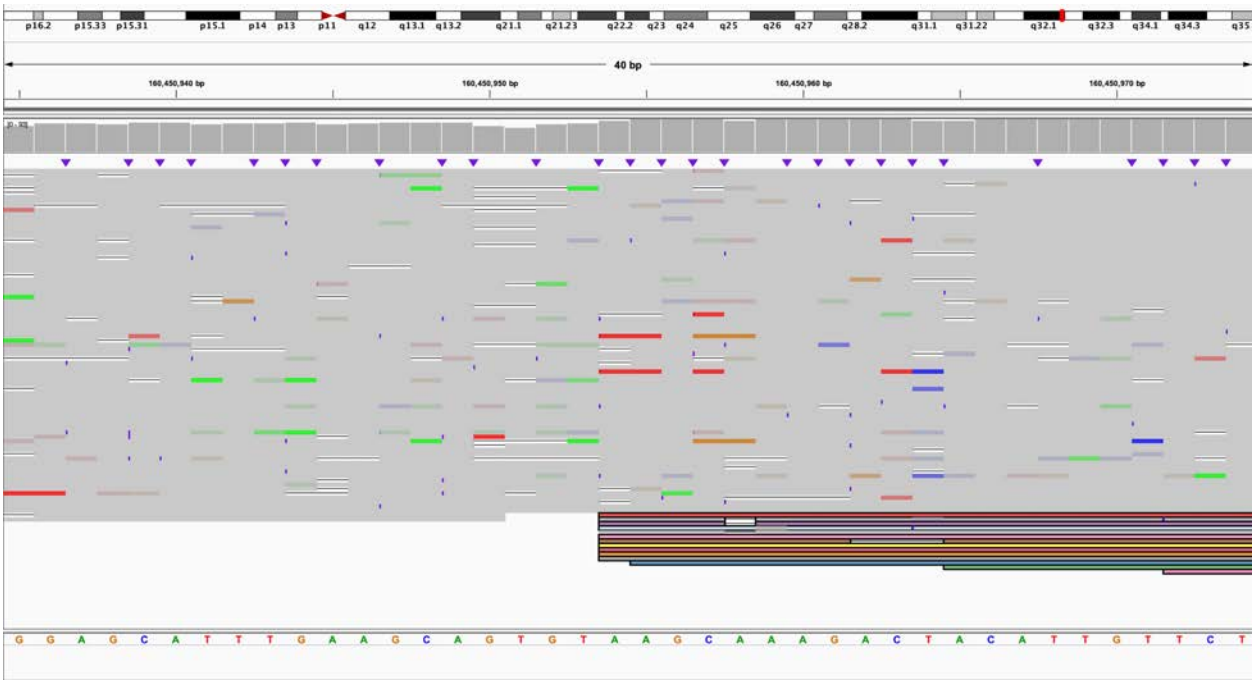

F. View of the fourth centromere-proximal breakpoint and amplification. Copy number estimate increases from 5x to 6x in this region (Table S9). IGV view is of chr4:160,450,935-160,450,974.

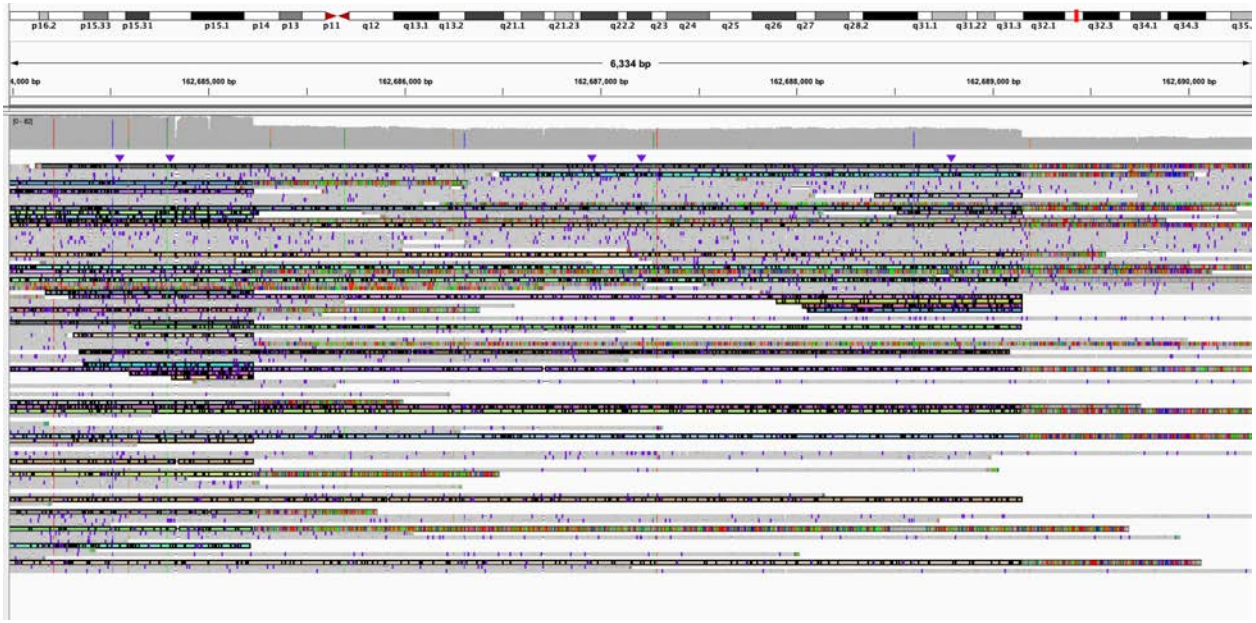

G. View of the telomere-proximal region of the focal amplification of 4q. Reads that span both breakpoints are highlighted. Copy number estimate decreases from 6x to 4x, then from 4x to 2x over a 3,920 bp interval (Table S9). IGV view is of chr4:162,683,982-162,690,349.

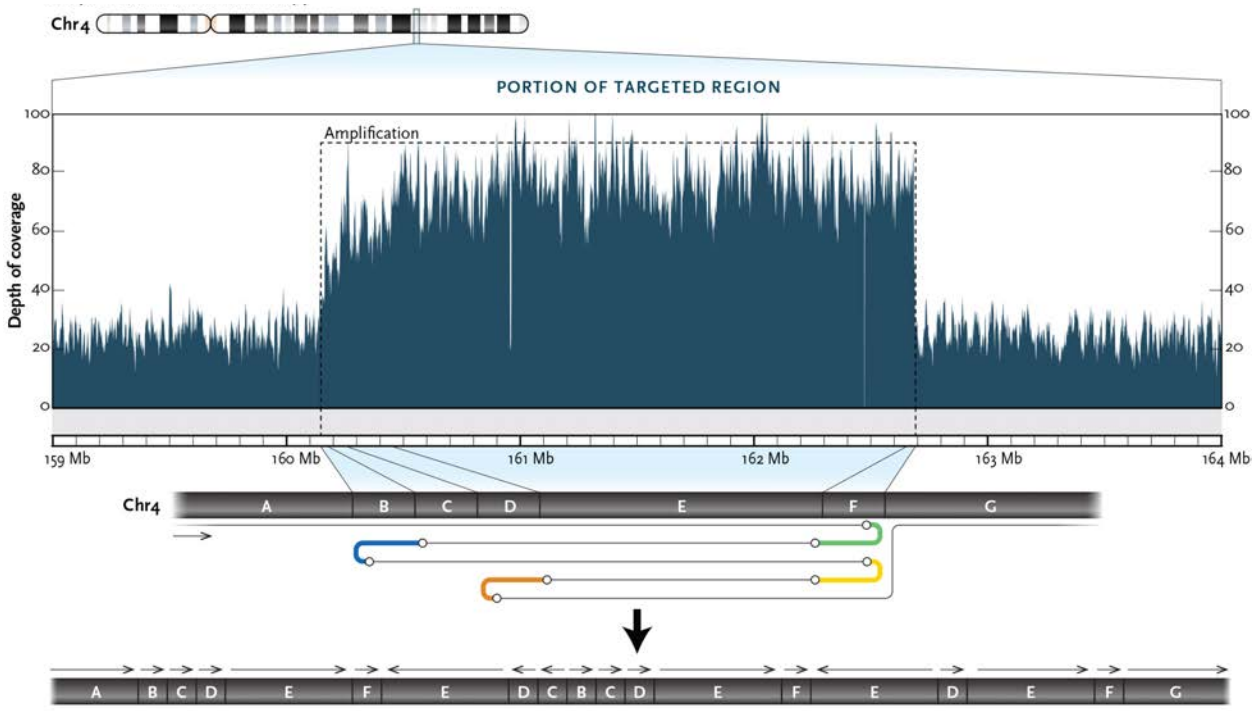

H. Estimate of the possible structure of the 4q amplification. We were not able to determine the exact order in which segments were duplicated. A possible arrangement of the region is shown based on this estimate.

Figure S28. S035, duplications of 8q24 and 16p13.11 identified by clinical testing.

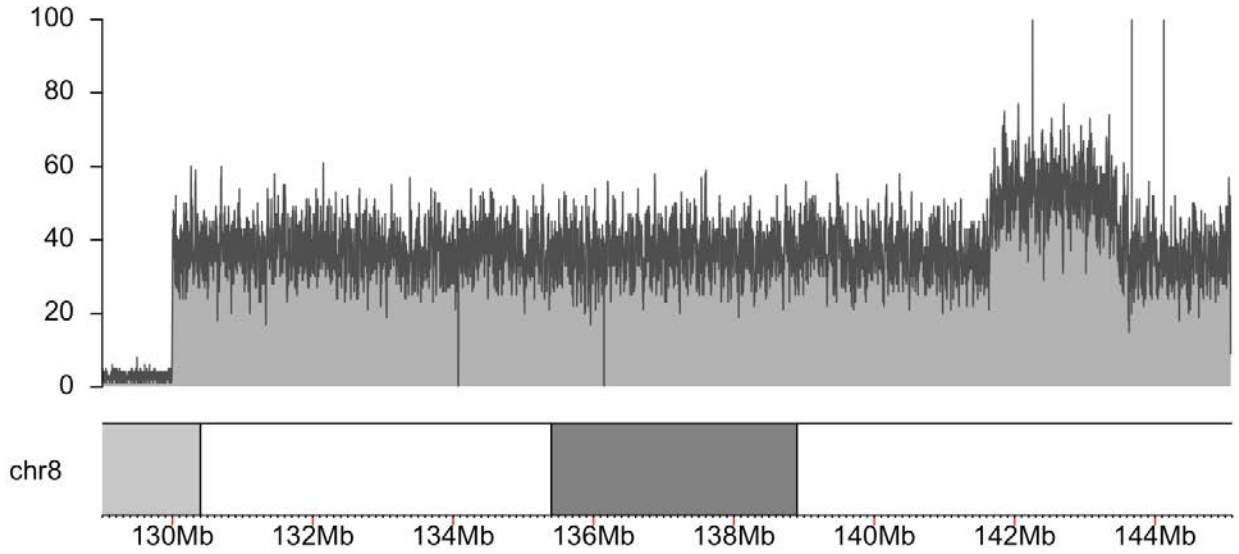

A. Coverage of chromosome 8 target region.

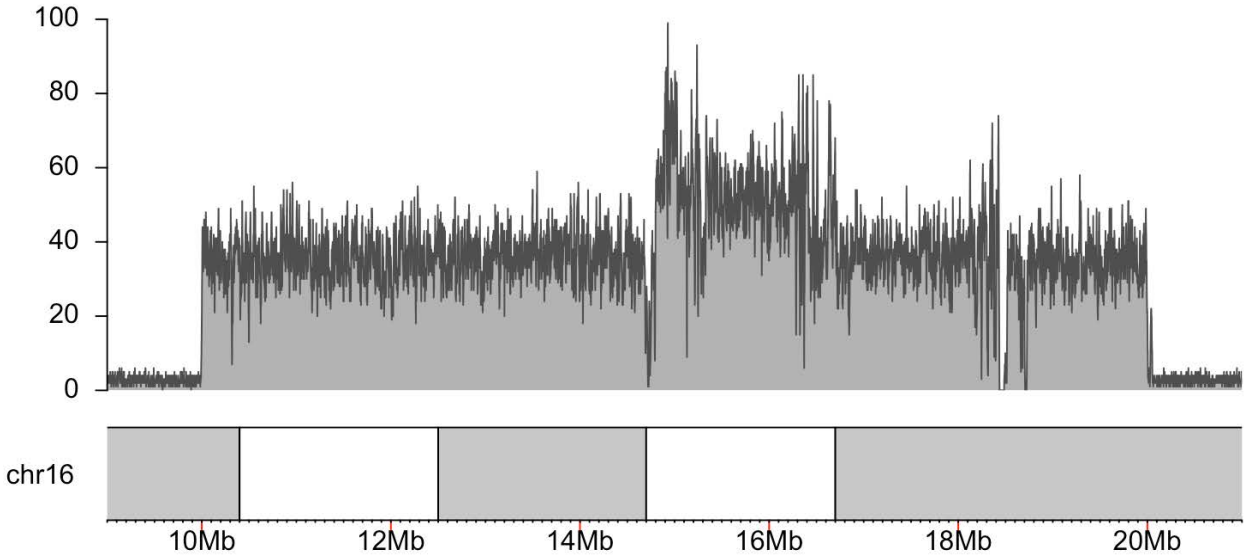

B. Coverage of chromosome 16 target region.

C. Centromere-proximal end of the chromosome 8 duplication, reads spanning the duplication are indicated by color. IGV coordinates are chr8:141,645,041-141,645,164.

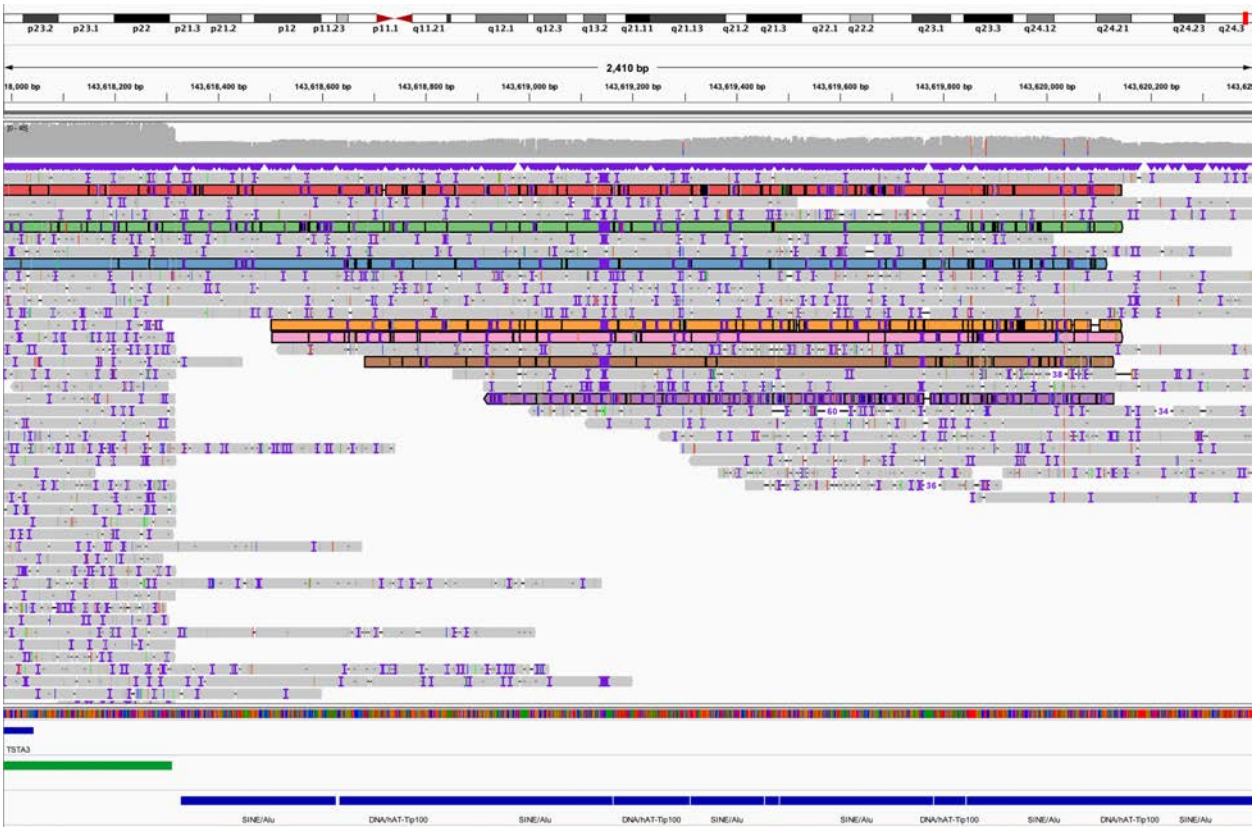

D. Telomere-proximal end of the chromosome 8 duplication shows that the duplication occurred within a TE-dense region. Reads on the 5' end of the image span an approximately 8 kbp deletion. Reads colored as in C. IGV coordinates are chr8:143,617,985-143,620,407.

Figure S29. S036, individual with multiple rearrangements and translocations of chromosomes 5, 6, 10, and 18.

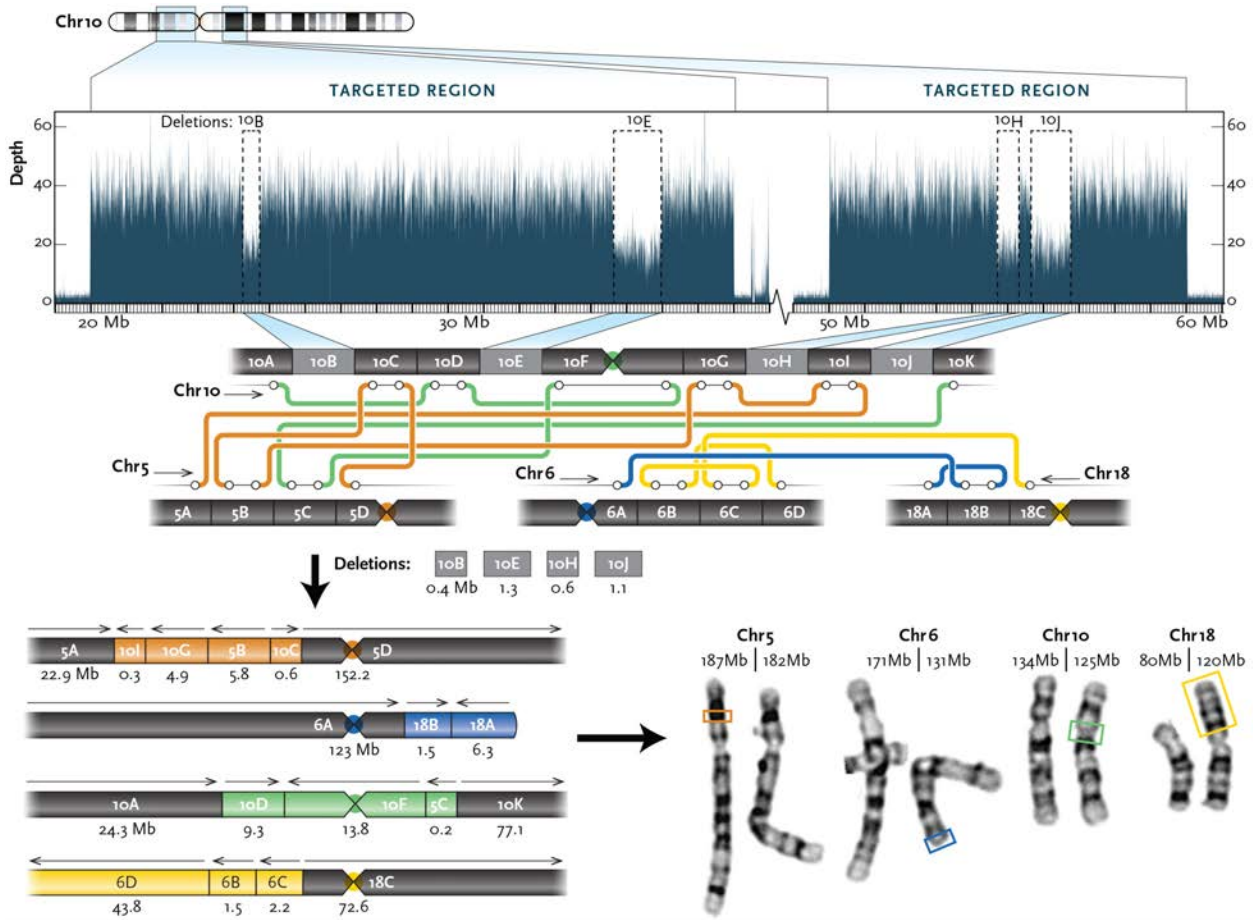

A. In a child with multiple deletions of chromosome 10, karyotyping revealed translocations between chromosomes 6 and 18 along with a pericentric inversion of chromosome 10. LRS identified additional translocations involving chromosomes 10 and 5 as well as several additional intrachromosomal rearrangements. Rearrangements can be resolved by following the subway plot for each derivative chromosome. Estimates of the reconstructed chromosome sizes are shown along with where they are estimated to correspond to on the karyotype (colored boxes).

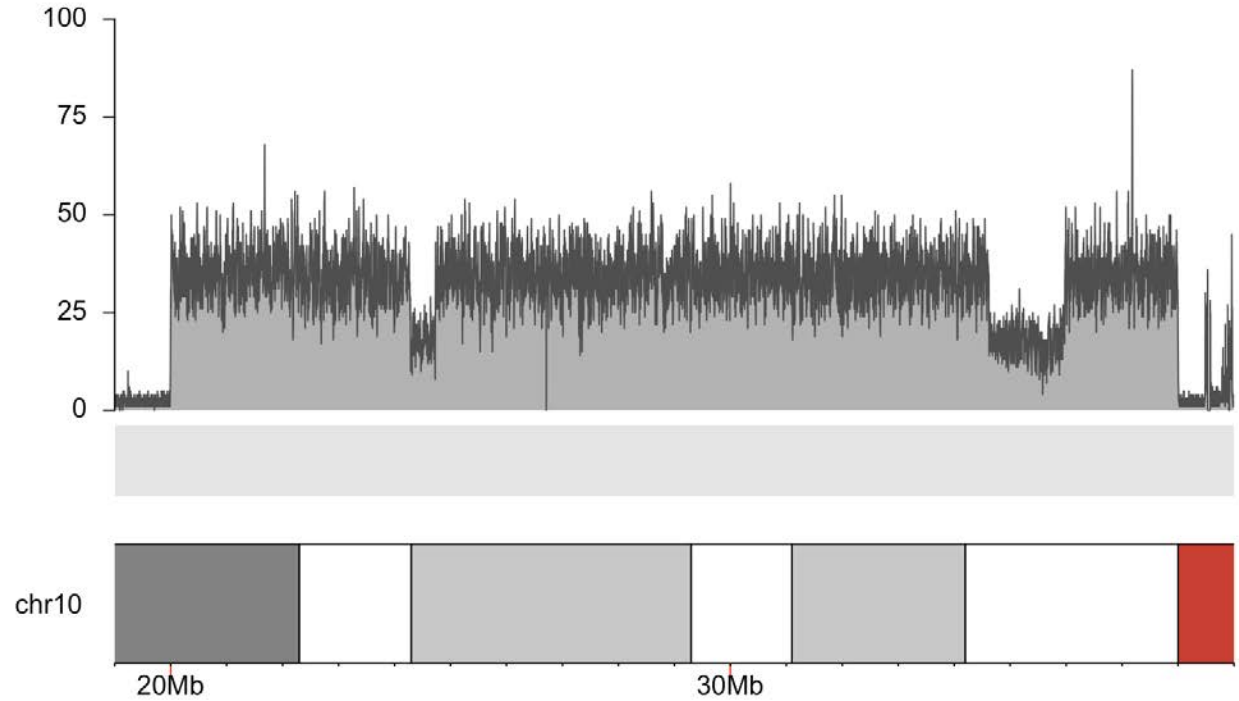

B. Coverage of chromosome 10p target region from the first readfish run.

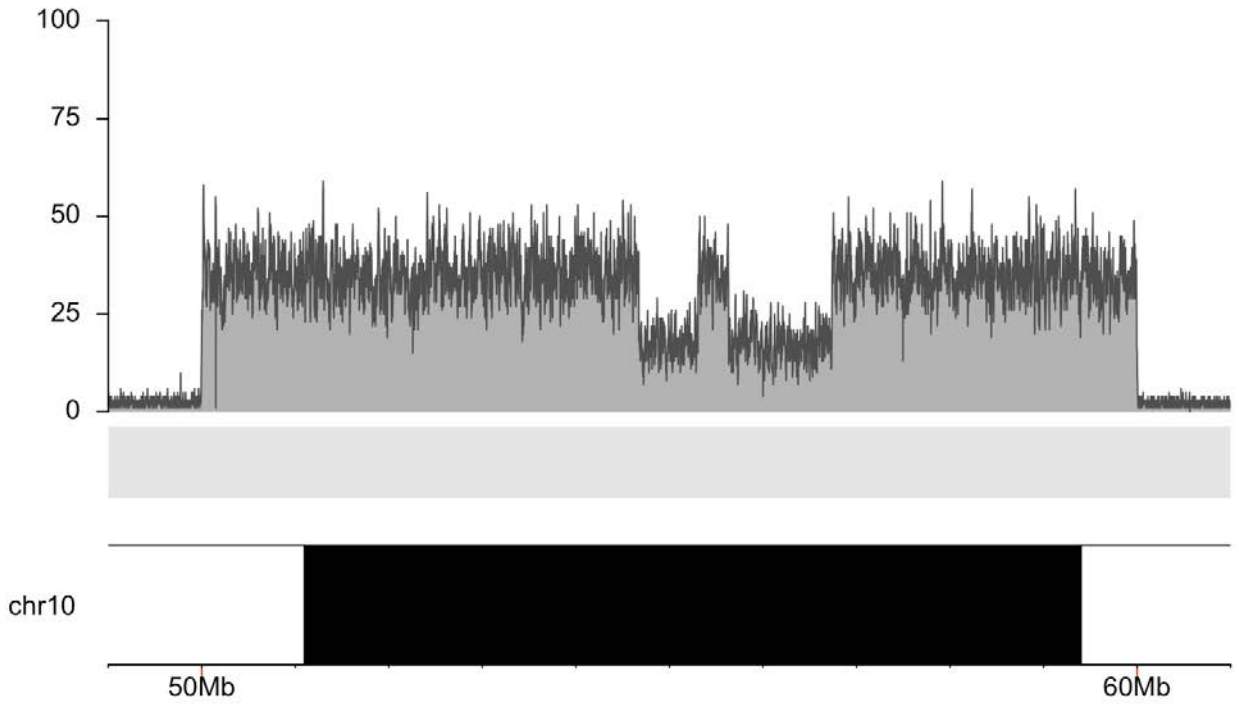

C. Coverage of chromosome 10q target region from the first readfish run.

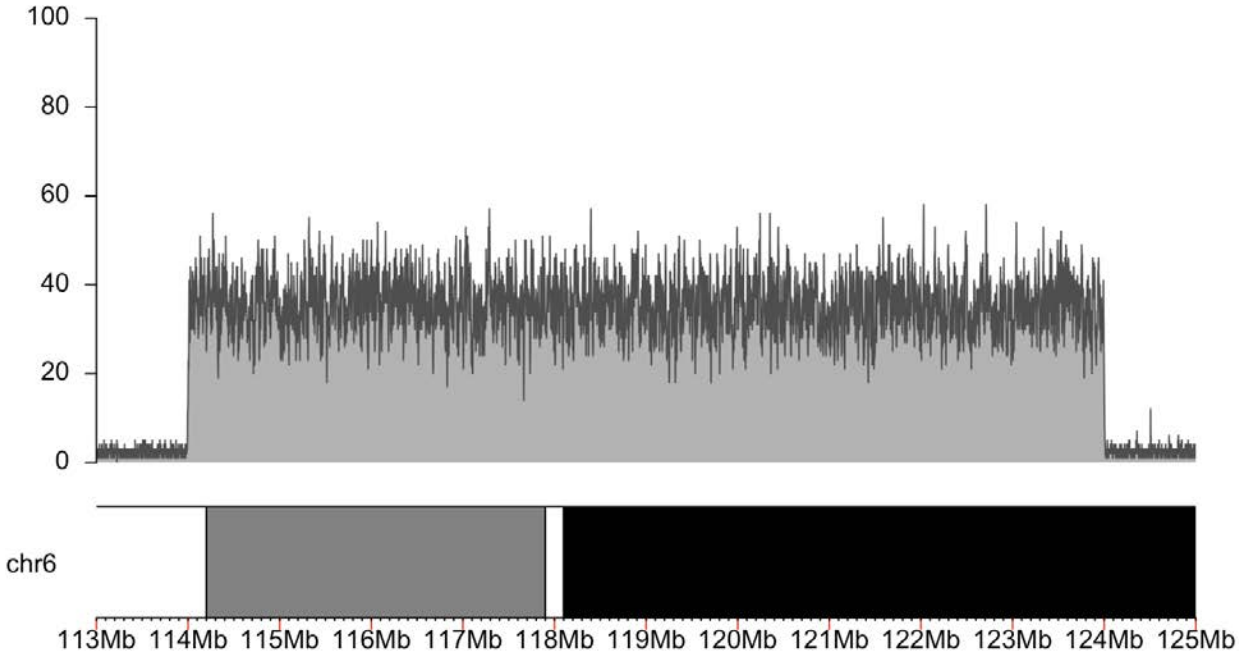

D. Coverage of chromosome 6 target region from the first readfish run.

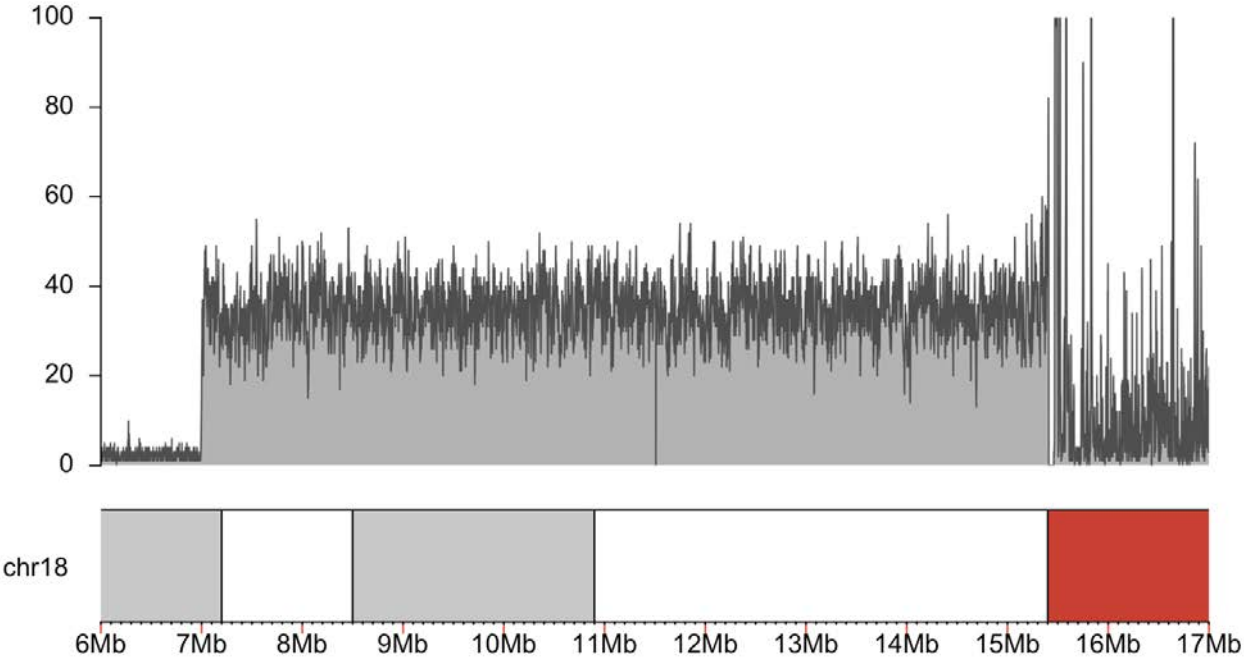

E. Coverage of chromosome 18 target region from the first readfish run.

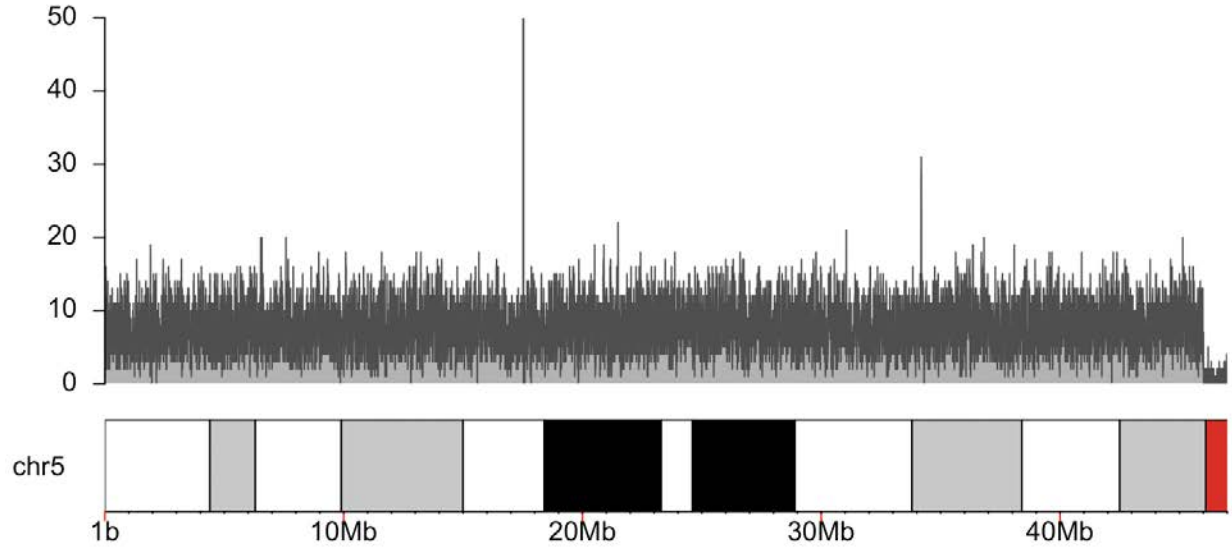

F. Coverage of chromosome 5 target region from the second readfish run.

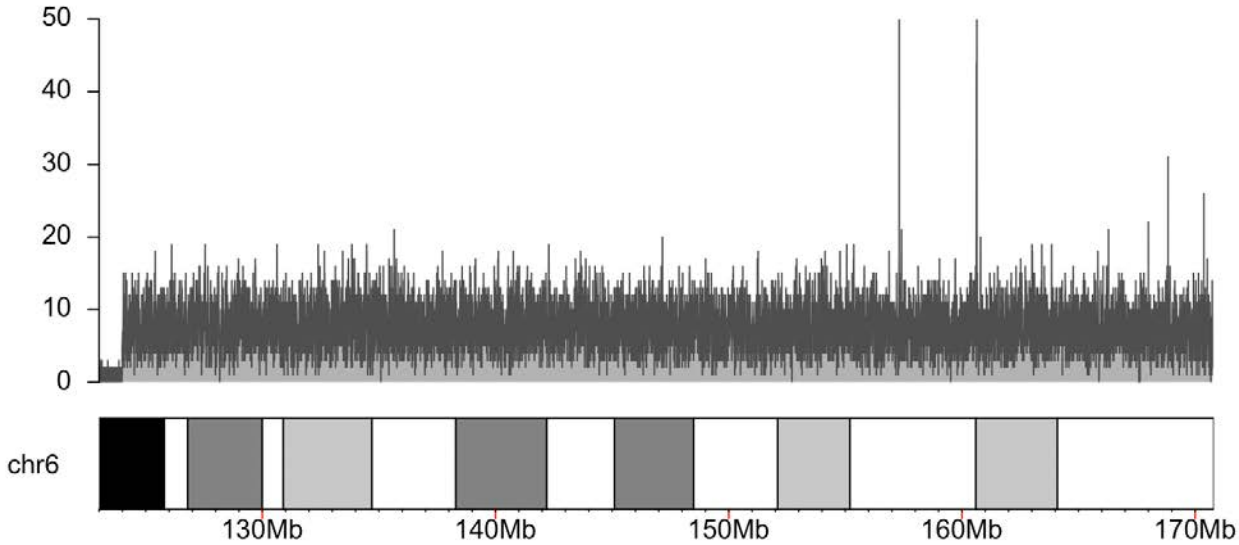

G. Coverage of chromosome 6 target region from the second read fish run.

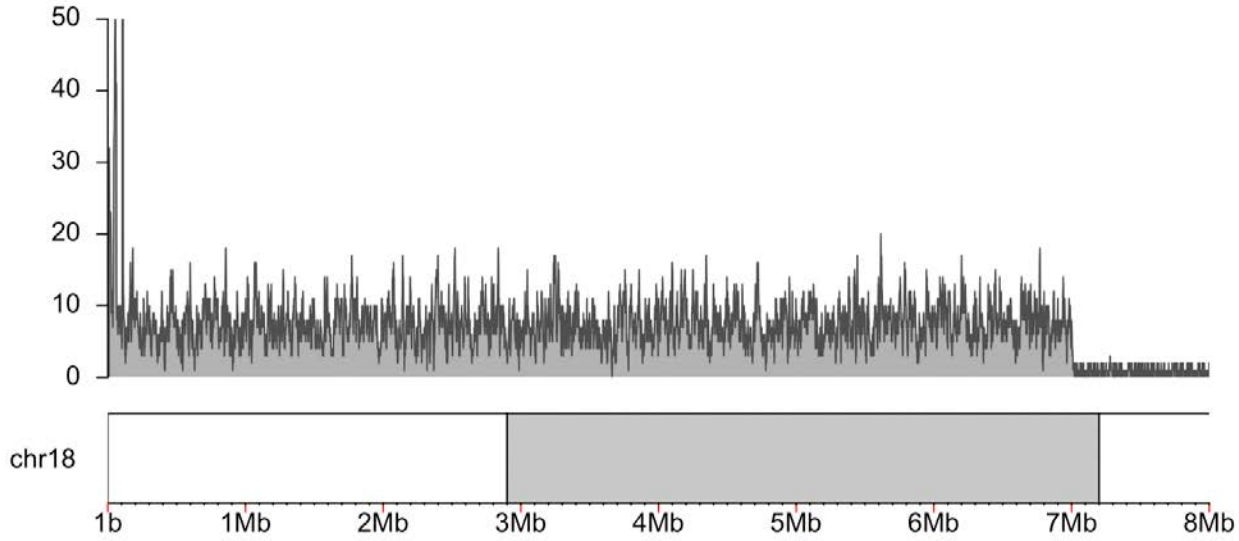

H. Coverage of chromosome 18 target region from the second readfish run.

I. Karyotype of the individual, arrows denote derivative chromosomes.

J: 3' end of 10:A bisects *KIAA1217* (IGV: chr10:24,286,090-24,286,130) and is linked to the 5' end of 10:D which bisects *GPR158* (IGV: chr10:25,278,377-25,278,417). This is the beginning of derivative chromosome 10.

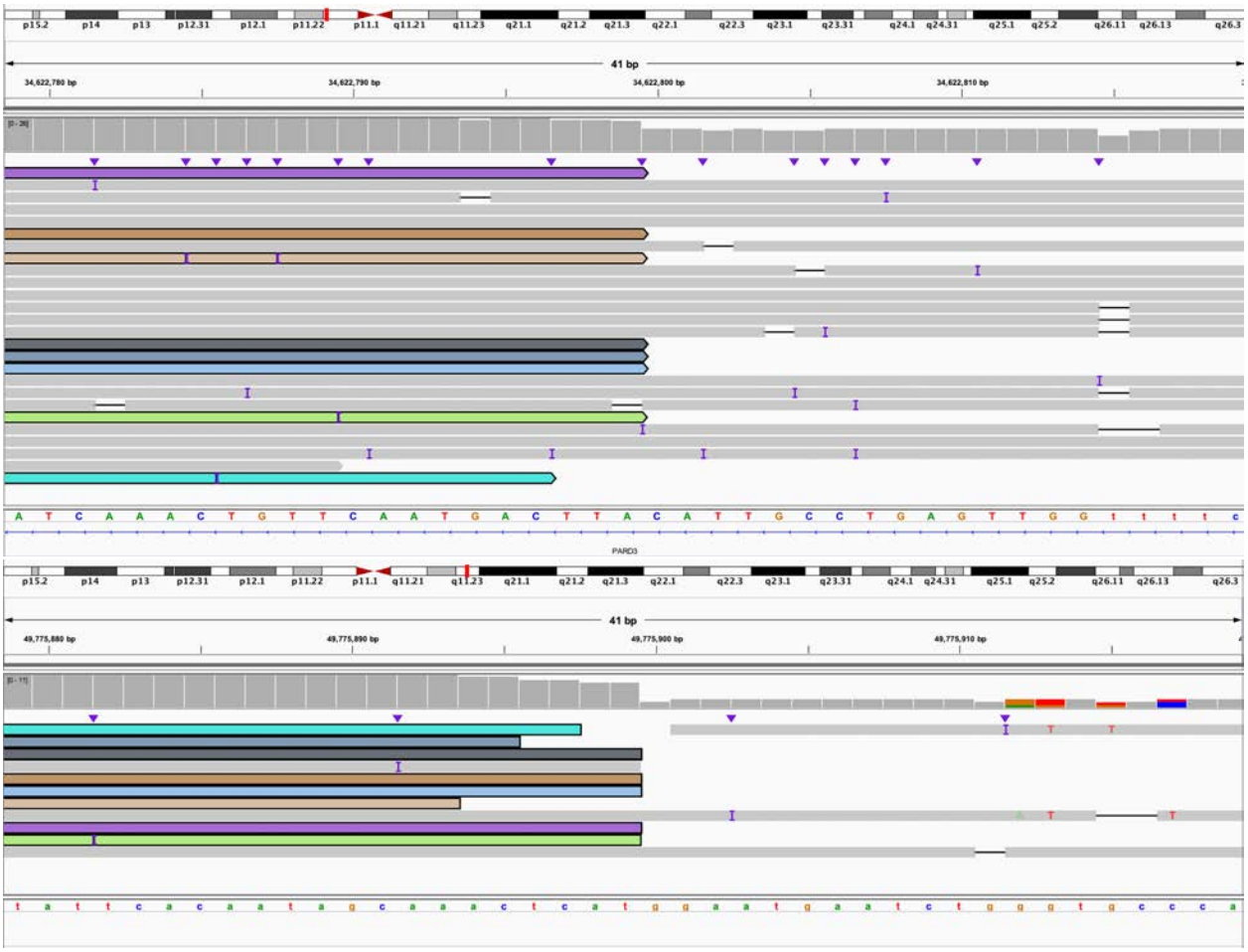

K: 3' end of 10:D bisects *PARD3* (IGV: chr10:34,622,779-34,622,819) and is linked to the 3' end of 10:F (IGV: chr10:49,775,879-49,775,919). This is within derivative chromosome 10.

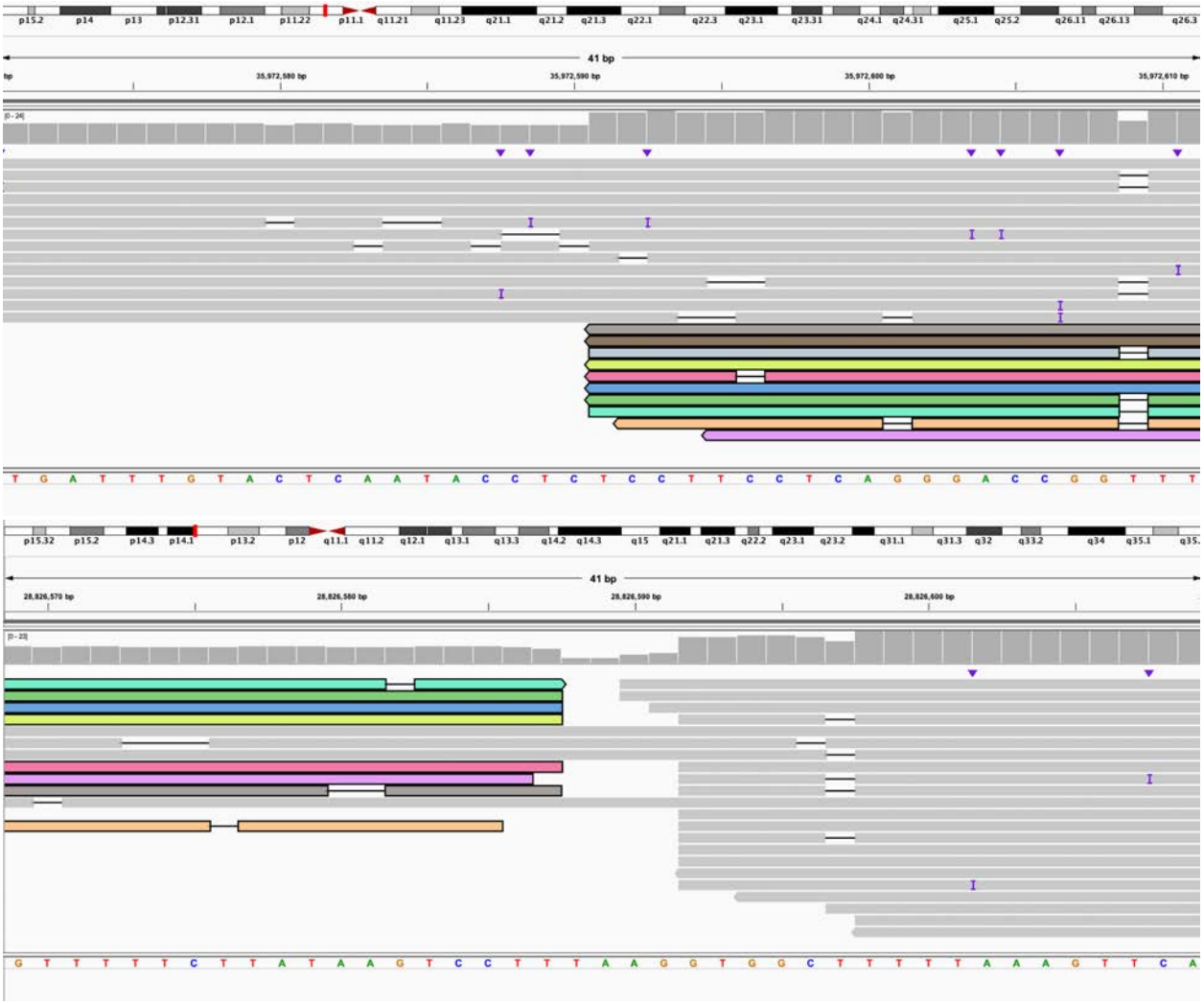

L: 5' end of 10:F (IGV: chr10:35,972,571-35,972,611) is linked to the 3' end of 5:C (IGV: chr5:28,826,569-28,826,609). This is within derivative chromosome 10.

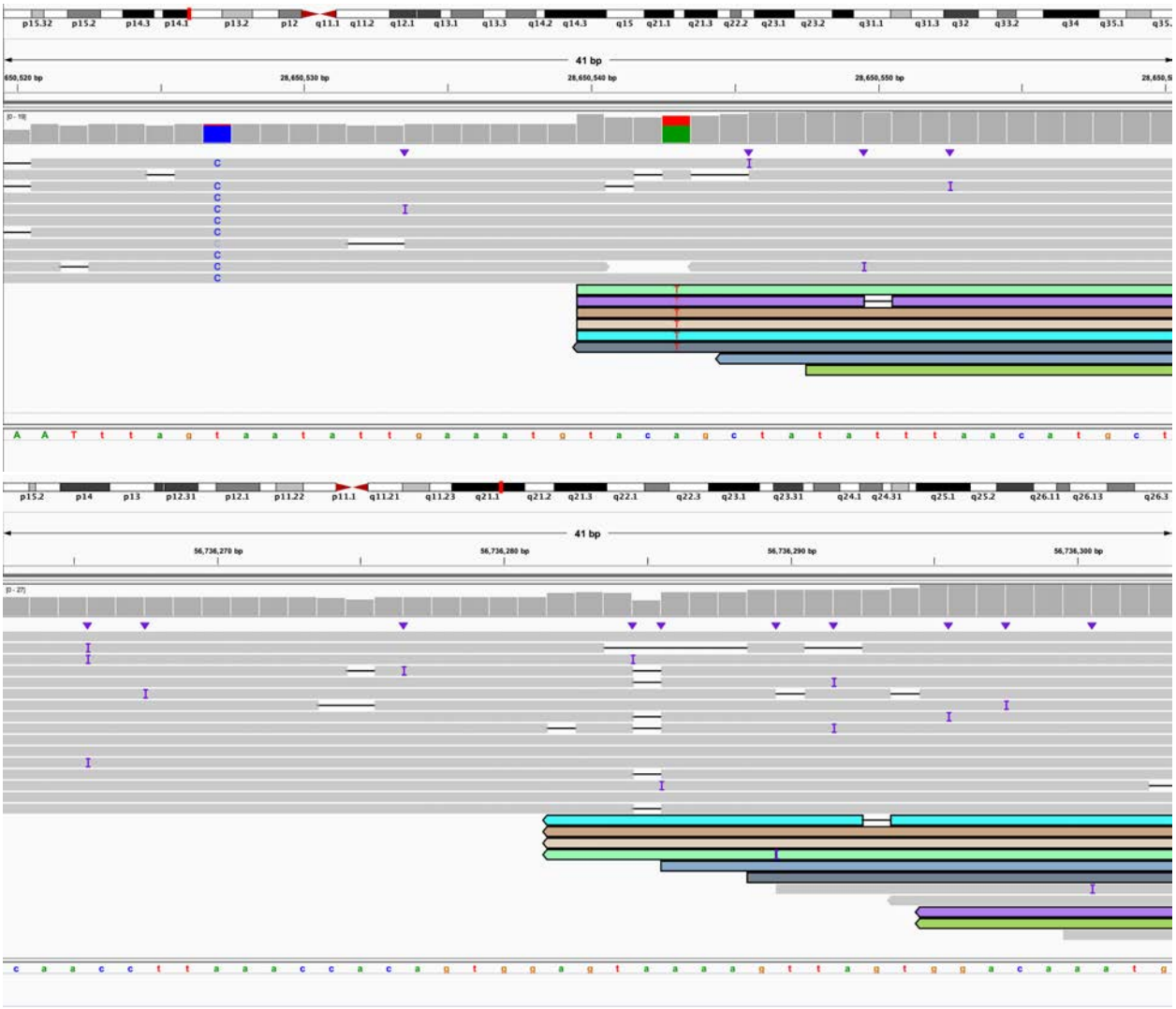

M: 5' end of 5:C (IGV: chr5:28,650,520-28,650,560) is linked to the 5' end of 10:K (IGV: chr10:56,736,263-56,736,303). This is the end of derivative chromosome 10.

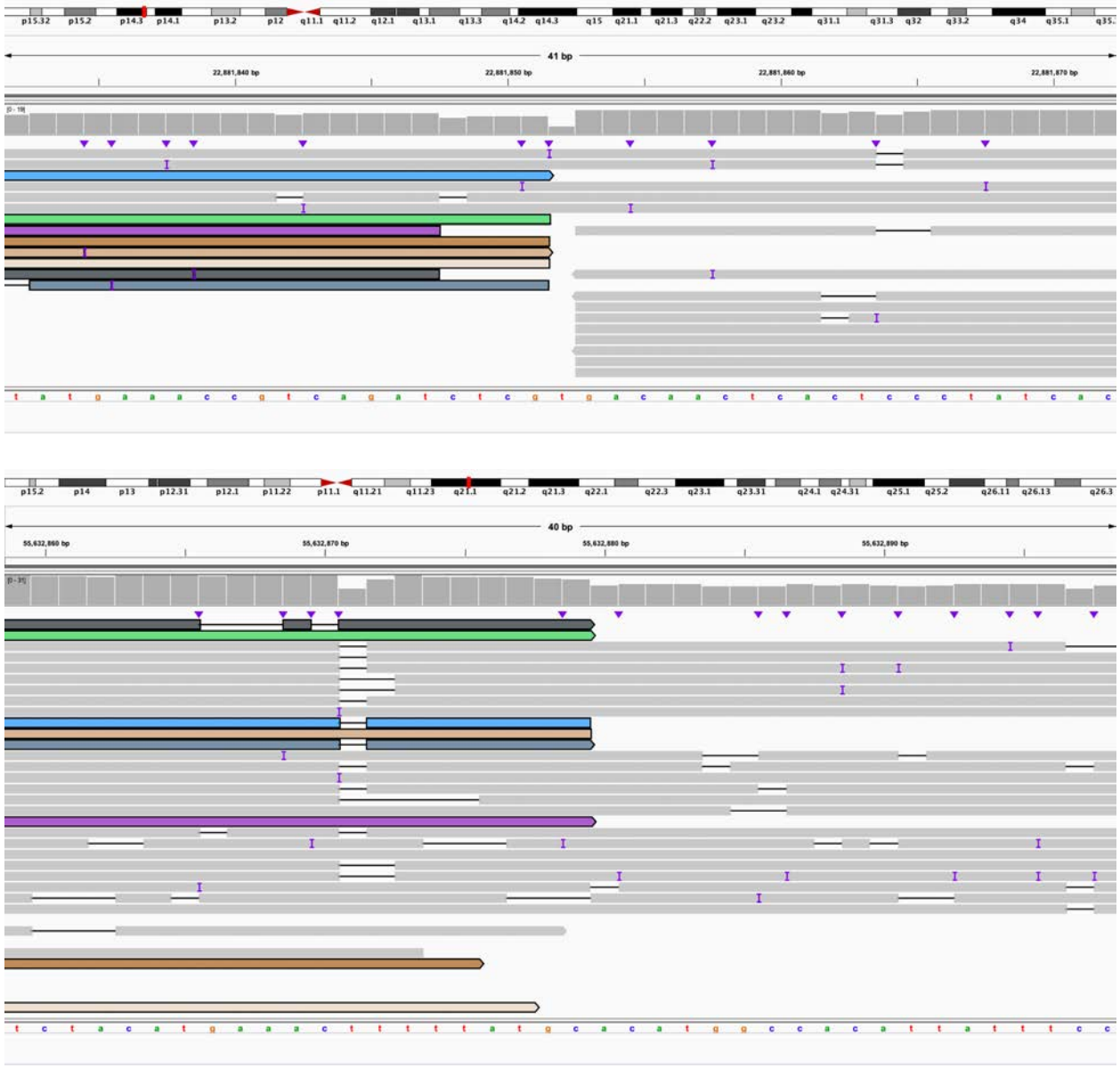

N: 3' end of 5:A (IGV: chr5:22,881,832-22,881,872) linked to 3' end of 10:I (IGV: chr10:55,632,859-55,632,898). This is the beginning of derivative chromosome 5.

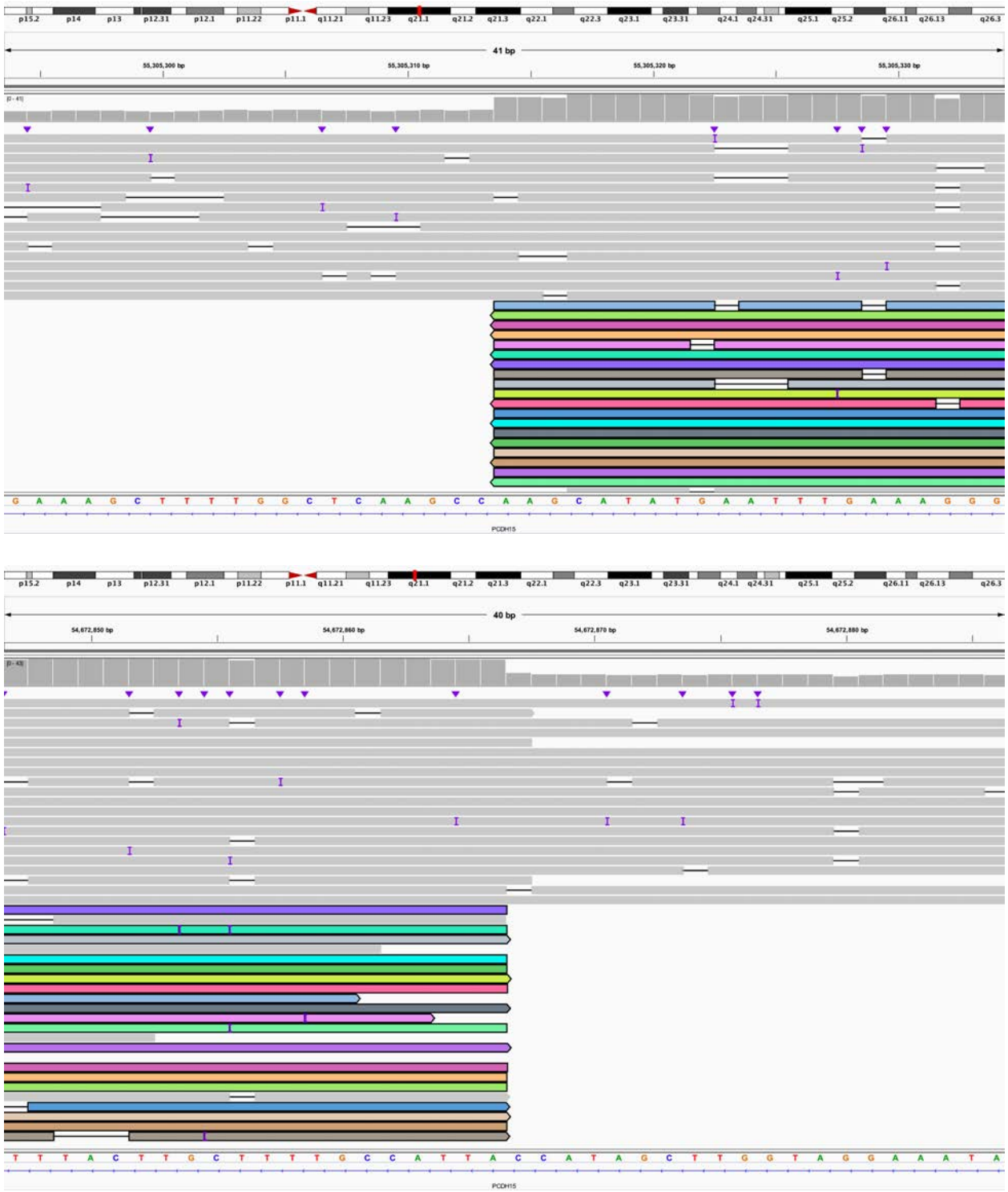

O: 5' end of 10:I bisects *PCDH15* (IGV: chr10:55,305,294-55,305,334) linked to 3' end of 10:G which also bisects *PCDH15* (IGV: chr10:54,672,847-54,672,886). This is within derivative chromosome 5.

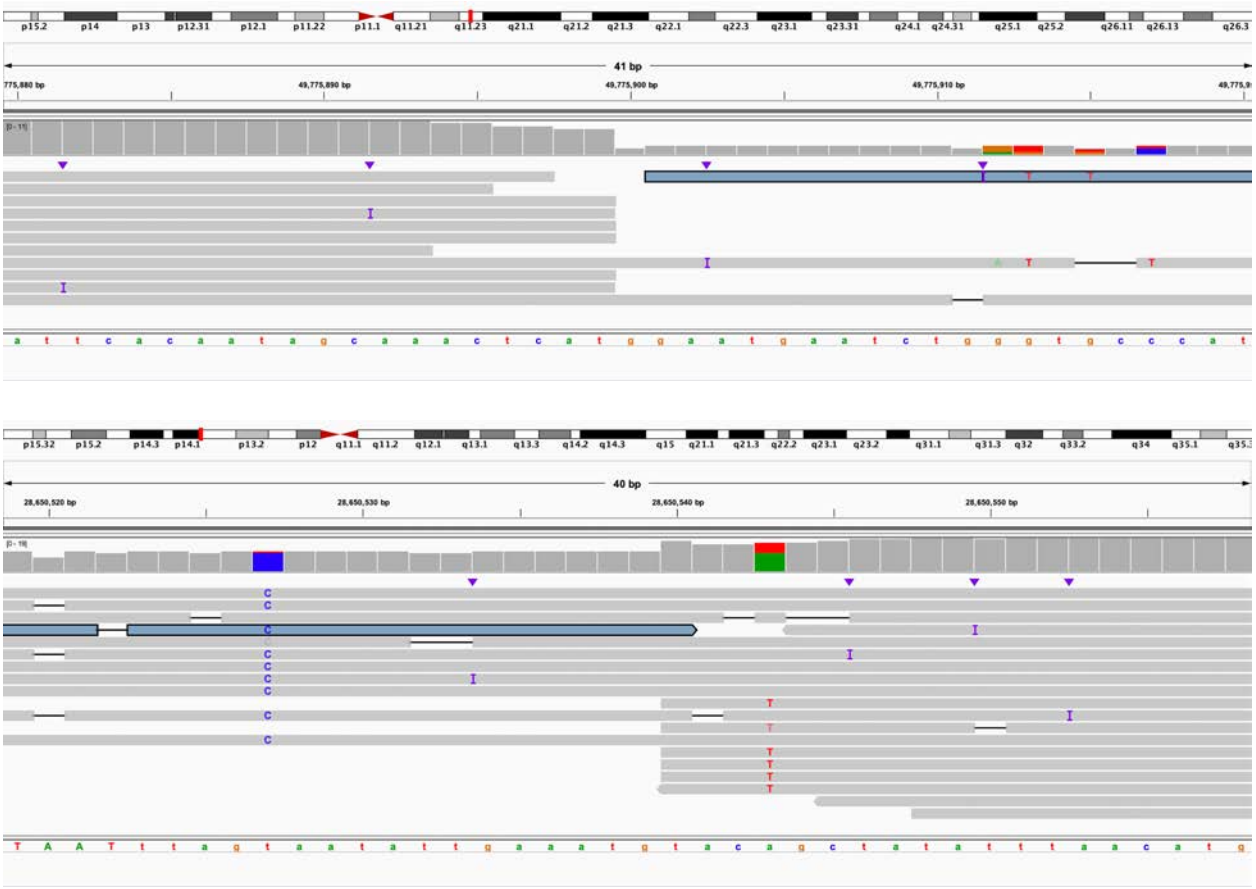

P: 5' end of 10:G (IGV: chr10:49,775,880-49,775,920) linked to 3' end of 5:B (IGV: chr5:28,650,519-28,650,558). This is within derivative chromosome 5.

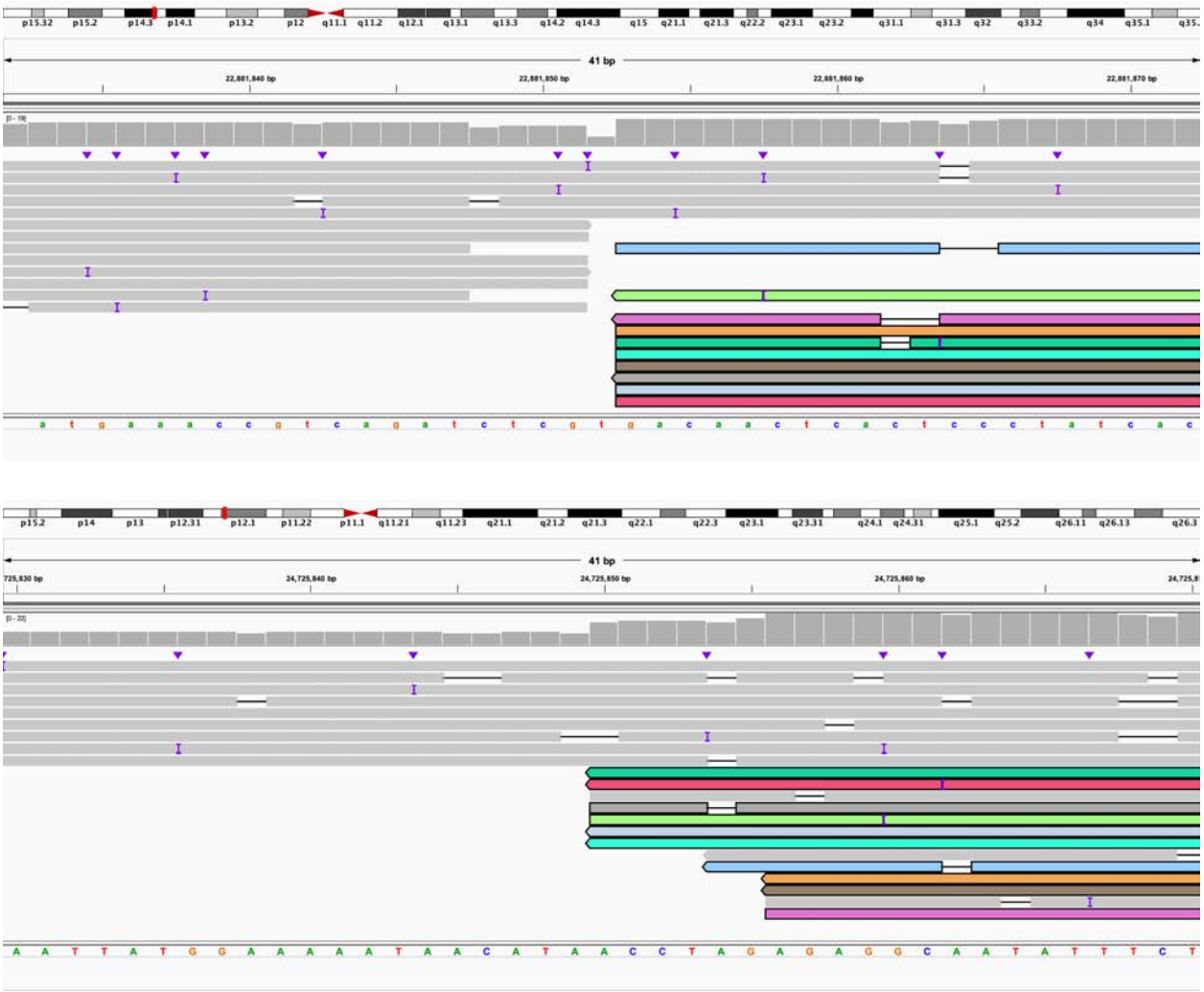

Q: 5' end of 5:B (IGV: chr5:22,881,832-22,881,872) linked to 5' end of 10:C (IGV: chr10:24,725,830-24,725,870). This is within derivative chromosome 5.

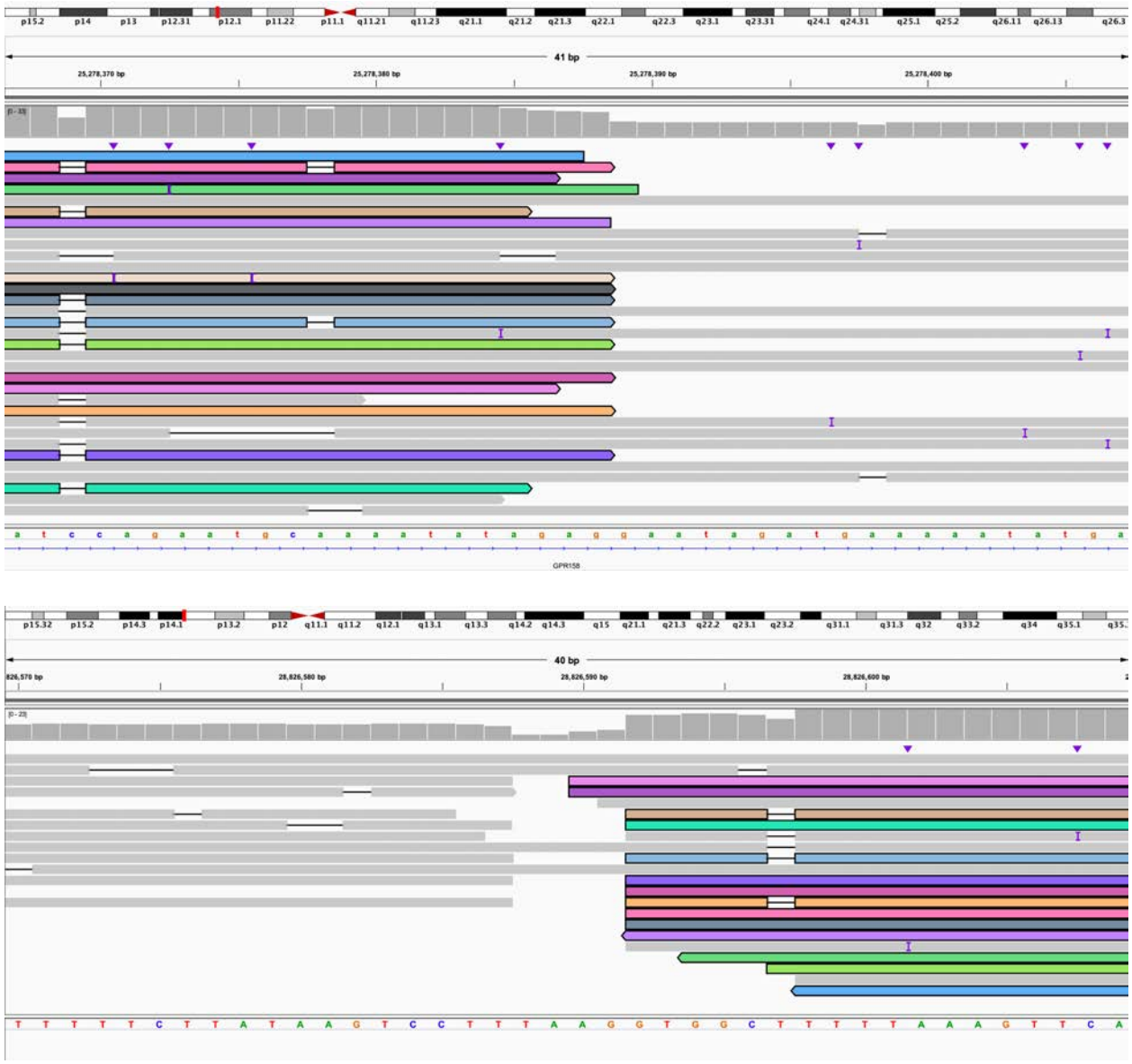

R: 3' end of 10:C is within *GPR158* (IGV: chr10:25,278,367-25,278,407) and is linked to 5' end of 5:D (IGV: chr5:28,826,570-28,826,609). This is the end of derivative chromosome 5.

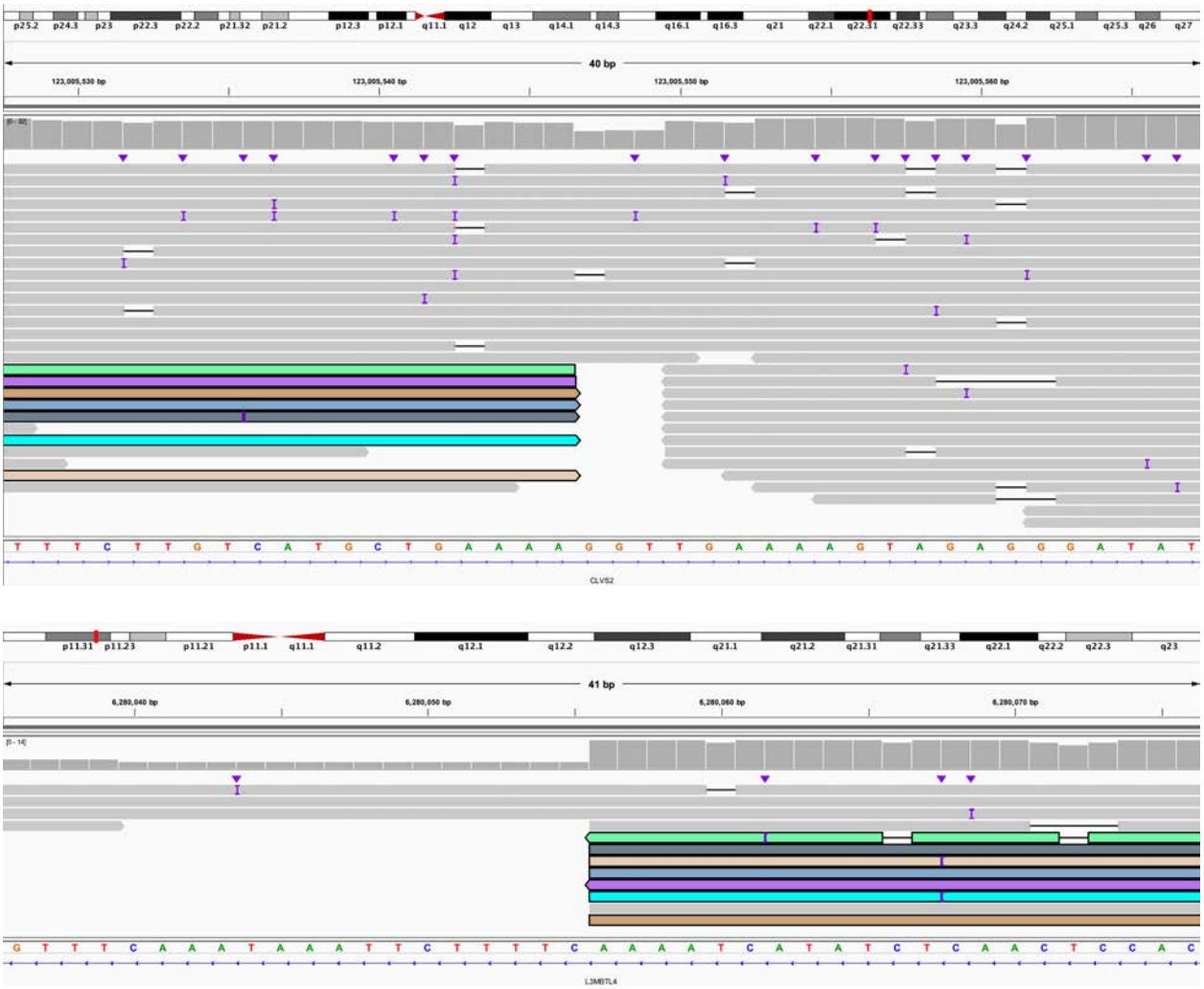

S: 3' end of 6:A bisects *CLVS2* (IGV: chr6:123,005,528-123,005,567) linked to 5' end of 18:C which bisects *L3MBTL4* (IGV: chr18:6,280,036-6,280,076). This is the beginning of derivative chromosome 6.

T: 3' end of 18:C (IGV: chr18:7,279,949-7,279,989) linked to 3' end of 18:A which bisects *L3MBTL4* (IGV: chr18:6,275,113-6,275,152). This is the end of derivative chromosome 6.

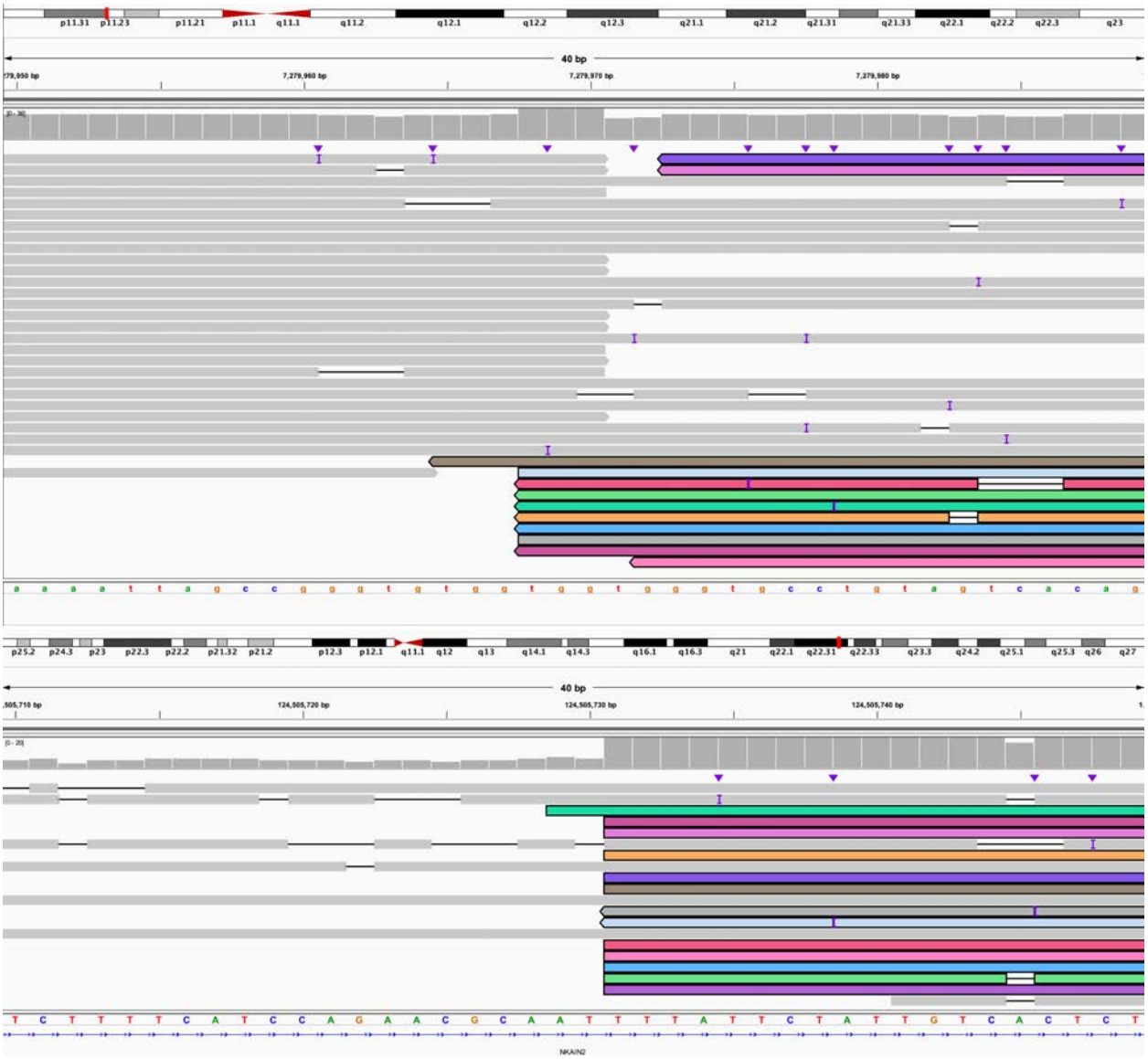

U: 5' end of 18:D (IGV: chr18:7,279,950-7,279,989) linked to 5' end of 6:C which bisects *NKAIN2* (IGV: chr6:124,505,710-124,505,749). This is the beginning of derivative chromosome 18.

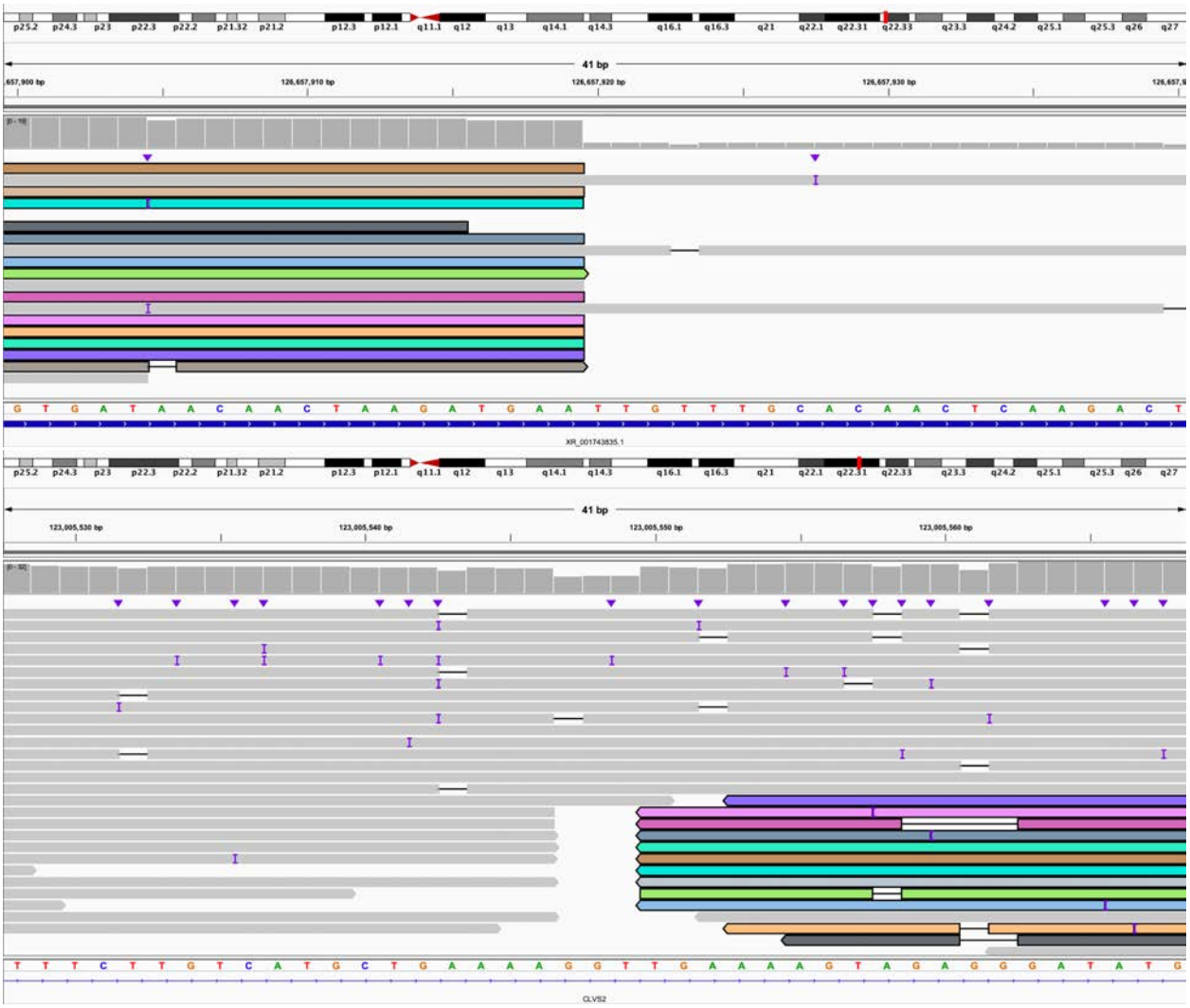

V: 3' end of 6:C bisects *XR_001743835.1* (IGV: chr6:126,657,900-126,657,940) linked to 5' end of 6:B which bisects *CLVS2* (IGV: chr6:123,005,528-123,005,568). This is within derivative chromosome 18.

W: 3' end of 6:B bisects *NKAIN2* (IGV: chr6:124,505,249-124,505,393) linked to 5' end of 6:E which bisects *XR_001743835.1* (IGV: chr6:126,680,021-126,680,060). This is the end of derivative chromosome 18.

Figure S30. S082, individual with deletion of *RBM20* and duplication involving *RAI1* and *PMP22*.

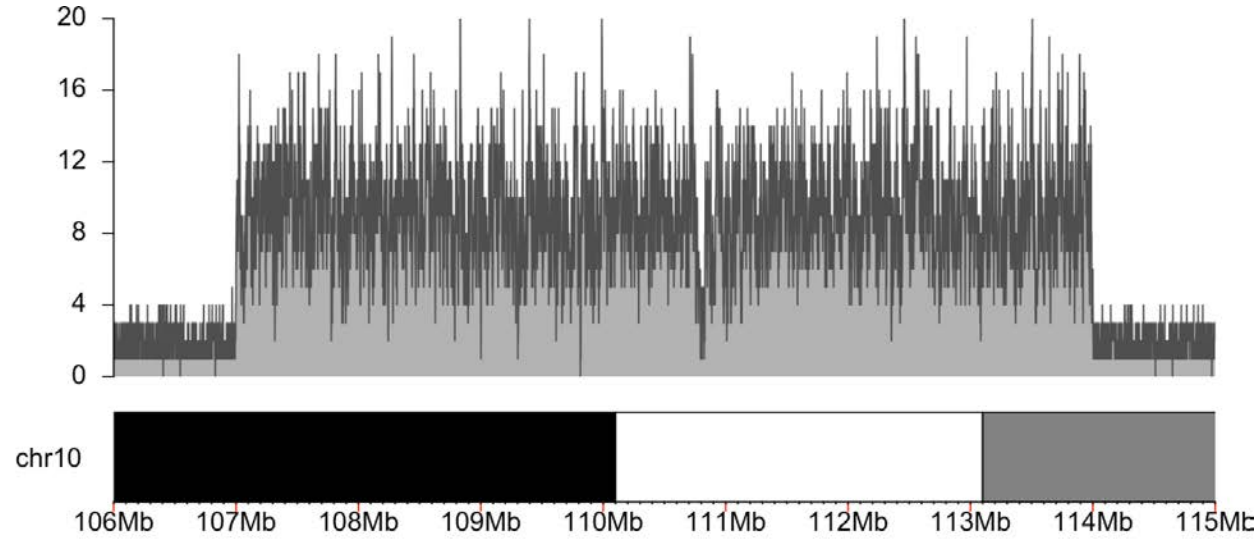

A. Coverage of chromosome 10 target region.

B: 5' end of deletion within RBM20 (IGV: chr10:110,755,668-110,755,707) is linked to 3' end of deletion (IGV: chr10:110,829,742-110,829,781).

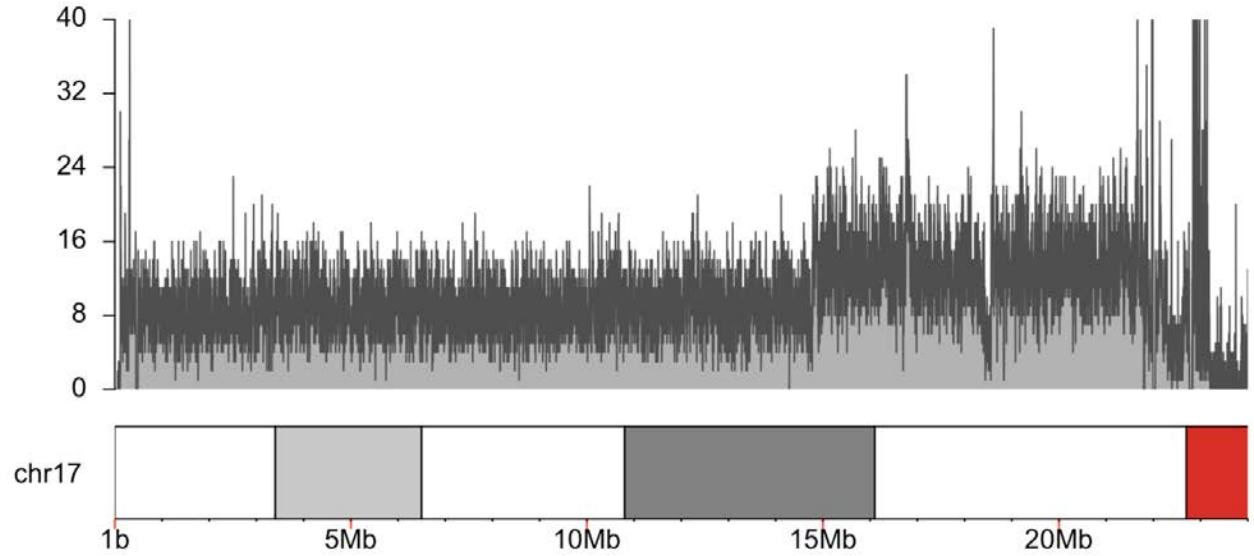

C: Coverage of chromosome 17 target region.

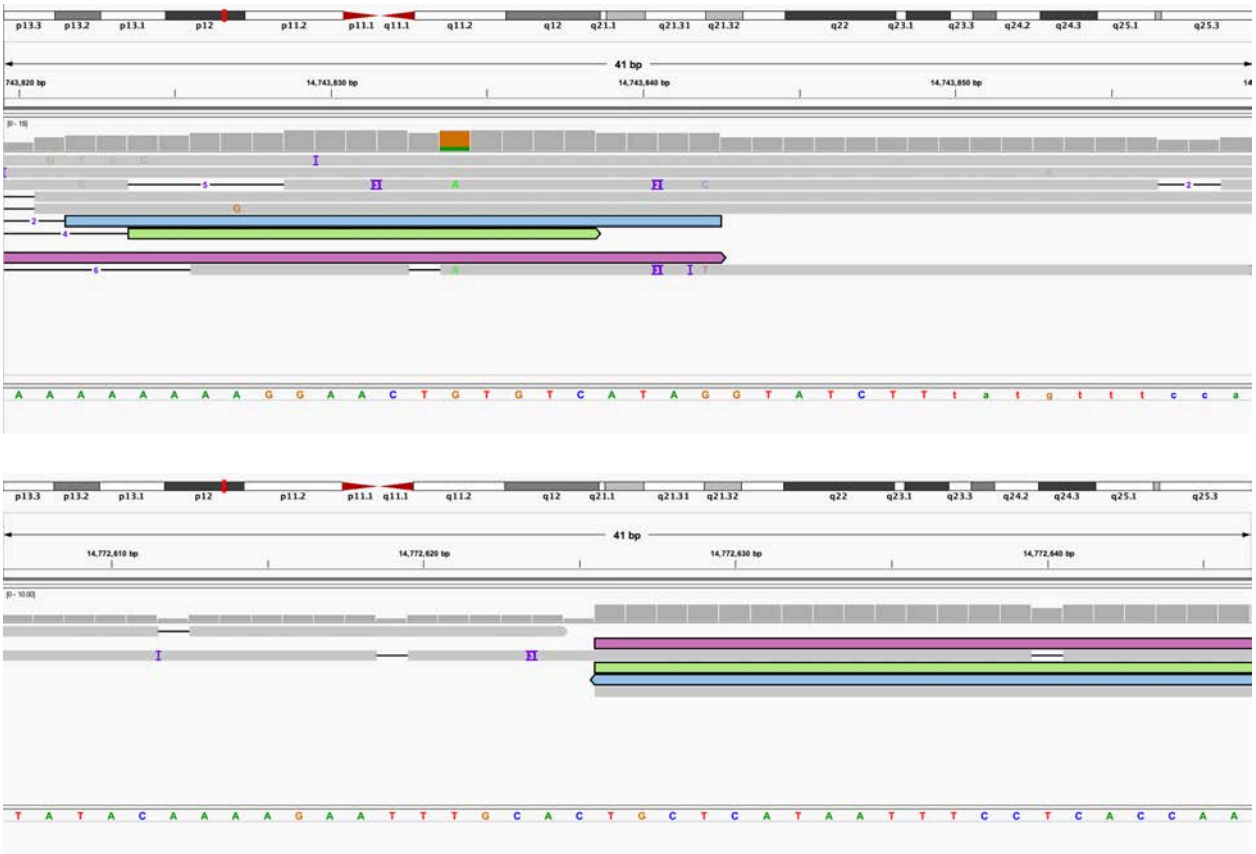

D: 5' end of A (IGV: chr17:14,743,820-14,743,859) is linked to 3' end of C (IGV: chr17:14,772,607-14,772,646) and results in a 29kb deletion.

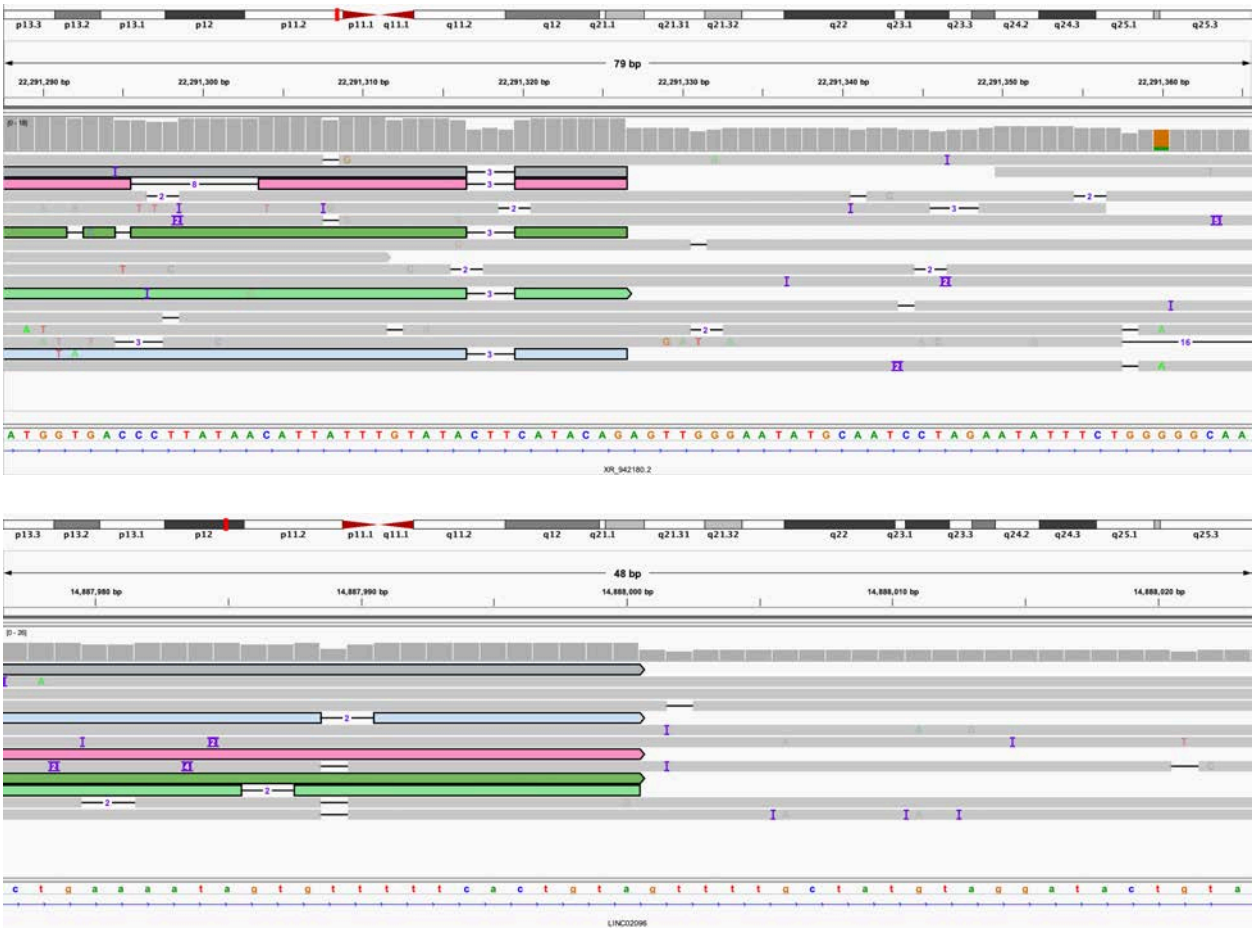

E: 5’ end of F (IGV: chr17:22,291,288-22,291,365) is connected to the 5’ end of D (IGV: chr17:14,887,977-14,888,023).

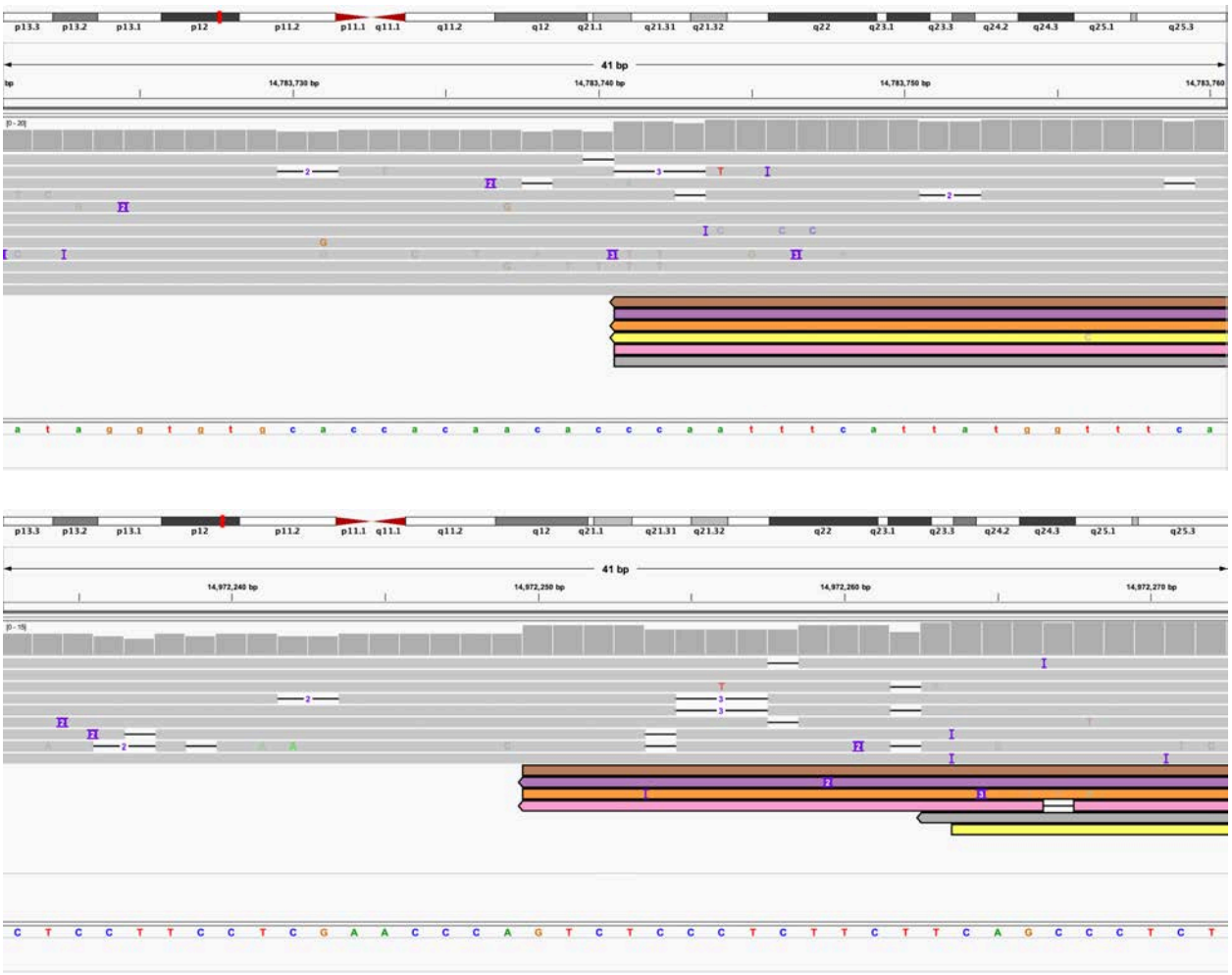

F: 3’ end of D (IGV: chr17:14,783,721-14,783,760) is connected to the 3’ end of F (IGV: chr17:14,972,233-14,972,272).

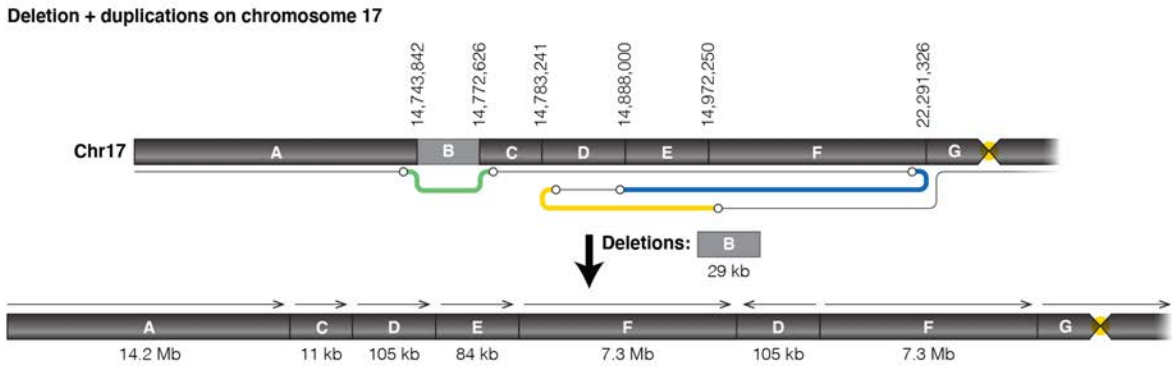

G: Cartoon of complex rearrangement on chromosome 17.

Figure S31. S083, individual with terminal deletion and proximal duplication of chromosome 4.

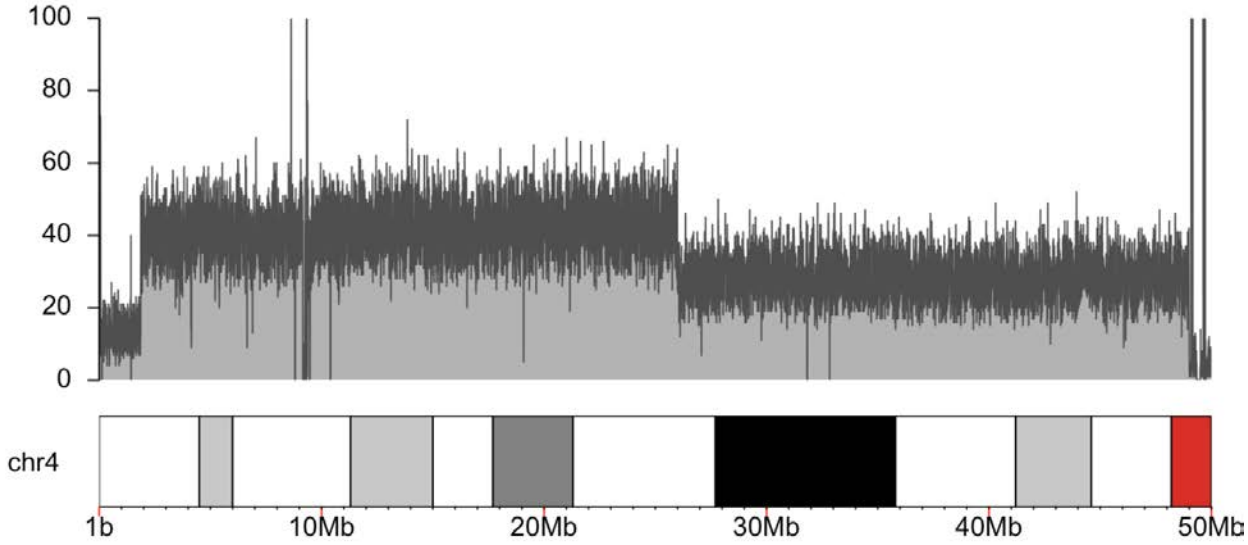

A. Coverage of target region showing terminal deletion followed by proximal duplication.

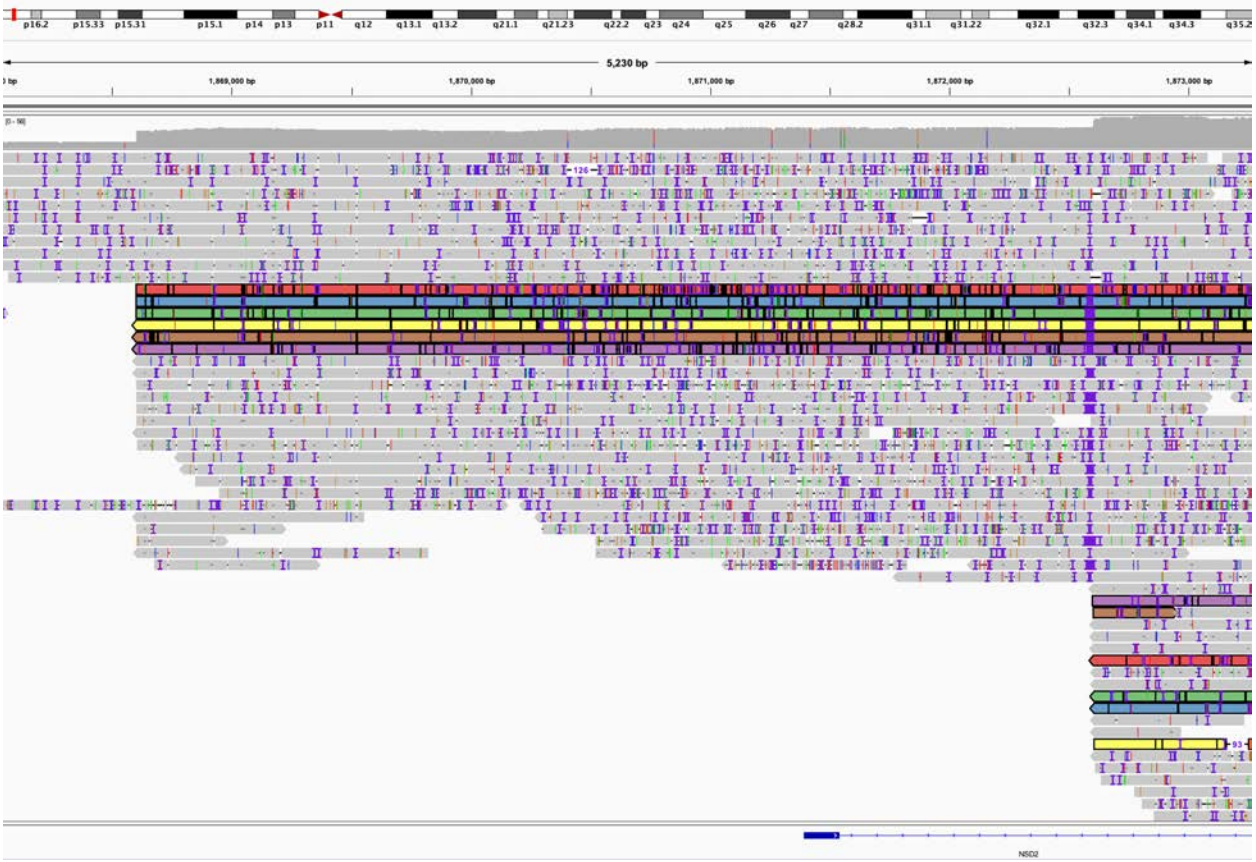

B. IGV view of deletion and duplication breakpoints. A small number of reads are highlighted to show the relationship between the duplicated region and the deletion. IGV view is of chr4:1,867,951-1,873,179.

C. IGV view of the end of the duplication breakpoint. There is no clear termination of the duplication, suggesting a terminal event. IGV view is of chr4:25,985,086-25,994,389.

Figure S32. S002 (*ALMS1*), IGV views of known inherited stop variant and *Alu* insertion.

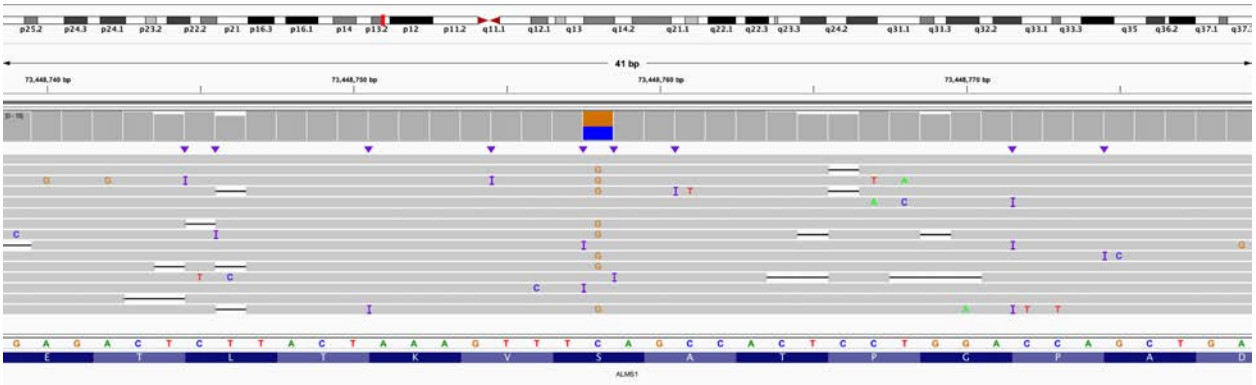

A. IGV view of all reads showing the known paternally inherited C>G that results in a stop codon. IGV coordinates for the screenshot are chr2:73,448,739-73,448,779.

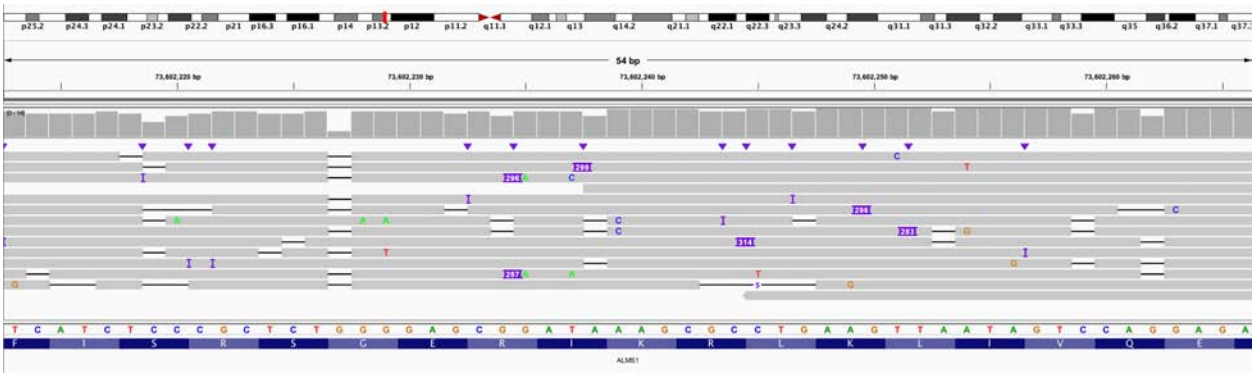

B. Screenshot of ~300 bp insertion in exon 20 that represents an *Alu* insertion, all reads are shown. IGV view is chr2:73,602,213-73,602,266.

Figure S33. S003 (*NPHP4*), IGV views of inherited stop, splice variant, and data showing variant does affect splicing.

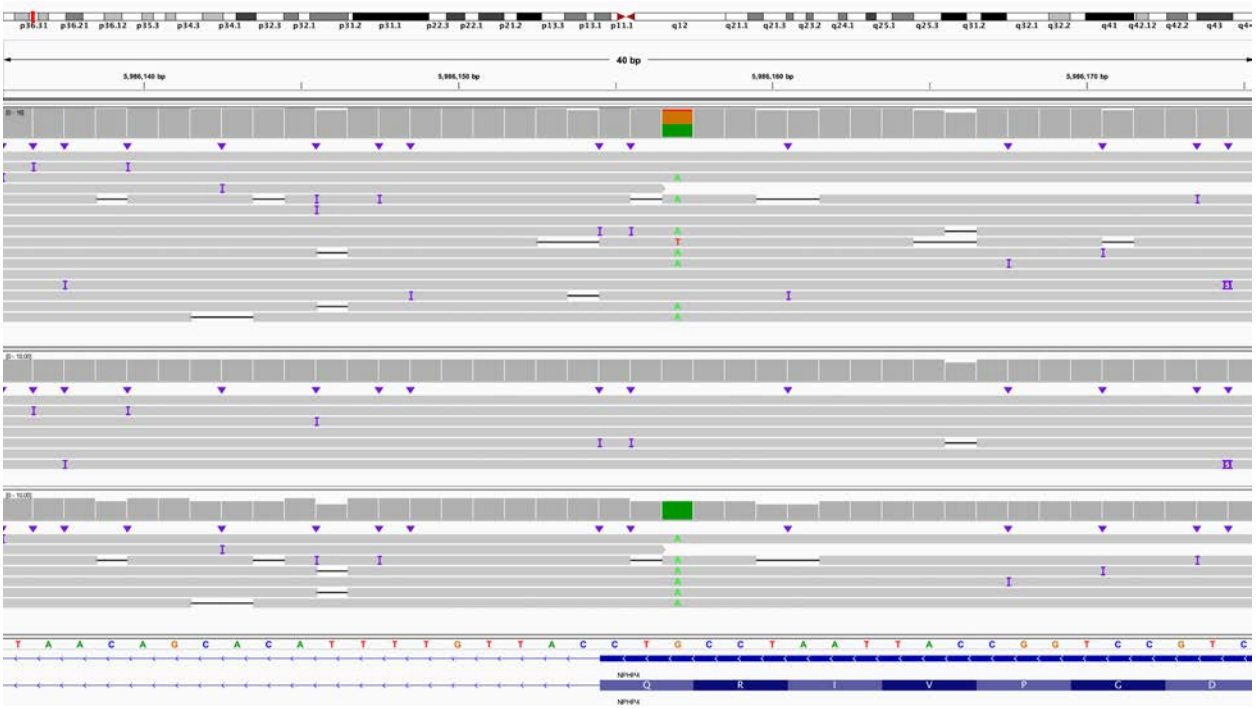

A. IGV view of all reads (top track) and reads phased into two haplotypes (middle and bottom tracks). DNA sequence and gene body are located below. The known paternally inherited G>A is located in the bottom haplotype. IGV screenshot is from chr1:5,986,136-5,986,175.

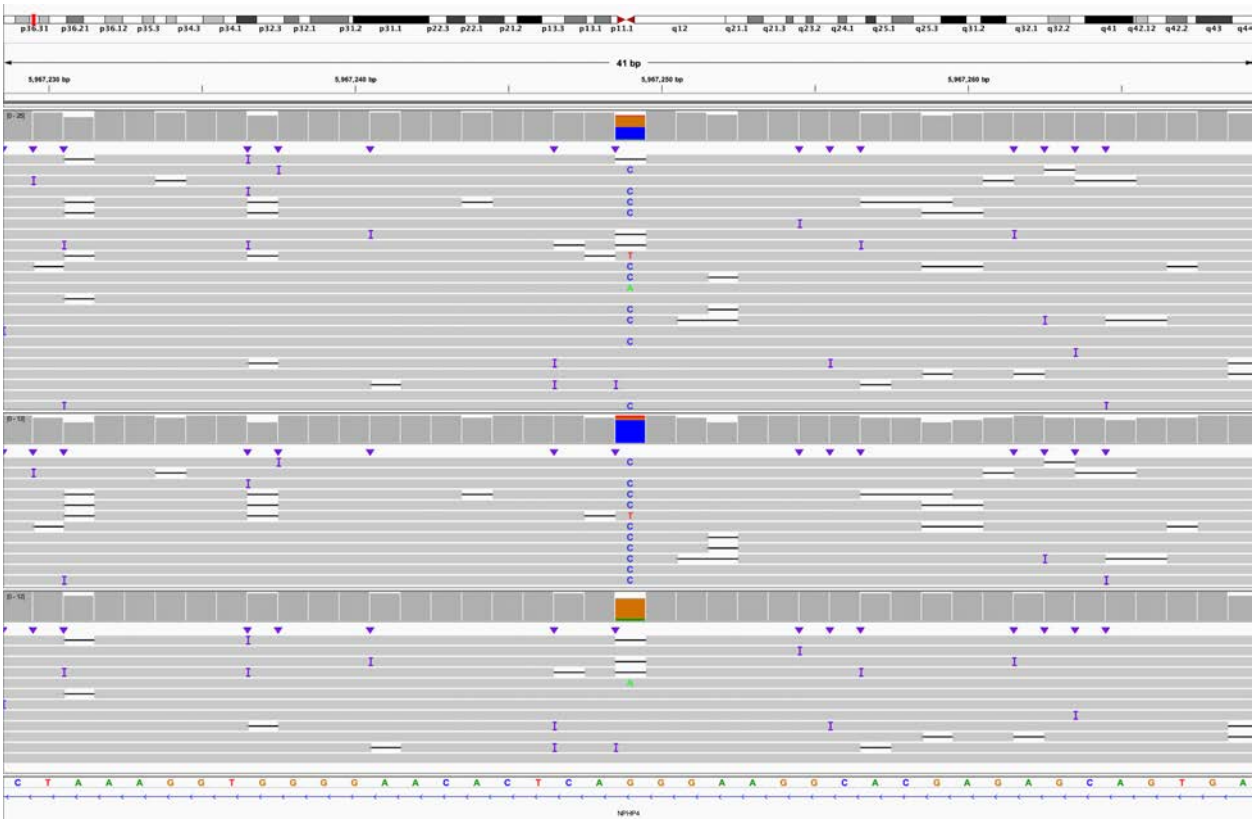

B. IGV view with reads as in A showing the G>C predicted to create a novel splice donor site on a different haplotype than the known paternally inherited G>A in A. IGV screenshot is from chr1:5,967,229-5,967,269.

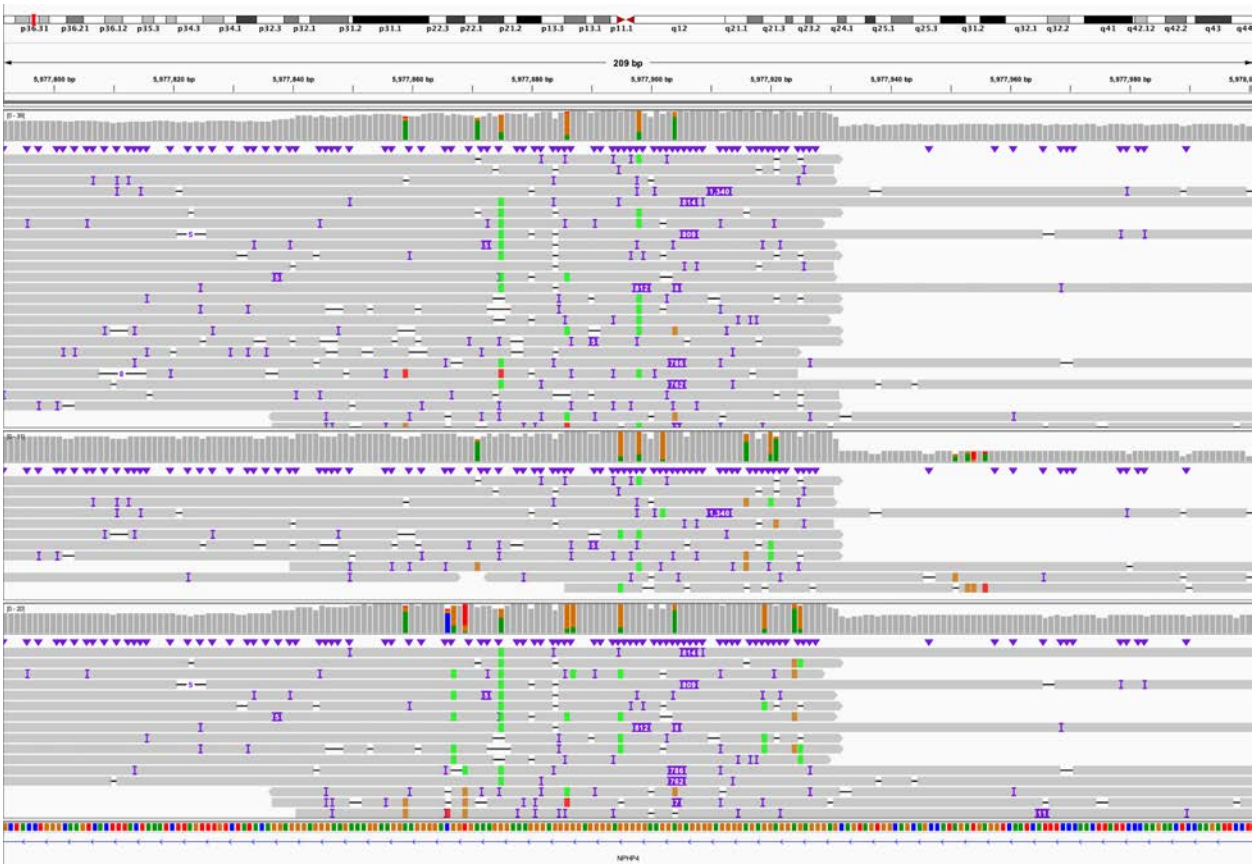

C. Analysis of SVs using both SVIM and Sniffles identified two insertions within an AG-rich repeat in an intron of *NPHP4* at approximately chr1:5,977,890. Phasing of reads separated all reads into a haplotype containing the ~800 bp insert and another containing the ~1,340 bp insert, similar to sizes observed in both nonhuman primates and human samples [4]. IGV screenshot is from chr1:5,977,792-5,978,001.

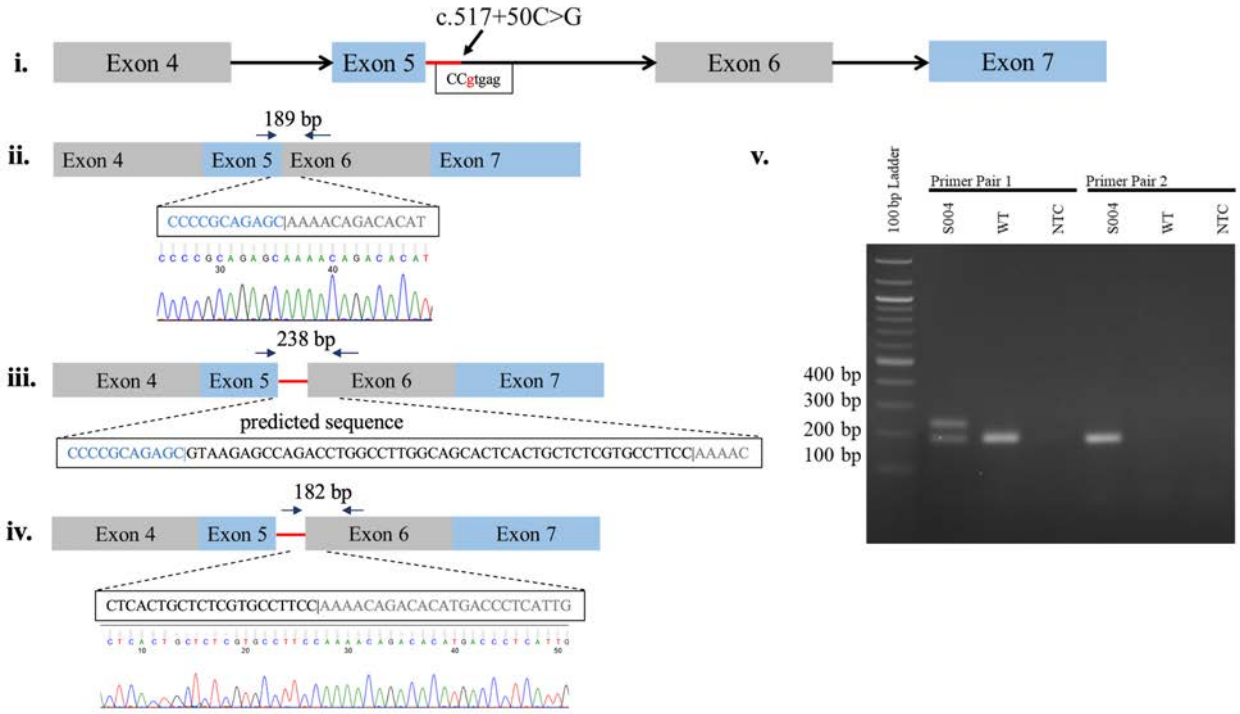

D. Splicing defect caused by deep intronic *NPHP4* variant in individual S004. **i.** *NPHP4* exon structure around the c.517+50C>G variant predicted to generate a new splice donor site (gtgag). **ii.** Normal splice isoform indicating primer pair 1 spanning the Exon 5-6 junction and corresponding Sanger sequencing of the PCR product. **iii.** Predicted aberrant transcript with inclusion of 49 intronic base pairs indicating predicted PCR product size for primer pair 1. **iv.** Predicted aberrant transcript indicating predicted PCR product size for primer pair 2, which should only amplify the aberrant transcript and corresponding Sanger sequencing of the PCR product. **v.** PCR products from S004 and unaffected fibroblast cDNA. Bands match the sizes predicted in B-D. NPHP4 reference sequence: NM_015102.4. bp=base pairs; NTC=No Template Control PCR; WT=wild-type, unaffected fibroblast cDNA.

Figure S34. S004 (*VARS2*), IGV view of known inherited variant.

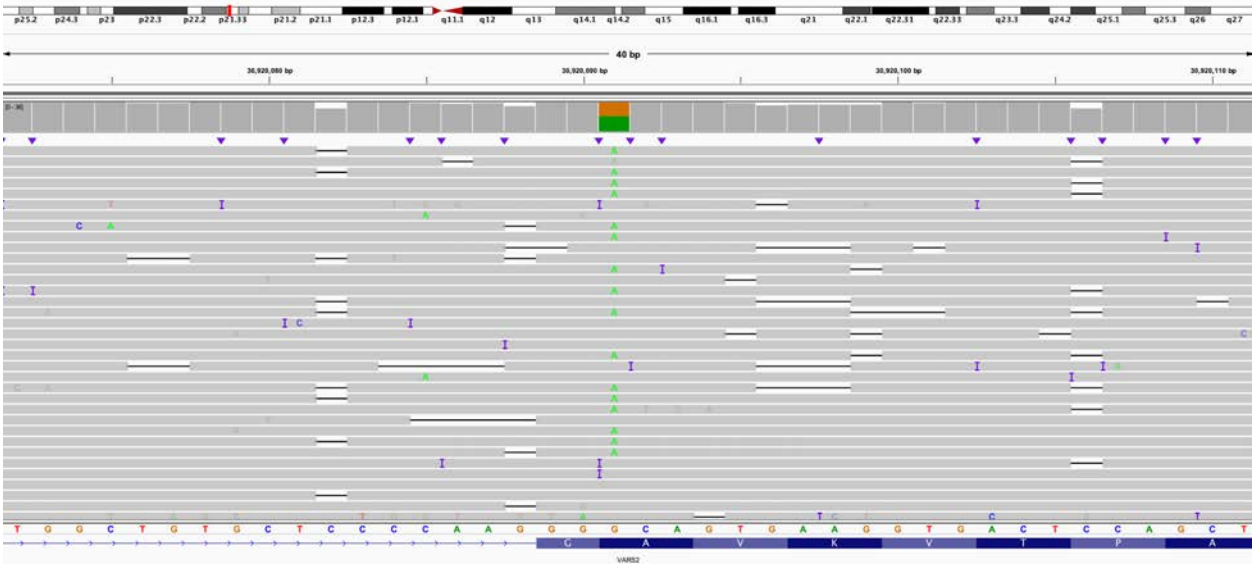

A. IGV view of known pathogenic paternally inherited G>A. No second variant was found in this case. IGV view is of chr6:30,920,072-30,920,111.

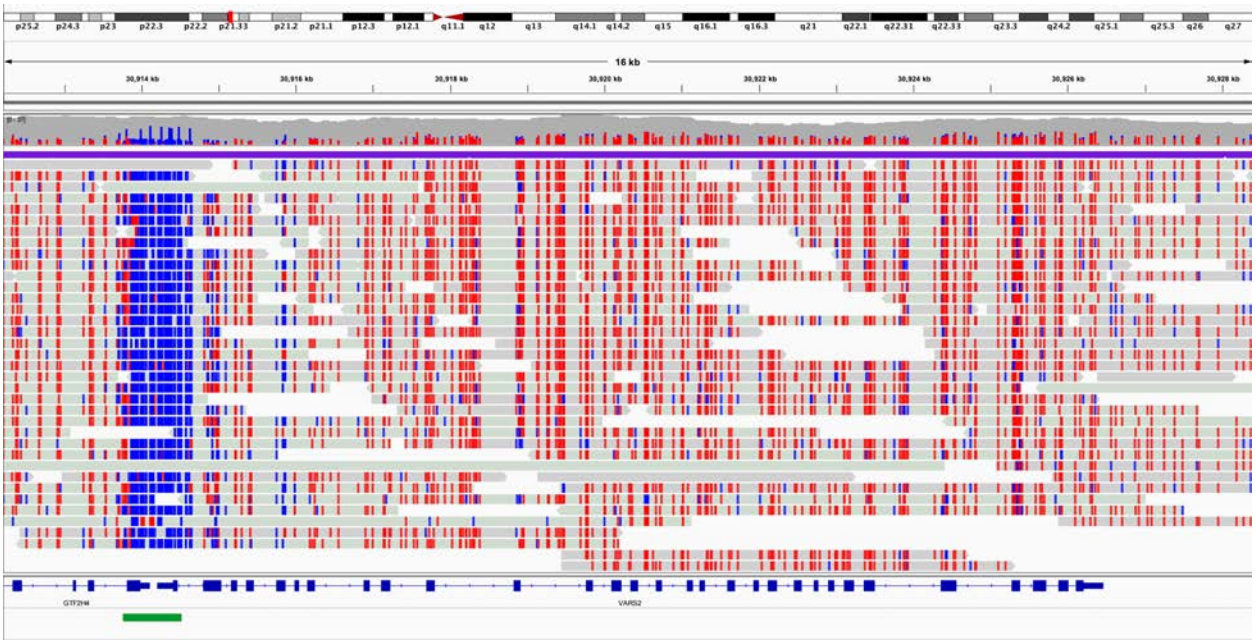

B. Analysis of reads reveals no change in methylation at the 5' UTR of *VARS2*. In this view, blue represents a hypomethylated region, suggesting an open 5' region and promoter. The green box under the promoter indicates the position of the CpG island. IGV view is chr6:30,912,208-30,928,459.

Figure S35. S008 (*HPRT1*), view of inversion and FISH results.

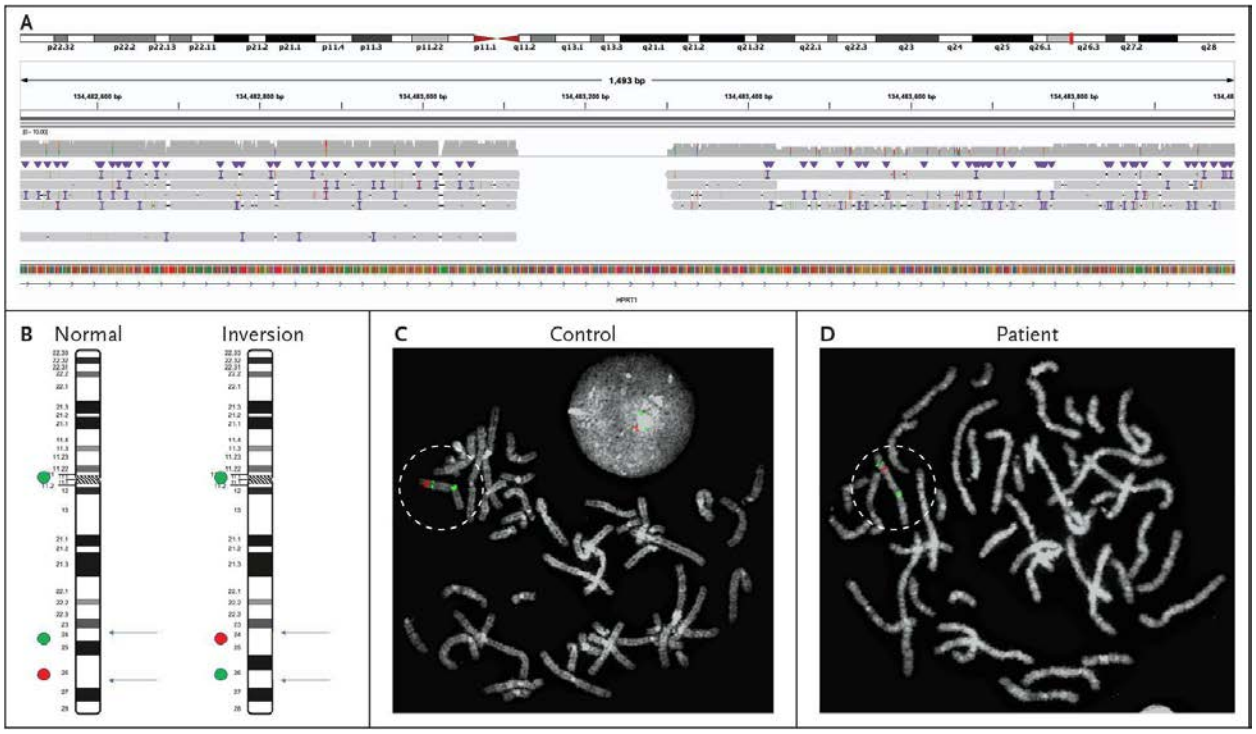

A. T-LRS suggested an approximately 17 Mbp inversion bisected *HPRT1*. Reads on the left partially mapped to approximately chrX:117,359,013 and reads on the right partially mapped to chrX:117,488,245. IGV view is chrX:134,482,505-134,484,004. **B.** FISH probes were designed to confirm the presence of an inversion. **C.** Image from control case, dashed circle highlights X chromosome. **D.** Image from the individual confirmed the presence of a 17 Mbp inversion reported as inversion (X)(q24q26.3), dashed circle highlights the X chromosome.

Figure S36. S009 (*DMD*), IGV view of AGAA expansion and frequency in SSC samples.

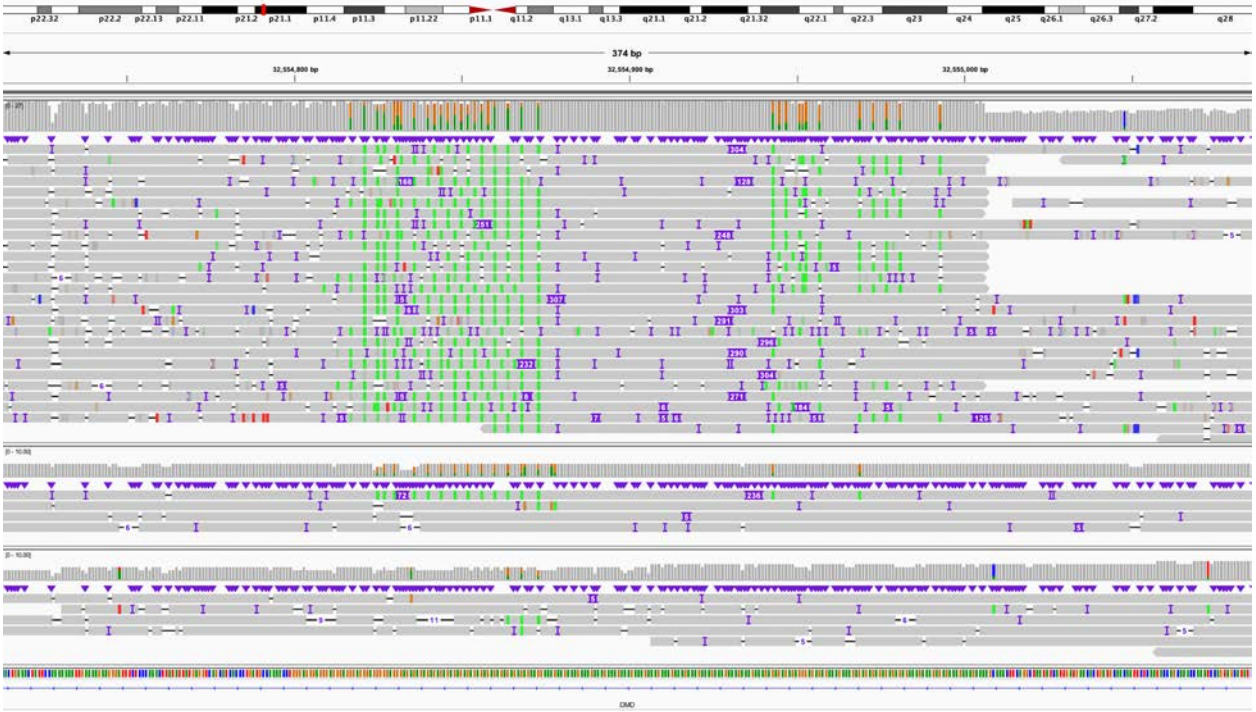

A. Expansion of an AGAA repeat represents a variant of uncertain significance in a child with a clinical diagnosis of Duchenne muscular dystrophy, but no molecular diagnosis. This view shows the insertion in intron 16 of the gene that is homozygous in the proband (top panel) and heterozygous in the bottom panel (the insert is divided into a 72 bp insert and a 236 bp insert). Bottom panel is from the proband's unaffected full brother who does not have an insertion at this position. IGV view is of chrX:32,554,713-32,555,087.

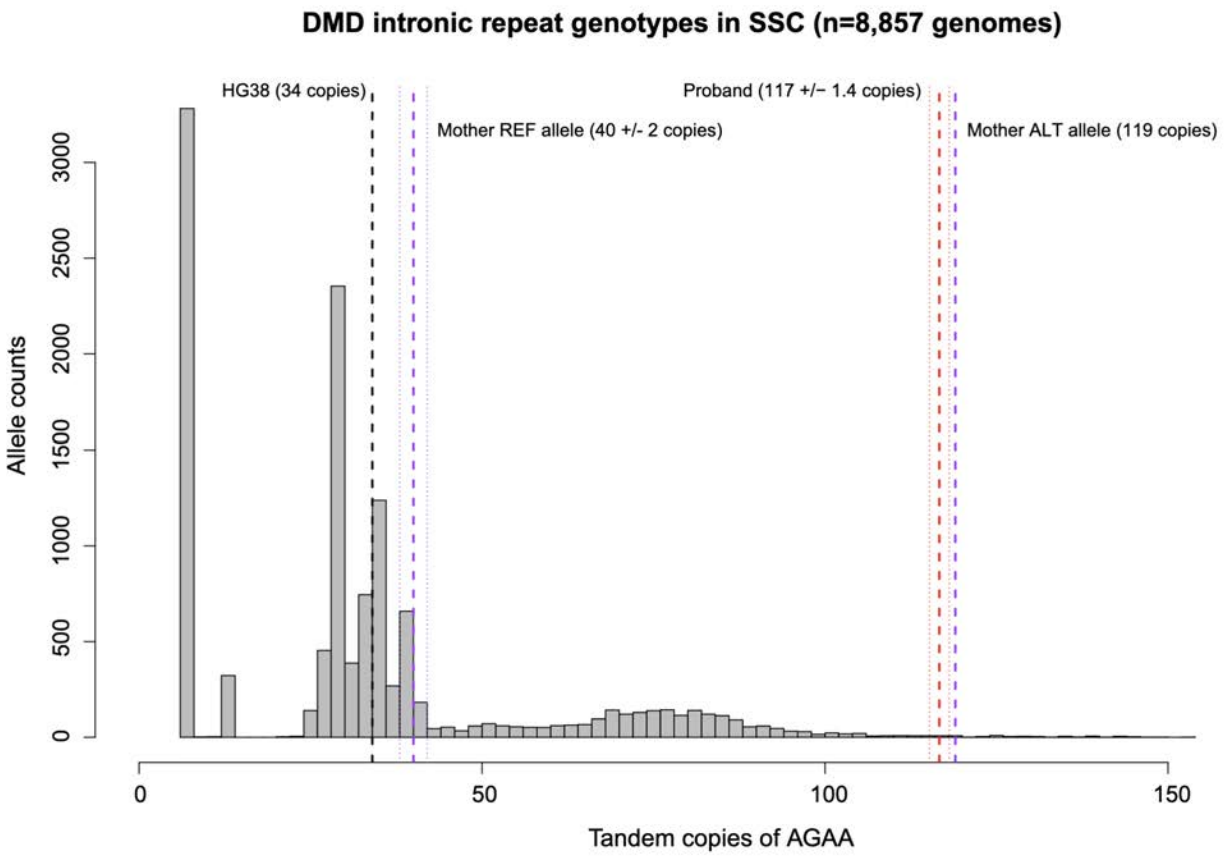

B. Histogram showing the number of individuals predicted to have an expansion of the AGAA repeat at the same position as the proband within the SSC collection. Position of the repeat expansion in the proband is shown in red, the length of the two haplotypes from the proband's mother is shown in red.

Figure S37. S013 (*HPS1*), IGV view of inherited variant and deletion identified by LRS.

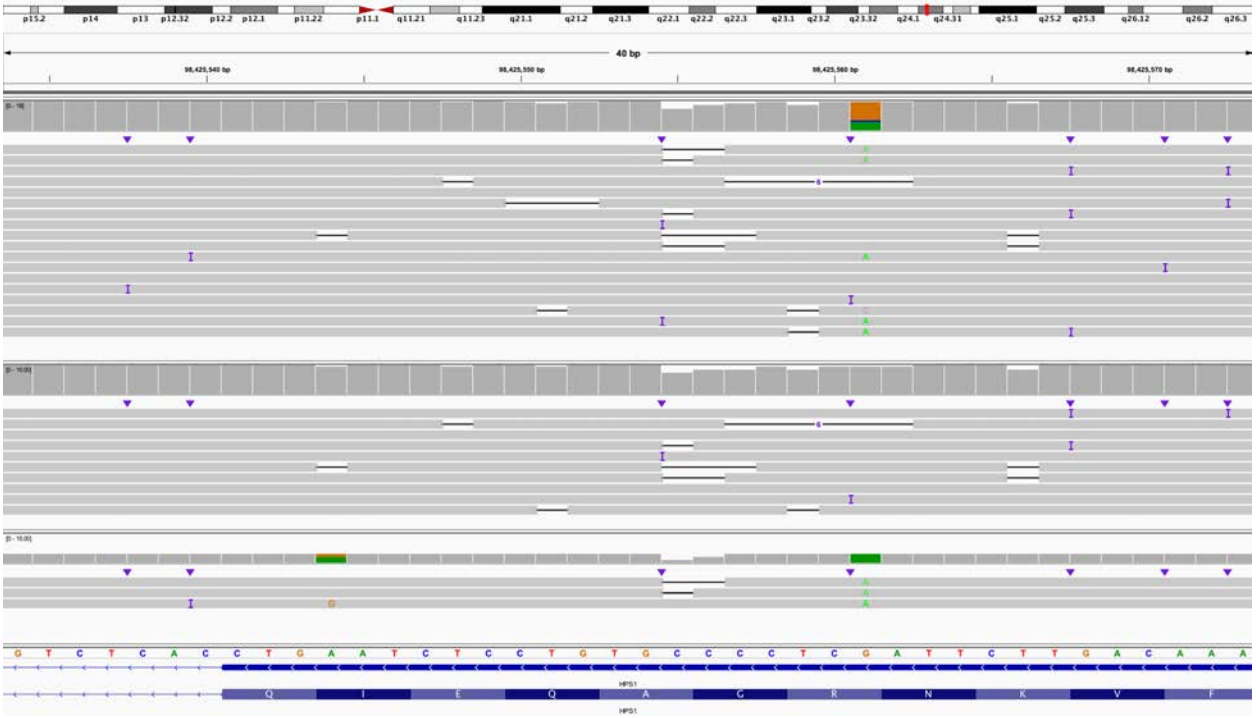

A. Screenshot of known paternally inherited pathogenic G>A variant. IGV view is of chr10:98,425,534-98,425,573. All reads are shown in the top track, haplotype 1 is the middle, and haplotype 2 is the bottom. Haplotype 2 is assumed to be the paternal track as the known paternally inherited G>A is in that track.

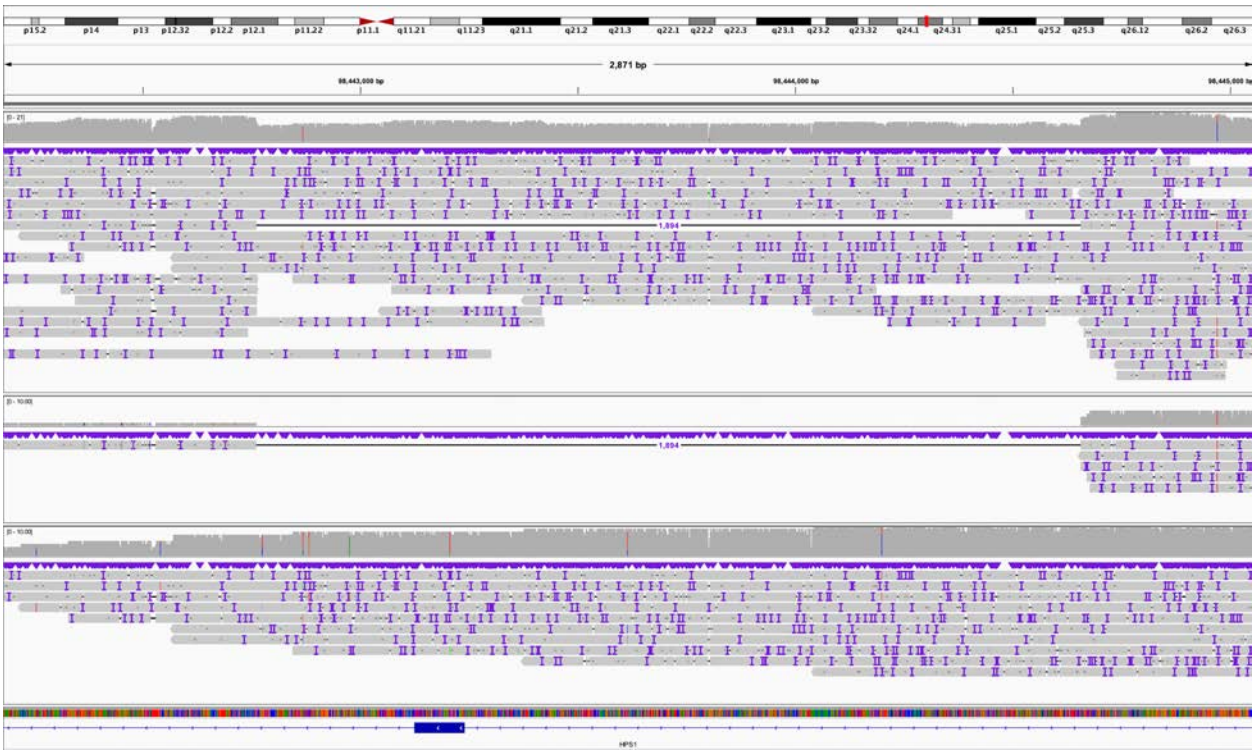

B. SV calling identified an approximately 1,900 bp deletion that included all of exon 3 on a different haplotype than the known G>A. Tracks are the same as in A. Screenshot from chr10:98,442,300-98,445,184.

Figure S38. S018 (*PAH*), known inherited splice variant identified, no second variant found.

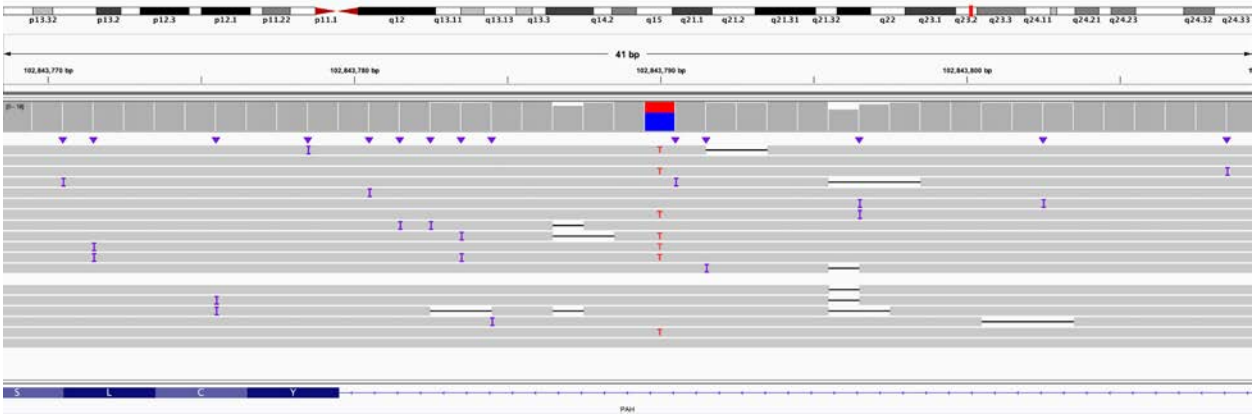

A. IGV view of previously known inherited pathogenic C>T splice variant. No second variant was found in this case. IGV view is of chr12:102,843,769-102,843,809.

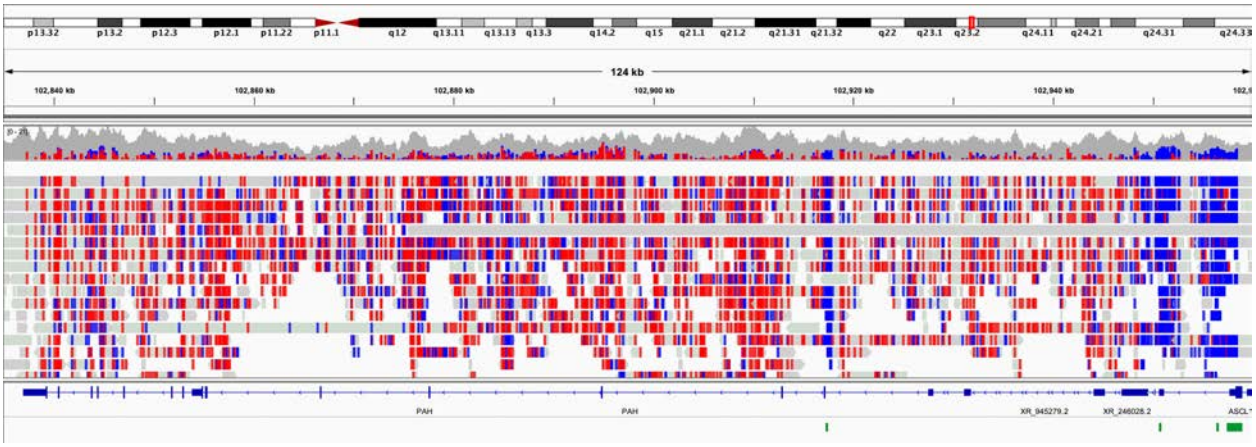

B. Bisulfite view of the entire *PAH* gene showing no hypermethylation near the 5' end of the gene (blue). Green blocks at the bottom of the image represent CpG islands. In this view, blue represents a CpG that is not methylated while red represents a methylated CpG.

Figure S39. S025 (*ABCA4*), the previously known variant and a 1,500 bp insertion can be phased into different haplotypes.

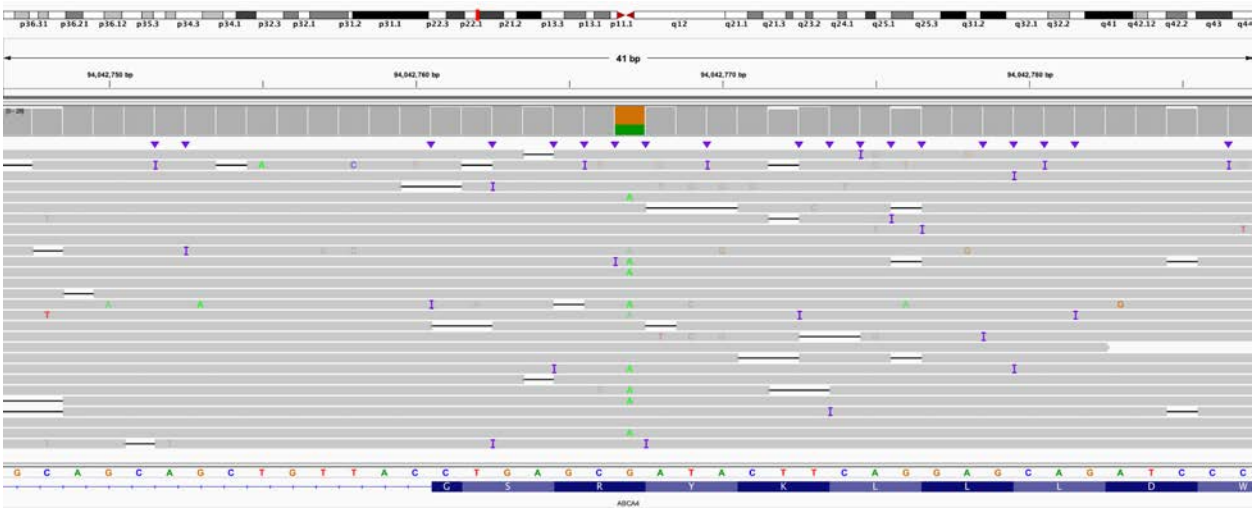

A. IGV screenshot of long reads showing the previously identified inherited pathogenic variant. IGV view is of chr1:94,042,747-94,042,787.

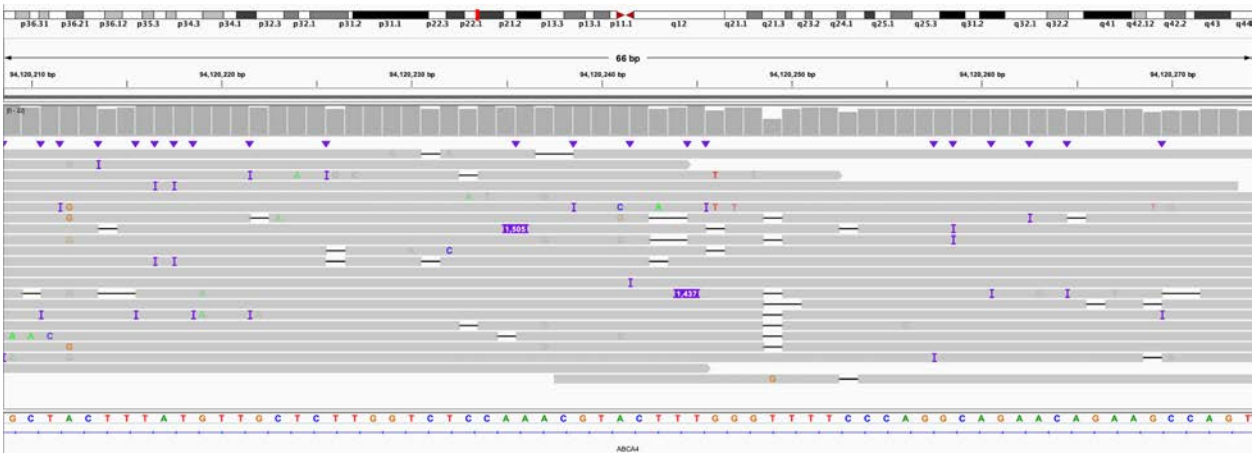

B. IGV screenshot of long reads showing two reads that include the 1,500 bp insertion in intron 1 of *ABCA4*. Several reads on either side of the region include the insertion and are soft clipped. IGV view is of chr1:94,120,209-94,120,274.

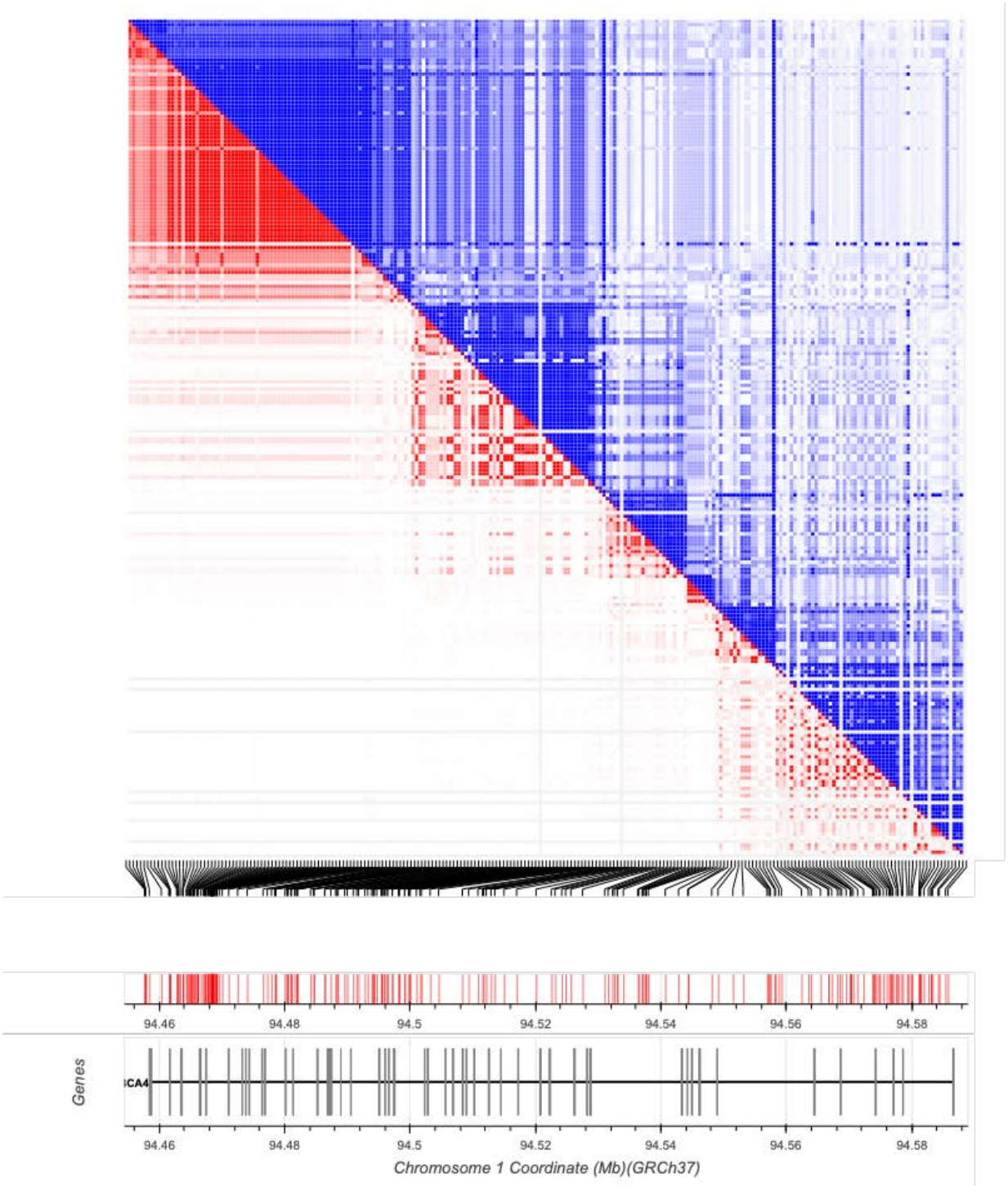

C. The linkage disequilibrium matrix represents R^2 and D' values in the lower and upper diagonal of the heatmap, respectively. Higher intensity colors represent higher linkage disequilibrium. Using orthogonal Illumina WGS data from S025, we identified all SNVs overlapping *ABCA4* using GATK, followed by calculating all pairwise R^2 and D' values using the 1000 Genomes Project Phase III genotypes.

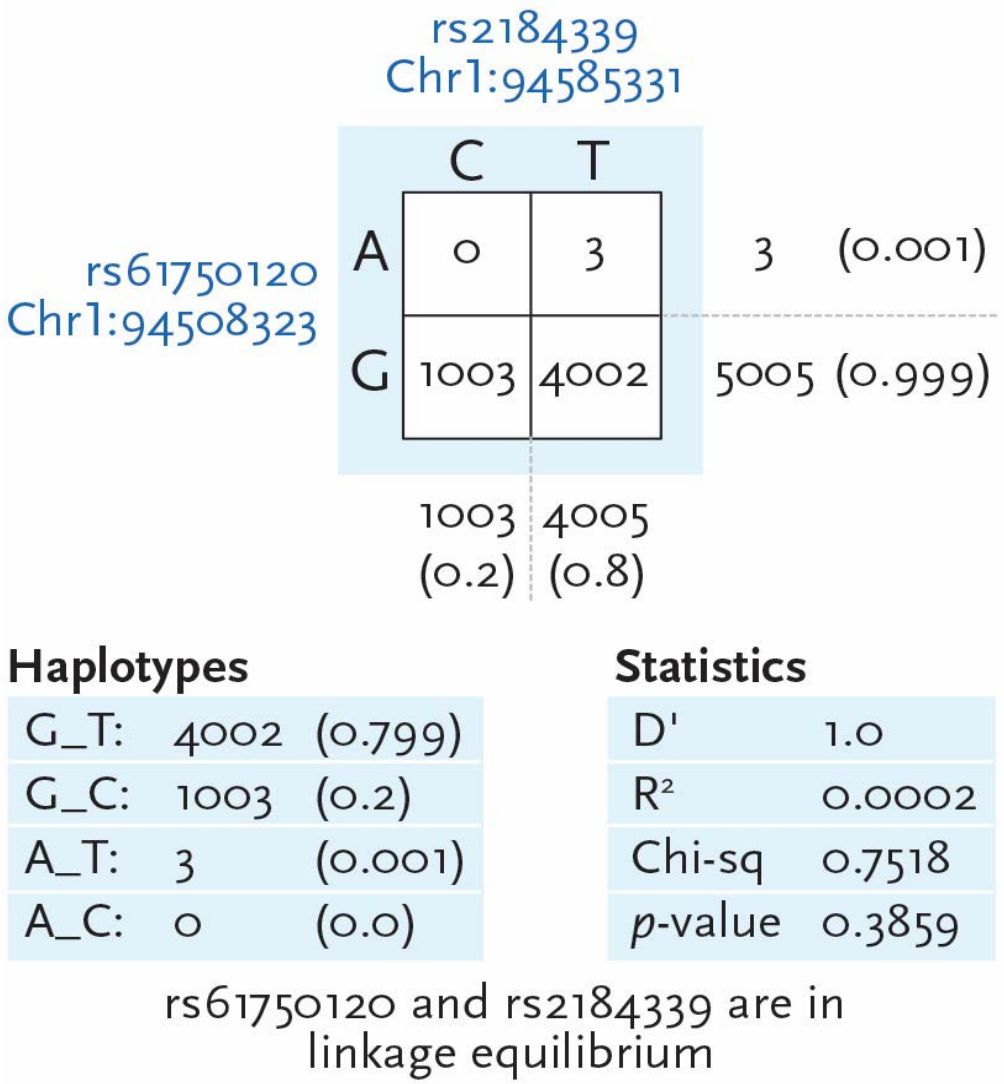

D. Phasing detail. The missense mutation on exon 22 corresponds to rs61750120 (G>A), while rs2184339 (T>C) has its alternative allele on the same allele as the 1.5 kbp insertion. Using the 1000 Genomes Project variation data (Machiela and Chanock 2015), we confirmed that the A allele of rs61750120 and the C allele of rs2184339 were never observed on the same haplotype (D'=1 and R^2=0.0001).

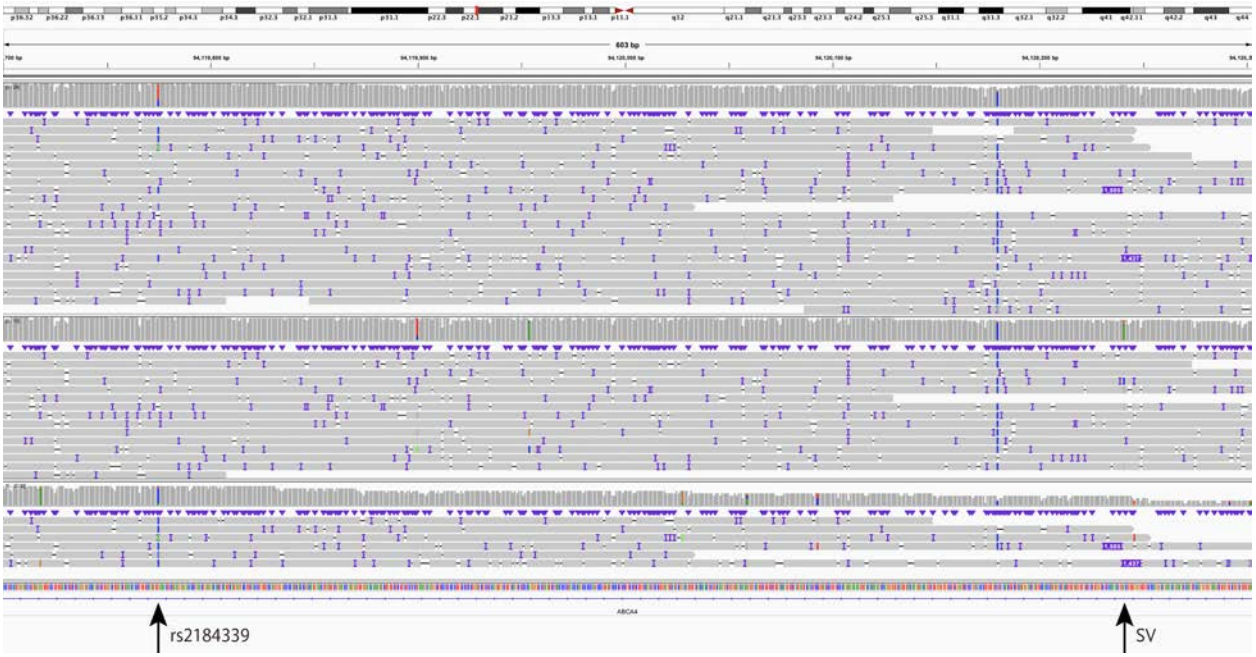

E. Phasing of long reads shows that rs2184339 (T>C) is present on reads with the 1,500 bp insertion. Most reads terminating at the insertion site are soft clipped. IGV view is of chr1:94,119,700-94,120,304.

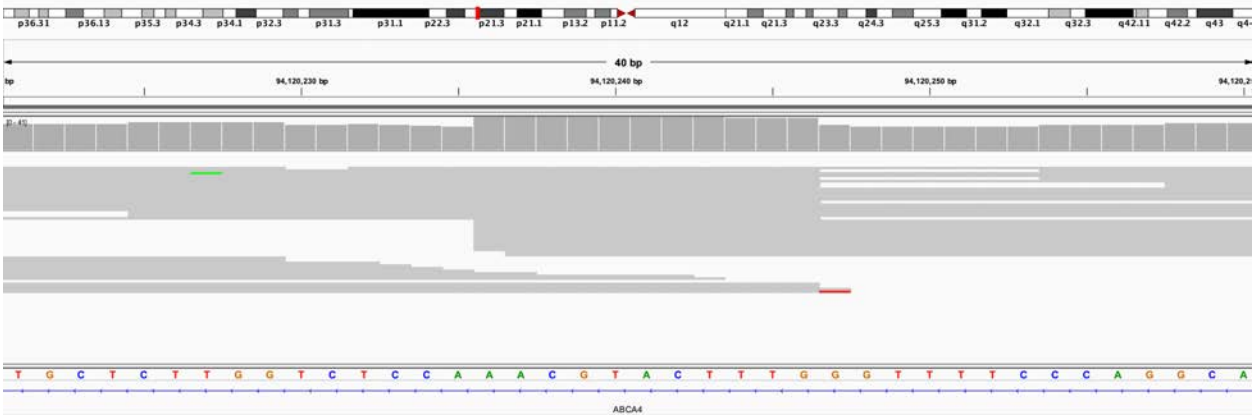

F. Analysis of short-read sequencing data reveals a 9 bp target site duplication at the position of the suspected insertion. IGV view is of chr1:94,120,221-94,120,260.

Figure S40. S047 (*AGL*), known single-nucleotide deletion, second hit is 1.5 kbp deletion.

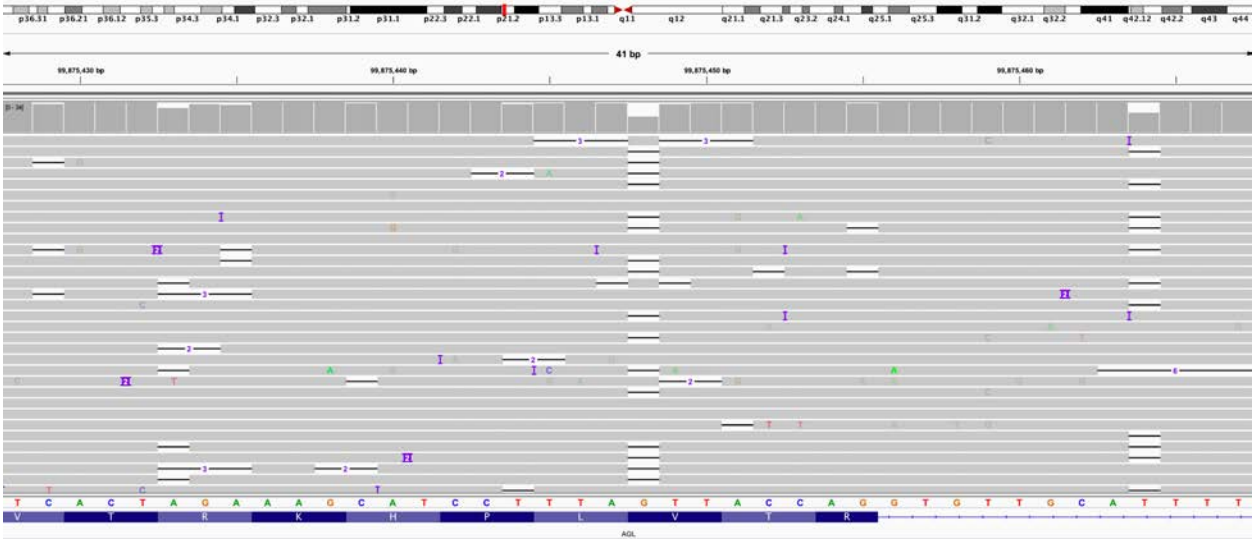

A. IGV screenshot of previously identified single-nucleotide deletion (view is chr1:99,875,428-99,875,467).

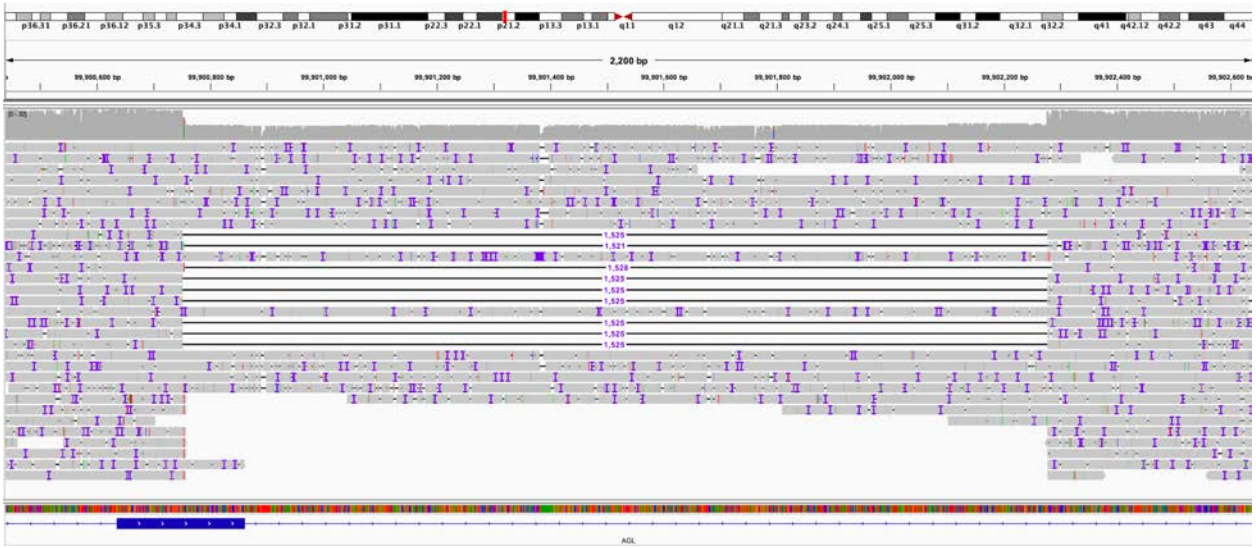

B. IGV screenshot of 1,525 bp deletion (coordinates are chr1:99,900,752-99,902,276) identified by Sniffles and SVIM (view is of chr1:99,900,438-99,902,636).

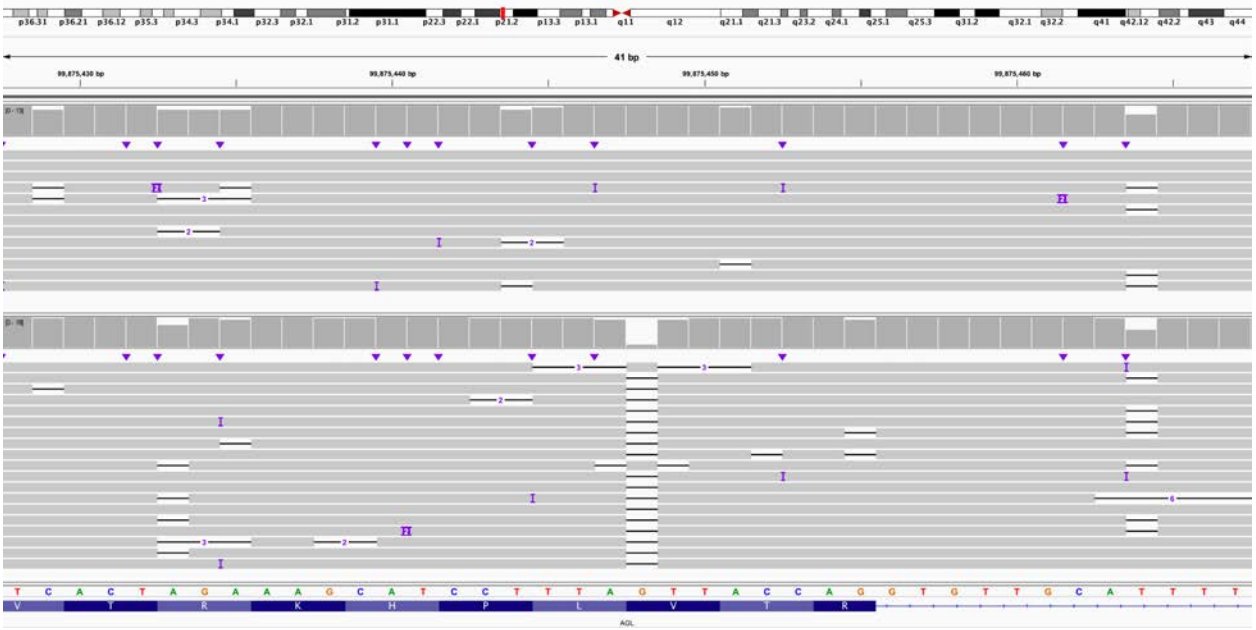

C. Longshot phased the reads into two haplotypes (HP1 and HP2) and suggests that the single-nucleotide deletion is on a different haplotype than the 1,525 bp deletion. IGV view is chr1:99,875,428-99,875,467.

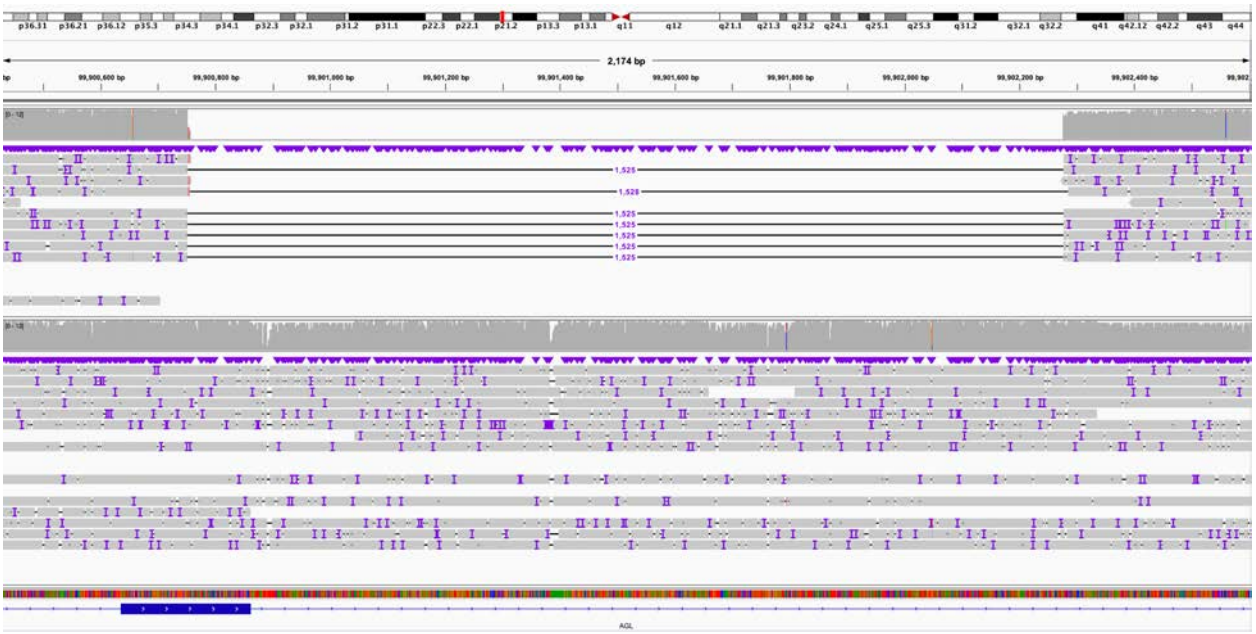

D. Longshot phased the reads into two haplotypes (HP1 and HP2) and suggests that the single-nucleotide deletion is on a different haplotype than the 1,525 bp deletion. IGV view is chr1:99,900,428-99,902,600.

Figure S41. S056 (*WDR19*), IGV views of inherited and splice variants identified by LRS.

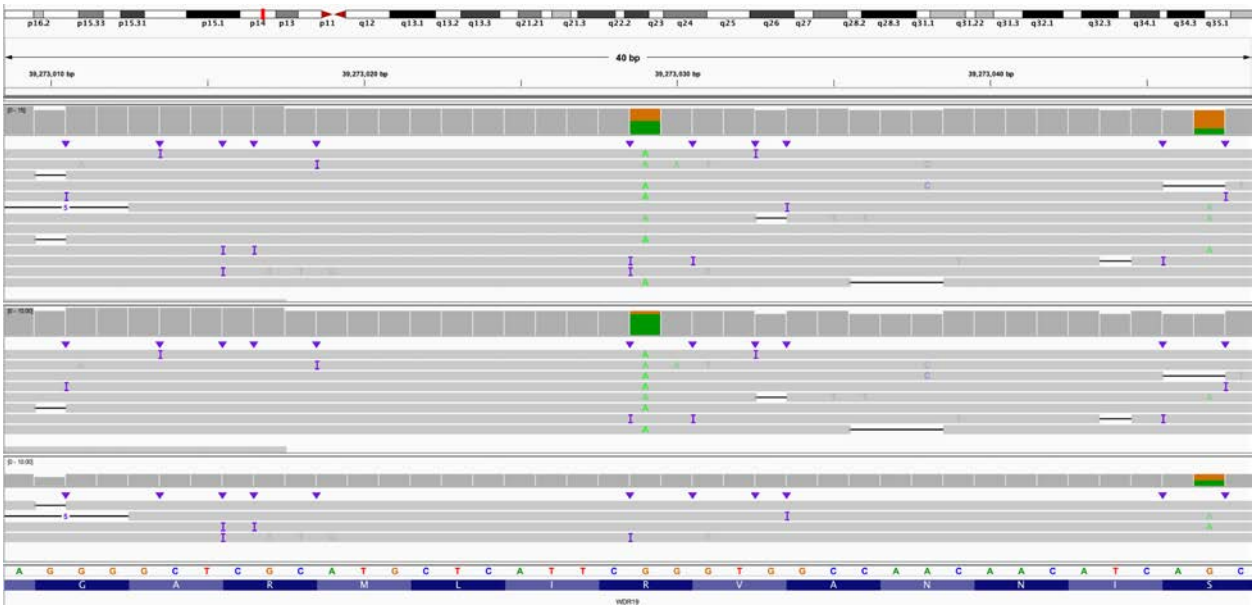

A. IGV view of known pathogenic inherited G>A. Top panel is all reads, middle panel is haplotype 1, and bottom panel is haplotype 2. IGV view is of chr4:39,273,009-39,273,048.

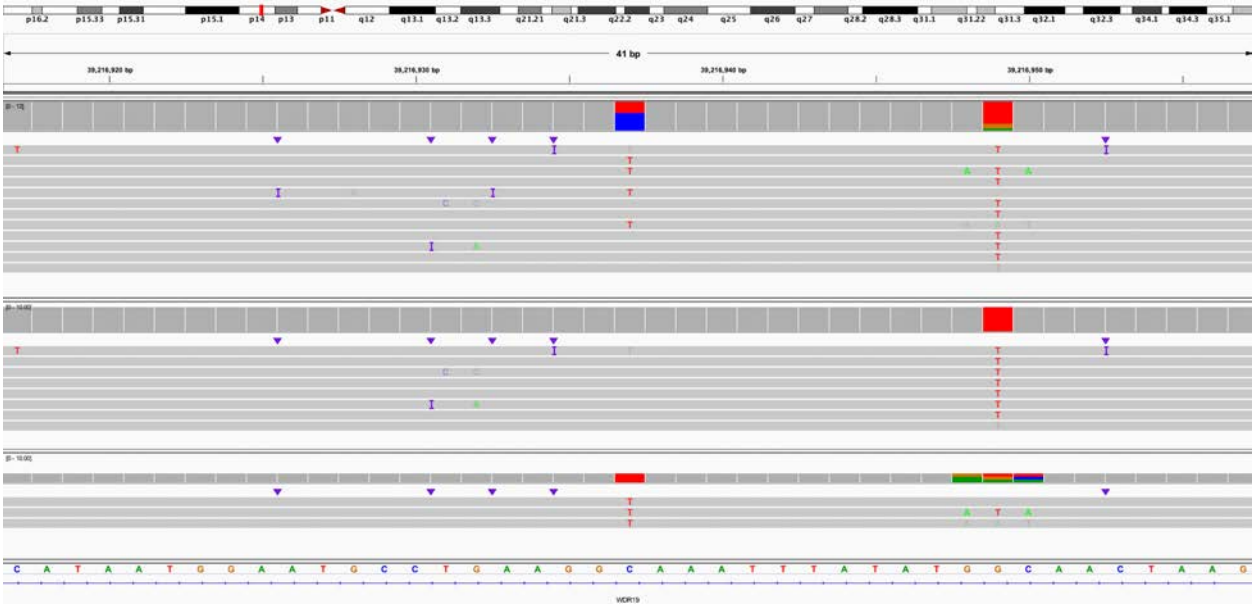

B. An intronic C>A variant in haplotype 2 is predicted to increase the likelihood this position acts as both a splice acceptor and donor. IGV view is of chr4:39,216,917-39,216,957.

Supplementary Tables

Table S1: Sample summary, DNA source, flow cells and libraries used per sample.

Type	Individual	DNA Source	Flow cells used	Libraries used	Summary of sample
Missing Variant (10)	S002	Blood	1	1	Single variant in *ALMS1*
	S003	Fibroblast	2	2	Single variant in *NPHP4*
	S004	Blood	3	3	Single variant in *VARS2*
	S008	Blood	2	3	No variant in *HPRT1*
	S009	Blood	3	4	No variant in *DMD*
	S013	Blood	1	2	Single variant in *HPS1*
	S018	Blood	1	1	Single variant in *PAH*
	S025	Blood	1	1	Single variant in *ABCA4*
	S047	Blood	1	1	Single variant in *AGL*
	S056	Blood	1	1	Single variant in *WDR19*
Phasing (2)	S071	Blood	1	1	Two variants in *METTL5*
	S086	Blood	2	2	Two variants in *KIAA1109*, one mosaic
Repeat Expansion (10)	S011	Saliva	1	1	Expansions of both *ATXN3* and *ATXN8OS*
	S039	Cell line	1	1	Expansion of *FMR1*
	S040	Cell line	1	1	Expansion of *FXN*
	S041	Cell line	1	1	Expansion of *FXN*
	04-01	Blood	1	1	Expansion and methylation of *XYLT1*
	06-01	Saliva	2	2	Expansion and methylation of *XYLT1*
	04-02	Fibroblasts	1	1	Mother of 04-01
	04-03	Saliva	1	1	Father of 04-01
	06-02	Saliva	1	1	Mother of 06-01
	06-03	Saliva	1	1	Father of 06-01
SV Case - Complex (8)	S014	Blood	1	1	Three noncontiguous deletions of chr6
	S020	Blood	2	3	Multiple deletions of chr4 and chr14, multiple translocations
	S021	Blood	2	2	Multiple mosaic deletions of chr8
	S022	Blood	1	1	Amplification of 4q with adjacent region of homozygosity
	S035	Blood	1	1	Two duplications
	S036	Blood	2	2	Four deletions on chr10, multiple translocations
	S082	Blood	1	1	Deletion of chr10, duplication on chr17
	S083	Blood	1	1	Deletion and duplication of chr4
SV Case - Simple (14)	BK144-03	Blood	1	1	22q13.3 deletion
	BK180-03	Blood	1	1	15q11-q13 duplication
	BK294-03	Blood	1	1	22q11.2 duplication
	BK364-03	Blood	1	1	1p36.11 duplication
	BK397-101	Blood	1	1	16p11.2 deletion
	BK430-103	Blood	1	1	16p11.2 duplication
	BK482-101	Blood	1	1	1q21.1 duplication
	BK487-101	Blood	1	1	1q21 deletion
	BK506-03	Blood	1	1	5p15.33 deletion
	S016	Blood	1	1	Tandem duplication in *CTNND2*
	S023	Blood	1	1	Mosaic ring 18
	S046	Blood	1	1	Unbalanced translocation between chr4 and chr15
	S060	Blood	1	1	Translocation between chr12 and chr17 in an individual with campomelic dysplasia
	S063	Fibroblast	1	1	Known SVA insertion in *BRCA1*

Table S2: Per sample sequencing targets, coverage, and average read length.

Individual	Target chr	Target start	Target end	Size of target region (bp)	Target, gene, or target	Average coverage of whole genome (x)	Average coverage of target region (x)	Average length of all reads (bp)	Average length of reads in target region (bp)
Simple SV cases									
BK144-03	22	17,500,000	50,818,000	33,318,000	22q13.3 del	3.5	14.7	539	2,133
BK180-03	15	20,000,000	35,000,000	15,000,000	15q11-q13 dup	3.6	61.5	524	4,289
BK294-03	22	17,500,000	50,818,000	33,318,000	22q11.2 dup	3.5	33.7	524	4,617
BK364-03	1	24,000,000	30,000,000	6,000,000	1p36.11 dup	2.0	21.2	427	3,692
BK397-101	16	26,500,000	35,300,000	8,800,000	16p11.2 del	0.7	12.5	865	6,230
BK430-103	16	25,000,000	35,000,000	10,000,000	16p11.2 dup	1.5	17.0	612	4,057
BK482-101	1	140,000,000	155,000,000	15,000,000	1q21.1 dup	2.2	22.8	417	2,258
BK487-101	1	140,000,000	155,000,000	15,000,000	1q21 del	1.6	36.9	515	6,883
BK506-03	5	1	8,000,000	7,999,999	5p15.33 del	2.7	15.8	443	3,814
S016	5	11,026,788	12,124,078	1,097,290	*CTNND2* dup	1.8	25.3	440	4,626
S023	18	1	5,000,000	4,999,999	8p	2.2	23.1	561	5,106
	18	45,000,000	80,373,285	35,373,285	8q	2.2	21.4	561	5,947
S046	4	180,000,000	190,214,555	10,214,555	translocation	2.0	9.8	436	2,757
	15	90,000,000	101,991,189	11,991,189	translocation	2.0	17.7	436	3,068
S060	12	45,000,000	65,000,000	20,000,000	translocation	2.0	27.2	579	6,574
	17	65,000,000	80,000,000	15,000,000	translocation	2.0	26.3	579	6,801
S063	17	42,000,000	44,000,000	2,000,000	SVA insertion	2.1	18.8	724	5,925
Repeat expansion cases									
S011	14	92,041,011	92,101,011	60,000	*ATXN3*	2.7	8.3	481	1,099
	13	70,109,384	70,169,384	60,000	*ATXN8OS*	2.7	9.2	481	1,197
S039	X	147,862,037	147,962,037	100,000	*FMR1*	2.1	10.0	450	3,772
S040	9	69,007,285	69,067,285	60,000	*FXN*	1.6	21.2	483	5,649
S041	9	69,007,285	69,067,285	60,000	*FXN*	0.9	15.5	484	8,134
04-01	16	16,500,000	18,000,000	1,500,000	*XYLT1*	2.5	18.2	474	5,170
06-01	16	16,500,000	18,000,000	1,500,000	*XYLT1*	2.3	8.0	415	2,121
04-02	16	16,500,000	18,000,000	1,500,000	*XYLT1*	0.9	11.5	511	5,815
04-03	16	16,500,000	18,000,000	1,500,000	*XYLT1*	2.3	4.7	894	2,308
06-02	16	16,500,000	18,000,000	1,500,000	*XYLT1*	0.4	3.0	645	3,276
06-03	16	16,500,000	18,000,000	1,500,000	*XYLT1*	1.1	2.2	470	2,036
Cases with complex copy number changes									
S014	6	150,000,000	165,000,000	15,000,000	-	2.7	13.3	420	2,105
S020	2	1	36,300,000	36,299,999	1st run	1.9	16.3	872	6,639
	4	65,000,000	78,000,000	13,000,000	1st run	1.9	14.4	872	6,556
	10	59,474,150	80,320,091	20,845,941	1st run	1.9	16.3	872	6,569
	14	20,881,587	24,829,792	3,948,205	1st run	1.9	12.1	872	6.549
	10	41700000	59,475,000	17,775,000	2nd run	0.6	9.2	785	7,158
	4	51800000	65,000,000	13,200,000	2nd run	0.6	7.3	785	8,057
	4	78000000	100,000,000	22,000,000	2nd run	0.6	7.2	785	8,072
	14	25900000	50,000,000	24,100,000	2nd run	0.6	7.4	785	8,239
S021	8	1	145,138,636	145,138,635	-	4.9	34.7	642	3,603
S022	4	162611564	190000000	27,388,436	-	2.0	31.2	634	8,158
	15	22,000,000	23,500,000	1,500,000	-	2.0	31.8	634	6,003
S035	8	130,000,000	145,138,636	15,138,636	-	2.7	38.7	538	5,712
	16	10,000,000	20,000,000	10,000,000	-	2.7	38.5	538	5,671
S036	6	114,000,000	124,000,000	10,000,000	1st run	2.6	35.7	602	6,443
	18	7,000,000	16,000,000	9,000,000	1st run	2.6	34.9	602	6,010
	10	20,000,000	38,000,000	18,000,000	1st run	2.6	33.4	602	6,487
	10	50,000,000	60,000,000	10,000,000	1st run	2.6	32.4	602	6,446
	5	1	46,000,000	45,999,999	2nd run	0.7	7.8	828	8,413
	6	124,000,000	170,805,979	46,805,979	2nd run	0.7	7.6	828	8,511
	18	1	7,000,000	6,999,999	2nd run	0.7	7.8	828	7,535
S082	10	107,000,000	114,000,000	7,000,000	-	1.7	9.3	663	3,003
	17	1	23,000,000	23,000,000	-	1.7	10.3	663	2,916
S083	4	1	49,000,000	49,000,000	-	2.2	34.3	628	6,407
Phasing cases									
S071	2	169,780,000	169,850,000	70,000	*METTL5*	0.7	9.6	487	5,937
S086	4	121,200,000	123,300,000	2,100,000	*KIAA1109*	2.8	29.4	480	4,723

Missing variant cases									
S002	2	73,200,000	73,800,000	600,000	*ALMS1*	1.4	17.0	608	6,780
S003	1	5,762,810	6,092,425	329,615	*NPHP4*	2.9	21.6	792	6,232
S004	6	30814208	31026459	212,251	*VARS2*	3.5	41.9	640	6,443
S008	X	134,360,165	134,600,668	240,503	*HPRT1*	2.5	7.2	1,151	7,160
S009	X	31,019,219	33,439,460	2,420,241	*DMD*	6.9	29.5	501	3,344
S013	10	98,316,193	98,546,963	230,770	*HPS1*	3.7	18.7	751	3,484
S018	12	102,736,889	103,058,441	321,552	*PAH*	2.1	11.4	459	2,102
S025	1	93,000,000	95,000,000	2,000,000	*ABCA4*	3.2	23.1	574	3,392
S047	1	98,000,000	102,000,000	4,000,000	*AGL*	1.6	23.5	491	5,753
S056	4	35,000,000	43,000,000	8,000,000	*WDR19*	1.4	22.1	537	8,282

Table S3: Overview of individuals with a known single structural variant.

Individual	Previously known result	Confirmation of known result	Additional information gained with T-LRS	Previously reported event	Events seen by LRS
BK144-03	22q13.3 deletion	Identified the known deletion.	Identified exact position of deletion breakpoints.	1 deletion	1 deletion
BK180-03	15q11-q13 duplication	Identified the known duplication.	None	1 duplication	1 duplication
BK294-03	22q11.2 duplication	Identified the known duplication.	None	1 duplication	1 duplication
BK364-03	1p36.11 duplication	Identified the known duplication.	Identified the exact position of the duplication breakpoints and found that the duplication is tandem.	1 duplication	1 duplication
BK397-101	16p11.2 deletion	Identified the known deletion.	None	1 deletion	1 deletion
BK430-103	16p11.2 duplication	Identified the known duplication.	None	1 duplication	1 duplication
BK482-101	1q21.1 duplication	Identified the known duplication.	None	1 duplication	1 duplication
BK487-101	1q21 deletion	Identified the known deletion.	None	1 deletion	1 deletion
BK506-03	5p15.33 deletion	Identified the known deletion.	Appears to be an unbalanced translocation between chr5 and chr12. Short-read data from the individual agrees and the translocation is not found in parental short-read data.	1 deletion	Translocation between chr5 and chr12
S016	Tandem duplication in *CTNND2*	Identified the known duplication and confirmed it is tandem.	None	1 duplication	1 duplication
S023	Mosaic ring 18 in 40% of cells.	See decreased coverage in regions reported on the array.	None.	2 mosaic deletions	2 mosaic deletions
S046	Unbalanced translocation between chr4 and chr15.	Identified the translocation via coverage.	Identified exact position of translocation breakpoints.	Translocation	Translocation
S060	Translocation between chr12 and chr17	Identified the translocation	Exact position of translocation breakpoints	Translocation	Translocation
S063	SVA insertion in *BRCA1*	Identified SVA insertion	None, this served as a control	SVA insertion	SVA insertion

Table S4: Overview of individuals with repeat expansions, including expected and observed repeat expansion sizes.

Individual	Gene(s)	Repeat	Previously reported repeat size	Repeat position	BP added to window for repeat assay	Number of reads spanning window	Average repeat lengths (% difference from expected if known)
S011	*ATXN3*	CAG	Clinically reported as 74 and 28 repeats	chr14:92071012-92071052	100	10	25 (11%), 77 (4%)
S011	*ATXN8OS*	CAG	Clinically reported as 80 and 25 repeats	chr13:70139385-70139429	25	8	15 (40%), 73 (9%)
S039	*FMR1*	CGG	Coriell sample 06897, reported as 477 repeats.	chrX:147911980-147912111	200	3	386 (19%)
S040	*FXN*	GAA	Coriell sample 16789, reported as 750 and 1000 repeats.	chr9:69,037,285-69,037,302	50	4	333 (56%), 1049 (5%)
S041	*FXN*	GAA	Coriell sample 15850, reported as 650 and 1030 repeats.	chr9:69,037,285-69,037,302	50	9	647 (1%), 958 (7%)
04-01	*XYLT1*	GGC	Previously reported expansion.	chr16:17470921-17470922	500	4	758
04-02	*XYLT1*	GGC	Mother of 04-01, reported as one wild-type and one premutation allele.	chr16:17470921-17470922	50	16	97, 221
04-03	*XYLT1*	GGC	Father of 04-01, reported as two wild-type alleles.	chr16:17470921-17470922	50	2	71
06-01	*XYLT1*	GGC	Previously reported expansion.	chr16:17470921-17470922	500	5	224
06-02	*XYLT1*	GGC	Mother of 06-01, reported as one wild-type and one premutation allele	chr16:17470921-17470922	50	1	81
06-03	*XYLT1*	GGC	Father of 06-01, reported as two wild-type alleles	chr16:17470921-17470922	50	1	78

Table S5: Per-read details of individuals with *ATXN3*, *ATXN8OS*, *FMR1*, and *FXN* repeat expansions.

Read ID	Repeat Length (bp)	Repeats (Estimate)	Repeat Group	Average Number of Repeats
S011 - ATXN3				
c4b0552d-118e-4d6b-9411-09b0861262fe	55	18	1	25
616cf7f8-a13f-429a-b0c5-825f1a15da3d	72	24	1	
e133bc59-4c37-4c5c-8ce9-b206180058eb	77	26	1	
eadb0392-728a-4437-8e5e-c2814638894f	79	26	1	
2f107739-f4a6-40f0-b52b-252132f992f3	85	28	1	
137c7831-3cb4-4f7c-99b6-196a969702dc	218	73	2	77
72ed9321-3c6b-4cab-b508-83d6efc1efc0	230	77	2	
b6a6b164-c767-4514-b723-4a6643a0f3f5	231	77	2	
e6c40588-04c8-4a17-b740-fc1990995267	232	77	2	
0fa6df78-d10e-42f8-9e1e-6db5a907d858	250	83	2	
S011 - ATXN8OS				
9712bb2f-b1fb-40db-9e05-6f708b6443e4	41	14	1	15
3e0a7cc1-ee7f-47ff-97f4-9516cbebb21e	43	14	1	
d5eea8a6-f1d5-459f-b865-bff3c35a26b3	44	15	1	
c03fb6ab-a4a1-4518-b946-ad650f578e25	46	15	1	
70fec058-32ab-4270-aaa6-1984af7b1402	197	66	2	73
4f49b32d-139c-4beb-b831-9c4a5b7a19be	206	69	2	
a7304699-9d25-4843-b587-cb84de848b84	226	75	2	
489bde02-eae6-4270-a7db-1e488b61ccfd	245	82	2	
S039 - FMR1				
5fac5744-2c5c-4211-88c8-5b9ee3a20752	759	253	1	386
b215ab66-d863-46d3-878e-69d3d855a302	1448	483	1	
ef287abe-e2a4-4b0e-8121-1de041a53f77	1268	423	1	
S040 - FXN				
44970178-6c34-48e8-afd9-f529d6bda0e2	985	328	1	333
1e915a81-c955-4c88-8946-b3e73d371b64	1004	335	1	
afddceb3-0802-404d-a61c-24ecdba887db	1007	336	1	
a66018cb-a390-4cb6-89f4-b9c0073e68f8	3147	1049	2	1049
S041 - FXN				
a93466ef-353b-403d-a2ec-d5439867b826	1788	596	1	647
b1ac947d-e98d-41f4-b5ca-d464e3668388	1939	646	1	
8164bc3d-6cae-4928-a975-e695c48bc757	1963	654	1	
0bfda482-97a2-42c8-ad67-798ebf2bd5b8	2079	693	1	
bf8f85f8-f878-4f38-aefc-b7aa0009b8ae	2415	805	2	958
89100931-0b2b-4938-a882-f7c81652858a	2895	965	2	
20ad64ba-a1b7-4371-93f8-e3c425c2c008	2996	999	2	
d13da846-f4f3-45ba-806a-0f77f50bb71a	3000	1000	2	
c0a0f7ad-c30a-4e40-ab51-fe00b1ab699a	3058	1019	2	

Table S6: Per-read details of *XYLT1* repeat expansions.

Read ID	Repeat Length (bp)	Insert between *Kpn*I cut sites (bp)	Repeats	Repeat Group	Average Number of Repeats
04-01 - XYLT1					
71ed6a24-3280-465a-8114-338c0eb6308d	1846	4435	615	1	758
c522d590-4165-47ac-9d4e-fb98f391bc13	2861	5450	954	1	
beb4b5c7-293c-4f69-b275-d393c6a3ae34	1591	4180	530	1	
a09207e2-a9cc-4cb6-9e12-f9fb56214399	2800	5389	933	1	
04-02 - XYLT1					
b2bebdb7-8e03-4b86-833f-445c1c2cd1d0	167	2756	56	1	97
7c629eb4-81f6-4d27-988b-b827b81419a2	282	2871	94	1	
775ca9d2-16b7-43f2-8855-6ef25cfd26a0	283	2872	94	1	
0cce5876-2f35-44f8-835f-867f08e4e571	288	2877	96	1	
879df89f-3293-4bec-93ec-073c985c3a18	288	2877	96	1	
83d4020e-16f1-4b94-95d8-1bf48fca6de6	295	2884	98	1	
970f3e26-1807-42d3-b15e-4c85a25b6ab4	433	3022	144	1	
0edbaf14-3d7e-46a2-a03d-268c784560f3	603	3192	201	2	221
b09a91bf-aee4-4fc0-a7bf-51d7cb1ad126	615	3204	205	2	
40767c26-5d0c-467d-bdcf-c1a6346d4229	641	3230	214	2	
f85efe4f-2d32-4a6d-a217-165c6dbdc661	645	3234	215	2	
b0a508ce-069d-43ac-865e-7b7cd900eb70	653	3242	218	2	
5c6ac009-694d-4f86-9511-8708f952a81c	688	3277	229	2	
4e315aca-60a8-4e61-8cd6-c08f129d701a	693	3282	231	2	
227e44ce-2051-4169-9b25-17cfdb50a4c5	716	3305	239	2	
011e133a-ea64-43fd-a4f4-0c2cfc8fe56e	725	3314	242	2	
04-03 - XYLT1					
bba6d56d-5293-4c5b-bd03-327dc12f7ece	218	2807	73	1	71
370138b9-090a-4fb0-80bc-01723888a41b	209	2798	70	1	
06-01 - XYLT1					
c66d7ab6-2ec4-417d-9445-d1d68ef3cf8e	668	3257	223	1	224
7db4e75c-c2f7-4029-9c6e-a8e06ff269a6	720	3309	240	1	
210471f7-0e15-436e-862f-85557ad3d4ff	734	3323	245	1	
8f3c0400-f5dc-47e2-bc69-611a477181bf	622	3211	207	1	
5e39f080-90c9-4f3d-ba8b-bed01bef0caa	616	3205	205	1	
06-02 - XYLT1					
236a7c09-2c88-4ee8-b2b3-fda20bc625c1	243	2832	81	1	81
06-03 - XYLT1					
9e7e1ed4-ebc2-4b30-a8ea-4c561d87e793	235	2824	78	1	78

Table S7: Summary of individuals with complex SVs, including previously known events and new events identified by T-LRS.

Individual	Previously known result	Confirmation of known result	Additional information gained with T-LRS	Total previously known events	Total new events
S014	Three noncontiguous deletions of chromosome 6.	Identified the three deletions seen on array	Identified two additional deletions and one rearrangement, and found no pathogenic or likely pathogenic variants in deleted regions.	3	3
S020	Two deletions of 4q and one of 14q identified on the array. Karyotype revealed translocation between chromosomes 2, 4, 10, and 14.	Identified the three deletions seen on array and several translocations between chromosomes 2, 4, 10, and 14.	Identified one additional deletion on chromosome 4 and two on chromosome 10. Found the exact position of all translocation breakpoints, revealing two that bisected genes with AD phenotypes. Identified additional rearrangement breakpoints within chromosome 10 and chromosome 14 not involved in a deletion or translocation.	7	22
S021	Terminal 3.2 Mbp loss of 8p23.3 to p23.2 with a copy state of 1. Adjacent interstitial 3.7 Mbp mosaic loss of 8p23.2 to p23.1 with a copy state between 1 and 2. Terminal 50 Mbp mosaic gain of 8q22.1 to q24.3 with a copy state between 2 and 3.	Confirmed mosaic loss and gain seen on array.	Find that a common 400 kbp duplication on 8p not reported on the array appears to be inverted and attached to the chromosome 8 not carrying a deletion.	3	1
S022	Focal amplification of 4q (copy state 4 or greater) with adjacent region of homozygosity and 15q11.2 duplication.	See the amplification of 4q32, homozygosity of 4q, and duplication in 15q11.2.	Determined the structure of the tandem amplification on chr 4 and confirmed 5 copies of the amplification (6 with the wild-type chromosome). Do not see breakpoints of the 15q11.2 duplication, but do see the duplication. No methylation differences or pathogenic variants in the homozygous region.	2	0
S035	Duplications of 8q24 and 16p13.11	Both duplications observed.	Found that 8q duplication is tandem and identified exact breakpoints. Could not identify the exact position of the 16p13.11 duplication that is flanked by segmental duplications.	2	0
S036	Four deletions on chr 10, karyotype found translocation between chr 18 and 6 and pericentric inversion of chr10.	Identified four deletions and found the t(6;18).	Found additional translocations between chromosome 10 and chromosome 5 as well as additional rearrangements on chromosomes 6, 10, and 18.	7	13
S082	Single pathogenic deletion on chr 10. One complex likely pathogenic CNV on chr 17 with two deletions and three duplications.	Identified the deletion on chr 10. Identified the two deletions and three duplications on chr 17.	Determined that the duplications are rearranged and inverted.	6	2
S083	Deletion of distal arm of 4p, duplication of 4p proximal to the deletion.	Identified the deletion and duplication.	Determined the exact position of the deletion and duplication breakpoints.	2	0

Table S8: Known and new events observed for individuals with known complex SVs.

	Known				Observed				New Events			
Individual	Deletion	Duplication	Translocation	Rearrangement	Deletion	Duplication	Translocation	Rearrangement	Deletion	Duplication	Translocation	Rearrangement
S014	3	0	0	0	5	0	0	1	2	0	0	1
S020	3	0	4	0	5	0	11	13	2	0	7	13
S021	2	1	0	0	2	1	0	1	0	0	0	1
S022	0	2	0	0	0	2	0	0	0	0	0	0
S035	0	2	0	0	0	2	0	0	0	0	0	0
S036	4	0	2	1	6	0	8	6	2	0	6	5
S082	3	3	0	0	3	3	0	0	0	0	0	2
S083	1	1	0	0	1	1	0	0	0	0	0	0

Table S9: Details of focal amplification of 4q in individual S022.

Region	Size (bp)	Copy number estimate	Coverage	Increase or decrease in coverage from prior
chr4:160,000,000-160,143,267	143,267	2	31.3	
chr4:160,143,268-160,165,900	22,632	3	43.9	12.6
chr4:160,165,901-160,248,169	82,268	4	62.7	18.8
chr4:160,248,170-160,450,953	202,783	5	76.0	13.3
chr4:160,450,954-162,685,228	2,234,274	6	93.8	17.8
chr4:162,685,229-162,689,149	3,920	4	57.6	-36.2
chr4:162,689,150-162,700,000	110,850	2	30.6	-27.0

Table S10: Rearrangement numbers and sizes for individual S014.

Chr	Segment	Start	End	Size (bp)	Source/Type
6	A	1	153,854,905	153,854,904	-
6	B	153,854,906	154,095,842	240,936	Deletion
6	C	154,095,843	154,587,147	491,304	Inversion
6	D	154,587,148	154,588,799	1,651	Deletion
6	E	154,588,800	154,661,283	72,483	-
6	F	154,661,284	156,456,517	1,795,233	Deletion
6	G	156,456,518	156,460,113	3,595	Inversion
6	H	156,460,118	156,464,495	4,377	-
6	I	156,464,502	157,015,124	550,622	-
6	J	157,015,125	158,766,820	1,751,695	Deletion
6	K	158,766,821	164,500,069	5,733,248	-
6	L	164,500,070	164,654,921	154,851	Deletion
6	M	164,654,922	170,805,979	6,151,057	-

Table S11: Genes impacted by S014 breakpoints.

Chr	Breakpoint	Gene affected by breakpoint	Previously known based on clinical testing?	OMIM phenotype
6	B/C	*OPRM1*	Y	none
6	I/J	*ARID1B*	Y	Autosomal dominant: Coffin-Siris syndrome I
6	K/L	*EZR*	Y	none

Table S12: Rearrangement numbers and sizes for individual S020.

Chr	Segment	Start	End	Size (bp)	Source/Type	Validated with HiFi?
2	A	1	7,777,990	7,777,989	Derivative 14	Yes
2	B	7,777,996	16,235,712	8,457,716	Derivative 4	Yes
2	C	16,235,711	242,193,529	225,957,818	Derivative 2	Yes
4	A	1	67,572,970	67,572,969	Derivative 4	Yes
4	B	67,572,971	70,140,499	2,567,528	Deletion	Yes
4	C	70,140,500	73,061,492	2,920,992	Derivative 14	Yes
4	D	73,061,493	73,129,559	68,066	Deletion	Yes
4	E	73,129,560	73,446,127	316,567	Derivative 10	Yes
4	F	73,446,129	73,771,830	325,701	Derivative 10	Yes
4	G	73,771,831	74,581,615	809,784	Deletion	Yes
4	H	74,581,616	74,794,351	212,735	Derivative 14	Yes
4	I	74,794,352	74,831,249	36,897	Derivative 14	Yes
4	J	74,831,250	75,039,118	207,868	Derivative 4	Yes
4	K	75,039,137	77,012,176	1,973,039	Derivative 4	Yes
4	L	77,012,175	79,626,721	2,614,546	Derivative 14	Yes
4	M	79,626,720	81,632,570	2,005,850	Derivative 4	Yes
4	N	81,632,570	190,214,555	108,581,985	Derivative 2	Yes
10	A	1	50,382,094	50,382,093	Derivative 10	Yes
10	B	50,382,092	50,563,505	181,413	Derivative 10	Yes
10	C	50,563,501	50,649,777	86,276	Derivative 10	Yes
10	D	50,694,777	51,260,021	565,244	Derivative 10	Yes
10	E	51,260,022	51,840,878	580,856	Deletion	Yes
10	F	51,840,879	53,548,486	1,707,607	Derivative 10	Yes
10	G	53,548,487	53,563,514	15,027	Derivative 14	Yes
10	H	53,563,515	53,584,434	20,919	Deletion	Yes
10	I	53,584,435	56,035,820	2,451,385	Derivative 4	Yes
10	J	56,035,823	65,519,829	9,484,006	Derivative 4	Yes
10	K	65,519,828	67,462,235	1,942,407	Derivative 10	Yes
10	L	67,462,259	74,772,273	7,310,014	Derivative 10	Yes
10	M	74,772,269	76,402,382	1,630,113	Derivative 4	Yes
10	N	76,402,383	133,797,422	57,395,039	Derivative 4	Yes
14	A	1	20,934,810	20,934,809	Derivative 14	Yes
14	B	20,934,811	22,881,931	1,947,120	Deletion	Yes
14	C	22,881,932	107,043,718	84,161,786	Derivative 10	Yes
			Total Size	334,539,803	Derivative 2	
			Total Size	151,177,985	Derivative 4	
			Total Size	146,979,108	Derivative 10	
			Total Size	34,512,995	Derivative 14	

Table S13: Genes impacted by S020 breakpoints.

Chr	Breakpoint	Gene affected by breakpoint	Previously known based on clinical testing?	OMIM phenotype
4	A/B	*STAP1*	Y	none
4	B/C	*CSN1S2BP*	N	none
4	C/D	*COX18*	N	none
4	D/E	*ANKRD17*	N	none
4	E/F	*AFP*	N	Autosomal dominant: hereditary persistence of alpha-fetoprotein; autosomal recessive: alpha-fetoprotein deficiency
4	H/I	*BTC*	N	none
4	J/K	*PARM1*	N	none
4	K/L	*SEPTIN11*	N	none
10	A/B, B/C	*SGMS1*	N	none
10	D/E, E/F	*PRKG1*	N	Autosomal dominant: aortic aneurysm, familial thoracic
10	K/L	*CTNNA3*	N	Autosomal dominant: arrhythmogenic right ventricular dysplasia, familial
10	M/N	*LRMDA*	N	Autosomal recessive: Albinism, oculocutaneous, type VII

Table S14: Rearrangement numbers and sizes for individual S036.

Chr	Segment	Start	End	Size (bp)	Source/Type
5	A	1	22,881,851	22,881,850	Derivative 5
5	B	22,881,853	28,650,540	5,768,687	Derivative 5
5	C	28,650,540	28,826,587	176,047	Derivative 10
5	D	28,826,592	181,538,259	152,711,667	Derivative 5
6	A	1	123,005,546	123,005,545	Derivative 6
6	B	123,005,550	124,505,324	1,499,774	Derivative 18
6	C	124,505,731	126,657,919	2,152,188	Derivative 18
6	D	126,657,920	126,680,039	22,119	Deletion
6	E	126,680,040	170,805,979	44,125,939	Derivative 18
10	A	1	24,286,112	24,286,111	Derivative 10
10	B	24,286,113	24,725,849	439,736	Deletion
10	C	24,725,850	25,278,388	552,538	Derivative 5
10	D	25,278,408	34,622,799	9,344,391	Derivative 10
10	E	34,622,800	35,972,590	1,349,790	Deletion
10	F	35,972,591	49,775,899	13,803,308	Derivative 10
10	G	49,775,901	54,672,866	4,896,965	Derivative 5
10	H	54,672,867	55,305,313	632,446	Deletion
10	I	55,305,314	55,632,879	327,565	Derivative 5
10	J	55,632,880	56,736,281	1,103,401	Deletion
10	K	56,736,282	133,797,422	77,061,140	Derivative 10
18	A	1	6,275,133	6,275,132	Derivative 6
18	B	6,275,134	6,280,055	4,921	Deletion
18	C	6,280,056	7,279,970	999,914	Derivative 6
18	D	7,279,968	80,373,285	73,093,317	Derivative 18
			Total Length	187,139,272	Derivative 5
			Total Length	130,280,591	Derivative 6
			Total Length	124,670,997	Derivative 10
			Total Length	120,871,218	Derivative 18

Table S15: Genes impacted by S036 breakpoints.

Chr	Breakpoint	Gene affected by breakpoint	Previously known based on clinical testing?	OMIM phenotype
6	A/B	*CLVS2*	N	none
6	B/C	*NKAIN2*	N	none
10	A/B	*KIAA1217*	N	none
10	C/D	*GPR158*	N	none
10	D/E	*PARD3*	Y	none
10	F/G, G/H, H/I	*PCDH15*	Y	Autosomal dominant and autosomal recessive: Usher syndrome, type 1D/F digenic
18	A/B, C/D	*L3MBTL4*	N	none

Table S16: Summary of individuals with missing variants.

Individual	Clinical workup	Confirmation of inherited variant	Variant found by T-LRS	Confirmation or supporting findings
S002	CMA normal, exome with paternally inherited stop in *ALMS1*, consistent with suspected diagnosis of Alström syndrome. Deletion/duplication analysis of *ALMS1* negative.	Confirmed the known paternally inherited variant.	*Alu* insertion in exon 20	Clinically confirmed
S003	CMA normal, exome with paternally inherited stop in *NPHP4*, consistent with suspected diagnosis of NPH. Deletion/duplication analysis of *NPHP4* negative.	Confirmed the known paternally inherited variant.	Intronic splice variant	Confirmed by qPCR
S004	CMA normal, exome identified single paternally inherited pathogenic variant in *VARS2*, deletion/duplication analysis of *VARS2* negative.	Confirmed the known paternally inherited pathogenic p.A420T.	No second hit found.	n/a
S008	Biochemical diagnosis of Lesch-Nyhan based on enzyme analysis. CMA normal, sequencing and deletion/duplication analysis of *HPRT1* negative.	No pathogenic SNVs or copy number changes observed, consistent w/clinical testing.	Identified an inversion within *HPRT1* and confirmed with PCR.	Clinically confirmed
S009	Suspected diagnosis of Duchenne muscular dystrophy. Sequencing and deletion/duplication analysis of *DMD* negative. Muscle biopsy consistent with diagnosis. The proband's maternal uncle died of muscular dystrophy.	No pathogenic SNVs or copy number changes observed, consistent w/clinical testing.	Identified a candidate AGAA repeat expansion in intron 16.	Mom is heterozygous, unaffected brother has wild-type allele
S013	CMA normal, exome with paternally inherited stop in *HPS1*, consistent with suspected diagnosis of Hermansky-Pudlak syndrome. No deletion/duplication analysis done.	Confirmed the known paternally inherited variant.	Identified 1,900 bp deletion that removes exon 3.	Clinically confirmed with exon-level array
S018	Elevated phenylalanine, exome with single pathogenic variant in *PAH*.	Confirmed the known inherited variant.	No second hit found.	No second hit found with short-read sequencing
S025	Diagnosed with Stargardt disease by clinical retinal exam. Exome with single pathogenic variant in *ABCA4*. No second hit seen on research WGS.	Confirmed the known pathogenic variant.	~1,500 bp transposable element insertion in the first intron.	Insertion is present in Illumina short-read data.
S047	Diagnosed with glycogen storage disease III. Exome revealed single-nucleotide deletion resulting in frameshift. Research SR-WGS was negative.	Confirmed the known pathogenic variant.	1,525 bp deletion that removed part of exon 3 and results in frameshift.	Deletion present in Illumina SR-WGS data.
S056	CMA normal, exome with single pathogenic variant in *WDR19*, consistent with presumed diagnosis of Sensenbrenner syndrome. Deletion/duplication analysis negative.	Confirmed the known inherited variant.	Intronic splice variant	None

Table S17: Reads used to calculate length of AGAA motif in individual S009.

Read ID/Contig	Start Pos	End Pos	Period Size	Copy Number	Percent Matches	Percent Indels	Score	Motif
268a7f22-1c5e-40a6-b50a-764cc962ecd4:20612-21234	84	562	4	118.5	94	2	753	AAGA
33430113-f292-4c8a-abaa-ef24685b0275:9126-9747	90	540	4	117	79	15	393	AAGA
ab709b56-560e-442b-b415-6538973c978d:4402-4955	66	485	4	107.5	86	10	505	AAGA
157b7b75-7a60-4e4e-8717-6bfa1fc8424f:3823-4453	81	569	4	121.8	92	5	720	AAGA
4683a48e-1bd4-430f-a361-712f000d8ff1:14088-14711	84	562	4	119.8	93	4	727	AAGA
622462ec-1093-4532-91dc-a8366bd9f712:1867-2467	83	537	4	116.8	91	6	620	AAAG
aee7ddf8-5473-4c67-9e45-65ddb6b3512b:1667-2278	78	556	4	120.2	91	5	695	AGAA
4885dba3-b149-4870-b903-eb240a6f34e0:1488-2110	85	562	4	119.5	96	1	762	AAGA
ffc51d09-c8a1-4308-a843-9540a3c812ea:1304-1906	83	546	4	113.8	78	13	297	AAGA
Average				117.2				
Excluded read IDs containing TGTT motif								
1fd6ae08-37dc-47e1-8804-28117b821352								
8f3ea358-76e1-41a7-88a7-ef0e287b4c77								
37a6233f-91bb-4a5f-909d-e3951cc855be								

Table S18: Predicted strength of the canonical splice donor site at the Exon 1–Intron 1 boundary of *ABCA4* (NM_000350) and alternative sites introduced by the ~1,500 bp insertion in individual S025.

Splice donor	SpliceSiteFinder-like	MaxEntScan	NNSPLICE	GeneSplicer	Human Splice Finder
Canonical	81.70	8.90	1.00	5.20	84.70
Alternative	90.10	8.00	0.90	-	95.00
Alternative	81.50	7.20	0.80	0.60	90.80
Splice acceptor	**SpliceSiteFinder-like**	**MaxEntScan**	**NNSPLICE**	**GeneSplicer**	**Human Splice Finder**
Canonical	95.25	10.87	0.99	12.03	92.11
Alternative	93.50	10.00	1.00	3.20	90.60
Alternative	88.54	7.30	1.00	1.50	79.83
Alternative	77.80	6.10	0.60	2.30	78.50
Alternative	83.20	5.90	0.70	-	85.80
Alternative	71.70	5.70	-	1.60	79.50
Alternative	74.60	6.90	0.60	-	78.30

While the SV is absent from all accessible population genetic databases (gnomAD, BRAVO), assessment by multiple *in silico* prediction tools suggest a strong likelihood of pathogenicity. Specifically, the deep residual neural network SpliceAI predicts a splice-altering consequence of the pre-mRNA through the introduction of a *de novo* donor site by the insertion event (Δ score = 0.33, high recall). The ~1,500 bp insertion sequence itself contains two strong alternative splice donors and six alternative splice acceptors. The relative strength of these alternative donors and acceptors indicates a high probability of competition with canonical sites. One alternative donor site in particular exhibits a stronger splice signal than the canonical donor site at the Exon 1–Intron 1 boundary is the most probable site of alternative splicing leading to the inclusion of the 5' portion of the intron in the final mRNA transcript. Length of color bars (blue = donor, green = acceptor) are proportioned to the respective scales of each algorithm: SpliceSiteFinder-Like (0-100), MaxEntScan (0-16), NNSPLICE (0-1), Gene Splicer (0-15), Human Splice Finder v.3.1 (0-100).

Table S19: Accession numbers or contact information for original sequencing data.

Individual	Data Accession or ID	Contact	Email
S002	phs000693	Danny E. Miller, MD, PhD	danny.miller@seattlechildrens.org
S003	phs000693	Danny E. Miller, MD, PhD	danny.miller @seattlechildrens.org
S004	phs000693	Danny E. Miller, MD, PhD	danny.miller@seattlechildrens.org
S008	phs000693	Danny E. Miller, MD, PhD	danny.miller@seattlechildrens.org
S009	phs000693	Danny E. Miller, MD, PhD	danny.miller@seattlechildrens.org
S011	phs000693	Danny E. Miller, MD, PhD	danny.miller@seattlechildrens.org
S013	phs000693	Danny E. Miller, MD, PhD	danny.miller@seattlechildrens.org
S014	phs000693	Danny E. Miller, MD, PhD	danny.miller@seattlechildrens.org
S016	phs000693	Danny E. Miller, MD, PhD	danny.miller@seattlechildrens.org
S018	phs000693	Danny E. Miller, MD, PhD	danny.miller@seattlechildrens.org
S020	phs000693	Danny E. Miller, MD, PhD	danny.miller@seattlechildrens.org
S021	phs000693	Danny E. Miller, MD, PhD	danny.miller@seattlechildrens.org
S022	phs000693	Danny E. Miller, MD, PhD	danny.miller@seattlechildrens.org
S023	phs000693	Danny E. Miller, MD, PhD	danny.miller@seattlechildrens.org
S025	TBD	Danny E. Miller, MD, PhD	danny.miller@seattlechildrens.org
S035	phs000693	Danny E. Miller, MD, PhD	danny.miller@seattlechildrens.org
S036	phs000693	Danny E. Miller, MD, PhD	danny.miller@seattlechildrens.org
S039	phs000693	Danny E. Miller, MD, PhD	danny.miller@seattlechildrens.org
S040	phs000693	Danny E. Miller, MD, PhD	danny.miller@seattlechildrens.org
S041	phs000693	Danny E. Miller, MD, PhD	danny.miller@seattlechildrens.org
S046	phs000693	Danny E. Miller, MD, PhD	danny.miller@seattlechildrens.org
S047	TBD	Priya Kishnani, MD	priya.kishnani@duke.edu
S056	phs000693	Danny E. Miller, MD, PhD	danny.miller @seattlechildrens.org
S060	phs000693	Danny E. Miller, MD, PhD	danny.miller@seattlechildrens.org
S063	http://dx.doi.org/10.1136/jmedgenet-2020-107320		
S071	phs000693	Danny E. Miller, MD, PhD	danny.miller@seattlechildrens.org
S082	phs000693	Danny E. Miller, MD, PhD	danny.miller@seattlechildrens.org
S083	phs000693	Danny E. Miller, MD, PhD	danny.miller@seattlechildrens.org
S086	phs000693	Danny E. Miller, MD, PhD	danny.miller@seattlechildrens.org
04-01	TBD	Heather Mefford, MD, PhD	heather.mefford@stjude.org
04-02	TBD	Heather Mefford, MD, PhD	heather.mefford@stjude.org
04-03	TBD	Heather Mefford, MD, PhD	heather.mefford@stjude.org
06-01	TBD	Heather Mefford, MD, PhD	heather.mefford@stjude.org
06-02	TBD	Heather Mefford, MD, PhD	heather.mefford@stjude.org
06-03	TBD	Heather Mefford, MD, PhD	heather.mefford@stjude.org
BK144-03	phs000693	Danny E. Miller, MD, PhD	danny.miller@seattlechildrens.org
BK180-03	phs000693	Danny E. Miller, MD, PhD	danny.miller@seattlechildrens.org
BK294-03	phs000693	Danny E. Miller, MD, PhD	danny.miller@seattlechildrens.org
BK364-03	phs000693	Danny E. Miller, MD, PhD	danny.miller@seattlechildrens.org
BK397-101	phs000693	Danny E. Miller, MD, PhD	danny.miller@seattlechildrens.org
BK430-103	phs000693	Danny E. Miller, MD, PhD	danny.miller@seattlechildrens.org
BK482-101	phs000693	Danny E. Miller, MD, PhD	danny.miller@seattlechildrens.org
BK487-101	phs000693	Danny E. Miller, MD, PhD	danny.miller@seattlechildrens.org
BK506-03	phs000693	Danny E. Miller, MD, PhD	danny.miller@seattlechildrens.org

Supplemental References

1. Miller, D.E., Squire, A., and Bennett, J.T. (2019). A child with autism, behavioral issues, and dysmorphic features found to have a tandem duplication within CTNND2 by mate-pair sequencing. Am J Med Genet A.

2. Walsh, T., Casadei, S., Munson, K.M., Eng, M., Mandell, J.B., Gulsuner, S., and King, M.-C. (2020). CRISPR–Cas9/long-read sequencing approach to identify cryptic mutations in BRCA1 and other tumour suppressor genes. J Med Genet jmedgenet-2020-107320.

3. LaCroix, A.J., Stabley, D., Sahraoui, R., Adam, M.P., Mehaffey, M., Kernan, K., Myers, C.T., Fagerstrom, C., Anadiotis, G., Akkari, Y.M., et al. (2019). GGC Repeat Expansion and Exon 1 Methylation of XYLT1 Is a Common Pathogenic Variant in Baratela-Scott Syndrome. Am J Hum Genetics *104*, 35–44.

4. Sulovari, A., Li, R., Audano, P.A., Porubsky, D., Vollger, M.R., Logsdon, G.A., Consortium, H.G.S.V., Warren, W.C., Pollen, A.A., Chaisson, M.J.P., et al. (2019). Human-specific tandem repeat expansion and differential gene expression during primate evolution. Proc National Acad Sci *116*, 201912175.

5. Guo, H., Duyzend, M.H., Coe, B.P., Baker, C., Hoekzema, K., Gerdts, J., Turner, T.N., Zody, M.C., Beighley, J.S., Murali, S.C., et al. (2019). Genome sequencing identifies multiple deleterious variants in autism patients with more severe phenotypes. Genet Med *21*, 1611–1620.